

Acetonitrile Exchange Kinetics on Di- and Trivalent Lanthanide Ions

THÈSE N° 4114 (2008)

PRÉSENTÉE LE 27 JUIN 2008

À LA FACULTE SCIENCES DE BASE
LABORATOIRE DE CHIMIE INORGANIQUE ET BIOINORGANIQUE
PROGRAMME DOCTORAL EN CHIMIE ET GÉNIE CHIMIQUE

ÉCOLE POLYTECHNIQUE FÉDÉRALE DE LAUSANNE

POUR L'OBTENTION DU GRADE DE DOCTEUR ÈS SCIENCES

PAR

Gabriella Éva BÓDIZS

M.Sc. in chemistry, Babeş - Bolyai University, Cluj-Napoca, Roumanie
et de nationalité roumaine

acceptée sur proposition du jury:

Prof. P. Vogel, président du jury
Prof. L. Helm, directeur de thèse
Prof. M. Botta, rapporteur
Prof. P. J. Dyson, rapporteur
Dr E. Jakab Toth, rapporteur



ÉCOLE POLYTECHNIQUE
FÉDÉRALE DE LAUSANNE

Suisse
2008

*Édesapám Gábor János (1949–2006)
emlékére*

Acknowledgements

Even if a PhD thesis is a personal work it can not be completed alone. Herein I would like to express my gratitude to those who helped me in one way or in another to accomplish this work.

First and foremost, I would like to express my heartfelt gratitude to Prof. Lothar Helm, my thesis supervisor, for his guidance and support all along these years. His unconditional trust in my work as well as his encouragements and patience helped me to pursue in the most difficult moments of my thesis.

I would like to thank Prof. André Merbach and Prof. Lothar Helm not only for introducing me to the fascinating world of lanthanides, but also for giving me the chance to work in their groups and for the outstanding working conditions that they provided to me. During the course of this work they were for me an invaluable source of inspiration. Particular thanks to Prof. André Merbach for his continuous interest he showed about my work and for his constructive remarks about this manuscript.

I am grateful to the members of my thesis jury, Prof. Pierre Vogel (president), Dr. Éva Jakab-Tóth, Prof. Mauro Botta and Prof. Paul Dyson, for having kindly accepted to expertise my thesis. I am deeply indebt to Dr. Gábor Laurency and to Prof. Paul Dyson for their trust and support. Without their help and encouragements at the beginning of my career at EPFL I would have never pursued a research work at the PhD level.

A part of the work discussed in this manuscript has been performed in collaboration with Prof. Ingo Krossing and Dr. Ines Raabe. I could not thank them enough for all the fruitful discussions we had, for their precious help in the synthesis and X-ray crystal structure determinations (interpretations and data collections), as well for the IR and Raman measurements.

I would like to acknowledge the technical support of Dr. Euro Solari regarding the glove box and for the ICP and elemental analyses, as well as for Dr. Rosario Scopelliti for the X-ray crystal structures. I can not forget the precious help of the mechanical workshop given by

Carlo Bregonzi, Yves Morier and Roger Ith whenever I needed it; and, that of the famous “Magasin” team by Gladys Pache, Annelise Carrupt, Giovanni Petrucci and Jacky Gremaud for their permanent kindness. Martial Rey (NMR), Patrick Favre (electronic) and Donald Zbinden (computer) were also always there to come to rescue me. As well I would like to express my appreciation to Emanuela Mancianti and Maria Szuman for their administrative support.

I am particularly grateful to those who have introduced me to the measurement techniques used in this thesis: Dr. Rémi Dessapt (glove box and variable-temperature NMR), Dr. Gaëlle Nicolle (variable-pressure NMR and matlab programs), Dr. Sabrina Laus (relaxometry), Dr. Edina Balogh (UV-Vis), Dr. Meriem Benmelouka and Dr. Alain Borel (EPR) as well as Dr. Zoltán Béni (synthesis under inert atmosphere).

I am indebted to the people who revised my work: Dr. Ines Raabe and Dr. Caroline Canizzo; and, to Caroline (again), Hugues Jaccard and Dr. Fabrice Riblet for the French version of the abstract. Your questions and suggestions helped me to improve this manuscript.

Many thanks to all my actual and former colleagues from the LCIB and GCIB groups for providing an enjoyable and stimulating atmosphere. It was a real pleasure for me to have very interesting discussions with you over various topics during lunch time. In particular I would like to thank Céline, Caroline, Ines, Edina, Gaëlle, Corinne, Angelique, Fabrice, Jérôme, Alain, Laci, Zoli and Hugues. Your support and enthusiasm made me feel better when I was upset.

These acknowledgements would not be complete without thanking all my friends who have rendered my stay in Lausanne and in Switzerland enjoyable. The list is too long, thus I would like to thank them collectively.

Last but not least, my profound gratitude goes to my family. I would like to thank my parents, Gábor Irén and János, and my sister Lázini Hajnal and her family, Sandu and Evelin, for their unconditional support, love and encouragements that they gave to me when I was so far from them. Most of all, my special thanks goes to my husband, Csabi. I would have never been able to complete this thesis without your love, support and patience. Köszönöm!

Table of content

Abstract.....	5
Version abrégée.....	6
Symbols and abbreviations	7
I Introduction	11
I.1 Lanthanide ions: general properties and applications	13
I.2 Solvation and coordination number of lanthanide ions	16
I.3 Interaction of lanthanides with anions.....	18
I.4 General aspects of solvent exchange	19
I.4.1 Classification of exchange mechanisms	21
I.4.2 Determination of solvent exchange mechanisms.....	22
I.5 Solvent exchange on lanthanide complexes	26
I.5.1 Water exchange	26
I.5.2 Non-aqueous solvent exchange	28
I.6 Objectives of the thesis	30
I.7 References.....	32
II Synthesis and characterization of homoleptic $[\text{Ln}(\text{CH}_3\text{CN})_n][\text{Al}(\text{OC}(\text{CF}_3)_3)_4]_3$ complexes	35
II.1 Introduction.....	37
II.2 Synthesis of $[\text{Ln}(\text{CH}_3\text{CN})_n][\text{Al}(\text{OC}(\text{CF}_3)_3)_4]_3$ complexes	39
II.3 Characterisation of $[\text{Ln}(\text{CH}_3\text{CN})_n][\text{Al}(\text{OC}(\text{CF}_3)_3)_4]_3$ complexes in solid state.....	40
II.3.1 X-ray crystal structures	40
II.3.2 IR and Raman spectroscopy	47
II.4 Characterisation of $[\text{Ln}(\text{CH}_3\text{CN})_n][\text{Al}(\text{OC}(\text{CF}_3)_3)_4]_3$ complexes in solution	51
II.4.1 Conductivity	51
II.4.2 NMR chemical shift measurements	54
II.4.2.1 Hetero-nuclear NMR chemical shifts	55
II.4.2.2 Bulk magnetic susceptibility shifts	58
II.4.3 ^{19}F NMR measurements	60
II.4.4 UV-Vis spectroscopy	65
II.4.4.1 UV-Vis spectra of $[\text{Nd}(\text{CH}_3\text{CN})_9][\text{Al}(\text{OC}(\text{CF}_3)_3)_4]_3$	66
II.4.4.2 UV-Vis spectra of $[\text{Eu}(\text{CH}_3\text{CN})_9][\text{Al}(\text{OC}(\text{CF}_3)_3)_4]_3$	67
II.5 Conclusion.....	71
II.6 References	72

III	Acetonitrile exchange on $[\text{Ln}(\text{CH}_3\text{CN})_9][\text{Al}(\text{OC}(\text{CF}_3)_3)_4]_z$ where $\text{Ln} = \text{Gd}^{3+}$ and Eu^{2+}	75
III.1	Introduction	77
III.2	Acetonitrile exchange on the isoelectronic Gd^{3+} and Eu^{2+} ions	78
III.2.1	Experimental part	78
III.2.1.1	Sample preparation	78
III.2.1.2	^{14}N NMR spectroscopy	78
III.2.1.3	^1H NMRD	79
III.2.1.4	EPR spectroscopy	79
III.2.1.5	Data analysis	80
III.2.2	Equations for the simultaneous analysis of the NMR and EPR data for Gd^{3+} and Eu^{2+} ions in acetonitrile solution	80
III.2.2.1	^{14}N NMR spectroscopy	80
III.2.2.2	^1H NMRD	83
III.2.2.3	EPR spectroscopy	85
III.3	Results and discussions	86
III.3.1	Determination of the solvent exchange rate constants	88
III.3.2	Rotational correlation times by ^1H NMRD	92
III.3.3	Electron spin relaxation by EPR	94
III.4	Conclusion	96
III.5	References	97
IV	Acetonitrile exchange on $[\text{Ln}(\text{CH}_3\text{CN})_n][\text{Al}(\text{OC}(\text{CF}_3)_3)_4]_3$ where $n = 9, \text{Ln}^{3+} = \text{Nd}$ and Dy; $n = 8, \text{Ln}^{3+} = \text{Tm}$	101
IV.1	Introduction	103
IV.2	Acetonitrile exchange on Nd^{3+}, Dy^{3+} and Tm^{3+} ions	104
IV.2.1	Experimental part	104
IV.2.1.1	Sample preparation	104
IV.2.1.2	^{14}N NMR spectroscopy	104
IV.2.1.3	^1H NMRD	104
IV.2.1.4	Data analysis	105
IV.2.2	Equations for the analysis of the ^{14}N NMR and ^1H NMRD data for Nd^{3+} , Dy^{3+} and Tm^{3+} ions in acetonitrile solution	105
IV.2.2.1	^{14}N NMR spectroscopy	105
IV.2.2.2	^1H NMRD	109
IV.3	Results and discussions	113
IV.3.1	Determination of the solvent exchange rate constants	113
IV.3.2	Rotational correlation times and electron spin relaxations by ^1H NMRD and $1/T_{1\rho}$ of ^{14}N NMR	119
IV.4	Conclusion	124
IV.5	References	126

V	Conclusions	129
V.1	Conclusions	131
V.2	References	136
VI	Experimental section	137
VI.1	General experimental techniques and measurements	139
VI.1.1	General procedures and starting materials	139
VI.1.2	Elemental analysis	140
VI.1.3	X-ray diffraction and crystal structure determination.....	140
VI.1.4	Conductivity	140
VI.1.5	IR and Raman spectroscopy	140
VI.1.6	UV-Vis spectroscopy	141
VI.1.7	NMR spectroscopy	141
VI.1.8	¹ H NMRD	142
VI.1.9	EPR spectroscopy	143
VI.2	Synthesis and characterization of compounds used in this work	143
VI.2.1	Synthesis of Li[Al(OC(CF ₃) ₃) ₄]	143
VI.2.2	Synthesis of Ag[Al(OC(CF ₃) ₃) ₄].....	144
VI.2.3	Synthesis of [Bu ₄ N][Al(OC(CF ₃) ₃) ₄]	145
VI.2.4	Synthesis of [Nd(CH ₃ CN) ₉][Al(OC(CF ₃) ₃) ₄] ₃ 1	146
VI.2.5	Synthesis of [Eu(CH ₃ CN) ₉][Al(OC(CF ₃) ₃) ₄] ₃ 2 and 2a	147
VI.2.6	Synthesis of [Gd(CH ₃ CN) ₉][Al(OC(CF ₃) ₃) ₄] ₃ 3	148
VI.2.7	Synthesis of [Dy(CH ₃ CN) ₉][Al(OC(CF ₃) ₃) ₄] ₃ 4	149
VI.2.8	Synthesis of [Tm(CH ₃ CN) ₈][Al(OC(CF ₃) ₃) ₄] ₃ 5	150
VI.2.9	Synthesis of Ln(CH ₃ CN) ₃ (CF ₃ SO ₃) ₃ , Ln = Eu, Gd.....	151
VI.3	References.....	152
VII	Appendix.....	153
VII.1	Generalities	155
VII.2	Experimental data for chapter II.....	156
VII.3	Experimental data for chapter III	195
VII.4	Experimental data for chapter IV	205
VII.5	References	212
	Curriculum Vitae	213
	Publications	214
	Poster presentations.....	215

Abstract

The knowledge and understanding of the mechanism as well as the rate constant of the solvent exchange reactions are fundamental, since these reactions represent an important step in complex formation reactions on metal ions. Solvent exchange reactions in aqueous or non-aqueous solutions are the simplest chemical reactions on metal cations: a solvent molecule situated in the first coordination sphere of the ion is replaced by another one, generally entering from the bulk. In this work acetonitrile was chosen as non-aqueous solvent medium. For lanthanides, CH_3CN is a weakly coordinating, labile, uncharged ligand; therefore homoleptic acetonitrile lanthanide complexes could be used as essential synthetic precursors to produce a wide range of compounds under non-aqueous conditions. The presence of the anion in the first coordination sphere of the metal ion can considerably change the solvent exchange rate; therefore it is imperative that solvent exchange reactions to be studied on homoleptic metal complexes.

This study has been devoted to the synthesis of homoleptic acetonitrile lanthanide complexes like $[\text{Ln}(\text{CH}_3\text{CN})_n][\text{Al}(\text{OC}(\text{CF}_3)_3)_4]_3$ ($n = 9$, $\text{Ln}^{3+} = \text{Nd, Eu, Gd, Dy}$; $n = 8$, $\text{Ln}^{3+} = \text{Tm}$); and to the understanding of the acetonitrile exchange reaction on the lanthanide series. It has been found that in anhydrous acetonitrile nine-coordinated species are characteristic for lanthanides from the middle (Eu, Gd, Dy) and the beginning (Nd) of the Ln series, while for those from the end (Tm) eight-coordinated species are representatives. For the synthesized complexes, evidences that both in the solid state and in acetonitrile solution there is no direct metal–anion interaction are provided by: X-Ray diffraction, IR and Raman spectroscopy, conductivity and NMR techniques.

The rate constants of the acetonitrile exchange reaction as well as the rotational dynamics of the homoleptic acetonitrile Nd(III), Gd(III), Dy(III), Tm(III) and Eu(II) complexes have been achieved by variable temperature and multiple field ^{14}N NMR, ^1H NMRD or EPR measurements. It has been observed that the overall labilities of the CH_3CN ligands are the highest ones measured so far in non-aqueous solvents on lanthanides. It is most likely that the mechanistic pathway for the acetonitrile exchange reaction on the homoleptic nine-coordinated lanthanide ions follows a dissociative activation mode and an associative one for the eight-coordinated species.

Keywords: homoleptic acetonitrile lanthanide complexes, acetonitrile exchange, NMR, EPR.

Version abrégée

La connaissance et la compréhension des mécanismes ainsi que des constantes de vitesse des réactions d'échange de solvant sont fondamentales, particulièrement parce que ce type de réaction représente une étape importante dans les réactions de formation de complexes par des ions métalliques. Les réactions d'échange de solvant dans les milieux aqueux ou non-aqueux sont parmi les réactions chimiques les plus simples pour les cations métalliques: une molécule de solvant située dans la première sphère de coordination du métal est remplacée par une autre, généralement provenant du milieu environnant. Dans ce travail, l'acétonitrile a été choisi comme milieu de solvant non-aqueux, qui est pour les lanthanides, un ligand faiblement coordonnant, labile et neutre. De plus les complexes homoléptiques de lanthanides avec acétonitrile peuvent être utilisés comme précurseurs synthétiques essentiels pour produire une grande variété de composés en conditions non aqueuses. La présence d'un anion dans la première sphère de coordination du métal change considérablement la vitesse d'échange du solvant. Il est donc essentiel d'étudier les constantes de vitesse d'échange dans le cas de complexes homoléptiques.

Cette étude a été consacrée à la synthèse de complexes homoléptiques de lanthanides de formule générale $[\text{Ln}(\text{CH}_3\text{CN})_n][\text{Al}(\text{OC}(\text{CF}_3)_3)_4]_3$ ($n = 9$, $\text{Ln}^{3+} = \text{Nd}, \text{Eu}, \text{Gd}, \text{Dy}$; $n = 8$, $\text{Ln}^{3+} = \text{Tm}$) ainsi qu'à la compréhension de l'échange d'acétonitrile le long de la série des lanthanides. Dans l'acétonitrile anhydre, les espèces nonacoordinées ont été observées pour les lanthanides du milieu ($\text{Eu}, \text{Gd}, \text{Dy}$) et du début (Nd) de la série. Au contraire, les métaux de la fin de la série (Tm) forment des complexes octacoordinés. Pour les complexes synthétisés, l'absence d'interaction directe entre le centre métallique et l'anion a été prouvée aussi bien à l'état solide qu'en solution via de nombreuses techniques : diffraction des rayons X, spectroscopie IR et Raman, conductivité et RMN.

Les constantes de vitesses d'échange d'acétonitrile ainsi que la dynamique de rotation des complexes homoléptiques d'acétonitrile pour Nd(III) , Gd(III) , Dy(III) , Tm(III) et Eu(II) ont été déterminés par des études ^{14}N RMN, ^1H RMN ou RPE à température variable et à plusieurs champs. Il a été observé que les labilités globales des ligands CH_3CN sont les plus hautes jamais mesurées sur les lanthanides dans les solvants non aqueux. Vraisemblablement le mécanisme de la réaction d'échange d'acétonitrile pour les complexes de lanthanides nonacoordinés est dissociativement activé, alors que pour les complexes octacoordinés il s'agit d'un mécanisme de type associatif. **Mot-clefs:** complexes homoléptiques de lanthanides dans l'acétonitrile, échange d'acétonitrile, RMN, RPE.

Symbols and Abbreviations

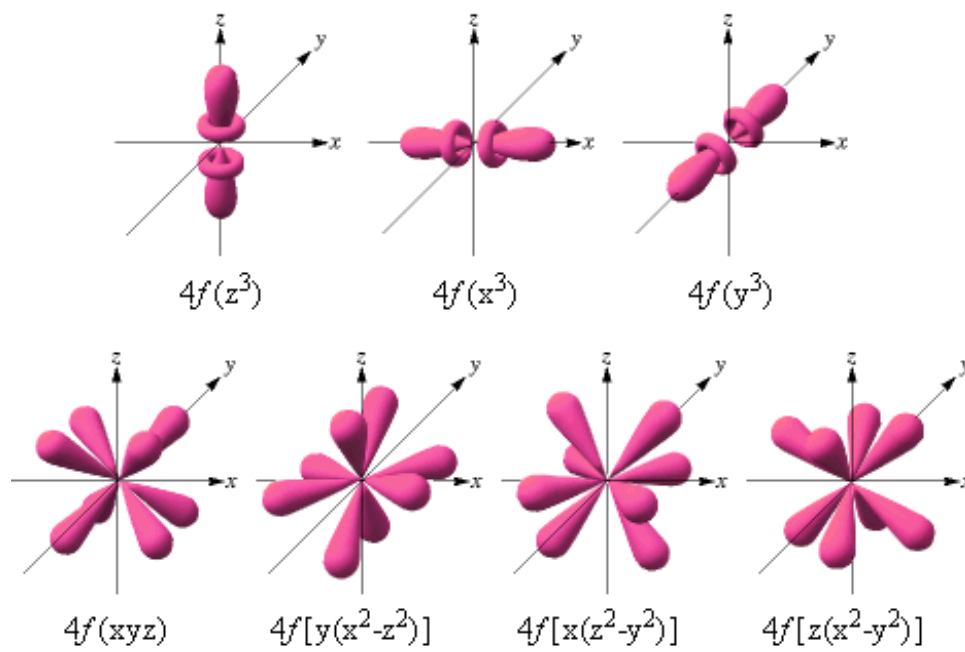
A/\hbar	scalar coupling constant
a_{LnH}	closest approach distance of the acetonitrile proton to the Ln complex
B_0	static magnetic field
BMS	Bulk Magnetic Susceptibility
Bu	n-butyl, $-\text{C}_4\text{H}_9$
CH_3CN	acetonitrile
CN	coordination number
C_{os}	outer-sphere constant
D_{LnH}	diffusion coefficient of the acetonitrile molecule (relative to the complex)
DIME	diethylene glycol dimethyl ether
DMSO	dimethylsulfoxide, $(\text{CH}_3)_2\text{SO}$
DMF	<i>N,N'</i> -dimethylformamide, $(\text{CH}_3)_2\text{NCOH}$
EPR	Electron Paramagnetic Resonance
E_{R}	activation energy for the rotation
E_{V}	activation energy for the modulation of the ZFS
E_{LnH}	activation energy for the diffusion of the acetonitrile molecule
Et	ethyl, $-\text{C}_2\text{H}_5$
EXAFS	Extended X-ray Absorption Fine Structure
FT-IR	Fourier Transform InfraRed
g_{L}	isotropic Landé factor
h	Planck constant
I	nuclear spin quantum number
ICP	Inductively Coupled Plasma
J	total angular quantum number
k_{B}	Boltzmann constant
k_{ex}	solvent exchange rate
LIS	Lanthanide Induced Shift
Ln	lanthanides
N_{A}	Avogadro constant
NMR	Nuclear Magnetic Resonance
NMRD	Nuclear Magnetic Relaxation Dispersion

[OTF] ⁻	triflate, [CF ₃ SO ₃] ⁻
[pftb] ⁻	perfluorotertbutoxyaluminate, [Al(OC(CF ₃) ₃) ₄] ⁻
<i>P_m</i>	mole fraction of the bound acetonitrile
pyO	pyridine N-oxide
<i>q</i>	solvation number per metal center
<i>R</i>	perfect gas constant
<i>R_i</i>	relaxation rate (= 1/ <i>T_i</i>)
<i>R₁^d</i>	diamagnetic contribution to the observed longitudinal relaxation rate
<i>R₁^{obs}</i>	observed longitudinal relaxation rate
<i>R₁^p</i>	paramagnetic contribution to the observed longitudinal relaxation rate
<i>r₁</i>	relaxivity
<i>r_{LnH}</i>	effective distance between the Ln electron charge and the ¹ H nucleus
<i>r_{LnN}</i>	effective distance between the Ln electron charge and the ¹⁴ N nucleus
<i>S</i>	electron spin quantum number
<i>T</i>	temperature
<i>T₁</i>	longitudinal relaxation time
<i>T₂</i>	transverse relaxation time
<i>T_{1e}</i>	electron longitudinal relaxation time
<i>T_{1A}</i>	longitudinal relaxation time of the diamagnetic reference
<i>T_{2e}</i>	electron transverse relaxation time
<i>T_{2A}</i>	transverse relaxation time of the diamagnetic reference
<i>T_{1m}</i>	longitudinal relaxation time of the bound acetonitrile molecule
<i>T_{2m}</i>	transverse relaxation time of the bound acetonitrile molecule
<i>T_{1r}</i>	reduced longitudinal relaxation time
<i>T_{2r}</i>	reduced transverse relaxation time
TEOF	triethy orthoformiate, HC(OEt) ₃
THF	tetrahydrofuran
TMP	trimethylphosphate
TMU	<i>N,N,N',N'</i> -tetramethylurea
TMS	tetramethylsilan
UV-Vis	Ultra-Violet-Visible
WCAs	Weakly Coordinating Anions
ZFS	Zero Field Splitting
<i>χ</i>	quadrupolar coupling constant

ΔH_{pp}	EPR peak to peak line width
ΔH^\ddagger	enthalpy of activation
ΔS^\ddagger	entropy of activation
ΔV^\ddagger	volume of activation
$\Delta\omega_m$	chemical shift difference between bound and bulk acetonitrile
$\Delta\omega_r$	reduced chemical shift difference
γ_I	nuclear gyromagnetic ratio
γ_S	electron gyromagnetic ratio
ε	molar extinction coefficient
η	asymmetry parameter
τ_{LnH}	diffusional correlation time
τ_m	acetonitrile mean residence correlation time
τ_R	rotational correlation time
τ_v	correlation time for the modulation of the ZFS
τ_S	electron relaxation time
μ_B	electron Bohr magneton
μ_{eff}	effective magnetic moment
ν	frequency
ω	angular frequency
ω_A	angular frequency of the diamagnetic reference
ω_0	resonance frequency
ω_I	nuclear Larmor frequency
ω_S	electron Larmor frequency

Chapter I

Introduction



I.1 LANTHANIDE IONS: GENERAL PROPERTIES AND APPLICATIONS

The fifteen elements La, Ce, Pr, Nd, Pm, Sm, Eu, Gd, Tb, Dy, Ho, Er, Tm, Yb and Lu (Table I-1) are generally called lanthanides because their chemical properties are similar to that of the first element of the series, lanthanum. Lanthanides together with Sc and Y are also often called rare earths.

Table I-1. Electronic configuration of lanthanides and their trivalent ions as well as their ionic radius for the nine coordinated species.

Element	Symbol	Atomic number	Ln electronic configuration	Ln ³⁺ electronic configuration	Ln ³⁺ ionic radius / Å ^[1]
Lanthanum	La	57	[Xe]5d ¹ 6s ²	[Xe]4f ⁰	1.216
Cerium	Ce	58	[Xe]4f ¹ 5d ¹ 6s ²	[Xe]4f ¹	1.196
Praseodymium	Pr	59	[Xe]4f ³ 6s ²	[Xe]4f ²	1.179
Neodymium	Nd	60	[Xe]4f ⁴ 6s ²	[Xe]4f ³	1.163
Promethium	Pm	61	[Xe]4f ⁵ 6s ²	[Xe]4f ⁴	1.144
Samarium	Sm	62	[Xe]4f ⁶ 6s ²	[Xe]4f ⁵	1.132
Europium	Eu	63	[Xe]4f ⁷ 6s ²	[Xe]4f ⁶	1.120
Gadolinium	Gd	64	[Xe]4f ⁷ 5d ¹ 6s ²	[Xe]4f ⁷	1.107
Terbium	Tb	65	[Xe]4f ⁹ 6s ²	[Xe]4f ⁸	1.095
Dysprosium	Dy	66	[Xe]4f ¹⁰ 6s ²	[Xe]4f ⁹	1.083
Holmium	Ho	67	[Xe]4f ¹¹ 6s ²	[Xe]4f ¹⁰	1.072
Erbium	Er	68	[Xe]4f ¹² 6s ²	[Xe]4f ¹¹	1.062
Thulium	Tm	69	[Xe]4f ¹³ 6s ²	[Xe]4f ¹²	1.052
Ytterbium	Yb	70	[Xe]4f ¹⁴ 6s ²	[Xe]4f ¹³	1.042
Lutetium	Lu	71	[Xe]4f ¹⁴ 5d ¹ 6s ²	[Xe]4f ¹⁴	1.032

In contrary to their name “rare earths”, most of the lanthanides are relatively abundant in the earth’s crust. They can be found especially as oxides, Table I-2, or in different minerals like: apatite, monazite, bastnasite, cerite, gadolinite, xenotime as phosphates and fluorocarbonates. The global concentration of rare earths has the same magnitude as that of zinc (0.016 %) and is largely superior to those of lead and silver. The most abundant lanthanide in the earth crust is cerium, which can be situated between that of copper and tin. The less abundant lanthanides are: europium, terbium and lutetium, whose concentrations are comparable with those of

mercury and cadmium. It has to be mentioned that promethium ^{61}Pm is a radioactive element which doesn't exist in nature. It is produced as unstable isotope during nuclear fission of the uranium ion (^{92}U).

Table I-2. Rare earth abundances in the earth crust as metal oxides.^[a]

Rare earth	Oxide	Abundance / ppm	Rare earth	Oxide	Abundance / ppm
Y	Y_2O_3	28	Gd	Gd_2O_3	6.4
La	La_2O_3	18	Tb	Tb_4O_7	0.9
Ce	CeO_2	46	Dy	Dy_2O_3	5
Pr	Pr_6O_{11}	5.5	Ho	Ho_2O_3	1.2
Nd	Nd_2O_3	24	Er	Er_2O_3	4
Pm	-	-	Tm	Tm_2O_3	0.4
Sm	Sm_2O_3	6.5	Yb	Yb_2O_3	2.7
Eu	Eu_2O_3	0.5	Lu	Lu_2O_3	0.8

^[a] http://www.sfc.fr/Donnees/mine/tera/textera.htm#Teneurs_minerais

The electronic configuration of lanthanides is $[\text{Xe}]4f^{n+1}6s^2$, presenting the successive filling of the $4f$ sub-shell (n varies from 0 to 14). La, Gd and Lu are exceptions, having $[\text{Xe}]4f^n5d^16s^2$ configuration. The $4f$ orbitals (Figure I-1) lie inside the completely filled $5s^2$ and $5p^6$ orbitals, therefore the $4f$ electrons do not contribute to the valence shell. Generally, lanthanides are trivalent, but they can also be divalent (Sm, Eu, Yb) or tetravalent (Ce, Pr, Tb) in the case where the electronic configuration of the $4f$ orbitals is empty ($4f^0$), half-filled ($4f^7$) or filled ($4f^{14}$) (underlined elements make exception from the rule). As the atomic number increases across the series, the nuclear charge increases and the electrons are more and more attracted to the nucleus, resulting in a decrease of the ionic radii, allowing thus to them small differences in their chemical properties. This is known as *lanthanide contraction*. The magnetic properties of the lanthanides can be attributed to the unpaired $4f$ electrons. With the exception of La^{3+} (f^0), Lu^{3+} (f^{14}), Ce^{4+} (f^0) and Yb^{2+} (f^{14}) which are diamagnetic the lanthanide ions have from 1 to 7 unpaired electrons which assign them paramagnetic properties. Eu^{3+} is also diamagnetic in the ground state, but the low lying paramagnetic states are populated at room temperature. Generally lanthanide ions are colored, having characteristic UV spectra due to the $f-f^*$ transitions, excepting Gd^{3+} , Yb^{3+} and Lu^{3+} ions, which are colorless.

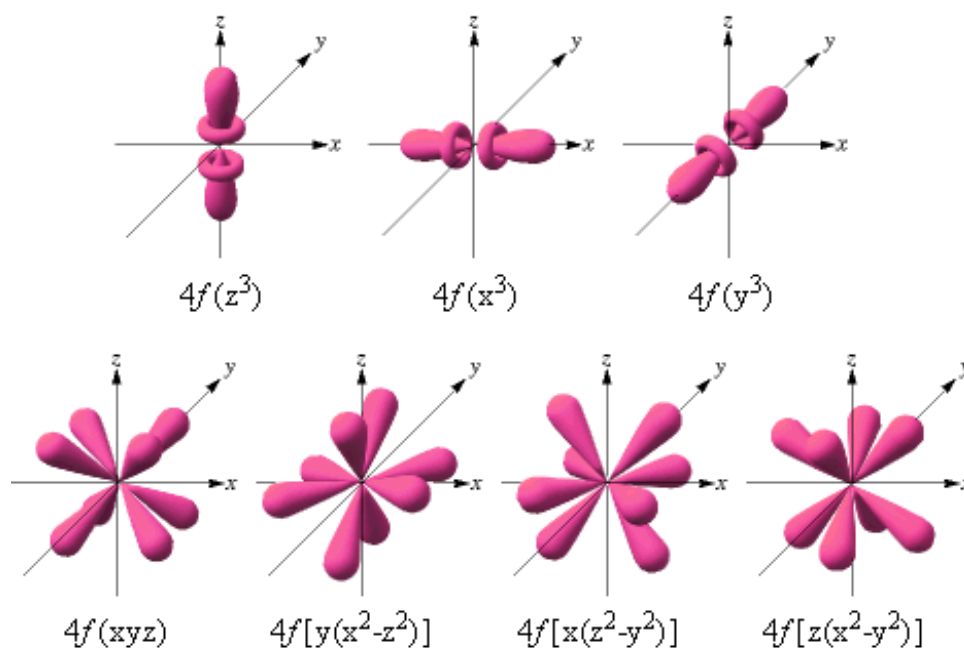


Figure I-1. Representation of the 4f orbitals.

Due to the above mentioned specific physical and chemical properties lanthanide ion complexes have a wide range of industrial applications. For example in glass industry some rare earth oxides are used to decolorize glasses,^[2] cerium complexes are used to improve the performance of high quality glasses. Cerium oxide is the best polishing agent known for glass, a property resulting from its natural hardness (due to its compact fluorite structure) and from the chemical reaction which takes place at the silica-cerium oxide interface.^[3] Neodymium (blue-violet), erbium (pink), praseodymium (green) are used to color some special glasses. Rare earth sulphides are used for coloration in plastic industry (La_2S_3 - yellow, Ce_2S_3 - red, Pr_2S_3 - green, Dy_2S_3 - orange)^[4] where they shown a good stability under UV exposure and no significant change in color with temperature (up to 300°C). Many other areas can be mentioned where rare earths are used extensively, for example perovskite mixed oxides (LaTO_3 , T = Co, Ni, Cu...) for oxidation catalysis,^[5] doped lanthanum-gallium oxide LaGaO_3 as a potential electrolyte for low temperatures,^[6] lanthanum-gallium based glasses for optical fiber amplifiers,^[7] rare earth organic derivatives as catalysts in a number of preparations of polymers and elastomers, and in medicine Gd^{3+} chelates are used as MRI contrast agents to improve the image contrast between the healthy and diseased tissues.^[8]

I.2 SOLVATION AND COORDINATION NUMBER OF LANTHANIDE IONS

Ions in solutions always react in solvated form and generally the ion solvation shell is changed as chemical reactions take place. So it is very important to know the composition and the structure of the solvated ions as well as the dynamics for understanding all chemical processes in solution.

The most common model of ion solvation is the concentric shell model, in which, the existence of several coordination shells around the solvated ion is adopted.^[9] In the first shell, generally called inner or first coordination sphere, solvent and/or ligand molecules have direct contact to the central metal ion. The total number of bonds with solvent and/or ligand molecules in the first coordination sphere is the **Coordination Number (CN)** of the ion. The second coordination shell represents the extended sphere where the solvent and/or ligand molecules are more or less influenced by the charge density of the cation. In the bulk there is interaction only between the solvent and/or ligand molecules.

The coordination number of lanthanide ions in solutions varies between 6 and 12.^[1] The small increase in the ionic radii by about 0.3 Å, from the coordination number of 6 to 12, implies that lanthanide complexes can easily adapt their coordination number to the nature of the coordinating ligand, solvent or counter ion. At the same time, the small decrease of the ionic radii from La to Lu by about 0.2 Å, in the case of the same coordination number, reveals that slight steric effects will also be involved in their complexes. Lanthanide ions in solutions are generally stable due to the fact that the 4*f* orbitals are protected from external interactions by the 5*s* and 5*p* orbitals. Therefore, the bonding and stereochemistry of lanthanide complexes and solvates are largely determined by ion-dipole interaction between the cation and solvent/ligand molecules, while the number of solvent/ligand molecules in the first coordination sphere and their geometrical arrangements will be largely influenced by steric requirements.

Lanthanides are hard acids and prefer hard donors like: F, O or N. In water the bond strength varies as follows: Ln-F > Ln-O >> Ln-N >> Ln-S ≈ Ln-P.^[10] After many years of contentious discussions (from 1950's to beginning of 1990's) about the coordination number of lanthanide ions in water, CN it is now well established from neutron scattering,^[11, 12] X-ray scattering,^[13, 14] extended X-ray absorption fine structure (EXAFS),^[15] density^[16, 17] and spectrophotometric

techniques^[18, 19] or quite recently by ^{17}O NMR spectroscopy and DFT calculations.^[20] The lighter ions, La^{3+} - Nd^{3+} , are predominantly nine-coordinate, Pm^{3+} - Eu^{3+} exist in equilibrium between eight- and nine-coordinate states, and the heavier ions, Gd^{3+} - Lu^{3+} , are predominantly eight-coordinate. This change in CN is nicely reflected in the evolution of the absolute partial molar volumes, V_{abs}^0 , measured along the lanthanide series in aqueous $\text{Ln}(\text{ClO}_4)_3$ solutions, Figure I-2.^[21] The CN values of lanthanide ions in aqueous solutions are sometimes in contrast to that observed in solid state. Hence, X-ray diffraction studies have shown that in solid state tricapped trigonal prismatic $[\text{Ln}(\text{H}_2\text{O})_9]^{3+}$ structure is characteristic for $\text{Ln}^{3+} = \text{La}^{3+}, \text{Pr}^{3+}, \text{Sm}^{3+}, \text{Gd}^{3+}, \text{Ho}^{3+}, \text{Er}^{3+}, \text{Yb}^{3+}$, and Lu^{3+} in the presence of CF_3SO_3^- , EtOSO_3^- and BrO_3^- counter ions and octahedral $[\text{Ln}(\text{H}_2\text{O})_6]^{3+}$ structure for $\text{Ln}^{3+} = \text{La}^{3+}, \text{Tb}^{3+}$, and Er^{3+} in the presence of ClO_4^- counter ion.^[19]

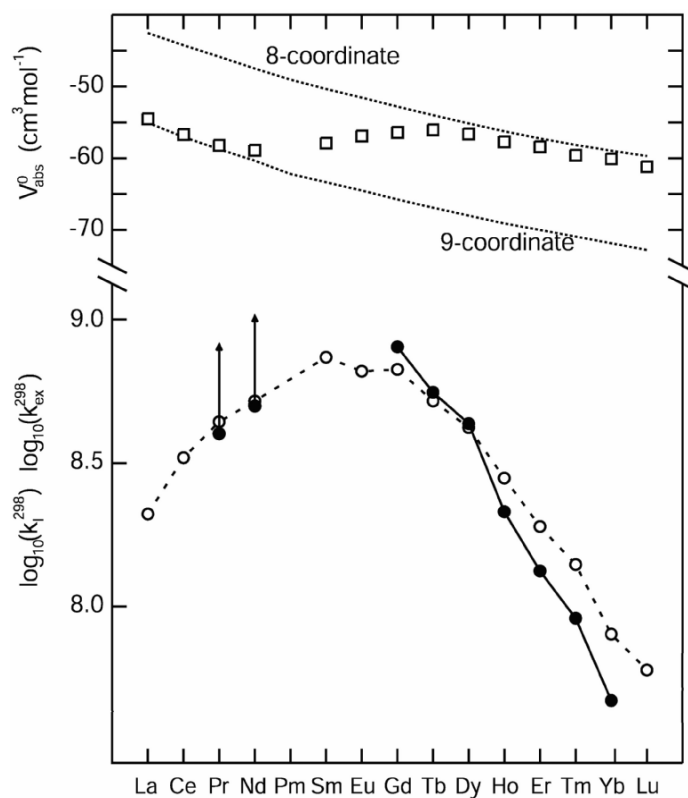


Figure I-2. Absolute partial molar volumes, V_{abs}^0 , of $[\text{Ln}(\text{H}_2\text{O})_n]^{3+}$ in aqueous $\text{Ln}(\text{ClO}_4)_3$ solutions (\square), compared with calculated values for $[\text{Ln}(\text{H}_2\text{O})_8]^{3+}$ and $[\text{Ln}(\text{H}_2\text{O})_9]^{3+}$ (upper and lower dotted lines, respectively). Interchange rate constants k_i , for substitution of SO_4^{2-} on $[\text{Ln}(\text{H}_2\text{O})_n]^{3+}$ are shown as (\circ), and water exchange rate constants (at 298 K) for $[\text{Ln}(\text{H}_2\text{O})_8]^{3+}$ are shown as (\bullet).^[21]

The determination of the coordination number of lanthanides in solution, especially in non-aqueous organic solvents, is very difficult due to: i) small solubility in non-aqueous organic

solvents of lanthanide complexes; ii) small absorption coefficients; iii) equilibrium between species having the same coordination number but different coordination polyhedra and thus different spectroscopic properties; iv) equilibrium between species differing in constitution by one, or more, bounded solvent molecules.^[22] Nevertheless some studies were carried out in this field.^[10] These works reveal that: a decrease even by two units of the coordination number along the lanthanide series can be present in non-aqueous solvents; the coordination number is highly influenced by the solvent composition; lanthanide ions can expand their coordination shell in the presence of strong donors, like DMSO; and, typically in non-polar solvents most of the weakly coordinating anion often interact with lanthanides.

I.3 INTERACTION OF LANTHANIDES WITH ANIONS

Interaction of lanthanides with effectively coordinating anions like halides ($X^- = Cl^-, Br^-$), nitrate (NO_3^-) or thiocyanate (NCS) to form monodentate, bidentate or bridged complexes or with perchlorate (ClO_4^-) and triflate ($CF_3SO_3^-$) which were, for a long time, believed to be non-coordinating anions to the lanthanides has been treated a lot over the years.^[10] Assiduous research in this field led to the subsequent conclusions.

In 1976 Smith *et al.*^[23] found the 8-coordinate specie $[LaCl_3(CH_3OH)_5]$ in methanol solution, proving the inner sphere coordination of chloride ion to lanthanides. In 1991 Ishiguro and Takahashi^[24] worked on complexation of rare-earth ions ($Ln = La - Lu$) by chloride in DMF. The formation of $[LnCl]^{2+}$, $[LnCl_2]^+$, $[LnCl_3]$ and $[LnCl_4]^-$ complexes has been evidenced.

In 1928 Quill *et al.*^[25] observed that the absorption spectra of some Ln^{3+} ions undergo substantial modifications upon addition of nitric acid. In 1979 Bünzli and Yersin,^[26] from luminescence spectra, also clearly point out the inner-sphere complexation of nitrate in water. Later, in 1983 Mabillard,^[27] from FT-IR spectra, evidenced the bidentate coordination of nitrate ion to lanthanides in anhydrous acetonitrile.

In 1993 Depaoli *et al.*^[28] reported the crystal and molecular structure of the homologous complexes $Ln(NCS)_3(THF)_4$, in which the unusual dual mono- ($Ln-NCS$) and bidentate ($Ln-NCS-Ln$) behavior of NCS ligand is sustained by the presence of octa-coordination. In 1992

Takahashi and Ishiguro^[29] reported the formation of thiocyanato complexes of $\text{Ln}^{3+} = \text{La, Nd, Tb, Ho, Tm, Yb}$ ions in DMF.

Inner-sphere interactions of perchlorate (ClO_4^-) ions with lanthanides does not occur in strong donor solvents such as H_2O , DMF or DMSO as was revealed by conductivity, absorption, luminescence, NMR and FT-IR data (Lugina *et al.* 1973,^[30] Pisaniello *et al.* 1983,^[31] Bünzli and Yersin 1982^[32]). But, in organic solvents having a weak to moderate donor strength inner-sphere complexes are formed. Evidence of this interaction has been brought by conductivity measurements which have shown for $\text{La}^{3+} = \text{Nd, Eu, Er}$ ions 2:1 electrolytes in anhydrous methanol (Zholdakov *et al.* 1971),^[33] anhydrous acetonitrile (Bünzli and Mabillard 1986),^[34] and methanol containing water (Legendziewicz *et al.* 1986).^[35] The FT-IR spectra of lanthanide perchlorate recorded by Bünzli *et al.* 1982,^[22] 1991,^[36] display absorption for monodentate and bidentate perchlorates in the first coordination sphere.

The triflate ion, CF_3SO_3^- , was also believed to be non-coordinating but in 1987 Pilloud and Bünzli^[37] have shown that lanthanide triflate solutions in propylene carbonate form 2:1 electrolytes, pointing to inner-sphere complexation. In 1987 Bünzli *et al.*^[38] conclude that in methanol the affinity of triflate is similar to that of the perchlorate ion. Di Bernardo *et al.* in 1993,^[39] in anhydrous acetonitrile, by FT-IR technique proved the complexing ability of triflate to lanthanide ions.

I.4 GENERAL ASPECTS OF SOLVENT EXCHANGE

The determination of solvation properties of metal cations constitutes an important step for cation complexation studies, when first coordination shell solvent molecules are generally replaced by donor atoms of the ligand upon complexation.^[40] It is therefore crucial to determine the structure and dynamics of uncomplexed cations in solution.

Solvent exchange reactions in aqueous or non-aqueous solutions are the simplest chemical reactions on metal cations: a solvent molecule situated in the first coordination shell of the ion is replaced by another one, generally entering from the second shell or the bulk, Eq. I-1. In solvent exchange reactions due to the fact that reagents and products are identical, there is no Gibbs free energy change (ΔG° of the reaction is zero).



The solvent exchange rate, k_{ex} , is the inverse of τ_m , which represents the mean residence time of a particular solvent molecule in the first coordination shell of the metal ion before it is replaced by another one from the bulk.^[19] The most studied solvent exchange reaction over the years was the water exchange. Figure I-3 shows that the water exchange rate constant on metal ions, k_{H_2O} , covers nearly 20 orders of magnitude.

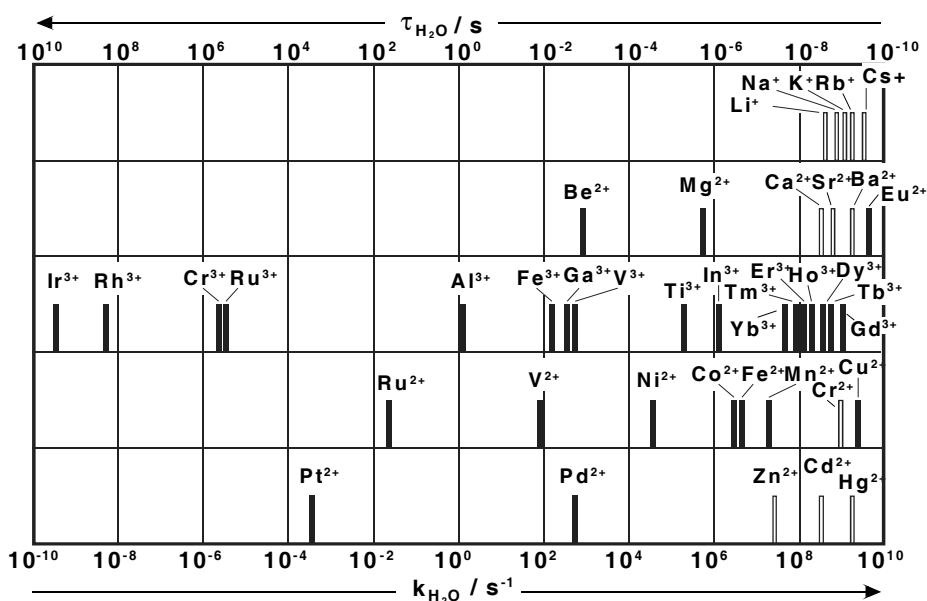


Figure I-3. Mean residence lifetimes, τ_{H_2O} , of a particular water molecule in the 1st coordination shell of a given metal ion and the corresponding water exchange rates at 298 K. The filled bars indicate directly determined values by NMR, and the empty bars indicate values deduced from ligand substitution studies.^[21]

As it can be seen the measured water exchange rates vary considerably with the nature of the cation. The slowest water exchange measured was for the Ir³⁺ ion ($k_{ex} [Ir(H_2O)_6]^{3+} = 1.1 \times 10^{-10}$ s⁻¹ at 298 K)^[41] on which, a water molecule spends ~ 300 years ($\tau_m = 9 \times 10^9$ s at 298 K) in the first coordination shell before it is replaced by another one from the bulk. In opposite to the Ir³⁺ ion, Eu²⁺ shows the fastest directly measured water exchange rate ($k_{ex} [Eu(H_2O)_7]^{2+} = 4.4 \times 10^9$ s⁻¹ at 298 K)^[42] where, the water molecule in the first coordination shell spends only about 200 ps ($\tau_m = 2 \times 10^{-10}$ s at 298 K).

The metal ions can be classified into three groups. The first group is represented by the main group metal ions. The exchange rate constants for these ions vary because these ions differ mainly in ionic radius and electric charges, which implies a coordination number range from 4 to 10.^[43] The second group is formed by the d-transition metal ions, which are in general hexa-coordinated, with the exception of Pt^{2+} and Pd^{2+} (which are four-coordinated, square planar), and Sc^{3+} (which might be hepta-coordinated).^[44] The solvent exchange rate constants for these ions are strongly dependent by the occupancy of the d-orbitals. The third group involves the lanthanide and actinide ions, which can be from six coordinated (for bulky non-aqueous solvents) to eight or nine coordinated (for water molecules). The solvent exchange rate constants are mainly influenced by the decrease of the ionic radius along the series and by the subsequent change in the coordination number.

Solvent exchange reactions on metal ions have been reviewed by Lincoln,^[19] Dunand^[45] and Helm.^[21, 46] They concluded that the rates of solvent exchange vary in a smaller extent with nature of the solvent (mostly due to his size) than with the nature of the cation (due to the ionic configuration, charge and ionic radii).

I.4.1 Classification of the Exchange Mechanisms

The mechanistic classification generally accepted for ligand substitution reactions proposed by Langford and Gray in 1965^[47] is also accepted for the solvent exchange reactions. In their classification Langford and Gray divided ligand substitution reactions in three categories of stoichiometric mechanisms: *associative* (**A**) where an intermediate of increased coordination number is formed, *dissociative* (**D**) where an intermediate of reduced coordination number is formed, and *interchange* (**I**) where there is no kinetically detectable intermediate. In Equation I-4, $\text{MX}_n \dots \text{Y}$ represents an outer-sphere complex.





Furthermore, they distinguished two categories of *intimate mechanisms*: those with an associative activation mode (**a**), where the reaction rate is sensitive to the nature of the entering group, and those with a dissociative mode (**d**), where the reaction rate is not sensitive to the variation of the entering group, but to the variation of the leaving group. All **A** mechanisms must be associatively and all **D** mechanisms must be dissociatively activated. The interchange mechanisms (**I**) include a continuous spectrum of transition states where the degree of bond-making between the entering ligand and the complex is very substantial for **I_a** mechanism and negligible for **I_d** mechanism and inversely for bond-breaking.^[48, 49] For a solvent exchange reaction, the forward and backward reaction coordinates must be symmetrical. Thus, for an **I_a** mechanism both the entering and the leaving solvent molecule must have considerable bonding to the metal ion at the transition state. Inversely, for an **I_d** mechanism with negligible bond-making for the entering solvent molecule, the leaving one is also necessarily weakly bound.

I.4.2 Determination of the Solvent Exchange Rate and Mechanism

Only a few experimental techniques are available to directly measure the exchange rates.^[45, 50] The measurement of solvent exchange rates in solution is today widely performed by Nuclear Magnetic Resonance spectroscopy (NMR). A common method is the observation of the NMR lineshape.^[51] If the exchange rate constant is in the range defined by the natural linewidth of the NMR resonance and there is a chemical shift difference between the resonance signals of bulk solvent and solvent molecules in the 1st coordination shell (both in rad s⁻¹), the solvent exchange rate constant can be directly determined from the NMR spectrum. This means that rates in the order of several hundreds s⁻¹ can be measured by ¹H or ¹³C as well as rates of order of 10⁶ s⁻¹ if chemical shift differences are large due to paramagnetic effects. Even faster exchange rates can be determined using methods based on relaxation rate measurements.^[52, 53] Using these methods, the fastest rate measured by NMR up to now is 4.4 × 10⁹ s⁻¹ for the water exchange rate on Eu²⁺ aqua ion.^[42] Relatively slow exchange reactions from 0.1 to 10 s⁻¹ can be followed using magnetization transfer technique. By exciting spins on a chemical site, well defined by its NMR signal, and observing how this excitation is transferred by the

chemical reaction to another site, reaction rates can be obtained if the reaction proceeds faster than nuclear spin relaxation.^[54, 55] Very slow reactions can be followed by isotopic labeling techniques. The solvent molecules in the 1st coordination sphere of the metal ion or the bulk solvent can be labeled either using stable isotopes as for example ²H, ¹³C, ¹⁵N or ¹⁷O or either radioactive isotopes as ¹⁴C or ³H. The exchange of the labeled molecules can be followed with different techniques like NMR or mass spectroscopy. To accelerate reactions, measurements can be performed at high temperatures like it has been done on the [Ir(H₂O)₆]³⁺ complex.^[41]

The microscopic nature of the mechanism of the exchange reaction is not directly accessible by experimental methods. In general, reaction mechanisms can be deduced by experimentally testing the sensitivity of the reaction rate to a variety of chemical and physical parameters such as temperature, pressure or concentration.

The solvent exchange rate, k_{ex} , can be determined from the variable temperature NMR measurements as well as the entropy, ΔS^\ddagger , and the enthalpy, ΔH^\ddagger , of activation, Eq. I-5:

$$\frac{1}{\tau_m} = k_{ex} = \frac{k_B T}{h} \exp \left\{ \frac{\Delta S^\ddagger}{R} - \frac{\Delta H^\ddagger}{RT} \right\} = \frac{k_{ex}^{298} T}{298.15} \exp \left\{ \frac{\Delta H^\ddagger}{R} \left(\frac{1}{298.15} - \frac{1}{T} \right) \right\} \quad \text{Eq. I-5}$$

The variation of the enthalpy, ΔH^\ddagger , and entropy, ΔS^\ddagger , of activation obtained from variable temperature NMR experiments can be a guide to a mechanistic change. Thus **d**-activated reactions tend to have greater ΔH^\ddagger values than do **a**-activated reactions, and ΔS^\ddagger tends to be positive for **d**- and negative for **a**-activated reactions. However, the magnitudes of the contributions to these two parameters arising from interactions that occur beyond the 1st coordination shell can be uncertain; hence the determination of ΔS^\ddagger is often prone to systematic errors, especially if the temperature range for experimental determination of the exchange rate constant is small. An adequate choice for the determination of solvent exchange mechanism is the measurement of the volume of activation, ΔV^\ddagger , for which, the precision of measurement is high and there is a direct relationship between its sign and the increase or decrease of the rate constant with pressure. Therefore, the dependency of the solvent exchange rate constant with pressure leads to the determination of the volume of activation, ΔV^\ddagger , Equation I-6, ^[56] which is strongly interconnected with the reaction mechanism. The volume of activation is defined as the difference between the partial molar volumes of the

transition state and the reactants. It is related to the pressure variation of the rate constant at a constant temperature T by the following equation:^[57]

$$\left(\frac{\partial \ln(k)}{\partial P}\right)_T = -\frac{\Delta V^\ddagger}{RT} \quad \text{Eq. I-6}$$

Assuming that ΔV^\ddagger is slightly pressure dependent Eq. I-6 leads to the approximate Eq. I-7:

$$\ln\left(\frac{k_P}{k_0}\right) = -\frac{\Delta V_0^\ddagger P}{RT} + \frac{\Delta\beta^\ddagger P^2}{2RT} \quad \text{Eq. I-7}$$

where k_P and k_0 are the rate constants at pressures P and 0, respectively, ΔV_0^\ddagger is the activation volume at $P = 0$ and $\Delta\beta^\ddagger$ is the compressibility coefficient of activation.^[57] For exchange reactions with water, a highly electrostricted solvent, the quadratic term in Eq. I-7 is small compared to the linear one, for pressures generally applied in kinetic studies (typically 0 – 200 MPa). Therefore in aqueous solution $\Delta V^\ddagger \cong \Delta V_0^\ddagger$.^[58] In non-aqueous solvents, however the pressure variation of $\ln(k)$ is often non-linear and therefore the compressibility coefficient of activation can not be neglected.^[59]

The interpretation of the activation volume for solvent exchange reactions on metal ions is based on the transition state theory,^[60] where no differences due to pressure variation in solvent interactions beyond the first coordination shell are taken into account. The measured ΔV^\ddagger is usually considered to be the combination of an intrinsic and an electrostriction contribution. The intrinsic contribution, ΔV_{int}^\ddagger , results from a change in internuclear distances and angles within the reactants during the formation of the transition state, whereas the electrostriction contribution, ΔV_{elec}^\ddagger , arises from changes in the electrostriction between the transition state and the reactant. For solvent exchange processes, where the charge of the complex remains unchanged, $\Delta V_{elec}^\ddagger \approx 0$ and therefore $\Delta V^\ddagger \cong \Delta V_{int}^\ddagger$. Consequently, the observed activation volume is a direct measure of the degree of bond-formation and bond-breaking on going to the transition state, assuming no changes in bond length of the non-exchanging solvent molecules.

Figure I-4 visualizes the pressure induced changes of the measured exchange rate constants and the underlying solvent exchange reaction mechanism. In a **d**-activated exchange process,

the approach to the transition state is characterized mainly by *bond-breaking* and results in an increase in volume, which means a decrease in the observed reaction rate constant, k_p [Eq. I-7]. In an **a**-activated exchange process, the approach to the transition state is characterized mainly by *bond-formation* and results in a decrease in volume which means an increase in k_p . Briefly, $\Delta V^\ddagger > 0$ is indicative of dissociatively activated processes and $\Delta V^\ddagger < 0$ is indicative of associatively activated processes. However, it is less easy to decide on the basis of activation volumes if the mechanism is a limiting associative **A**, or dissociative **D**, or an interchange **I** with a relatively strong contribution of the entering solvent molecule **I_a**, or with a negligible contribution of the entering solvent molecule **I_d**. The absolute value of the activation volume, $|\Delta V^\ddagger|$, can serve as guideline: the larger $|\Delta V^\ddagger|$, the closer the mechanism is to a limiting **A** or **D**.

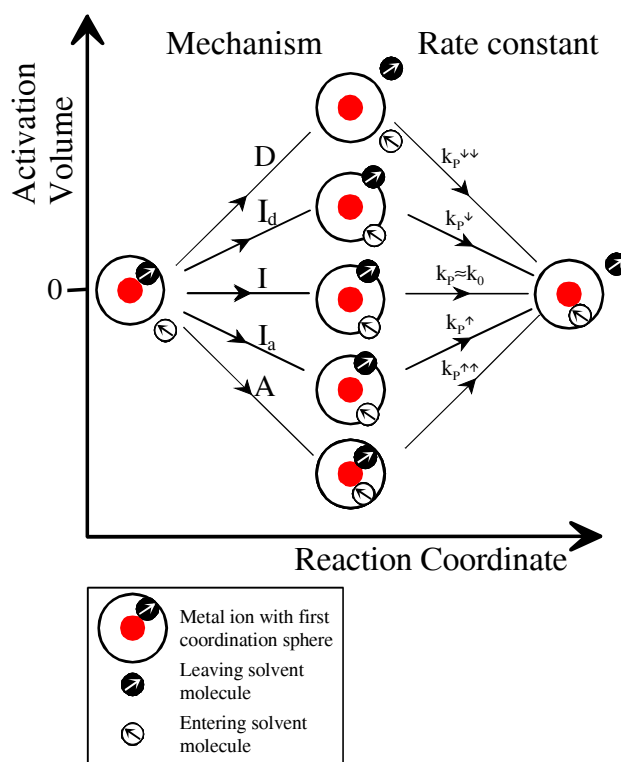


Figure I-4. Volume profiles, connected to the transition states, for the spectrum of solvent exchange processes.^[46]

I.5 SOLVENT EXCHANGE ON LANTHANIDE COMPLEXES

I.5.1 Water Exchange

The most studied solvent exchange reaction on lanthanide complexes is the water exchange. For lanthanide complexes the lifetime, τ_m , of a water molecule in the first coordination sphere is in the order of 10^{-8} s, which means that the rate of exchange of a water molecule approaches the rate of diffusion of the molecules between the inner- and outer-coordination sphere. According to the fast exchange rates observed one can conclude that monodentate ligands are very labile on lanthanide complexes which make the study of substitution reaction mechanisms difficult.

As it was mentioned above, there are a few articles which deal with the number of water molecules in the first coordination sphere of lanthanides.^[61-64] Therefore, it has been proved that the early lanthanides (La^{3+} to Nd^{3+}) are nine coordinated, the late lanthanides (Gd^{3+} to Lu^{3+}) are eight coordinated and Pm^{3+} , Sm^{3+} and Eu^{3+} ions exist in an equilibrium between nine- and eight-coordinate species. Table I-3 shows that k_{ex} decreases from Gd^{3+} to Yb^{3+} for the eight coordinated aqua ions along the lanthanide series, with the systematic decrease of the ionic radius. Both ΔS^\ddagger and ΔV^\ddagger are negative, but the activation volume is far from the value of $-12.9 \text{ cm}^3 \text{ mol}^{-1}$ calculated with Swaddle's semi-empirical model for the reaction volume for $\text{CN} = 8 \rightarrow \text{CN} = 9$ on lanthanides^[65] and from the value of $-11 \text{ cm}^3 \text{ mol}^{-1}$ measured by variable pressure UV-Vis experiments on the equilibrium $[\text{Ce}(\text{H}_2\text{O})_8]^{3+} + \text{H}_2\text{O} \rightleftharpoons [\text{Ce}(\text{H}_2\text{O})_9]^{3+}$.^[66] Therefore, an I_a mechanism has been attributed for water exchange on $[\text{Ln}(\text{H}_2\text{O})_8]^{3+}$. The decrease of the exchange rate constants from Gd^{3+} to Yb^{3+} is understandable: according to an I_a mechanism, the transition state for the water exchange is close to an ennea-coordinate Ln^{3+} , which is more and more less favoured for the smaller ions (Table I-3).^[21] The same decrease is observed for the interchange rate constants, k_i , between an inner sphere water molecule and a SO_4^{2-} ion from the outer sphere Gd^{3+} to Lu^{3+} , Figure I-2.^[67]

For the light lanthanides the kinetic effect is not sufficient to enable the determination of k_{ex} by ^{17}O transverse NMR relaxation rate measurements at 9.4 T. For $[\text{Pr}(\text{H}_2\text{O})_9]^{3+}$ and $[\text{Nd}(\text{H}_2\text{O})_9]^{3+}$, which have the most favourable chemical shifts at the beginning of the lanthanide series, measurements at 14.1 T allowed the determination of only a lower limits of

k_{ex} . For the three other lighter paramagnetic lanthanides ions, Ce^{3+} , Pm^{3+} and Sm^{3+} , the kinetic effect and the chemical shifts are too small to enable the determination of the water exchange rate by ^{17}O NMR relaxation rate measurements.

Table I-3. Rate constants and activation parameters for water exchange on lanthanide aqua ions.^[21]

Complex	$k_{ex}^{298\text{ a)}}$ / 10^7 s^{-1}	ΔH^\ddagger / kJ mol^{-1}	ΔS^\ddagger / $\text{J K}^{-1}\text{ mol}^{-1}$	ΔV^\ddagger / $\text{cm}^3\text{ mol}^{-1}$	Mech.	Ref.
Eu²⁺						
$[\text{Eu}(\text{H}_2\text{O})_7]^{2+}$	500 ^{b)}	15.7	-7.0	-11.3	I_a, A	[42, 68, 69]
Ln³⁺						
$[\text{Nd}(\text{H}_2\text{O})_9]^{3+}$	≥ 50					[61]
$[\text{Pr}(\text{H}_2\text{O})_9]^{3+}$	≥ 40					[61]
$[\text{Gd}(\text{H}_2\text{O})_8]^{3+}$	83.0	14.9	-24.1	-3.3	I_a	[62]
$[\text{Tb}(\text{H}_2\text{O})_8]^{3+}$	55.8	12.1	-36.9	-5.7	I_a	[63, 64]
$[\text{Dy}(\text{H}_2\text{O})_8]^{3+}$	43.4	16.6	-24.0	-6.0	I_a	[63, 64]
$[\text{Ho}(\text{H}_2\text{O})_8]^{3+}$	21.4	16.4	-30.5	-6.6	I_a	[63, 64]
$[\text{Er}(\text{H}_2\text{O})_8]^{3+}$	13.3	18.4	-27.8	-6.9	I_a	[63, 64]
$[\text{Tm}(\text{H}_2\text{O})_8]^{3+}$	9.1	22.7	-16.4	-6.0	I_a	[63, 64]
$[\text{Yb}(\text{H}_2\text{O})_8]^{3+}$	4.7	23.3	-21.0			[63, 64]

a) First order rate constant for the exchange of a particular coordinated water molecule.^[19]

b) The value originally published for a CN = 8 in ref.^[69] was corrected for CN = 7 in ref.^[68]

The eight- and nine-coordinate Ln^{3+} -aqua ions adopt in aqueous solution a square antiprism geometry (SAP) and a tricapped trigonal prism geometry (TTP), respectively. Consequently, the transition state, $[\text{Ln}(\text{H}_2\text{O})_9]^{3+}$, in an **I_a** water exchange mechanism on $[\text{Ln}(\text{H}_2\text{O})_8]^{3+}$ is proposed to have a TTP geometry, similar to the one observed in the solid state for the whole series. This leads to the possible mechanistic path for water exchange on $[\text{Ln}(\text{H}_2\text{O})_8]^{3+}$ illustrated in Figure I-5.

It can be well understood by taking the reverse case of an exchange on $[\text{Ln}(\text{H}_2\text{O})_9]^{3+}$ (case of the early lanthanides) that the transition state should have a metal centre with lower CN, like $[\text{Ln}(\text{H}_2\text{O})_8]^{3+}$. In this latter case the water exchange should proceed through an **I_d** mechanism

with a transition state that adopts SAP geometry. This change in mechanism has been supported by a computational study using classical molecular dynamics simulation.^[21]

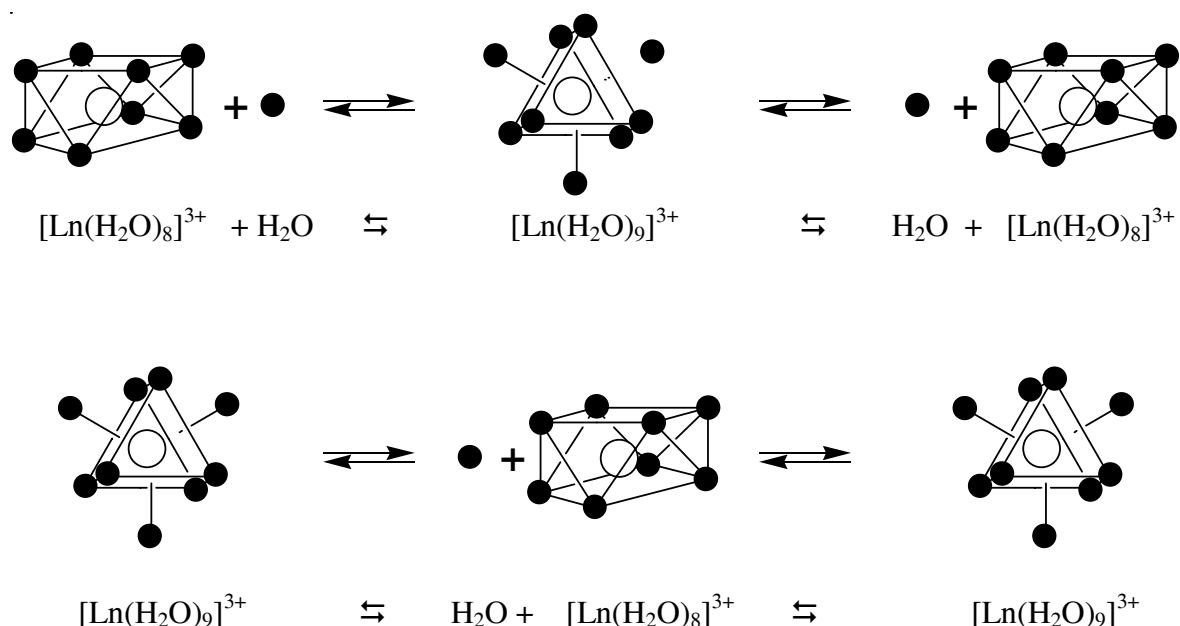
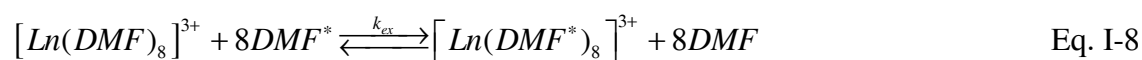


Figure I-5. Possible mechanistic paths for water exchange on eight- and nine-coordinate lanthanides.^[45]

I.5.2 Non-aqueous Solvent Exchange

The only non-aqueous solvent exchange studied over the lanthanide series are the DMF and TMU, whereas DMSO exchange reaction was studied only on the $[\text{Gd}(\text{DMSO})_8](\text{CF}_3\text{SO}_3)_3$ complex (Table I-4).

The exchange of DMF on lanthanides, Equation I-8, has been studied by using solutions of lanthanide perchlorate complexes in neat solvent and in CD_3NO_2 diluent.^[31]



Pisaniello *et al.*^[31] proved by conductivity and ^{35}Cl NMR studies that there is no complexation by ClO_4^- in the inner coordination sphere of the lanthanides in DMF solution. They also demonstrated the presence of an equilibrium between eight- and nine-coordinated species for the light lanthanides like Ce^{3+} , Pr^{3+} , and Nd^{3+} . For the heavier lanthanides the presence of eight DMF molecules in the first coordination sphere is characteristic. Due to this

equilibrium it was impossible to determine the kinetic parameters as well as the reaction mechanism for the light lanthanide complexes, while for the heavier one from Tb³⁺ to Yb³⁺ the kinetic parameters and the reaction mechanism for the DMF exchange was determined by ¹H NMR measurements (Table I-4).

Table I-4. Rate constants and activation parameters for non-aqueous solvent exchange on trivalent lanthanides.^[21]

Ln³⁺	<i>r</i>_{Ln}^{a)} / pm	<i>k</i>_{ex}^{298 b)} / s⁻¹	ΔH^\ddagger / kJ mol⁻¹	ΔS^\ddagger / J K⁻¹ mol⁻¹	ΔV^\ddagger / cm³ mol⁻¹	Mech.	Ref.
[Ln(DMF)₈]³⁺							
Tb ³⁺	104.0	19 × 10 ⁶	14.1	-58	+5.2	I_d	[31]
Dy ³⁺	102.7	6.3 × 10 ⁶	13.8	-69	+6.1	I_d	[31]
Ho ³⁺	101.5	3.6 × 10 ⁶	15.3	-68	+5.2	I_d	[31]
Er ³⁺	100.4	13 × 10 ⁶	23.6	-30	+5.4	D and I_d	[31]
Tm ³⁺	99.4	31 × 10 ⁶	33.2	+10	+7.4	D	[31]
Yb ³⁺	98.5	99 × 10 ⁶	39.3	+40	+11.8	D	[31]
[Ln(DMSO)₈]³⁺							
Gd ³⁺	105.3	6.2 × 10 ⁶	32.8	-4.7	+8.2	I_d	[70]
[Ln(TMU)₆]^{3+ c)}							
Tb ³⁺	92.3	1380	38.2	-56.7		-	[71]
Dy ³⁺	91.2	1290	38.6	-56.0		-	[71]
Ho ³⁺	90.1	510	40.9	-55.9		-	[71]
Y ³⁺	90.0	253	27.1	-108		D	[72]
Er ³⁺	89.0	214	35.5	-81.3		D	[71]
Tm ³⁺	88.0	145	29.3	-105		D	[73]
Yb ³⁺	86.8	65.5	38.3	-81.8		D	[71]
Lu ³⁺	86.1	41.9	41.7	-74		D	[74]
Sc ³⁺	74.5	0.90	68.6	-15.7		D	[75]

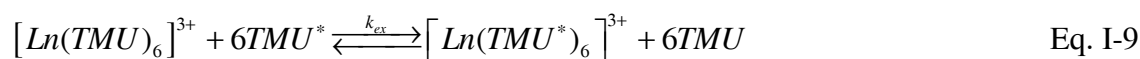
^{a)} Eight- and six- coordinate ionic radii from ref.^[76]

^{b)} First order rate constant for the exchange of a particular coordinated solvent molecule.^[19]

^{c)} In CD₃CN diluent.

The exchange process of DMF is characterized by a systematic increase of ΔH^\ddagger , by a change from negative to positive ΔS^\ddagger , and by a positive ΔV^\ddagger as the ionic radius decreases. The apparent conflict in ΔS^\ddagger and ΔV^\ddagger for Tb^{3+} , Dy^{3+} and Ho^{3+} in DMF solution can be attributed to a decrease in degree of freedom accompanying the formation of a nine coordinate transition state which forms in an interchange mechanism. In this way for the DMF exchange process a **d**-activation mode was assigned, with a mechanistic crossover from **I_d** to limiting **D** at Er^{3+} .^[77]

As the size of monodentate ligands bound to Ln^{3+} increases, so the coordination number decrease. Thus, in tetrametyurea (TMU) $[\text{Ln}(\text{TMU})_6]^{3+}$ is the dominant species. The exchange of TMU on $[\text{Ln}(\text{TMU})_6]^{3+}$, Equation I-9, has been studied in CD_3CN diluent.



The data presented in Table I-4 clearly shows that a decrease in coordination number results in a drastic decrease in lability. k_{ex} was found to be independent on TMU concentration, consistent with the operation of a **D** mechanism. The decrease in k_{ex} and increase in ΔH^\ddagger from Er^{3+} to Lu^{3+} with decrease in ionic radii is consistent with the increasing strength of Ln^{3+} -TMU bonding being a dominant factor in a **d**-activated exchange mechanism.

Exchange of DMSO on lanthanides has only be studied on $[\text{Gd}(\text{DMSO})_8]^{3+}$ so far.^[70] The rate constant measured is more than 2 orders of magnitude slower than that for the water exchange. While comparing the positive ΔV^\ddagger measured on $[\text{Gd}(\text{DMSO})_8]^{3+}$ with the negative one found for $[\text{Gd}(\text{H}_2\text{O})_8]^{3+}$ one can conclude that the activation mode for the two solvents are different. DMSO exchange follows a **d**-activation mode like that for DMF, while H_2O exchange follows an **a**-activation mode.

I.6 Objectives of the thesis

As metal ions in solution always react in solvated form, the investigation of the solvation processes is of particular importance for understanding the reactivity of metal ions in solutions. The simplest metal ion solvation process is the solvent exchange reaction. Aqueous and non-aqueous solvent exchange reactions on metal ions have already been extensively

studied during the years, but data about non-aqueous solvent exchange reaction on the lanthanides series are quite scarce (see subsection I.5). Due to the difficulty of working under anhydrous conditions with the “water hungry” lanthanide ions and due to the poor coordinating ability of the uncharged acetonitrile ligand, acetonitrile exchange reactions on the lanthanide series have never been studied before.

Therefore, the major goal of this work was to understand the solution dynamics of acetonitrile lanthanide salts in acetonitrile solution. This was achieved by variable temperature and multiple field ^{14}N and ^1H NMR or EPR measurements (Chapter III and IV). An understanding of the properties of solutions of the metal salts requires the knowledge of the composition and structure of the first coordination sphere of the metal ion. Acetonitrile lanthanide salts without any anion in the first coordination sphere of the metal are difficult to synthesize due to the poor coordinating ability of the acetonitrile. Therefore most of the generally known “non-coordinating” anions in acetonitrile coordinate to lanthanides. Since the solvent exchange reaction can be considerably influenced by the presence of a coordinating anion, the first objective of this work was the synthesis of homoleptic acetonitrile lanthanide complexes (Chapter II). To further analyze the solution dynamics of these homoleptic acetonitrile lanthanide salts in acetonitrile it was imperative to characterize the synthesized complexes, in both solid state and in solution (Chapter II and VI).

I.7 REFERENCES

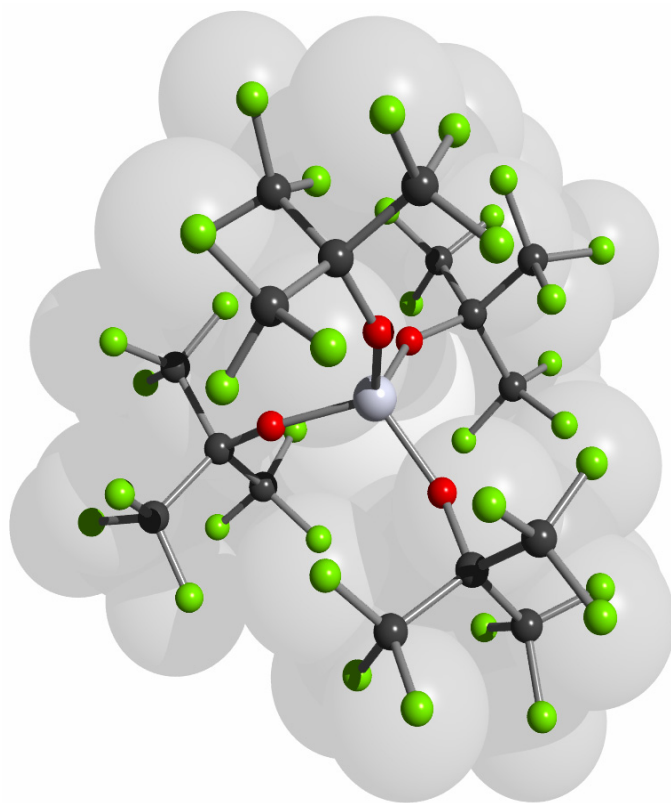
- [1] R. D. Shannon, *Acta Cryst., Sect. A* **1976**, A32, 751.
- [2] P. Maestro, *J. Less Com. Met.* **1985**, 111, 43.
- [3] R. V. Horrigan, **1981**, 164, 101.
- [4] R. Perrin, E. Wimmer, *Phys. Rev. B* **1996**, 55, 2428.
- [5] T. Seyama, *Properties and applications of perovskite type oxides*, Dekker, M., **1993**.
- [6] T. Ishihara, H. Matsuda, Y. Takita, *Sol. St. Ionics* **1995**, 79, 147.
- [7] D. S. Hewack, *Elec. Lett.* **1994**, 30, 968.
- [8] A. E. Merbach, E. Toth, *The Chemistry of Contrast Agents in Medical Magnetic Resonance Imaging*, Wiley: Chichester ed., **2001**.
- [9] J. E. Enderby, G. W. Neilson, *Rep. Prog. Phys.* **1981**, 44, 593.
- [10] J.-C. G. Bünzli, A. Milicic-Tang, in *Handbook on the Physics and Chemistry of Rare Earth* (Eds.: K. A. Gschneidner, L. a. J. Eyring), Elsevier Science B. V., **1995**, pp. 305.
- [11] C. Cossy, A. C. Barnes, J. E. Enderby, A. E. Merbach, *J. Chem. Phys.* **1989**, 90, 3254.
- [12] L. Helm, A. E. Merbach, *Eur. J. Solid State Inorg. Chem.* **1991**, 28, 245.
- [13] A. Habenschuss, F. H. Spedding, *J. Chem. Phys.* **1980**, 73, 442.
- [14] A. Habenschuss, F. H. Spedding, *J. Chem. Phys.* **1979**, 70, 3758.
- [15] T. Yamaguchi, M. Nomura, H. Wakita, H. Ohtaki, *J. Chem. Phys.* **1988**, 89, 5153.
- [16] F. H. Spedding, P. F. Cullen, A. Habenschuss, *J. Phys. Chem.* **1974**, 78, 1106.
- [17] F. H. Spedding, L. E. Shiers, M. A. Brown, J. L. Derer, D. L. Swanson, A. Habenschuss, *J. Chem. Eng. Data* **1975**, 20, 81.
- [18] K. Miyakawa, Y. Kaizu, H. Kobayashi, *J. Chem. Soc., Faraday Trans.* **1988**, 84, 1517.
- [19] S. F. Lincoln, A. E. Merbach, *Adv. Inorg. Chem.* **1995**, 42, 1.
- [20] K. Djanashvili, C. Platas-Iglesias, J. A. Peters, *Dalton Trans.* **2008**, 602.
- [21] L. Helm, A. E. Merbach, *Chem. Rev.* **2005**, 105, 1923.
- [22] J.-C. G. Bünzli, C. Mabillard, J.-R. Yersin, *Inorg. Chem.* **1982**, 21, 4214.
- [23] L. S. Smith Jr., D. C. McCain, D. L. Wertz, *J. Am. Chem. Soc.* **1976**, 98, 5125.
- [24] S. Ishiguro, R. Takahashi, *Inorg. Chem.* **1991**, 30, 1854.
- [25] L. Quill, P. W. Selwood, B. S. Hopkins, *J. Am. Chem. Soc.* **1928**, 50, 2929.
- [26] J.-C. G. Bünzli, J.-R. Yersin, *Inorg. Chem.* **1979**, 18, 605.
- [27] C. Mabillard, (Lausanne, Switzerland), **1983**.

-
- [28] G. Depaoli, P. Ganis, P. L. Zanonato, *Polyhedron* **1993**, *12*, 671.
- [29] R. Takahashi, S. Ishiguro, *J. Chem. Soc., Faraday Trans.* **1992**, *88*, 3165.
- [30] L. N. Lugina, N. K. Davidenko, K. B. Yatsimirskii, *Russ. J. Inorg. Chem. (Engl. Transl.)* **1973**, *18*, 1453.
- [31] D. L. Pisaniello, L. Helm, P. Meier, A. E. Merbach, *J. Am. Chem. Soc.* **1983**, *105*, 4528.
- [32] J.-C. G. Bünzli, J.-R. Yersin, *Helv. Chim. Acta* **1982**, *65*, 2498.
- [33] A. A. Zholdakov, L. N. Lugina, N. K. Davidenko, *Russ. J. Inorg. Chem. (Engl. Transl.)* **1971**, *16*, 265.
- [34] J.-C. G. Bünzli, C. Mabillard, *Inorg. Chem.* **1986**, *25*, 2750.
- [35] J. Legendziewicz, G. Oczko, B. Keller, *Bull. Pol. Acad. Sci. Ser. Chem.* **1986**, *34*, 257.
- [36] J.-C. G. Bünzli, V. Kasperek, *Inorg. Chim. Acta* **1991**, *182*, 101.
- [37] F. Pilloud, B. J.-C. G, *Inorg. Chim. Acta* **1987**, *139*, 153.
- [38] J.-C. G. Bünzli, A. E. Merbach, R. M. Nielson, *Inorg. Chim. Acta* **1987**, *139*, 151.
- [39] P. Di Bernardo, G. R. Choppin, R. Portanova, P. L. Zanonato, *Inorg. Chim. Acta* **1993**, *207*, 85.
- [40] J. M. Lehn, *Struct. Bonding* **1973**, *161*, 1.
- [41] A. Cusanelli, U. Frey, D. T. Richens, A. E. Merbach, *J. Am. Chem. Soc.* **1996**, *118*, 5265.
- [42] P. Caravan, É. Tóth, A. Rockenbauer, A. E. Merbach, *J. Am. Chem. Soc.* **1999**, *121*, 10403.
- [43] H. Ohtaki, T. Radnai, *Chem. Rev.* **1993**, *93*, 1157.
- [44] P. Smirnov, H. Wakita, T. Yamaguchi, *J. Phys. Chem. B* **1998**, *102*, 4802.
- [45] F. A. Dunand, L. Helm, A. E. Merbach, *Adv. Inorg. Chem.* **2003**, *54*, 1.
- [46] L. Helm, A. E. Merbach, *Coord. Chem. Rev.* **1999**, *187*, 151.
- [47] C. H. Langford, H. B. Gray, *Ligand Substitution Processes*, Benjamin, W. A., New York, **1965**.
- [48] A. E. Merbach, *Pure Appl. Chem.* **1982**, *54*, 1479.
- [49] A. E. Merbach, *Pure Appl. Chem.* **1987**, *59*, 161.
- [50] L. Helm, G. M. Nicolle, A. E. Merbach, *Adv. in Inorg. Chem.* **2005**, *2005*, 327.
- [51] J. Sandström, *Dynamic NMR Spectroscopy*, Academic Press, London, **1982**.
- [52] T. J. Swift, R. E. Connick, *J. Chem. Phys.* **1962**, *37*, 307.
- [53] J. R. Zimmerman, W. E. Brittin, *J. Phys. Chem.* **1957**, *61*, 1328.
- [54] S. Forsén, R. A. Hoffman, *J. Chem. Phys.* **1963**, *39*, 2892.
-

- [55] J. J. Led, H. Gesmar, *J. Magn. Reson.* **1982**, *49*, 444.
- [56] R. van Eldik, *Inorganic High Pressure Chemistry: Kinetics and Mechanisms*, Elsevier, Amsterdam, **1986**.
- [57] D. R. Stranks, *Pure Appl. Chem.* **1974**, *38*, 303.
- [58] R. van Eldik, *Inorganic High-Pressure Chemistry*, Elsevier, Amsterdam, **1986**.
- [59] K. E. Newman, F. K. Meyer, A. E. Merbach, *J. Am. Chem. Soc.* **1979**, *101*, 1470.
- [60] C. A. Eckert, *Ann. Rev. Phys. Chem.* **1972**, *23*, 239.
- [61] D. H. Powell, A. E. Merbach, *Magn. Reson. Chem.* **1994**, *32*, 739.
- [62] K. Micskei, D. H. Powell, L. Helm, E. Brücher, A. E. Merbach, *Magn. Reson. Chem.* **1993**, *31*, 1011.
- [63] C. Cossy, L. Helm, A. E. Merbach, *Inorg. Chem.* **1988**, *27*, 1973.
- [64] C. Cossy, L. Helm, A. E. Merbach, *Inorg. Chem.* **1989**, *28*, 2699.
- [65] T. W. Swaddle, *Can. J. Chem.* **1983**, *61*, 472.
- [66] G. Laurenczy, A. E. Merbach, *Helv. Chim. Acta* **1988**, *71*, 1971.
- [67] D. P. Fay, D. Litchinsky, N. J. Purdie, **1969**, *73*, 544.
- [68] G. Moreau, L. Helm, J. Purans, A. E. Merbach, *J. Phys. Chem. A* **2002**, *106*, 3034.
- [69] P. Caravan, A. E. Merbach, *Chem. Comm.* **1997**, 2147.
- [70] R. Dessapt, L. Helm, A. E. Merbach, *J. Phys. Condens. Matter* **2004**, *14*, S1027.
- [71] S. F. Lincoln, A. White, *Inorg. Chim. Acta* **1990**, *168*, 265.
- [72] D. L. Pisaniello, S. F. Lincoln, A. F. Williams, A. Jones, *Aust. J. Chem.* **1981**, *34*, 495.
- [73] S. F. Lincoln, A. White, *Polyhedron* **1986**, *5*, 1351.
- [74] S. F. Lincoln, A. M. Hounsflow, A. Jones, *Aust. J. Chem.* **1982**, *35*, 2393.
- [75] D. L. Pisaniello, S. F. Lincoln, *J. Chem. Soc., Dalton Trans.* **1980**, 699.
- [76] R. D. Shannon, *Acta Crystallogr., Sect. A* **1976**, *32*, 751.
- [77] D. L. Pisaniello, L. Helm, D. Zbinden, A. E. Merbach, *Helv. Chim. Acta* **1983**, *66*, 1872.

Chapter II

Synthesis and characterization of homoleptic $[\text{Ln}(\text{CH}_3\text{CN})_n][\text{Al}(\text{OC}(\text{CF}_3)_3)_4]_3$ complexes



II.1 INTRODUCTION

Since their discovery, lanthanides and their complexes received considerable attention of many researchers. Several lanthanide complexes are used in organic syntheses as highly efficient catalysts.^[1] For some of these catalysts, their efficiency is strengthened in aqueous solution, whereas for others, the use of non-aqueous medium is imperative. In the former case, $Ln(CF_3SO_3)_3$ complexes are used as Lewis acid catalysts to promote Friedel-Crafts acylation reactions;^[2, 3] whilst in the latter, the $[{Eu(CH_3CN)_3(BF_4)_3}]_n$ complex is successfully used to initiate polymerization reactions of olefins.^[4]

Since the discovery of the $[{Eu(CH_3CN)_3(BF_4)_3}]_n$ complex, many attempts have been made to synthesize homoleptic lanthanide complexes with the labile, uncharged ligand CH_3CN . Some synthesis have failed, as reported for $ErCl_3(H_2O)_2(CH_3CN)_2$,^[5] $[(DIME)Yb(CH_3CN)_5][B_{12}H_{12}]$, $[(DIME)_2Yb(CH_3CN)_2][Hg(Fe(CO)_4)_2]$ and $[(C_5H_5N)_5Yb(CH_3CN)_2][Hg(Fe(CO)_4)_2] \cdot 2C_5H_5N$ ^[6] or $(CH_3CN)_nLn[BH_4]_2$ ($Ln = Eu, n = 2$; $Ln = Yb, n = 4$);^[7] while other synthesis were successful, as reported for $[Ln(CH_3CN)_9][AlCl_4]_3 \cdot CH_3CN$ ($Ln = La, Pr, Nd, Sm, Eu, Gd, Tb, Ho$ and Yb),^[8] $[Ln(CH_3CN)_9][AsF_6]_3 \cdot nCH_3CN$ ($Ln = La, n = 1$; $Ln = Sm, n = 3$) or $[Pr(CH_3CN)_9][AlCl_4]_3 \cdot CH_3CN$ and $[Yb(CH_3CN)_8][AlCl_4]$,^[9] $[Pr(CH_3CN)_9][SnCl_5(CH_3CN)]_3$ $[Pr(CH_3CN)_9][SnCl_5(THF)]_{2.5}[SnCl_5(CH_3CN)]_{0.5}$ ^[10] or $[Yb(CH_3CN)_8][BPh_4]_2$.^[11]

In this study, in order to determine the acetonitrile exchange rate and mechanism on lanthanide ions, homoleptic acetonitrile lanthanide complexes were sought that do not have any coordinated counter ion in the first coordination sphere of the metal ion in solid state, neither in solution. None of the above mentioned complexes correspond to these requirements. In the compounds $[Pr(CH_3CN)_9][SnCl_5(THF)]_{2.5}[SnCl_5(CH_3CN)]_{0.5}$ and $[Pr(CH_3CN)_9][SnCl_5(CH_3CN)]_3$,^[10] there are two types of CH_3CN : some are coordinated to Pr and the others to Sn. Therefore, it would not be evident to which exchange the measured acetonitrile exchange rate can be attributed. Shen and his co-workers^[8] reported that in solution the conductivity value measured for the $[Sm(CH_3CN)_9][AlCl_4]_3 \cdot CH_3CN$ salt revealed a 2:1 electrolyte type. For the synthesis of $[Ln(CH_3CN)_9][AsF_6]_3 \cdot nCH_3CN$ ($Ln = La, n = 1$; $Ln = Sm, n = 3$) complexes, characterized by Deacon *et al.*,^[9] the starting materials used are highly unstable at room temperature and their preparation is extremely time consuming (3 weeks).

The main problem in synthesizing homoleptic acetonitrile lanthanide complexes is the coordination to the metal center of the counter ions. Consequently, the objective of the study presented in this chapter was the selection of a suitable counter ion, which may not compete with CH_3CN for coordination sites during the exchange reaction, and the elaboration of an easy synthetic way for the preparation of homoleptic lanthanide acetonitrile complexes.

Generally the term “non-coordinating” anion was used when a coordinating anion, such as a halide X^- , was replaced by a complex anion, such as $[\text{CF}_3\text{SO}_3]^-$, $[\text{ClO}_4]^-$, $[\text{BF}_4]^-$, $[\text{AlX}_4]^-$ or $[\text{MF}_6]^-$ ($\text{X} = \text{Cl-I}$; $\text{M} = \text{P, As, Sb, etc.}$). However, for lanthanide complexes, most of the above mentioned anions which are, at least in aqueous solution, known to be non-coordinating; in non-aqueous solvents often compete with organic ligands for coordinating to the metal center. This is true especially in the case of the weakly coordinating acetonitrile ligand as mentioned above and in Chapter I.

“Non-coordinating” or more correctly called “Weakly Coordinating Anions” (WCAs), which minimally interact with cations, have been widely studied in the past decade.^[12-14] Ideally, these anions should possess the following properties: i) no basic or nucleophilic sites, such as lone pairs, hydridic hydrogens and easily ionized single or multiple bonds; ii) resistance to oxidation and iii) the largest possible size to minimize electrostatic attraction. From the new generation of WCAs,^[13, 14] $[\text{B}(\text{C}_6\text{F}_5)_4]^-$,^[15] $[\text{CB}_{11}\text{H}_6\text{X}_6]^-$ ($\text{X} = \text{Cl, Br}$)^[16, 17] or $[\text{Al}(\text{OC}(\text{CF}_3)_3)_4]^-$ ^[18-20] (Figure II-1), the very stable and chemically robust $[\text{Al}(\text{OC}(\text{CF}_3)_3)_4]^-$ anion was chosen to the preparation of homoleptic acetonitrile lanthanide complexes, due to its cheap and easy preparation.

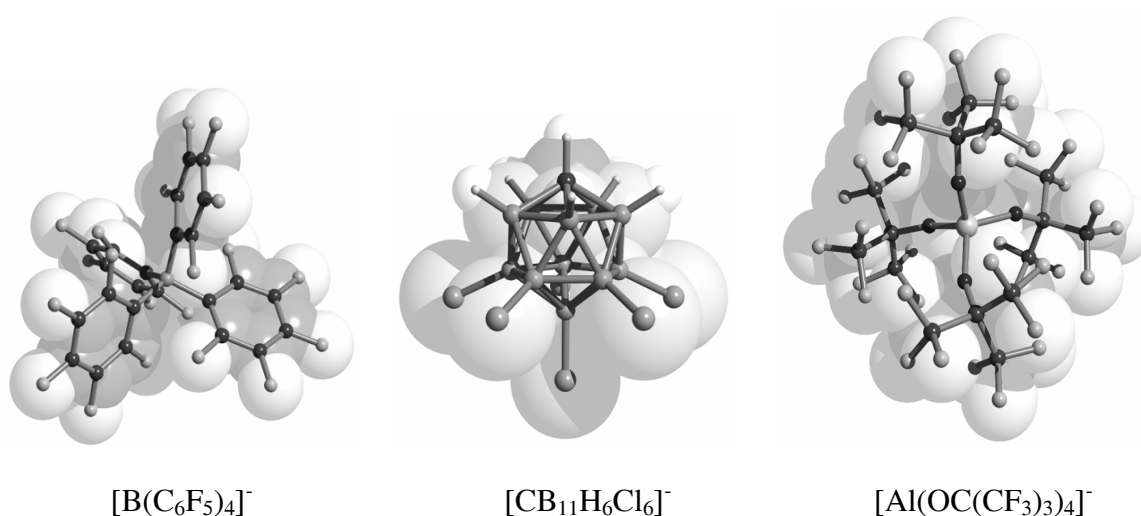
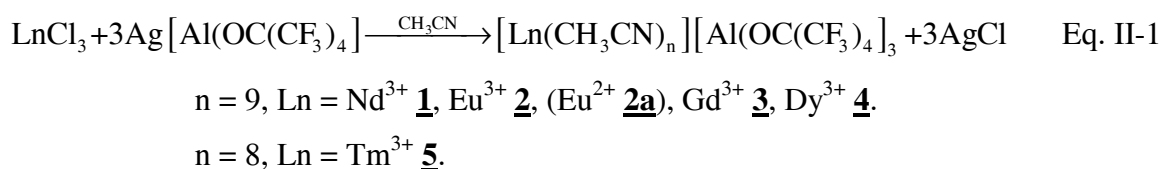


Figure II-1. Structures of selected weakly coordinating anions.^[14]

In this chapter the straightforward one step synthesis of stable, homoleptic complexes $[\text{Ln}(\text{CH}_3\text{CN})_n][\text{Al}(\text{OC}(\text{CF}_3)_3)_4]_3$ ($n = 9$, $\text{Ln}^{3+} = \text{Nd}, \text{Eu}, \text{Gd}, \text{Dy}$; $n = 8$, $\text{Ln}^{3+} = \text{Tm}$) is reported. Evidence that there is no direct metal–anion interaction in solid state and in acetonitrile solution of the complexes will be presented by elemental analysis, X-ray diffraction, conductivity and NMR techniques.

II.2 SYNTHESIS OF $[\text{Ln}(\text{CH}_3\text{CN})_n][\text{Al}(\text{OC}(\text{CF}_3)_3)_4]_3$ COMPLEXES

Reacting anhydrous lanthanide chlorides with $\text{Ag}[\text{Al}(\text{OC}(\text{CF}_3)_3)_4]$ in CH_3CN leads to the homoleptic $[\text{Ln}(\text{CH}_3\text{CN})_n][\text{Al}(\text{OC}(\text{CF}_3)_3)_4]_3$ complexes by the following metathesis reaction (Eq. II-1):



Using a slight excess of the $[\text{Al}(\text{OC}(\text{CF}_3)_3)_4]^-$ salt allowed the complete elimination of chlorines from lanthanides. The complexes **1** to **5** are soluble in polar solvents and insoluble in non-polar solvents like CH_2Cl_2 . Therefore, the excess of $\text{Ag}[\text{Al}(\text{OC}(\text{CF}_3)_3)_4]$ can be easily removed from **1** to **5** by several washings with CH_2Cl_2 , since $\text{Ag}[\text{Al}(\text{OC}(\text{CF}_3)_3)_4]$ is highly soluble in CH_2Cl_2 . After filtration, the pure compounds (elemental analysis, NMR spectroscopy) crystallize easily by slow diffusion of CH_2Cl_2 onto a concentrated acetonitrile solution of the lanthanide complexes at room temperature. Using a column of amalgamated zinc,^[21] the acetonitrile solution of the Eu^{3+} salt **2** can be reduced to the Eu^{2+} salt **2a** (**2a** has been obtained only in solution).^[22-24] Several attempts to get crystals of $[\text{Eu}(\text{CH}_3\text{CN})_9][\text{Al}(\text{OC}(\text{CF}_3)_3)_4]_2$ **2a** suitable for X-ray diffraction failed.

Complexes **1** to **5** are hygroscopic; therefore all manipulations have to be done in inert dry atmosphere, using Schlenk or glove box techniques. The $\text{Ag}[\text{Al}(\text{OC}(\text{CF}_3)_3)_4]$ salt was prepared as previously described by Krossing^[20] (see Chapter VI). The non-coordinating ability of $[\text{Al}(\text{OC}(\text{CF}_3)_3)_4]^-$ anion towards lanthanides in acetonitrile was proved by conductometric measurements and ^{19}F -NMR spectroscopy (see below Section II.4.3).

The above described method represents an easy, one-step reaction which allows the synthesis of low-cost, analytically pure, stable homoleptic acetonitrile lanthanide complexes.

II.3 CHARACTERIZATION OF $[\text{Ln}(\text{CH}_3\text{CN})_n][\text{Al}(\text{OC}(\text{CF}_3)_3)_4]_3$ COMPLEXES IN SOLID STATE

II.3.1 X-Ray Crystal Structures

For the homoleptic $[\text{Ln}(\text{CH}_3\text{CN})_n][\text{Al}(\text{OC}(\text{CF}_3)_3)_4]_3$ complexes (except **2**), colorless crystals suitable for X-ray diffraction could be obtained in a few days at room temperature by slow diffusion of CH_2Cl_2 onto a concentrated acetonitrile solution of the lanthanide complexes (details of the data collections for the X-ray structure determinations can be found in Table II-1 and in Chapter VI). However, a detailed discussion of their solid-state structures is not possible, as in these compounds, many crystallographic problems arise. The rather poor quality of the data is due to the fact that for these compounds their unit cell dimensions (in all compounds $V \sim 12 \text{ nm}^3$) as well as the content of the asymmetric unit are in the same order of magnitude like for small proteins. The compounds **1**, **3** and **4** crystallize in the highly symmetric space group $Pna2_1$, and therefore, not many reflections are observed because of systematic lattice extinctions. Another difficulty arises from the spherical (S_4 symmetric) $[\text{Al}(\text{OC}(\text{CF}_3)_3)_4]^-$ anions, which tend to disorder in the solid state, even at temperatures as low as 100 K, and to form twinned structures.^[25-31] Besides, embedded (disordered) solvent molecules raise additional problems. It is worth to be mentioned that the co-crystallization of solvent molecules into $[\text{Ln}(\text{CH}_3\text{CN})_n][\text{anion}]_3$ complexes is not unusual as revealed by Shen and co-workers^[8] for $[\text{Sm}(\text{CH}_3\text{CN})_9][\text{AlCl}_4]_3 \cdot \text{CH}_3\text{CN}$ or Deacon et al.^[9] for $[\text{Pr}(\text{CH}_3\text{CN})_9][\text{AlCl}_4]_3 \cdot \text{CH}_3\text{CN}$ and $[\text{Ln}(\text{CH}_3\text{CN})_9][\text{AsF}_6]_3 \cdot n\text{CH}_3\text{CN}$ ($\text{Ln} = \text{La}$, $n = 1$; $\text{Ln} = \text{Sm}$, $n = 3$). Therefore, for the compounds **1**, **3** and **4**, only the AlO_4 tetrahedra of the $[\text{Al}(\text{OC}(\text{CF}_3)_3)_4]^-$ anion have been used for the refinement cycles, while the electron density of the $\text{C}(\text{CF}_3)_3$ moieties has been treated with the SQUEEZE routine included with the program package PLATON.^[32] Compound **5** is the only one that crystallizes in a space group with lower symmetry $P2_1/n$ and could therefore be refined without using SQUEEZE.

Table II-1. Crystallographic details for $[Nd(CH_3CN)_9][Al(OC(CF_3)_3)_4]_3 \cdot 4CH_2Cl_2$ (**1**·4CH₂Cl₂), $[Gd(CH_3CN)_9][Al(OC(CF_3)_3)_4]_3 \cdot 3CH_2Cl_2$ (**3**·3CH₂Cl₂), $[Dy(CH_3CN)_9][Al(OC(CF_3)_3)_4]_3 \cdot 3CH_2Cl_2 \cdot CH_3CN$ (**4**·3CH₂Cl₂·CH₃CN) and $[Tm(CH_3CN)_8][Al(OC(CF_3)_3)_4]_3 \cdot 2CH_2Cl_2 \cdot 2CH_3CN$ (**5**·2CH₂Cl₂·2CH₃CN).

	1 ·4CH ₂ Cl ₂	3 ·3CH ₂ Cl ₂	4 ·3CH ₂ Cl ₂ ·CH ₃ CN	5 ·2CH ₃ CN·2CH ₂ Cl ₂
Empirical formula	C ₇₀ H ₃₅ Al ₃ Cl ₈ F ₁₀₈ N ₉ O ₁₂ Nd	C ₆₉ H ₃₃ Al ₃ Cl ₆ F ₁₀₈ N ₉ O ₁₂ Gd	C ₇₁ H ₃₆ Al ₃ Cl ₆ F ₁₀₈ N ₁₀ O ₁₂ Dy	C ₇₀ H ₃₄ Al ₃ Cl ₄ F ₁₀₈ N ₁₀ O ₁₂ Tm
Fw	3754.85	3682.81	3729.11	3650.74
Crystal size [mm ³]	0.98 x 0.32 x 0.14	0.49 x 0.23 x 0.21	0.61 x 0.26 x 0.23	0.33 x 0.26 x 0.14
Crystal system	orthorhombic	orthorhombic	orthorhombic	monoclinic
Space group	<i>Pna</i> 2 ₁	<i>Pna</i> 2 ₁	<i>Pna</i> 2 ₁	<i>P</i> 2 ₁ / <i>n</i>
<i>a</i> [pm]	28.308(10)	28.3168(18)	28.161(5)	14.2601(3)
<i>b</i> [pm]	29.321(9)	29.3210(16)	29.301(5)	32.5092(6)
<i>c</i> [pm]	15.203(3)	15.1241(10)	15.2811(16)	26.3378(5)
α [°]	90	90	90	90
β [°]	90	90	90	95.8031(18)
γ [°]	90	90	90	90
<i>V</i> [nm ³]	12.619(6)	12.557(2)	12.609(3)	12.147(2)
<i>Z</i>	4	4	4	4
ρ_{calc} [Mg m ⁻³]	1.976	1.006	1.908	1.996
μ [mm ⁻¹]	0.817	0.448	0.953	1.063
Absorption correction	none	none	none	multi-scan
F (000)	7284	3680	7012	7072
Index range	-29 ≤ <i>h</i> ≤ 29 -29 ≤ <i>k</i> ≤ 30 -15 ≤ <i>l</i> ≤ 15	-38 ≤ <i>h</i> ≤ 38 -39 ≤ <i>k</i> ≤ 39 -17 ≤ <i>l</i> ≤ 17	-32 ≤ <i>h</i> ≤ 32 -34 ≤ <i>k</i> ≤ 34 -17 ≤ <i>l</i> ≤ 17	-17 ≤ <i>h</i> ≤ 17 -40 ≤ <i>k</i> ≤ 40 -32 ≤ <i>l</i> ≤ 32
Max 2 θ	21.51	29.16	24.51	26.37
<i>T</i> [K]	100(2)	100(2)	100(2)	140(2)
Diffractometer type	Bruker APEX II	Bruker APEX II	Bruker APEX II	Kuma KM4 CCD
Unique reflns. [<i>I</i> > 2 σ (<i>I</i>)]	7603	7377	13586	18493
Data / restraints / parameters	7603 / 592 / 331	7737 / 454 / 193	13586 / 537 / 295	18493 / 1875 / 54
GOOF	1.274	0.770	1.527	1.052
Final R1 [<i>I</i> > 2 σ (<i>I</i>)]	0.1578	0.1106	0.1561	0.0813
Final wR2	0.3834	0.2683	0.4095	0.1894
Largest residual peak [e Å ⁻³]	2.168	1.574	2.315	1.773
Largest residual hole [e Å ⁻³]	-0.910	-1.558	-1.407	-1.744

From the synthesized **1** to **5** complexes, the structure of **2** presents the most important disorder. However, **2** crystallize in the monoclinic space group $P2_1/n$ as all nine-coordinated $[\text{Ln}(\text{CH}_3\text{CN})_9][\text{Al}(\text{OC}(\text{CF}_3)_3)_4]_3$ complexes shown in Table II-1. Therefore, one can conclude that in **2** Eu^{3+} is coordinated probably to nine acetonitrile molecules.

For compounds **1**, **3** and **4**, as it has already been mentioned above, no straightforward structure refinement was possible, consequently their crystal structures are not suitable for detailed information on bond lengths and angles (see the relatively high values of R1 being between 11.06 % and 15.78 %). However, they still can be used as structural proofs for the non-coordination of the $[\text{Al}(\text{OC}(\text{CF}_3)_3)_4]^-$ anion in the first coordination sphere of the Ln^{3+} cation, as well as to determine how many CH_3CN ligands are coordinated. Thus, in complexes **1**, **3** and **4** the homoleptic lanthanide cations are all nine-coordinated with the N donor atoms in a mono-capped square antiprismatic array. If one considers the mentioned uncertainties in the inter-atomic distances of compounds **1**, **3** and **4**, one can still state that the Ln-N bond lengths found in the $[\text{Al}(\text{OC}(\text{CF}_3)_3)_4]^-$ salts are reasonable if compared with those in other compounds cited in the literature (see Table II-2).

The generally observed trend for homoleptic lanthanide complexes shows a decreasing of the Ln-coordinating atom distance along the series as the molecular weight of Ln increase.^[9, 33, 34] Even with the mentioned uncertainties this trend can be also observed in complexes **1** – **5**.

From Table II-2 can be seen that a scarce number of publications related to the crystal structures of homoleptic acetonitrile lanthanide complexes containing several lanthanide ions can be found.^[8-11] Thus, in 1990 Shen and co-workers^[8] were the first dealing with homoleptic acetonitrile lanthanide complexes. They have synthesized a series of lanthanide complexes formulated as $[\text{Ln}(\text{CH}_3\text{CN})_9][\text{AlCl}_4]_3 \cdot \text{CH}_3\text{CN}$ (Ln = La, Pr, Nd, Sm, Eu, Gd, Tb, Ho or Yb) independent of the lanthanide ion size, on the basis of analytical data and a crystal structure for Ln = Sm. Unfortunately, they did not submit the crystal structure of the Sm complex to the X-ray database; therefore no data about the arrangement of the N donor atom around the Sm ion as well as bond lengths or angles could be found.

Using the same anion, $[\text{AlCl}_4]^-$, Deacon *et al.*^[9] have published the crystal structures of the Pr and Yb complexes. They found for the Pr complex the same structure $[\text{Pr}(\text{CH}_3\text{CN})_9][\text{AlCl}_4]_3 \cdot \text{CH}_3\text{CN}$ as was probably found by Shen and co-workers,^[8] with a nine coordination of praseodymium having a tricapped trigonal prismatic arrangement of the N

donor atom around the metal center. However, a quite different structure for the Yb complex $[Yb(CH_3CN)_8][AlCl_4]_3$ has been found without a co-crystallized acetonitrile molecule and with only eight coordinated N atoms around the metal center in a square dodecahedral arrangement. These observations strengths the well-known fact that the coordination number of lanthanides often varies with the cation size. The same trend was observed using $[Al(OC(CF_3)_3)_4]^-$ as “non-coordinating” anion to lanthanides, where Ln = Nd, Eu, Gd, Dy and Tm: nine coordinated species for light and eight coordinated species for heavy lanthanides. Concerning the lanthanide 2+ ions, Evans *et al.*^[11] reported eight coordinated acetonitrile lanthanide complex for heavy lanthanide Yb^{2+} in $[Yb(CH_3CN)_8][B(C_6H_5)_4]_2$ using $[B(C_6H_5)_4]^-$ as counter ion. Consequently, one can conclude that the nature of the “non-coordinating” anion seems to not really influence the coordination number of homoleptic acetonitrile lanthanide complexes. Therefore, at the beginning of the series nine, whiles at the end of the series eight coordinated species are characteristic in the solid state structures of homoleptic acetonitrile lanthanide complexes.

Table II-2: Mean Ln-N distances, \bar{d}_{Ln-N} , and coordination polyhedron in different homoleptic $[Ln(CH_3CN)_n]^{3+}$ complexes (n = 8, 9). n. g. = value not given in the reference, MCSAP. = mono-capped square antiprismatic, DSAP = distorted square antiprism, TTP = tricapped trigonal prism, MCSP = mono-capped square prism, SD = square dodecahedron.

Complexes	Counter-anion	$\bar{d}_{Ln-N} / \text{\AA}$	T / K	Coordination polyhedron	Ref.
$[Nd(CH_3CN)_9]^{3+}$ (1)	$[Al(OC(CF_3)_3)_4]^-$	2.637(3)	100	MCSAP	this work
$[Gd(CH_3CN)_9]^{3+}$ (3)	$[Al(OC(CF_3)_3)_4]^-$	2.549(4)	100	MCSAP	this work
$[Dy(CH_3CN)_9]^{3+}$ (4)	$[Al(OC(CF_3)_3)_4]^-$	2.521(8)	100	MCSAP	this work
$[La(CH_3CN)_9]^{3+}$	$[AsF_6]^-$	2.629(3)	173	TTP	[9]
$[Sm(CH_3CN)_9]^{3+}$	$[AsF_6]^-$	2.534(6)	173	TTP	[9]
$[Sm(CH_3CN)_9]^{3+}$	$[AlCl_4]^-$	n.g.	n.g.	n. g.	[8]
$[Pr(CH_3CN)_9]^{3+}$	$[AlCl_4]^-$	2.591(4)	173	TTP	[9]
$[Pr(CH_3CN)_9]^{3+}$	$[SnCl_5]^{-a)}$	2.600(7)	180	TTP	[10]
$[Pr(CH_3CN)_9]^{3+}$	$[SnCl_5]^{-b)}$	2.577(3)	180	MCSP	[10]
$[Yb(CH_3CN)_8]^{3+}$	$[AlCl_4]^-$	2.393(2)	173	SD	[9]
$[Yb(CH_3CN)_8]^{2+}$	$[B(C_6H_5)_4]^-$	2.556(5)	158	DSAP	[11]
$[Tm(CH_3CN)_8]^{3+}$ (5)	$[Al(OC(CF_3)_3)_4]^-$	2.410(1)	140	DSAP	this work

^{a)} with THF and CH_3CN coordinated to the $[SnCl_5]^-$ anion. ^{b)} only CH_3CN solvent molecule coordinated to the $[SnCl_5]^-$ anion.

In Figure II-2, the cationic part of the compound **3** is shown. The $[\text{Ln}(\text{CH}_3\text{CN})_9]^{3+}$ cations in compounds **1** and **4** have analogue structures as can be seen in Appendix Figures A II-1 and A II-2. Due to their relatively high R1 value a detailed discussion related to bond lengths and angles is not pertinent for these compounds.

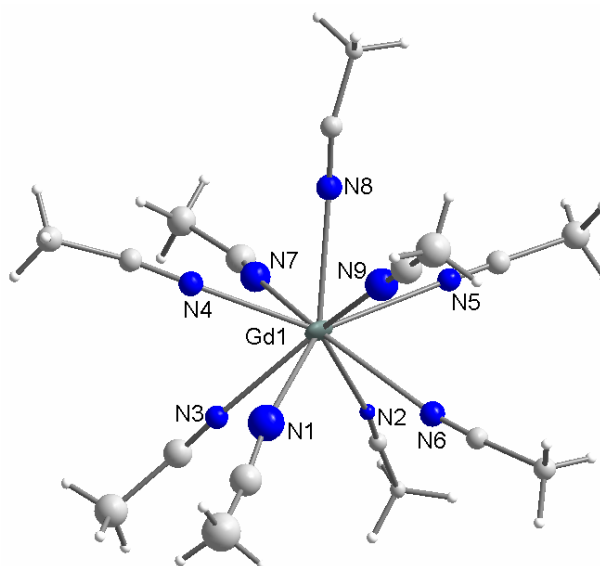


Figure II-2. Solid-state structure of the $[\text{Gd}(\text{CH}_3\text{CN})_9]^{3+}$ cation in compound **3**. The ellipsoids are drawn at the 25% probability level. The $[\text{Al}(\text{OC}(\text{CF}_3)_3)_4]^-$ anions as well as the embedded solvent molecules ($3\text{CH}_2\text{Cl}_2$) have been omitted for clarity.

The structure of the $[\text{Tm}(\text{CH}_3\text{CN})_8]^{3+}$ cation in **5** is displayed in Figure II-3 with the atom notation used, while the structure of the complex **5** without the embedded solvent molecules is shown in Figure II-4. Selected bond distances and angles are listed in Table II-3. The Tm salt crystallizes in the monoclinic space group $P2_1/n$ and, as it is characteristic for heavy lanthanides, Tm^{3+} is coordinated to eight acetonitrile molecules in a slightly distorted square antiprismatic manner.^[11, 34] The twist angle between the planes of the distorted square antiprism is 37° , whilst the angle formed by the N1, N3, N5, N7 and N2, N4, N6, N8 planes is 2.2° . The Tm-N distances are between 2.400(6) - 2.430(7) Å as listed in Table II-3.

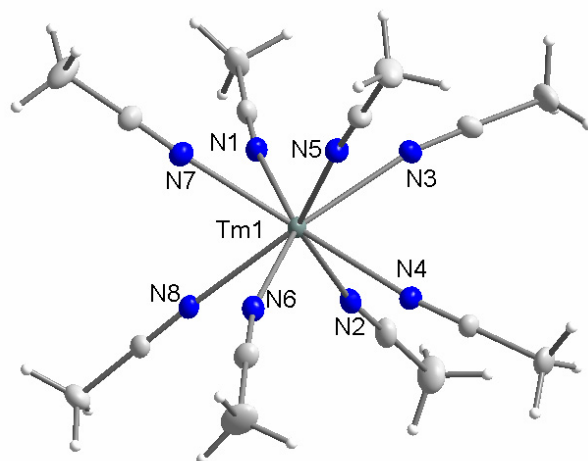


Figure II-3. Solid-state structure of the $[Tm(CH_3CN)_8]^{3+}$ cation in compound **5**. The ellipsoids are drawn at the 25% probability level. The $[Al(OC(CF_3)_3)_4]^-$ anions as well as solvent molecules ($2CH_2Cl_2$ and $2CH_3CN$) have been omitted for clarity.

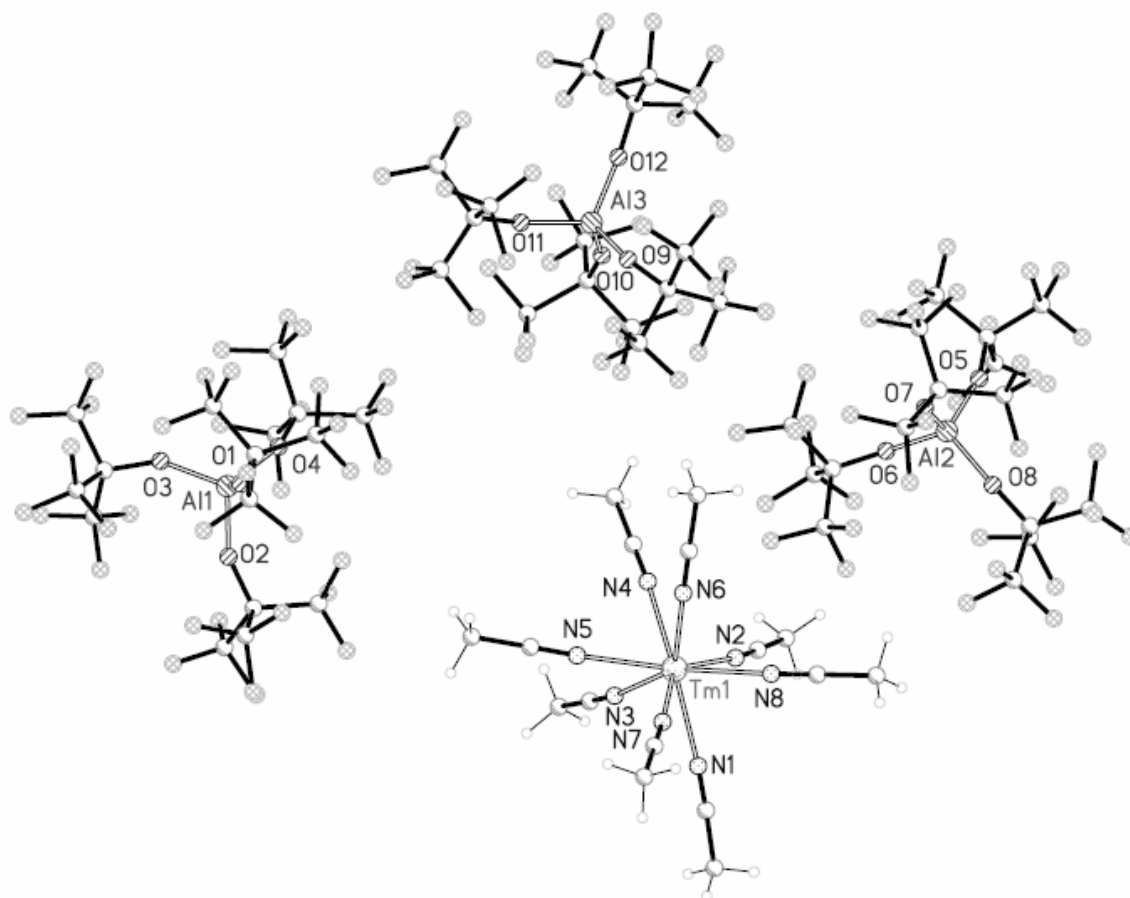
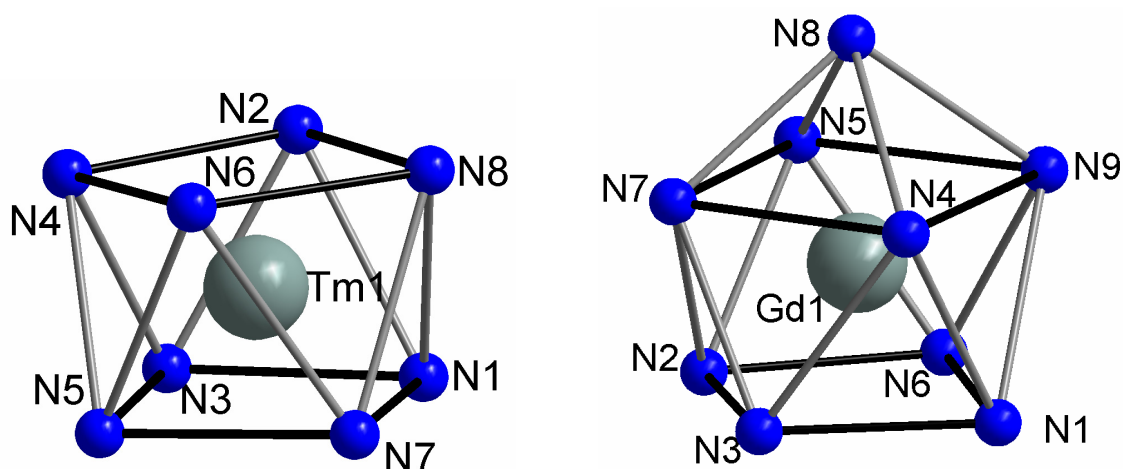


Figure II-4. ORTEP representation of the structure of $[Tm(CH_3CN)_8][Al(OC(CF_3)_3)_4]_3$ **5**. The embedded solvent molecules ($2CH_2Cl_2$ and $2CH_3CN$) have been omitted for clarity.

Table II-3. Selected bond lengths (Å) and angles (°) for [Tm(CH₃CN)₈][Al(OC(CF₃)₃)₄]₃ **5**:

<i>Bond lengths</i>		<i>Bond angles</i>	
Tm(1)-N(1)	2.407(6)	N(1)-Tm(1)-N(8)	79.4(2)
Tm(1)-N(2)	2.405(6)	N(3)-Tm(1)-N(2)	76.0(2)
Tm(1)-N(3)	2.400(6)	N(3)-Tm(1)-N(8)	143.1(2)
Tm(1)-N(4)	2.400(6)	N(4)-Tm(1)-N(1)	139.9(2)
Tm(1)-N(5)	2.400(6)	N(4)-Tm(1)-N(2)	72.6(2)
Tm(1)-N(6)	2.421(6)	N(4)-Tm(1)-N(3)	74.1(2)
Tm(1)-N(7)	2.430(7)	N(4)-Tm(1)-N(8)	116.2(2)
Tm(1)-N(8)	2.418(6)	N(5)-Tm(1)-N(1)	114.1(2)
		N(5)-Tm(1)-N(3)	73.4(2)
		N(5)-Tm(1)-N(4)	77.3(2)
		N(5)-Tm(1)-N(8)	141.9(2)

In Figure II-5, the coordination polyhedra of the nine- and the eight-coordinated lanthanide ions are shown, both having - distorted - C₄ symmetry. For the eight-fold coordination, the slightly distorted square antiprism polyhedron shown for complex **5** has been already found in homoleptic acetonitrile lanthanide complex as described by Evans.^[11] For the nine-fold coordination the mono-capped square antiprismatic coordination sphere found in **1**, **3** and **4** is slightly different from the representative tricapped trigonal prismatic symmetric arrangement described for the majority of nine-coordinated homoleptic acetonitrile lanthanide complexes presented in Table II-2.^[9, 10] However, mono-capped square antiprism arrangement was already been observed for the Ln-N bonds in [La(NH₃)₉][Cu(S₄)₂].^[34]

**Figure II-5:** Coordination polyhedra of the Tm in **5** (left, square antiprism) and Gd in **3** (right, capped square antiprisma).

II.3.2 IR and Raman Spectroscopy

For all the compounds discussed in this study, solid state IR and Raman spectra have been recorded. In Table II-4, their vibrational bands are listed together with those of free CH_3CN , $[\text{NEt}_4][\text{Al}(\text{OC}(\text{CF}_3)_3)_4]$ and $\text{Li}[\text{Al}(\text{OC}(\text{CF}_3)_3)_4]$. The latter two species have been chosen as models for a free, undisturbed (S_4 symmetric) and a strongly coordinated system respectively.^[35, 36] It can be seen from this table, that in all the $[\text{Ln}(\text{CH}_3\text{CN})_n][\text{Al}(\text{OC}(\text{CF}_3)_3)_4]_3$ salts, the anion bands are in very good agreement with those in $[\text{NEt}_4][\text{Al}(\text{OC}(\text{CF}_3)_3)_4]$, indicating pure ionic compounds without anion coordination. In the case of $\text{Li}[\text{Al}(\text{OC}(\text{CF}_3)_3)_4]$, in which the lithium cation is strongly coordinated to the anion, characteristic splitting of some anion bands ($974\text{ cm}^{-1} \rightarrow 964\text{ cm}^{-1}$ and 976 cm^{-1} ; $756\text{ cm}^{-1} \rightarrow 755\text{ cm}^{-1} + 760\text{ cm}^{-1}$; $572\text{ cm}^{-1} \rightarrow 572\text{ cm}^{-1} + 582\text{ cm}^{-1}$; $537\text{ cm}^{-1} \rightarrow 539\text{ cm}^{-1} + 546\text{ cm}^{-1}$) occurs. As these splitted bands are not observed in the compounds **1** to **5**, it can be stated that - even without a crystallographic proof - there is no $[\text{Al}(\text{OC}(\text{CF}_3)_3)_4]^-$ anion in the first coordination sphere of these complexes.

The vibrational energies of the CH_3CN change slightly upon coordination to lanthanides. The $\nu(\text{C-C})$ band, which is observed for the free ligand at 918 cm^{-1} , appears for all compounds **1** to **5** at higher wave numbers around 935 cm^{-1} . Also the $\nu(\text{C-N})$ stretching frequencies are shifted to higher frequencies (2283 cm^{-1}) if compared with free CH_3CN (2253 cm^{-1}), as expected on coordination.^[37] They are also in perfect agreement with those of $[\text{Ln}(\text{CH}_3\text{CN})_9][\text{AsF}_6]_3 \cdot n\text{CH}_3\text{CN}$ ($\text{Ln} = \text{La}$, $n = 1$; Sm , $n = 3$), $[\text{Ln}(\text{CH}_3\text{CN})_9][\text{AlCl}_4]_3 \cdot \text{CH}_3\text{CN}$ ($\text{Ln} = \text{Pr}$, Sm) and $[\text{Yb}(\text{CH}_3\text{CN})_8][\text{AlCl}_4]_3$.^[8, 9]

All samples for IR and Raman measurements were prepared in dry inert atmosphere. The IR spectra were recorded on a Nicolet Magna 760 spectrometer using a diamond Orbit ATR unit (extended ATR correction with refraction index 1.5 was used). Raman spectra were recorded at room temperature on a Bruker RAM II FT-Raman spectrometer (using a liquid nitrogen cooled, highly sensitive Ge detector) in sealed melting point capillaries.

Table II-4. Comparison of the IR and Raman spectra of **1**, **2**, **3**, **4** and **5** with those of free CH₃CN and of the [pftb]⁻ = [Al(OC(CF₃)₃)₄]⁻ anion in [NEt₄][pftb] and Li[pftb]. Bands assigned to the [Ln(CH₃CN)_n]³⁺ cations are marked in bold (vw = very weak, w = weak, mw = medium weak, m = medium, ms = medium strong, s = strong, vs = very strong, sh = shoulder).

IR	1		2		3		4		5		[pftb] ⁻ in [NEt ₄][pftb]		[pftb] ⁻ in Li[pftb]		CH ₃ CN		assignment
	Raman	IR	Raman	IR	Raman	IR	Raman	IR	Raman	IR	Raman	IR	Raman	IR	Raman	IR	
-	233 (w)	-	234 (w)	-	236 (w)	-	233 (w)	-	235 (w)	-	228 (w)	234 (w)	-	234 (mw)	-	-	C-C-
289 (w)	288 (w)	283 (w)	288 (w)	287 (w)	291 (w)	287 (w)	287 (w)	289 (w)	291 (w)	289 (w)	285 (mw)	289 (w)	289 (w)	297 (w)	-	-	C-C
315 (m)	323 (w)	315 (w)	322 (m)	315 (m)	324 (ms)	315 (m)	323 (w)	315 (m)	324 (m)	316 (m)	316 (m)	323 (ms)	-	316 (w)	-	-	C-C, Al-O
327 (w)	-	-	-	331 (vw)	-	331 (vw)	-	328 (w)	-	331 (w)	331 (w)	-	326 (w)	327 (m)	-	-	C-C, C-F, Al-O
355 (vw)	-	-	-	-	-	-	-	355 (vw)	-	-	-	-	-	-	383 (mw)	-	C-C-N
-	368 (w)	-	368 (w)	368 (w)	370 (w)	368 (w)	368 (w)	370 (w)	370 (w)	367 (mw)	367 (mw)	368 (w)	369 (w)	363 (w)	-	-	C-C, C-F, Al-O
376 (w)	-	376 (w)	-	380 (w)	-	380 (w)	-	375 (w)	-	377 (mw)	-	-	-	390 (w)	-	-	C-C, C-O
399 (m)	408 (w)	-	409 (mw)	417 (vw)	417 (m)	417 (vw)	414 (w)	407 (w)	418 (m)	-	-	-	-	-	-	-	C-C-N
447 (ms)	-	447 (m)	-	449 (ms)	-	449 (ms)	-	448 (ms)	-	446 (ms)	446 (ms)	-	-	-	-	-	C-C, C-O
-	-	-	-	-	-	-	-	-	-	-	-	-	464 (m)	-	-	-	-
537 (ms)	538 (w)	537 (mw)	538 (m)	537 (ms)	540 (w)	537 (ms)	539 (w)	537 (ms)	549 (w)	537 (m)	537 (m)	538 (w)	539 (m)	539 (mw)	-	-	C-C, C-O
-	-	-	-	-	-	-	-	-	-	-	-	-	546 (mw)	-	-	-	-
561 (ms)	562 (w)	561 (w)	561 (mw)	561 (ms)	563 (w)	561 (ms)	562 (w)	561 (ms)	563 (w)	562 (mw)	562 (mw)	563 (w)	562 (mw)	-	-	-	Al-O, C-C
572 (m)	572 (sh, w)	572 (vw, sh)	572 (sh, w)	572 (mw)	571 (sh, w)	572 (mw)	572 (sh, w)	572 (m)	572 (sh, w)	571 (w)	571 (w)	-	572+582 (m)	573 (mw)	-	-	Al-O, C-C

Table II-4 continued: Comparison of the IR and Raman spectra of **1**, **2**, **3**, **4** and **5** with those of free CH_3CN and of the $[pftb]^- = [Al(OC(CF_3)_3)_4]^-$ anion in $[NEt_4][pftb]$ and $Li[pftb]$. Bands assigned to the $[Ln(CH_3CN)_n]^{3+}$ cations are marked in bold (vw = very weak, w = weak, mw = medium weak, m = medium, ms = medium strong, s = strong, vs = very strong, sh = shoulder).

1		2		3		4		5		$[pftb]^-$ in $[NEt_4][pftb]$		$[pftb]^-$ in $Li[pftb]$		CH_3CN		assignment
IR	Raman	IR	Raman	IR	Raman	IR	Raman	IR	Raman	IR	Raman	IR	Raman	IR	Raman	
727 (ms)	-	727 (s)	-	727 (ms)	-	727 (ms)	-	727 (ms)	-	727 (s)	-	726 (s)	730 (s)	-	-	C-C, C-O
-	746 (ms)	-	746 (s)	-	748 (s)	-	746 (ms)	-	748 (ms)	-	747 (ms)	740 (ms)	745 (s)	-	-	-
755 (vw)	-	756 (vw)	-	756 (vw)	-	756 (vw)	-	756 (vw)	-	756 (mw)	-	756+760 (m)	-	-	-	C-C, C-O
-	798 (ms)	-	797 (s)	-	799 (s)	-	798 (ms)	-	799 (ms)	-	798 (s)	798 (m)	801 (w)	-	-	-
832 (mw)	-	832 (w)	-	833 (w)	-	832 (w)	-	832 (mw)	-	833 (m)	-	844 (ms)	843 (w)	-	-	Al-O, C-C
-	-	-	-	-	-	-	-	-	-	-	-	863 (ms)	-	-	-	Al-O, C-C
933 (vw)	936 (vw)	935 (w)	938 (w)	934 (vw)	942 (w)	937 (vw)	938 (vw)	-	942 (w)	-	-	936 (ms)	-	918 (vw)	922 (m)	C-C
-	-	-	-	-	-	-	-	-	-	-	-	964 (vs)	-	-	-	C-C
972 (vs)	978 (w)	972 (vs)	973 (vw)	972 (vs)	977 (vw)	972 (vs)	-	972 (vs)	977 (w)	973 (s)	978 (mw)	976 (vs)	978 (w)	-	-	C-C, C-F
-	-	-	-	-	-	-	-	-	-	-	-	-	-	1039 (w)	-	H-C-N
-	-	-	1135 (vw)	-	-	-	-	-	-	-	1139 (mw)	-	1113 (w)	-	-	C-C, C-F
1168 (m)	-	1170 (ms)	-	1171 (m)	-	1171 (m)	-	-	-	-	1173 (mw)	1184 (ms)	1171 (w)	-	-	C-C, C-F
1218 (vs)	-	1216 (vs)	1218 (vw)	1218 (vs)	-	1217 (vs)	-	1217 (vs)	-	1217 (vs)	-	1225 (vs)	1214 (mw)	-	-	C-C, C-F

Table II-4 continued: Comparison of the IR and Raman spectra of **1**, **2**, **3**, **4** and **5** with those of free CH₃CN and of the [pf₆]⁻ = [Al(OC(CF₃)₃)₄]⁻ anion in [NEt₄][pf₆] and Li[pf₆]. Bands assigned to the [Ln(CH₃CN)_n]³⁺ cations are marked in bold (vw = very weak, w = weak, mw = medium weak, m = medium, ms = medium strong, s = strong, vs = very strong, sh = shoulder).

1		2		3		4		5		[pf ₆] ⁻ in [NEt ₄][pf ₆]		[pf ₆] ⁻ in Li[pf ₆]		CH ₃ CN		assignment
IR	Raman	IR	Raman	IR	Raman	IR	Raman	IR	Raman	IR	Raman	IR	Raman	IR	Raman	
1244 (vs)	1245 (w)	1244 (vs)	1244 (w)	1245 (vs)	-	1245 (vs)	-	1245 (s)	-	1240 (s)	1235 (mw)	1243 (s)	1250 (mw)	-	-	C-C, C-F
-	-	-	-	-	-	-	-	-	-	1245 (s)	-	-	-	-	-	C-C, C-F
1275 (s)	1274 (w)	1275 (s)	1273 (w)	1275 (s)	1276 (w)	1275 (vs)	1271 (mw)	1275 (s)	1276 (w)	1274 (vs)	1274 (mw)	1270 (s)	1281 (mw)	-	-	C-C, C-F
1299 (ms)	-	1299 (ms)	1307 (w)	1299 (ms)	1308 (w)	1299 (s)	1308 (w)	1299 (ms)	1308 (w)	1298 (s)	1300 (m)	1297 (s)	-	-	-	C-C, C-F
1353 (m)	-	1353 (m)	-	1353 (m)	-	1353 (m)	-	1353 (m)	-	1353 (ms)	-	1353 (ms)	1337 (mw)	-	-	C-C, C-F
-	1377 (m)	1377 (vw)	1377 (m)	-	1379 (m)	1376 (vw)	1377 (m)	-	1379 (m)	-	-	-	-	1376 (ms)	1377 (w)	H-C-H, H-C-N
-	-	-	1416 (vw)	-	1420 (vw)	-	-	-	1420 (vw)	-	-	-	-	1444 (ms)	1448 (w)	H-C-H
2281 (m)	2284 (vs)	2283 (m)	2285 (vs)	2283 (mw)	2290 (vs)	2284 (m)	2286 (vs)	2286 (m)	2290 (vs)	-	-	-	-	2253 (vs)	2255 (s)	C-N
2310 (w)	2312 (ms)	2311 (w)	2313 (s)	2312 (vw)	2318 (s)	2313 (w)	2314 (ms)	2314 (w)	2318 (ms)	-	-	-	-	2292 (mw)	2295 (w)	C-N
2955 (vw)	2956 (s)	2956 (vw)	2956 (vs)	2955 (vw)	2957 (vs)	2955 (vw)	2955 (w)	2955 (vw)	-	-	-	-	-	2945 (vw)	2945 (vs)	C-H
-	3022 (mw)	-	3021 (w)	-	3023 (mw)	-	3024 (vs)	-	3023 (vs)	-	-	-	-	3002 (vw)	3004 (w)	C-H

II.4 CHARACTERIZATION OF $[\text{Ln}(\text{CH}_3\text{CN})_n][\text{Al}(\text{OC}(\text{CF}_3)_3)_4]_3$ COMPLEXES IN SOLUTION

II.4.1 Conductivity

The previous sections present some results proving that, in solid state, for complexes **1** to **5** there is no $[\text{Al}(\text{OC}(\text{CF}_3)_3)_4]^-$ anion coordination to the metal center. However, in solution the non-coordinating properties of the $[\text{Al}(\text{OC}(\text{CF}_3)_3)_4]^-$ anion towards the $[\text{Ln}(\text{CH}_3\text{CN})_n][\text{Al}(\text{OC}(\text{CF}_3)_3)_4]_3$ complexes might change. Therefore, in order to elucidate whether the $[\text{Al}(\text{OC}(\text{CF}_3)_3)_4]^-$ anion coordinates or not to the metal center in solution, conductivity measurements on each complex from **1** to **5** have been undertaken. Conductivity measurements can reveal the type of the electrolyte formed in solution: 3:1, e.g. $[\text{Ln}(\text{CH}_3\text{CN})_n][\text{Al}(\text{OC}(\text{CF}_3)_3)_4]_3$; 2:1, e.g. $[\text{Ln}(\text{CH}_3\text{CN})_n\text{Al}(\text{OC}(\text{CF}_3)_3)_4][\text{Al}(\text{OC}(\text{CF}_3)_3)_4]_2$; or 1:1 e.g. $[\text{Ln}(\text{CH}_3\text{CN})_n(\text{Al}(\text{OC}(\text{CF}_3)_3)_4)_2][\text{Al}(\text{OC}(\text{CF}_3)_3)_4]$. Therefore, the results can indicate whatever, in solution, there is or not any strong interaction between the metal center and the anions.

Conductance measurements of solutions are often used in coordination chemistry to determine the electrolyte type (1:1, 2:1 and 3:1).^[38] A commonly adopted procedure is to determine the specific conductivity, κ [$\text{ohm}^{-1} \text{cm}^{-1}$], of a solution by measuring the resistance, R , in an experimental cell of known cell constant (Eq. II-2).

$$\kappa = \frac{\text{cell const.}}{R} \quad \text{Eq. II-2}$$

The molar conductivity, Λ_M [$\text{ohm}^{-1} \text{cm}^2 \text{mol}^{-1}$], then can be easily calculated just by dividing the specific conductivity, κ [$\text{ohm}^{-1} \text{cm}^{-1}$], by the molar concentration [mol l^{-1}] of the solution (Eq. II-3):

$$\Lambda_M = \frac{\kappa}{c_M} \quad \text{Eq. II-3}$$

The majority of authors compute Λ_M values at a single concentration, which is generally 10^{-3} M, by using an assumed molecular weight. Then, the so obtained molar conductance is compared to the Λ_M values of a known electrolyte type.

The selection of an appropriate solvent for conductivity measurements is not straightforward. The solvent has to fulfill the following criteria: being inert to chemical reactions with the species in the solution; having a high dielectric constant and a low viscosity. An overview of some properties of non-aqueous solvents relevant to their use for conductivity measurements is listed in Table II-5.

Table II-5. Some relevant properties of non-aqueous solvents to their use in conductivity measurements.^[38]

Solvent	Dielectric constant, ϵ	Viscosity, η / $\text{g}^{-1} \text{sec}^{-1}$	Specific conductivity, κ / $\text{ohm}^{-1} \text{cm}^{-1}$
Acetone	20.7	0.295	5.8×10^{-8}
Nitromethane	35.9	0.595	6.56×10^{-7}
Nitrobenzene	34.8	1.634	9.1×10^{-7}
Methanol	32.7	0.545	1.5×10^{-7}
Ethanol	24.5	1.078	1.35×10^{-7}
Acetonitrile	37.5	0.325	4.2×10^{-7}
Dimethylformamide	36.7	0.796	$0.6 - 2.0 \times 10^{-7}$
Dimethylsulphoxide	46.7	1.960	3.0×10^{-8}

In the conductivity measurements performed in this study acetonitrile was chosen as solvent media in order to avoid the formation of new compounds, of different ion types, by solvolysis reaction with the solvents mentioned above. Acetonitrile has also the advantage of having a high dielectric constant and low viscosity. The measured specific conductivity of the pure solvent was $3.9 \times 10^{-7} \text{ ohm}^{-1} \text{cm}^{-1}$, which is in a good agreement with the previously published data.^[39, 40]

Geary^[38] summarized the expected ranges of the molar conductivity (Λ_M) for complexes of different electrolyte types at a concentration of 10^{-3} M , in common organic solvents (Table II-6). In the literature only a scarce number of publications can be found about molar conductivity values for 3:1 electrolytes in acetonitrile.^[4, 41-48] Particular attention should be attributed to the work of Burmeister *et al.*^[45] where extremely high molar conductivities [$\text{ohm}^{-1} \text{cm}^2 \text{mol}^{-1}$] were measured on $[\text{Ln}(\text{NCS})_6][(\text{n-C}_4\text{H}_9)_4\text{N}]_3$ complexes: 472 (Pr), 457 (Nd), 468 (Sm), 430 (Dy), 440 (Ho) and 417 (Er); or to the work of Seminara *et al.*^[46] where extremely low molar conductivities [$\text{ohm}^{-1} \text{cm}^2 \text{mol}^{-1}$] were measured on some $[\text{Ln}(\text{H}_2\text{O})_9][\text{CF}_3\text{SO}_3]_3$ complexes: 270 (Nd), 300 (Eu); 295 (Ho) and 285 (Tm) or

$[Ln(pyO)_8][CF_3SO_3]_3$ complexes: 305 (La), 290 (Nd), 310 (Eu), 305 (Ho). These extremely high and low molar conductivity values were excluded from the expected Λ_M ranges presented by Geary. The work of Prabhakaran *et al.*^[47] on $[Mn(DMSO)_6][ClO_4]_3$ and $[Mn(DMF)_6][ClO_4]_3$ show more classical Λ_M values of 361 and 390 $ohm^{-1} cm^2 mol^{-1}$, respectively.

Table II-6. Expected Λ_M [$ohm^{-1} cm^2 mole^{-1}$] ranges for complexes of different electrolyte types at 10^{-3} M in common organic solvents [$ohm^{-1} cm^2 mole^{-1}$].^[38]

Solvent	Electrolyte type		
	1:1	2:1	3:1
Nitromethane	75 – 95	150 – 180	220 – 260
Nitrobenzene	20 – 30	50 – 60	70 – 82
Acetone	100 – 140	160 – 200	270?
Acetonitrile	120 – 160	220 – 300	340 – 420
Dimethylformamide	65 – 90	130 – 170	200 – 240
Methanol	80 – 115	160 – 220	290 – 350
Ethanol	35 – 45	70 – 90	120?

In this study, all conductivity measurements were carried out in inert atmosphere in an argon filled glove box to avoid any contamination with water. The measurements were done at 25°C with a Metrohm 712 Conductometer working with a platinum electrode and having a cell constant of $0.814 cm^{-1}$. The molar conductivity values presented in Table II-7, measured on the $[Ln(CH_3CN)_n][Al(OC(CF_3)_3)_4]_3$ complexes **1** - **5**, are at the upper limit for the generally accepted molar conductivity values for 3:1 electrolytes type.

The studied complexes have extremely similar molar conductivity values, leading to the conclusion that all of them have the same behavior in acetonitrile.

Finally, one can conclude from the molar conductivity measurements that all $[Ln(CH_3CN)_n][Al(OC(CF_3)_3)_4]_3$ ($n = 9$: Ln = Nd, Eu, Gd, Dy; $n = 8$: Ln = Tm) complexes behave like 3:1 electrolytes in dilute acetonitrile solution. Therefore, the first coordination sphere of the metal center, even in acetonitrile solution, is free of any $[Al(OC(CF_3)_3)_4]^-$ anion.

Table II-7. Molar conductivity data for $[\text{Ln}(\text{CH}_3\text{CN})_n][\text{Al}(\text{OC}(\text{CF}_3)_3)_4]_3$ complexes measured in acetonitrile at 25°C.

Complexes	$c / \text{mmol l}^{-1}$	$\Lambda_M / \text{ohm}^{-1} \text{cm}^2 \text{mol}^{-1}$
$[\text{Nd}(\text{CH}_3\text{CN})_9][\text{Al}(\text{OC}(\text{CF}_3)_3)_4]_3$ 1	1.022	420.9
$[\text{Eu}(\text{CH}_3\text{CN})_9][\text{Al}(\text{OC}(\text{CF}_3)_3)_4]_3$ 2	0.918	419.7
$[\text{Gd}(\text{CH}_3\text{CN})_9][\text{Al}(\text{OC}(\text{CF}_3)_3)_4]_3$ 3	1.005	430.1
$[\text{Dy}(\text{CH}_3\text{CN})_9][\text{Al}(\text{OC}(\text{CF}_3)_3)_4]_3$ 4	1.029	420.2
$[\text{Tm}(\text{CH}_3\text{CN})_8][\text{Al}(\text{OC}(\text{CF}_3)_3)_4]_3$ 5	0.985	420.9

II.4.2 NMR Chemical Shift Measurements

Hetero-nuclear NMR chemical shift measurements were performed in order to predict the chemical shifts of all nuclei present in the samples with respect to the TMS primary reference resonance frequency; as well as bulk magnetic susceptibility shift measurements in order to determine the concentrations of the lanthanide ions.

Lanthanide ions (except La and Lu) have unpaired electrons in their 4*f* inner shells. Due to these unpaired electrons they have a paramagnetic character. The paramagnetism of 4*f* ions led to the discovery of the Lanthanides Induced Shift (LIS), which is very helpful in the interpretation of the NMR spectra of large molecules like nucleotides, amino acids or proteins.^[49, 50] In this way, Eu^{3+} , Tm^{3+} and Dy^{3+} complexes are widely used as shift reagents^[51-53] Also, due to their paramagnetism Gd^{3+} complexes are successfully used as MRI contrast agents.^[54, 55] In solution, a paramagnetic compound can affect nuclear spins by producing chemical shifts and/or by increasing the nuclear spin relaxation rates.

In general, a paramagnetic species can induce a chemical shift (Δ) in the resonance frequency of a nuclear spin via three mechanisms: the diamagnetic (Δ_d), the hyperfine ($\Delta_c + \Delta_p$) and the bulk magnetic susceptibility (Δ_χ) mechanisms (Eq. II-4).^[50]

$$\Delta = \Delta_d + \Delta_c + \Delta_p + \Delta_\chi \quad \text{Eq. II-4}$$

The diamagnetic shifts (Δ_d) are usually small (often neglected) and affect atoms of the ligands which are directly bonded to the paramagnetic metal center. They represent shifts which would have been observed if the paramagnetic metal center had been replaced by a diamagnetic metal ion (in the case of lanthanides by La^{3+} or Lu^{3+} , which contain no unpaired electrons).

The hyperfine shifts are influenced by a contact or scalar contribution (Δ_c) and by a dipolar or pseudo contact contribution (Δ_p). The contact or scalar contribution (Δ_c) results from through-bond transmission of unpaired spin density of the Ln^{3+} to the ligand nucleus in question. The dipolar or pseudo contact contribution (Δ_p) is the result of a through-space dipolar interaction between the magnetic moments of the unpaired electrons in Ln^{3+} and the nucleus under study.

Bulk Magnetic Susceptibility (BMS) shifts (Δ_χ) arise due to the partial alignment of the magnetic moments of the paramagnetic species by the magnetic field. As such, bulk magnetic susceptibility shifts affect all nuclei present in the sample whether they are directly bonded to the metal center or not.

In the case of the $[\text{Ln}(\text{CH}_3\text{CN})_n][\text{Al}(\text{OC}(\text{CF}_3)_3)_4]_3$ compounds **1** - **5**, one can not find a solvent which will be less coordinating to the metal center than CH_3CN and in which the salts are still soluble. Thus, for all chemical shift measurements neat anhydrous acetonitrile was used as solvent medium.

II.4.2.1 Hetero-nuclear NMR Chemical Shifts

To elucidate the chemical shifts of nuclides present in the $[\text{Ln}(\text{CH}_3\text{CN})_n][\text{Al}(\text{OC}(\text{CF}_3)_3)_4]_3$ **1** to **5** complexes, the measurements were done using the unified scale recommendation of IUPAC (see Chapter VI). Due to the fact that lanthanides are strongly paramagnetic some special care had to be undertaken. As a consequence, since the paramagnetism of lanthanides is different (which imply a different shift of the TMS signal), the proton resonance frequency of TMS had to be recorded individually for each complex. Therefore, for each compound, NMR spectra were recorded in anhydrous CH_3CN with some drops of TMS and without lock substance. Due to the fact that no lock substance was used particular attention had to be paid to not change the shim values once the proton resonance frequency of TMS was measured. In this way, once the proton resonance frequency of TMS as well as the X nuclide resonance frequency measured, the chemical shifts of all nuclides could be attributed by simply applying

the Eq. VI-1 and VI-2 as presented in Chapter IV. The used Ξ_{ref} values are listed in Table II-8. The so obtained chemical shifts for all X nuclides are listed in Table II-9. All spectra were recorded in 5 mm sealed NMR tubes on a Bruker DRX-400 spectrometer at 25°C.

Table II-8. Spin properties and frequency ratio values for nuclei present in the lanthanide complexes

Nuclear isotope	Nuclear spin	Natural abundance, X / %	Frequency ratio, Ξ / %	Reference compound	Sample conditions
^1H	1/2	99.98	100.000 000	Me_4Si	CDCl_3 , $\varphi = 1$ %
^{13}C	1/2	1.07	25.145 020	Me_4Si	CDCl_3 , $\varphi = 1$ %
^{19}F	1/2	100	94.094 011	CCl_3F	^[57]
^{14}N	1	99.63	7.226 317	CH_3NO_2	Neat/ CDCl_3
^{27}Al	5/2	100	26.056 859	$\text{Al}(\text{NO}_3)_3$	D_2O , 1.1 m

Krossing *et al.*^[58, 59] have shown that under some experimental conditions, $[\text{Al}(\text{OC}(\text{CF}_3)_3)_4]^-$ decomposes to give the fluoride-bridged $[(\text{F}_3\text{C})_3\text{CO})_3\text{Al-F-Al}(\text{OC}(\text{CF}_3)_3)_3]^-$ anion. The decomposition of the homoleptic $[\text{Al}(\text{OC}(\text{CF}_3)_3)_4]^-$ anion can be detected by drastic changes in the ^{27}Al and ^{19}F NMR spectra. Thus, in the ^{27}Al NMR spectra an extreme line broadening occurs (from $\Delta\nu_{1/2} = 6 - 130$ Hz to $\Delta\nu_{1/2} = 2200$ Hz) when fluorines are coordinated to the Al center. In the ^{19}F NMR spectra a bridging fluorine signal appears at $\delta_{\text{Al-F-Al}} = -185$ in addition to that of the $-\text{CF}_3$ groups at $\delta_{\text{CF}} = -76$. In the NMR spectra of the $[\text{Ln}(\text{CH}_3\text{CN})_n][\text{Al}(\text{OC}(\text{CF}_3)_3)_4]_3$ complexes none of the above mentioned evidences of anion decomposition can be observed. For each lanthanide complexes only one fluorine signal corresponding to the $-\text{CF}_3$ resonance and a very sharp $\Delta\nu_{1/2} = 3 - 5$ Hz ^{27}Al resonance were recorded (Table II-9).

Table II-9. Chemical shift values measured at 25°C on a Bruker DRX-400 for different $[Ln(CH_3CN)_n][Al(OC(CF_3)_3)_4]_3$ salts in CH_3CN with 1 % TMS.

	$[Ln(CH_3CN)_n][Al(OC(CF_3)_3)_4]_3$					$Ag[Al(OC(CF_3)_3)_4]^a)$
	Nd^{3+}	Eu^{3+}	Gd^{3+}	Dy^{3+}	Tm^{3+}	
$[Al(OC(CF_3)_3)_4]^-$	$^{27}Al^{b)}$	34.5	34.5	34.3	34.6	34.5
	$^{19}F^{b)}$	-76.0	-76.0	-76.2	-75.8	-76.0
	$^{13}C \quad \underline{CF_3}^{b,c)}$	121.1	121.0	121.0	121.3	121.5
	$\underline{OC}^{b)}$	78.4	78.9	78.7	79.1	80.0
CH_3CN	1H	2.0	2.0	1.8	2.0	-
	^{14}N	-131.6	-140.0	-139.1	-136.3	-140.2
	$^{13}C \quad \underline{CN}$	117.7	117.0	114.7	113.5	116.9
	$\underline{CH_3}^{d)}$	0.8	0.7	0.3	0.3	0.7

^{a)} in CD_3CN ; ^{b)} the chemical shift values obtained in this study are in concordance with those observed by Krossing; ^[19, 58] ^{c)} $^1J_{CF} = 292.62$ Hz; ^{d)} $^1J_{CH} = 136.18$ Hz.

II.4.2.2 Bulk Magnetic Susceptibility (BMS) Shifts

Usually, the metal ion content can be determined by titration or by using Inductively Coupled Plasma (ICP) methods. For lanthanides, a typical titration method consists of using EDTA at 5.6 - 6 pH with urotropine as buffer and xylenol orange as indicator. Unfortunately, in the case of $[\text{Ln}(\text{CH}_3\text{CN})_n][\text{Al}(\text{OC}(\text{CF}_3)_3)_4]_3$ complexes, titration with EDTA was not possible due to the presence of aluminium in each sample. As well, since the metal ion content had to be determined in acetonitrile solution, the ICP method was also not possible to use, due to the fact that, the calibration in the organic solvent (acetonitrile) in our measurements gave unsatisfactory results. Therefore, an alternative method had to be found to determine the lanthanide content of all sample solutions used in the acetonitrile exchange study on $[\text{Ln}(\text{CH}_3\text{CN})_n][\text{Al}(\text{OC}(\text{CF}_3)_3)_4]_3$ complexes.

The Evans method^[60, 61] is a useful technique for the accurate determination of the susceptibility of paramagnetic molecules in solution. It can also be used to determine the paramagnetic species concentration of a solution. By using this method, the Bulk Magnetic Susceptibility (BMS) shift of the ^1H NMR resonance signals for an inert reference compound is proportional to the concentration of the paramagnetic lanthanide ion (Eq. II-5). Basically, to obtain the paramagnetic lanthanide concentration, the BMS shift of an inert reference compound in the sample has to be compared with that of the chemical shift of an external reference.

The paramagnetic contribution to the BMS can be expressed as.^[62]

$$\Delta_\chi = \frac{4\pi cS}{T} \left(\frac{\mu_{\text{eff}}}{2.84} \right)^2 10^{-3} \quad \text{Eq. II-5}$$

where:

Δ_χ	paramagnetic contribution to BMS
c	concentration of the paramagnetic complex in $\text{mol}\cdot\text{l}^{-1}$
S	shape factor: 0 for a sphere, 1/3 for a cylinder parallel to the main magnetic field; -1/6 a cylinder perpendicular to the main magnetic field
T	temperature in K
μ_{eff}	effective magnetic moment of the particular lanthanide ion

For a given lanthanide complex, the concentration in the paramagnetic metal ion can be calculated by using the following simplified equation ($S = 1/3$ as the sample tubes were parallel to the main magnetic field), Eq. II-6:

$$c = \frac{3\Delta_\chi T}{4\pi} \left(\frac{2.84}{\mu_{eff}} \right)^2 10^{-3} \quad \text{Eq. II-6}$$

Practically, a regular 1H NMR spectrum was measured: the sample of the lanthanide complex in CH_3CN with a few drops of TMS was placed in the 5 mm NMR tube and a capillary tube with a reference (TMS in CH_3CN) was inserted. The resulting spectrum consisted of four peaks: a peak of CH_3CN in the paramagnetic sample, a peak of TMS in the paramagnetic sample, a peak of CH_3CN in the reference sample and a peak of TMS in the reference sample. The difference between the chemical shifts (Δ_χ , in ppm) of the two peaks of TMS is the paramagnetic contribution to the BMS and is related to the concentration of the paramagnetic ion via Eq. II-6. The same experiment was performed for all paramagnetic lanthanide ions used. The effective magnetic moments employed for the estimation of the metal ion concentrations are listed in Table II-10. Note that, after the oxidation of an Eu^{2+} solution by using the effective magnetic moment of 3.4 the expected concentration value for an Eu^{3+} solution was obtained.

Table II-10. Effective magnetic moments of the paramagnetic lanthanide ions^[50, 63]

Lanthanide ion	μ_{eff}
Nd^{3+}	3.68
Eu^{2+}	7.9
Eu^{3+}	3.4 - 3.51
Gd^{3+}	7.94
Dy^{3+}	10.6
Tm^{3+}	7.6

The accuracy and the limits of this method are correlated to the line widths of the two peaks of the TMS, in particular at low lanthanide concentration when the two peaks are close to each other. For a good resolution of the peaks, the difference in the chemical shifts should be at least two times the value of the half-widths of those peaks. Of course, the half-widths depend on the quality of shims. In our case, using a Bruker DRX-400 spectrometer, in general

the TMS line widths varied from 2 to 9 Hz. Thus, considering $\Delta\chi = 18$ Hz, the corresponding limiting concentration of Ln would be: 1.9 mM for Nd^{3+} ; 0.4 mM for Eu^{2+} ; 2.1 - 2.2 mM for Eu^{3+} ; 0.4 mM for Gd^{3+} ; 0.2 mM for Dy^{3+} and 0.4 mM Tm^{3+} . The concentrations used in our study were much higher than these limits and their exact values will be mentioned later on in the sections describing the data treatments.

II.4.3 ^{19}F NMR Measurements

Besides the conductivity results presented in Section II.4.1 additional evidence of the non-coordination of the $[\text{Al}(\text{OC}(\text{CF}_3)_3)_4]^-$ anion to the metal center in complexes **1** to **5** in acetonitrile solution were sought. In this section, the results of ^{19}F nuclear spin relaxation measurements are provided as a cross-check to support the conclusions of Section II.4.1.

As it has already been mentioned in the previous section, paramagnetic ions can affect nuclear spins in solutions not only by inducing chemical shifts, but also by increasing nuclear relaxation rates.^[50, 64] Thus, the presence of unpaired electron spins enhanced the nuclear spin relaxation rates of the species that are in the vicinity of the paramagnetic center.

By IR and Raman spectroscopy as well as by the X-ray crystal structures, it has been proved that in the solid state there is no coordination of the anion to the metal center in the $[\text{Ln}(\text{CH}_3\text{CN})_n][\text{Al}(\text{OC}(\text{CF}_3)_3)_4]_3$ complexes. Obviously, based on the above observation it can not be concluded that the anion will not coordinate to the metal center in solution either. In the $[\text{Al}(\text{OC}(\text{CF}_3)_3)_4]^-$ anion, since the oxygen centers, which are the most basic sites of the anion ($q = -0.24$),^[65] are sterically shielded by the bulky $-\text{C}(\text{CF}_3)_3$ groups, the only possible anion coordination can occur via the peripheric fluorine atoms ($q = -0.20$).^[65] In order to eliminate any doubt of anion coordination, ^{19}F -NMR relaxation rate measurements in acetonitrile solutions were performed for different ratios of the anion and metal concentrations.

In case of the coordination of an $[\text{Al}(\text{OC}(\text{CF}_3)_3)_4]^-$ anion, two types of ^{19}F spin species will be present in solution: inner sphere species and species in the bulk. By inner-sphere species there are denoted the spins that are directly bounded to the metal center. By species in the bulk there are denoted both: outer-sphere spins, which are in the proximity of the metal center, and

spins being in the bulk, far from the metal center. Due to diffusion and molecular motion present in solution, these species can exchange their places. The exchange between these species can take place slowly or rapidly on the NMR time scale. In the ^{19}F -NMR spectrum, for the case of a slow exchange reaction it would be possible to observe two signals attributed to the coordinated and bulk fluorine spins; while in the fast exchange reaction only one coalesced signal can be observed at a frequency corresponding to the weighted mean of the two individual ones. The ^{19}F -NMR spectra of all complexes **1** to **5** revealed only one fluorine signal at the frequency measured for the uncoordinated one in $[Al(OC(CF_3)_3)_4]^-$ (Table II-9). If fluorine coordinates to the paramagnetic metal center, the transverse relaxation rate of the ^{19}F spins should vary with the increase of the concentration of the $[Al(OC(CF_3)_3)_4]^-$ anion with respect to that of the metal one. Since, no significant variation in the transverse relaxation rate of the ^{19}F spins were observed for all complexes from **1** to **5** (Table II-11 and Appendix A II-7 to A II-11), it can be concluded that the $[Al(OC(CF_3)_3)_4]^-$ anion does not coordinate to lanthanides in acetonitrile solution. The paramagnetism of Eu^{2+} ion is considerably higher than that of the Eu^{3+} ion; therefore the effect on the relaxation rate of Eu^{2+} complex is more intense. In consequence, for the ^{19}F -NMR measurements we used **2a** instead of **2**.

Table II-11. ^{19}F -NMR data measured on $[\text{Eu}(\text{CH}_3\text{CN})_9][Al(OC(CF_3)_3)_4]_2$ **2a** and $[\text{Gd}(\text{CH}_3\text{CN})_9][Al(OC(CF_3)_3)_4]_3$ **3** at 376 MHz, 25°C in CH_3CN .

Sample	[Ln] / mmol kg ⁻¹	[anion]/[Ln]	$\Delta\nu_{1/2}$ / Hz	$1/T_{2\text{obs}}$ / s ⁻¹
$[\text{Eu}(\text{CH}_3\text{CN})_9][Al(OC(CF_3)_3)_4]_2$ 2a	10.08	3	11.4	36
		6	11.3	36
		9	10.4	33
$[\text{Gd}(\text{CH}_3\text{CN})_9][Al(OC(CF_3)_3)_4]_3$ 3	13.37	3	46	143
		6	51	159
		9	53	167
	8.56	3	45	140
		6	50	158
		9	45	142
	1.35	3	26	82

The apparently considerable differences between the ^{19}F -NMR relaxation rates and/or the line widths of the $[\text{Eu}(\text{CH}_3\text{CN})_9][Al(OC(CF_3)_3)_4]_2$ **2a** and $[\text{Gd}(\text{CH}_3\text{CN})_9][Al(OC(CF_3)_3)_4]_3$ **3** are

due to differences in the experimental setups: **3** was measured in spherical tubes placed in regular 10 mm NMR tubes for which the field inhomogeneity is not totally compensated, while **2a** was measured in 5 mm NMR tubes for which the field inhomogeneity is better compensated by shimming.

Furthermore, in order to strengthen the above mentioned conclusion, we performed similar ^{19}F NMR relaxation rate measurements in acetonitrile solution of $\text{Gd}(\text{CH}_3\text{CN})_3(\text{CF}_3\text{SO}_3)_3$ and $\text{Eu}(\text{CH}_3\text{CN})_3(\text{CF}_3\text{SO}_3)_2$. For each complex, the anion concentration was successively increased. In the literature, evidence of anion coordination to the metal center can be found for these complexes. Di Brenardo *et al.*^[42] showed by IR measurements that, in the acetonitrile solution of the $\text{Eu}(\text{CH}_3\text{CN})_3(\text{CF}_3\text{SO}_3)_3$ complex at least one $(\text{CF}_3\text{SO}_3)^-$ anion is coordinated to the metal center. Moreover, the IR measurements of the acetonitrile solution of the $\text{Eu}(\text{CH}_3\text{CN})_3(\text{CF}_3\text{SO}_3)_2$ complex also revealed vibrational bands for coordinated and uncoordinated triflates.

Due to fast exchange between the coordinated and bulk ^{19}F species, only one signal can be observed in the fluorine spectra of $\text{Gd}(\text{CH}_3\text{CN})_3(\text{CF}_3\text{SO}_3)_3$ and $\text{Eu}(\text{CH}_3\text{CN})_3(\text{CF}_3\text{SO}_3)_2$ complexes in acetonitrile. The experimentally observed relaxation rate is therefore the weighted sum of the contributions of these species, Eq. II-7:

$$\frac{1}{T_{2\text{obs}}} = P_{\text{is}} \frac{1}{T_{2\text{is}}} + P_{\text{bulk}} \frac{1}{T_{2\text{bulk}}} \quad \text{Eq. II-7}$$

$$P_{\text{is}} + P_{\text{bulk}} = 1 \quad \text{Eq. II-8}$$

$$\Delta\nu_{1/2} = \frac{1}{\pi T_{2\text{obs}}} \quad \text{Eq. II-9}$$

where:	$1/T_{2\text{obs}}$	observed transverse relaxation rate
	$1/T_{2\text{is}}$	transverse relaxation rate of the inner sphere-species
	$1/T_{2\text{bulk}}$	transverse relaxation rate of the species from the bulk
	P_{is}	mole fraction of the inner-sphere species
	P_{bulk}	mole fraction of the species from the bulk
	$\Delta\nu_{1/2}$	half height line with

Equations II-7 and II-8 are only valid when the inner-sphere molecules exchange rapidly (in the NMR time scale) with the molecules from the bulk.

Table II-12 presents the recorded transverse relaxation rates of the ^{19}F spins in the acetonitrile solution of the $Ln(CH_3CN)_3(CF_3SO_3)_z$ ($Ln^{z+} = Gd^{3+}, Eu^{2+}$) complexes. We can observe that by keeping the concentration of the paramagnetic ion constant, but increasing the concentration of the triflate in the solution, the transverse relaxation rate of the ^{19}F spin is decreasing. The only explication to this phenomenon is that there is a different weight of the contributions of the inner-sphere and bulk species to the observed relaxation rate. Inner-sphere spins feel the direct influence of the paramagnetic spins, leading to an enhanced relaxation rate. Their influence on the observed relaxation rate will not change by varying the anion concentration, since the number of the coordinated fluorine atoms will probably not increase. In contrast, the spins from the bulk are not that much influenced by the paramagnetism of the metal center. As a consequence, they have a much smaller relaxation rate than those being in direct contact with the paramagnetic spins. Therefore, by increasing the amount of anion, the amount of the bulk ^{19}F spin species in solution will increase. Since bulk ^{19}F spins have small relaxation rates, while increasing the anion concentration we observe a decrease in the measured observed relaxation rates. This theory is in a perfect agreement with the measured data.

Table II-12. ^{19}F -NMR data measured on $[Eu(CH_3CN)_3][CF_3SO_3]_2$ and $[Gd(CH_3CN)_3][CF_3SO_3]_3$ at 376 MHz, 25°C in CH_3CN .

Sample	[Ln] / mmol kg ⁻¹	[anion]/[Ln]	$\Delta\nu_{1/2}$ / Hz	$1/T_{2obs}$ / s ⁻¹
$[Eu(CH_3CN)_3][CF_3SO_3]_2$	9.43	3	316	991
		6	282	887
		9	253	795
$[Gd(CH_3CN)_3][CF_3SO_3]_3$	12.51	3	817	2568
		6	497	1561
		9	385	1210

Figures II-6 and II-7 present a comparison of the measured observed relaxation rates for the Eu^{2+} and Gd^{3+} complexes with both $[Al(OC(CF_3)_3)_4]^-$ and $(CF_3SO_3)^-$ anions.

In order to keep the concentration of the metal ions constant, the concentration of $[Al(OC(CF_3)_3)_4]^-$ was varied by adding solid $Ag[Al(OC(CF_3)_3)_4]$ to the acetonitrile solution of the Ln^{3+} complexes and $[Bu_4N][Al(OC(CF_3)_3)_4]$ in the case of Eu^{2+} (Eu^{2+} is oxidized to Eu^{3+} in the presence of Ag^+). The concentration of the $(CF_3SO_3)^-$ was varied by adding the

corresponding amount of solid $[\text{Bu}_4\text{N}][\text{CF}_3\text{SO}_3]$ salt to the acetonitrile solution of each metal ion. All measured data on **1** to **5** complexes are presented in the Appendix A II-7 to A II-11.

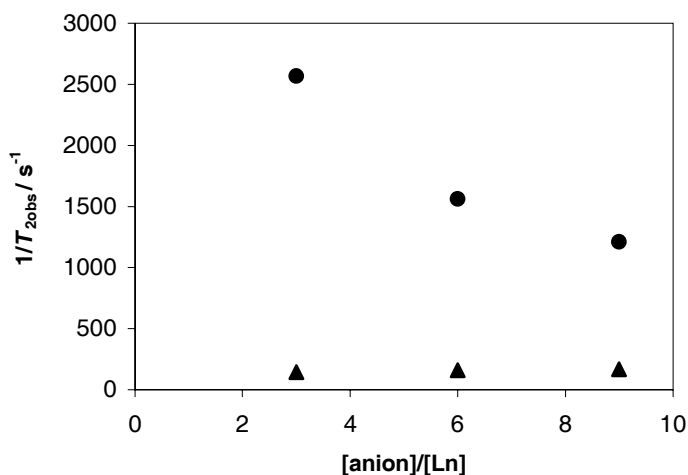


Figure II-6. ^{19}F NMR observed transverse relaxation rates for (●) $\text{Gd}(\text{CH}_3\text{CN})_3(\text{CF}_3\text{SO}_3)_3$ **3** and (▲) $[\text{Gd}(\text{CH}_3\text{CN})_9][\text{Al}(\text{OC}(\text{CF}_3)_3)_4]_3$ as a function of anion concentration variation.

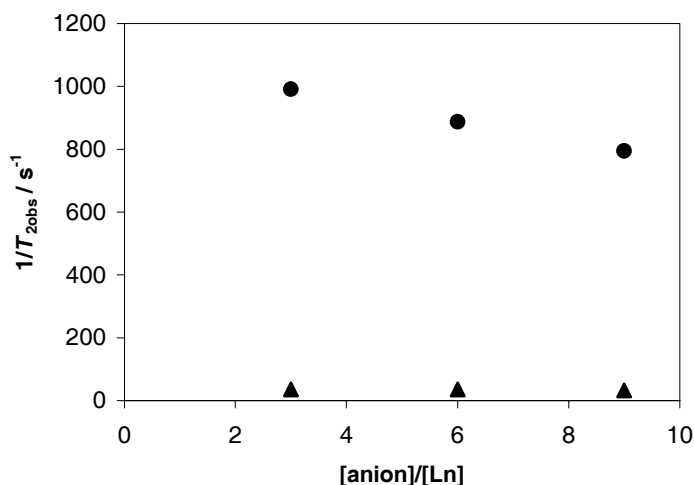


Figure II-7. ^{19}F NMR observed transverse relaxation rates for (●) $\text{Eu}(\text{CH}_3\text{CN})_3(\text{CF}_3\text{SO}_3)_2$ **2a** and (▲) $[\text{Eu}(\text{CH}_3\text{CN})_9][\text{Al}(\text{OC}(\text{CF}_3)_3)_4]_2$ as a function of anion concentration variation.

The results show that relaxation rate measurements can be a useful tool to elucidate whether an atom bearing a nuclear spin coordinates to a paramagnetic center or not. As a conclusion, the hypothesis that $[\text{Al}(\text{OC}(\text{CF}_3)_3)_4]^-$ anion does not coordinate to the paramagnetic centers in **1** to **5** lanthanide complexes in acetonitrile solution is confirmed.

II.4.4 UV-Vis Spectroscopy

UV-Vis spectroscopic measurements were performed on $[Nd(CH_3CN)_9][Al(OC(CF_3)_3)_4]_3$ **1** and $[Eu(CH_3CN)_9][Al(OC(CF_3)_3)_4]_3$ **2** to reveal whether there is or not some coordination equilibrium in the acetonitrile solution of these complexes.

It is well known that Ln^{3+} ions in solution are very labile towards ligand substitution.^[66, 67] In the solid state, owing to X-ray diffraction techniques, the determination of the inner sphere coordination number of lanthanides is straightforward. In solution, due to the above mentioned high lability, the determination of a precise coordination number is very difficult. Nevertheless, in the absorption spectra of several lanthanides, there are some $f-f$ transitions which are particularly sensitive to changes in the inner coordination sphere. Therefore, in function of the multiplicity of the observed transition it is possible to distinguish between different coordination states of the metal.

During the years, from the lanthanide series, solutions of europium complexes were the most studied by UV-Vis spectroscopy. This ion has a $4f^6$ configuration (Figure II-8) and a highly forbidden $^7F_0 \rightarrow ^5D_0$ transition between 577 - 581 nm. This transition is extremely affected in the presence of a ligand field and implies the pairing of two unpaired electrons of the $4f$ orbitals. The degree of variation of the transition compared to that of the free gaseous ion corresponds to the nephelauxetic effect described by Horrocks.^[68]

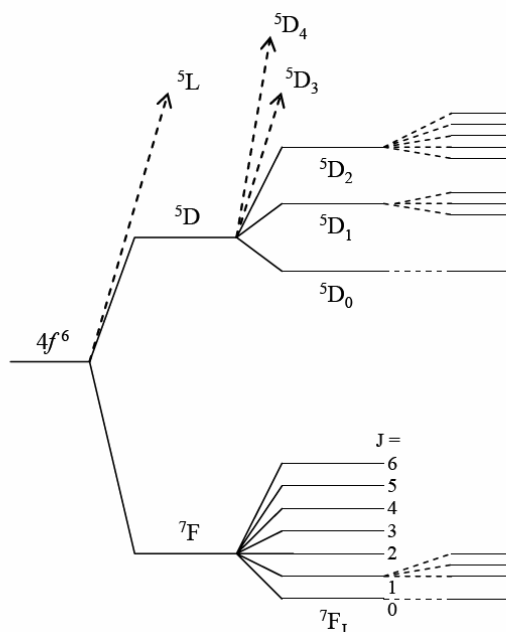


Figure II-8. Electronic configuration of the $4f^6$ electrons of the Eu^{3+} ion.

Some publications can be found in the literature where, an equilibrium between two coordination sites were observed for different Eu^{3+} and Nd^{3+} complexes: $\text{Eu}/\text{H}_2\text{O}$ complexes,^[69] Nd/DMF solvates,^[70] Nd/TMP solvates.^[70]

II.4.4.1 UV-Vis Spectra of $[\text{Nd}(\text{CH}_3\text{CN})_9][\text{Al}(\text{OC}(\text{CF}_3)_3)_4]_3$ 1

The $^4\text{I}_{9/2} \rightarrow ^2\text{P}_{1/2}$ (426 - 435 nm) absorption band in the electronic spectrum of Nd^{3+} is sensitive to environmental changes.^[71] Thus, in dimethylformamide solution the absorption spectra of the $\text{Nd}(\text{ClO}_4)_3/\text{DMF}$ reveals two signals: one for an eight (429.3 nm) and one for a nine (428.2 nm) coordinated species.^[70] These two species are in an equilibrium which can be shifted towards one of the species by varying the temperature or the pressure. As a result, high temperature and pressure stabilize the nine coordinated species. Pisaniello *et al.*^[70] found that in trimethylphosphate (TMP) the behavior of the visible spectra of $\text{Nd}(\text{CF}_3\text{SO}_3)_3/\text{TMP}$ with respect to temperature and pressure is similar to that of the $\text{Nd}(\text{ClO}_4)_3/\text{DMF}$. It also shows equilibrium between two solvated species, but in TMP the equilibrium is between a six and a seven coordinated species.

The UV-Vis spectra of an anhydrous acetonitrile solution of $\text{Nd}[\text{Al}(\text{OC}(\text{CF}_3)_3)_4]_3/\text{CH}_3\text{CN}$ 1 at variable temperatures (from 243 to 320 K) exhibit a single absorption band at 428.62 nm (Figure II-9), which proves that only one species is solvated. The variation of the absorbance upon temperature changes can be explained in term of a temperature dependence of the extinction coefficient (Figure II-10).

In the solid state, the X-ray structure of $\text{Nd}[\text{Al}(\text{OC}(\text{CF}_3)_3)_4]_3/\text{CH}_3\text{CN}$ 1 shows that there are nine acetonitrile molecules in the first coordination sphere of the neodymium ion. In analogy with the X-ray structure of 1, the position of the absorption band in DMF solution of $\text{Nd}(\text{ClO}_4)_3/\text{DMF}$ and with the well known fact that most of the light lanthanides are nine coordinated, one can conclude that in 1, the absorption band at 428.62 nm is due to the nine coordinated specie.

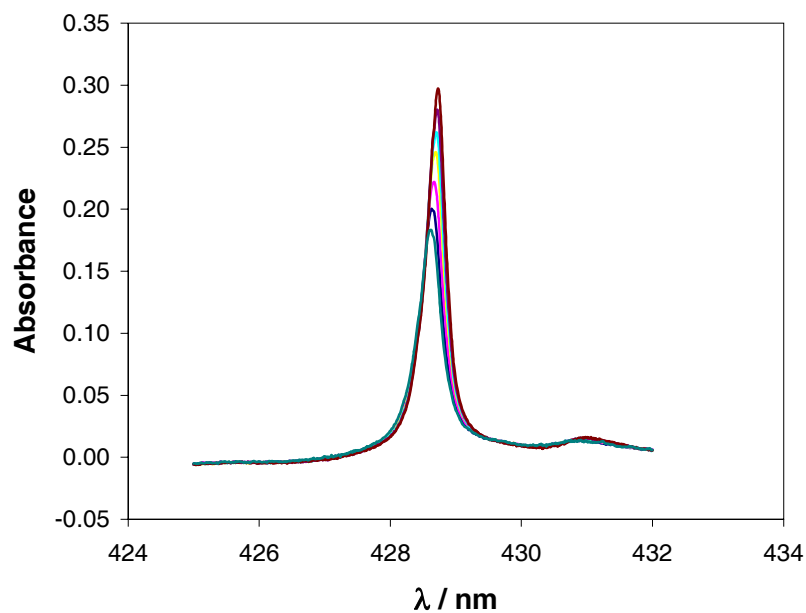


Figure II-9. UV-Vis spectra of **1** in CH_3CN recorded at variable temperature ($c_{Nd} = 10.2$ mM).

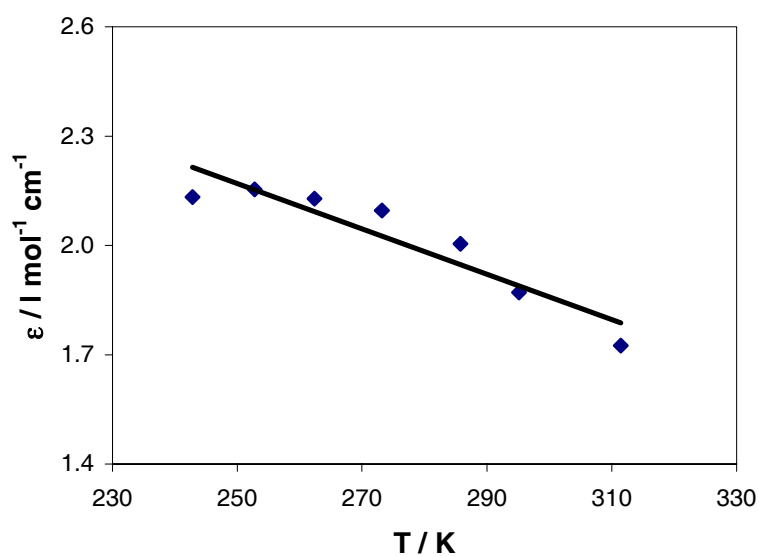


Figure II-10. Temperature dependence of the extinction coefficient for the $^4I_{9/2} \rightarrow ^2P_{1/2}$ transition in the CH_3CN solution of **1**.

II.4.4.2 UV-Vis Spectra of $[Eu(CH_3CN)_9][Al(OC(CF_3)_3)_4]_3$ **2**

The $^7F_0 \rightarrow ^5D_0$ (577 - 581 nm) transition band of Eu^{3+} is very sensitive to the coordination environment and is often used to test the presence of differently coordinated species in solution.^[68, 69, 72] Thus, Graeppi *et al.*^[69] have shown in a study on Eu^{3+}

poly(aminocarboxylate) complexes that the equilibrium is between eight and nine coordinated species. If one expects an $[\text{Eu}(\text{CH}_3\text{CN})_8]^{3+}/[\text{Eu}(\text{CH}_3\text{CN})_9]^{3+}$ equilibrium, one can estimate from the nephelauxetic parameters proposed by Horrocks^[68] that the absorption bands will be separated by about 0.21 nm.

The absorption spectra of an anhydrous acetonitrile solution of the $\text{Eu}[\text{Al}(\text{OC}(\text{CF}_3)_3)_4]_3/\text{CH}_3\text{CN}$ **2** reveals two signals: one at 578.1 nm and one at 579.2 nm, which are insensitive to the variation of temperature from 273 to 322 K, Figure II-11 (condensation problems hindered the measurements of a larger temperature range).

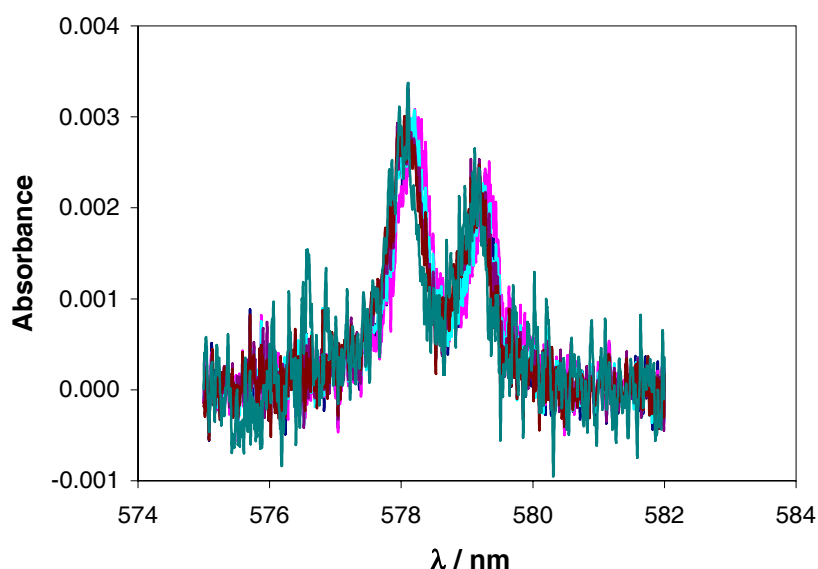


Figure II-11. UV-Vis spectra of **2** in CH_3CN recorded at variable temperature ($c_{\text{Eu}} = 8.2 \text{ mM}$).

From these results one can conclude that there is no coordination equilibrium in the acetonitrile solution of **2**. It is worth to note that high pressure absorption measurements could more clearly strengthen the statement of the absence of a coordination equilibrium, but unfortunately solubility and technical problems (only 2 cm cells are available for high pressure UV measurements) impeded this type of measurements. However, the statement of the absence of a coordination equilibrium is strengthened by the fact that the separation of the two absorption bands (1.1 nm) is much larger than that proposed by Horrocks^[68] for an equilibrium between differently coordinated species. Consequently, the discrepancy with the prediction made by Horrocks^[68] can be explained by the absence of the coordination equilibrium between $[\text{Eu}(\text{CH}_3\text{CN})_8]^{3+}/[\text{Eu}(\text{CH}_3\text{CN})_9]^{3+}$ and by the presence of two different species in the solution. These two species are probably: $[\text{Eu}(\text{CH}_3\text{CN})_n][\text{Al}(\text{OC}(\text{CF}_3)_3)_4]_3$ ($n =$

8 or 9 based on the X-ray structure and/or on the results presented by Moreau^[73]) and $[Eu(CH_3CN)_nCl]Cl_2$.

A fastidious study was performed with two different solutions in order to estimate qualitatively and quantitatively the presence of the absorption band at 579.2 nm. For the qualitative study $EuCl_3$ in CH_3CN was added to the anhydrous acetonitrile solution of **2** in CH_3CN . Figure II-12 clearly shows that successive addition of $EuCl_3$ in CH_3CN to **2** in CH_3CN increases progressively the intensity of the absorption band at 579.2 nm. In order to avoid any ambiguous interpretation of this phenomenon, due to the progressive addition of the Eu^{3+} ion as well with the $EuCl_3/CH_3CN$ solution, a quantitative study was done by progressive addition of a $CuCl$ in CH_3CN solution to a solution of **2** in CH_3CN (Figure II-13).

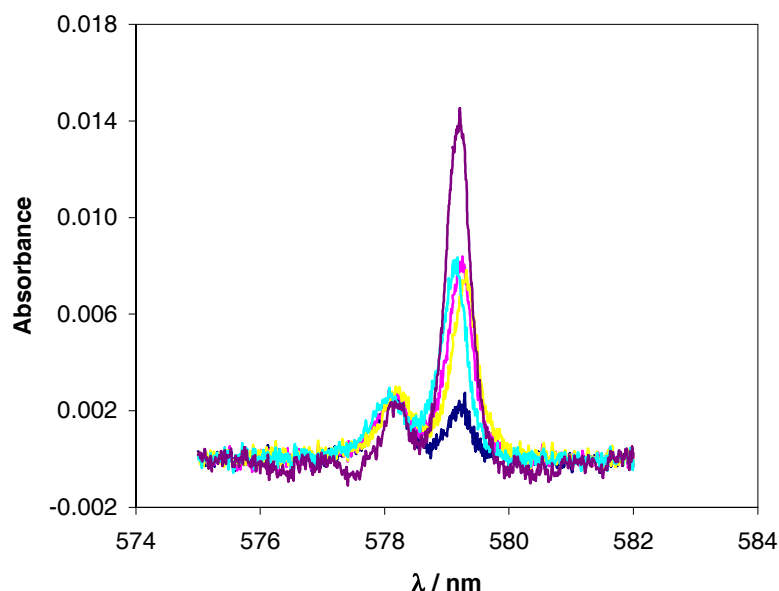


Figure II-12. Influence of the successive addition of an $EuCl_3$ solution in CH_3CN on the UV-Vis spectra of **2** in CH_3CN recorded at variable temperature ($c_{Eu} = 8.5$ mM).

Figures II-11, II-12 and II-13 clearly show that the absorption band at 578.1 nm is influenced neither by the temperature variation nor by the successive addition of chloride. So, it can be concluded that the absorption band at 579.2 nm is due to the ${}^7F_0 \rightarrow {}^5D_0$ transition of a species, in which probably one chloride counter ion is directly coordinated to europium besides the acetonitriles. Additionally, it is evident that the two species have a quite different extinction coefficient. Therefore, just by simply applying the Lambert-Beer law to the absorption of the Eu species and by using a linear regression in the calibration curve of the absorption of Eu-Cl

species vs. the concentration of the added CuCl, the following molar extinction coefficients were obtained: $\epsilon_{\text{Eu}} = 0.04 \text{ l mol}^{-1} \text{ cm}^{-1}$ and $\epsilon_{\text{Eu-Cl}} = 0.44 \text{ l mol}^{-1} \text{ cm}^{-1}$. It is denoted by Eu, the species where no anion is coordinated to the metal center, and by Eu-Cl, the species where besides the acetonitriles probably one chloride counter ion is directly coordinated to europium. From these results, it is obvious that the amount of chlorine in the initial solution of $\text{Eu}[\text{Al}(\text{OC}(\text{CF}_3)_3)_4]_3/\text{CH}_3\text{CN}$ **2** is very small.

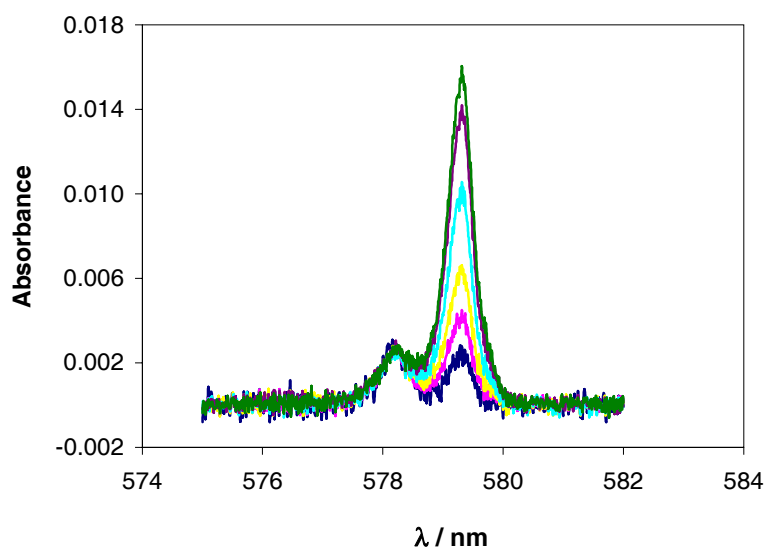


Figure II-13. Influence of the successive addition of an CuCl solution in CH_3CN on the UV-Vis spectra of **2** in CH_3CN recorded at variable temperature ($c_{\text{Eu}} = 7.7 \text{ mM}$; $c_{\text{Cu}} = 3.8 \text{ mM}$).

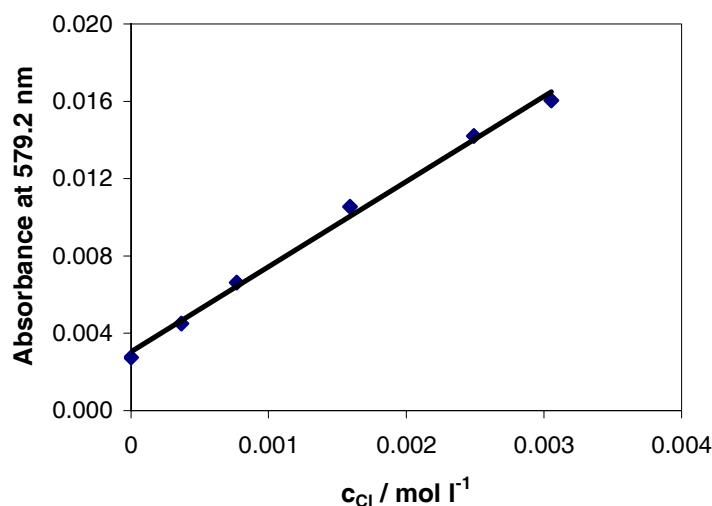


Figure II-14. Calibration curve representing the absorption of EuCl vs. the added chloride concentration.

Furthermore, from the calibration curve (Figure II-14) it was possible to calculate the initial content in chloride of **2** in CH_3CN . In this way, 0.07 % m/m chlorine content was found,

which is in a good agreement with the elemental analysis result ($< 0.1\%$ m/m). This negligible amount of chlorine in the acetonitrile solution of **2** is present as an impurity due to the fact that the starting material for the preparation of the europium salt was $EuCl_3$.

It can be concluded from the UV-Vis spectra of complex **2** that, there is no coordination equilibrium between two solvated species in the $Eu[Al(OC(CF_3)_3)_4]_3/CH_3CN$ solution. The absorption band at 578.1 nm is due to the $f-f$ transition of either $[Eu(CH_3CN)_8]^{3+}$ or $[Eu(CH_3CN)_9]^{3+}$ species. The two arguments proving this are: i) no splitting at variable temperature of the absorption band at 578.1 nm, and ii) the presence of the absorption band at 579.2 nm is due to the $EuCl$ absorption.

Finally, from the UV-Vis measurements, one can conclude that for the nine-coordinated Nd^{3+} and Eu^{3+} ions, there is no coordination equilibrium in the acetonitrile solution of complex **1** and **2**. By analogy, we presume that no coordination equilibrium should be present for the nine-coordinated Gd^{3+} ion (which is the neighbor ion of Eu) in complex **3**. For Dy^{3+} and Tm^{3+} ions, in complexes **4** and **5**, we assume from the X-ray diffraction data that the equilibrium in acetonitrile as well is fully shifted towards nine and eight coordinated species, respectively.

II.5 CONCLUSION

In this study the facile and straightforward one-step synthesis of five homoleptic acetonitrile lanthanide complexes $[Ln(CH_3CN)_n][Al(OC(CF_3)_3)_4]_3$ ($n = 9$: $Ln^{3+} = Nd, Eu, Gd, Dy$; $n = 8$: $Ln^{3+} = Tm$) **1** – **5** has been presented. It has been proved by IR and Raman spectroscopy as well as by the X-ray crystal structures that in the solid state there is no anion coordination to the metal center in the above mentioned complexes. The same conclusion was elaborated in the anhydrous acetonitrile solution of the complexes by conductivity and NMR measurements. UV-Vis spectroscopy results states that there is no coordination equilibrium in the acetonitrile solution of Nd^{3+} **1** and Eu^{3+} **2** complexes. Since in the literature equilibrium between differently coordinated species can be found only for the middle of the lanthanide series (Pm^{3+} , Sm^{3+} and Eu^{3+}), we assume the absence of a coordination equilibrium in the acetonitrile solution of Gd^{3+} **3**, Dy^{3+} **4** and Tm^{3+} **5** complexes as well.

II.6 REFERENCES

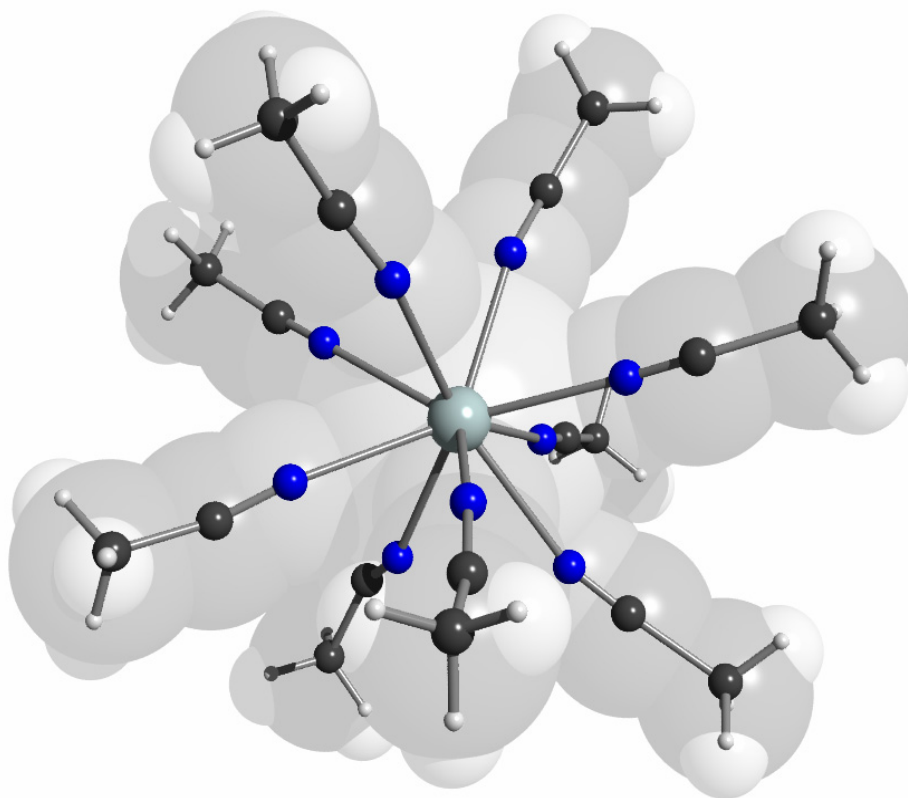
- [1] G. A. Molander, *Chem. Rev.* **1992**, 92, 26.
- [2] A. Kawada, M. Mitamura, S. Kobayashi, *J. Chem. Soc., Chem. Commun.* **1993**, 1157.
- [3] A. Kawada, S. Mitamura, S. Kobayashi, *Chem. Comm.* **1996**, 183.
- [4] R. R. Thomas, V. Chebolu, A. Sen, *J. Am. Chem. Soc.* **1986**, 108, 4096.
- [5] W. Errington, M. P. Spry, G. R. Willey, *Acta Cryst., Sect. C* **1998**, 54, 290.
- [6] J. P. White, H. Deng, E. P. Boyd, J. Gallucci, S. G. Shore, *Inorg. Chem.* **1994**, 33, 1685.
- [7] J. P. White, H. Deng, S. G. Shore, *Inorg. Chem.* **1991**, 30, 2337.
- [8] J.-Y. Hu, Q. Shen, Z.-S. Jin, *Chinese Sci. Bull.* **1990**, 35, 1090.
- [9] G. B. Deacon, B. Görtler, P. C. Junk, E. Lork, R. Mews, J. Petersen, B. Zemva, *J. Chem. Soc., Dalton Trans.* **1998**, 3887.
- [10] G. R. Willey, D. R. Aris, W. Errington, *Inorg. Chim. Acta* **2001**, 318, 97.
- [11] W. J. Evans, M. A. Johnston, M. A. Greci, T. S. Gummersheimer, J. W. Ziller, *Polyhedron* **2003**, 22, 119.
- [12] C. Reed, *Acc. Chem. Res.* **1998**, 31, 133.
- [13] S. H. Strauss, *Chem. Rev.* **1993**, 93, 927.
- [14] I. Krossing, I. Raabe, *Angew. Chem. Int. Ed.* **2004**, 43, 2066.
- [15] A. G. Massey, A. J. Park, *J. Organomet. Chem.* **1964**, 2, 245.
- [16] J. Plešek, T. Jelinek, S. Hermanek, B. Stibr, *Collect. Czech. Chem. Commun.* **1986**, 51, 819.
- [17] C. Reed, *Acc. Chem. Rev.* **1998**, 31, 133.
- [18] S. M. Ivanova, B. G. Nolan, Y. Kobayashi, S. M. Miller, O. P. Anderson, S. H. Strauss, *Chem. Eur. J.* **2001**, 7, 503.
- [19] I. Krossing, *Chem. Eur. J.* **2001**, 7, 490.
- [20] I. Krossing, A. Reisinger, *Coord. Chem. Rev.* **2006**, 250, 2721.
- [21] S. D. Clerc, R. A. Jewsbury, M. G. Mortimer, J. Zeng, *Anal. Chim. Acta* **1997**, 339, 225.
- [22] H. N. McCoy, *J. Am. Chem. Soc.* **1935**, 57, 1756.
- [23] H. N. McCoy, *J. Am. Chem. Soc.* **1936**, 58, 1577.
- [24] D. C. Foster, H. E. Kremers, *Anal. Chem.* **1953**, 25, 1921.
- [25] I. Raabe, S. Müller, N. Trapp, M. Kaupp, I. Krossing, *J. Chem. Soc., Dalton Trans.* **2008**, 946.

- [26] I. Krossing, A. Bihlmeier, I. Raabe, N. Trapp, *Angew. Chem. Int. Ed.* **2003**, *42*, 1531.
- [27] M. Gonsior, I. Krossing, L. Müller, I. Raabe, M. Jansen, L. v. Wüllen, *Chem. Eur. J.* **2002**, *8*, 4479.
- [28] I. Krossing, H. Brands, R. Feuerhake, S. Koenig, *J. Fluorine Chem.* **2001**, *112*, 82.
- [29] I. Krossing, *J. Am. Chem. Soc.* **2001**, *123*, 4603.
- [30] I. Krossing, L. v. Wüllen, *Chem. Eur. J.* **2002**, *8*, 700.
- [31] A. Reisinger, N. Trapp, I. Krossing, S. Altmannshofer, H. Verena, P. Manuel, W. S., *Angew. Chem. Int. Ed.* **2007**, *46*, 8295.
- [32] A. L. Spek, PLATON, A Multipurpose Crystallographic Tool ed., Utrecht University: Utrecht, The Nedrelands, **2007**.
- [33] C. Cossy, A. E. Merbach, *Pure Appl. Chem.* **1988**, *60*, 1785.
- [34] D. M. Young, G. L. Schimek, J. W. Kolis, *Inorg. Chem.* **1996**, *35*, 7620.
- [35] I. Raabe, I. Krossing, K. Wagner, K. Guttsche, *in preparation*.
- [36] I. Raabe, *Ecole Polytechnique Fédérale de Lausanne, Thèse N° 3809*, **2007**, 69.
- [37] R. A. Walton, *Q. Rev. Chem. Soc.* **1965**, *19*, 126.
- [38] W. J. Geary, *Coord. Chem. Rev.* **1971**, *7*, 81.
- [39] I. R. Beattie, P. J. Jones, M. Webster, *J. Chem. Soc. A* **1969**, 218.
- [40] J. V. Quagliano, J. T. Summers, S. Kida, L. M. Vallarino, *Inorg. Chem.* **1964**, *3*, 1557.
- [41] J. H. Forsberg, T. M. Kubik, T. Moeller, K. Gucwa, *Inorg. Chem.* **1971**, *10*, 2656.
- [42] P. Di Bernardo, G. R. Choppin, R. Portanova, P. L. Zanonato, *Inorg. Chim. Acta* **1993**, *207*, 85.
- [43] D. A. Durham, G. H. Frost, F. A. Hart, *J. Inorg. Nucl. Chem.* **1969**, *31*, 833.
- [44] C. D. Schmulbach, I. Y. Ahmed, *Inorg. Chem.* **1971**, *10*, 1902.
- [45] J. L. Burmeister, S. D. Patterson, E. A. Deardorff, *Inorg. Chim. Acta* **1969**, *3*, 105.
- [46] A. Seminara, E. Rizzarelli, *Inorg. Chim. Acta* **1980**, *40*, 249.
- [47] C. P. Prabhakaran, C. C. Patel, *J. Inorg. Nucl. Chem.* **1968**, *30*, 867.
- [48] N. P. Crawford, G. A. Melson, *J. Chem. Soc. A* **1969**, 427.
- [49] W. D. Horrocks, Jr., I. Sipe, J. P., *J. Am. Chem. Soc.* **1971**, *93*, 680.
- [50] J. A. Peters, J. Huskens, D. J. Raber, *Prog. Nucl. Magn. Reson. Spectrosc.* **1996**, *28*, 283.
- [51] Hinckley, *J. Am. Chem. Soc.* **1969**, *91*, 5160.
- [52] S. C.-K. Chu, Y. Xu, J. A. Balschi, C. S. J. Springer, *Magn. Reson. Med.* **1990**, *13*, 239.
- [53] C. T. W. Moonen, S. E. Anderson, S. Unger, *Magn. Reson. Med.* **1987**, *5*, 296.

- [54] A. E. Merbach, E. Toth, *The Chemistry of Contrast Agents in Medical Magnetic Resonance Imaging*, Wiley: Chichester ed., **2001**.
- [55] P. Caravan, J. J. Ellison, T. J. McMurry, R. B. Lauffer, *Chem. Rev.* **1999**, 99, 2293.
- [56] R. K. Harris, E. D. Becker, S. M. Cabral de Menezes, R. Goodfellow, P. Grangere, *Pure Appl. Chem.* **2001**, 73, 1795.
- [57] S. Brownstein, J. Bornais, *J. Magn. Reson.* **1980**, 38, 131.
- [58] A. Bihlmeier, M. Gonsior, I. Raabe, N. Trapp, I. Krossing, *Chem. Eur. J.* **2004**, 10, 5041.
- [59] I. Krossing, *J. Chem. Soc., Dalton Trans.* **2002**, 500.
- [60] D. F. Evans, *J. Chem. Soc.* **1959**, 2003.
- [61] D. F. Evans, G. V. Fazakerley, R. F. Phillips, *J. Chem. Soc. A* **1971**, 1931.
- [62] D. M. Corsi, C. Platas-Iglesias, H. van Bekkum, J. A. Peters, *Magn. Reson. Chem.* **2001**, 39, 723.
- [63] J. H. Van Vleck, in *The theory of electric and magnetic susceptibilities*, London: Oxford University Press, **1966**, p. 243.
- [64] J. Kowalewski, D. Kruk, G. Parigi, *Adv. in Inorg. Chem.* **2005**, 57, 41.
- [65] I. Krossing, I. Raabe, *Chem. Eur. J.* **2004**, 10, 5017.
- [66] L. Helm, A. E. Merbach, *Chem. Rev.* **2005**, 105, 1923.
- [67] F. A. Dunand, L. Helm, A. E. Merbach, *Adv. Inorg. Chem.* **2003**, 54, 1.
- [68] S. T. Frey, W. D. Horrocks, Jr., *Inorg. Chim. Acta* **1995**, 229, 383.
- [69] N. Graepi, D. H. Powell, G. Laurenczy, L. Zékany, A. E. Merbach, *Inorg. Chim. Acta* **1995**, 235, 311.
- [70] D. L. Pisaniello, P. J. Nichols, Y. Ducommun, A. E. Merbach, *Helv. Chim. Acta* **1982**, 65, 1025.
- [71] K. B. Yatsimirskii, N. K. Davidenko, *Coord. Chem. Rev.* **1979**, 27, 223.
- [72] E. Toth, O. M. Ni Dhubhghaill, G. Besson, L. Helm, A. E. Merbach, *Magn. Reson. Chem.* **1999**, 37, 701.
- [73] G. Moreau, R. Scopelliti, L. Helm, J. Purans, A. E. Merbach, *J. Phys. Chem. A* **2002**, 106, 9612.

Chapter III

Acetonitrile exchange on
 $[\text{Ln}(\text{CH}_3\text{CN})_9][\text{Al}(\text{OC}(\text{CF}_3)_3)_4]_z$ where
 $\text{Ln} = \text{Gd}^{3+}$ and Eu^{2+}



III.1 INTRODUCTION

Many studies on solvent exchange reactions in aqueous as well as non-aqueous solvents have been published in the literature,^[2] since Swift and Connick^[1] have described in 1962 the equations for the NMR line broadening in dilute aqueous solutions of paramagnetic ions. However, very few solvent exchange studies on lanthanides and especially in non-aqueous solvents have been carried out. Since then, Bünzli *et al.*^[3, 4] have established the following solvent affinity sequence for $Tb(ClO_4)_3$ and $Tb(NO_3)_3$ on the basis of luminescence data: $DMSO > DMF \sim H_2O > (CH_3)_2CO > CH_3CN$. This sequence is in agreement with the relative basicity of the various donors. More recently this sequence it was also proved to be valid for the $Eu(CF_3SO_3)_2$ complex.^[5] From the above mentioned series, the exchange of the most strongly coordinating DMSO solvent was recorded only for Gd.^[6] H_2O ^[7-13] and DMF ^[14, 15] solvent exchanges have been measured for almost the entire lanthanide series, while the exchange of the least coordinating CH_3CN solvent to lanthanides has never been the subject of a scientific paper. This can be explained by the difficulty to synthesize homoleptic acetonitrile lanthanide complexes, since even the well known weakly coordinating counter ions, such as ClO_4^- and $CF_3SO_3^-$, compete with the CH_3CN ligands for coordination sites.^[16] Nevertheless, due to the high lability of the uncharged acetonitrile ligand, homoleptic acetonitrile lanthanide complexes could be used as essential synthetic precursors to produce a wide range of compounds under non-aqueous conditions. Thus, it would be interesting to get an insight into the kinetics of the acetonitrile exchange reaction on lanthanides.

Divalent lanthanides have received only little attention from coordination chemists because of their strong redox instability. During the recent years interest in Eu^{2+} has been growing because this divalent ion is isoelectronic with the trivalent Gd^{3+} , the favourite magnetic center of contrast agents in medical Magnetic Resonance Imaging (MRI).^[17] It has been shown that Eu^{2+} is sufficiently stable to study structure and water exchange on the aqua ion and on chelate complexes.^[12] Since Eu^{2+} is more stable in acetonitrile than in water,^[18] the solvent exchange reaction in the former could be easily completed.

In this chapter, the study of acetonitrile exchange on $[Ln(CH_3CN)_9][Al(OC(CF_3)_3)_4]_z$ with Ln being one of the isoelectronic $S = 7/2$ ion (Gd^{3+} **3** or Eu^{2+} **2a**), will be presented. The acetonitrile exchange on metal ions can be studied both by 1H or ^{14}N NMR measurements. The coordination of an acetonitrile molecule to the metal center takes place through the

nitrogen atom. The ^{14}N nucleus, being nearest to the paramagnetic metal center, experiences a much larger chemical shifts than do the protons in the coordinated acetonitrile, allowing therefore a more accurate determination of the exchange parameters. As a consequence, in the following studies, the acetonitrile exchange kinetic studies on lanthanides have been completed by ^{14}N NMR measurements. The variable temperature and magnetic fields ^{14}N NMR study yields the kinetic parameters (k_{ex} , ΔH^\ddagger and ΔS^\ddagger) for the exchange of acetonitrile from the first coordination sphere of lanthanides and the bulk. The ^1H NMRD and EPR data permitted to determine the rotational correlation times (τ_R) of both complexes.

III.2 ACETONITRILE EXCHANGE ON THE ISOELECTRONIC Gd^{3+} AND Eu^{2+} IONS

III.2.1 Experimental Part

III.2.1.1 Sample Preparation

Acetonitrile solutions of $[\text{Ln}(\text{CH}_3\text{CN})_9][\text{Al}(\text{OC}(\text{CF}_3)_3)_4]_3$ ($\text{Ln} = \text{Gd}^{3+}$ **3**, Eu^{3+} **2**) were prepared by dissolving the solid lanthanide salts in pure, anhydrous acetonitrile. The pure solvent was kept over molecular sieves and the water content - analyzed by Karl Fischer titration - was less than 5 ppm. The acetonitrile solution of $[\text{Eu}(\text{CH}_3\text{CN})_9][\text{Al}(\text{OC}(\text{CF}_3)_3)_4]_2$ **2a** was obtained by passing the acetonitrile solution of $[\text{Eu}(\text{CH}_3\text{CN})_9][\text{Al}(\text{OC}(\text{CF}_3)_3)_4]_3$ **2** at least 7 times over a glass column filled with Zn/Hg amalgam.^[19] The metal content in the solutions was determined by the bulk magnetic susceptibility techniques described in Chapter II section 2.5.2.

III.2.1.2 ^{14}N NMR Spectroscopy

Longitudinal and transverse ^{14}N relaxation rates as well as chemical shift measurements on $[\text{Gd}(\text{CH}_3\text{CN})_9][\text{Al}(\text{OC}(\text{CF}_3)_3)_4]_3$ **3** ($c_{\text{Gd}} = 1.34 \text{ mmol kg}^{-1}$) and $[\text{Eu}(\text{CH}_3\text{CN})_9][\text{Al}(\text{OC}(\text{CF}_3)_3)_4]_2$ **2a** ($c_{\text{Eu}} = 17.43 \text{ mmol kg}^{-1}$) were performed at temperatures between 228.15 and 349.15 K on Bruker ARX-400 (9.4 T, 28.9 MHz) and Avance II-800 (18.8 T, 57.8 MHz) spectrometers. Bruker BVT-3000 temperature control units were used to maintain a constant temperature,

which was measured by the substitution technique.^[20] The samples were sealed under vacuum in glass spheres adapted to 10 mm NMR tubes to avoid susceptibility correction to the chemical shifts.^[21, 22] The longitudinal and transverse relaxation rates, $1/T_1$ and $1/T_2$, were obtained with the inversion-recovery^[23] and the Carr-Purcell-Meiboom-Gill^[24] spin echo techniques, respectively. The relaxation rates and chemical shifts were measured with regard to pure acetonitrile as external reference.

III.2.1.3 1H NMRD

Longitudinal 1H relaxation rates were measured at 238.15, 268.65, 298.15 and 319.15 K on $[Gd(CH_3CN)_9][Al(OC(CF_3)_3)_4]_3$ **3** ($c_{Gd} = 8.58 \text{ mmol L}^{-1}$) and at 238.15, 268.65 and 298.15 K on $[Eu(CH_3CN)_9][Al(OC(CF_3)_3)_4]_2$ **2a** ($c_{Eu} = 12.95 \text{ mmol L}^{-1}$). The measurements were performed on a Stellar Spinmaster FFC (Fast Field Cycling) relaxometer covering a continuum of magnetic fields from 7×10^{-4} to 0.47 T (corresponding to a proton Larmor frequency range 0.01 – 20 MHz) equipped with a VTC90 temperature control unit. The temperature was regulated by an air or N_2 gas flow. At higher fields, the measurements were performed on different Bruker spectrometers: Avance 200 (2.3 T, 100 MHz; 4.7 T, 200 MHz), ARX-400 (9.4 T, 400 MHz) and Avance II- 800 (18.8 T, 800 MHz). In each case, the temperature was measured by the substitution technique.^[20] The samples were placed in cylindrical sample holders placed into 10 mm NMR tubes. The diamagnetic correction of the pure acetonitrile to the 1H relaxation rates measured at 4.7 T were: 0.104 s^{-1} (238.15 K), 0.077 s^{-1} (268.65 K), 0.068 s^{-1} (298.15 K) and 0.065 s^{-1} (319.15 K).

III.2.1.4 EPR Spectroscopy

EPR spectra of $[Gd(CH_3CN)_9][Al(OC(CF_3)_3)_4]_3$ **3** ($c_{Gd} = 19.23 \text{ mmol kg}^{-1}$) and $[Eu(CH_3CN)_9][Al(OC(CF_3)_3)_4]_2$ **2a** ($c_{Eu} = 17.43 \text{ mmol kg}^{-1}$) were recorded in continuous wave mode at Q- (35 GHz) and X-band (9.4 GHz) on a Bruker ELEXSYS E500 spectrometer at temperatures between 231.65 and 331.05 K. A controlled nitrogen gas flow was used to maintain a constant temperature, which was measured by the substitution technique.^[20] The microwave frequency was measured using a frequency counter embedded in the standard

microwave bridge (X-band) or an external Hewlett-Packard 5353B frequency counter (Q-band).

III.2.1.5 Data Analysis

The simultaneous least-squares fit of ^{14}N NMR, ^1H NMRD and EPR data were performed by the Visualiseur/Optimiseur programs^[25, 26] on a Matlab platform, version 6.5. The errors of the fitted parameters correspond to one standard deviation. The EPR spectra were analyzed by fitting Lorentzian functions using the NMRICMA program^[27] for Matlab.

III.2.2 Equations for the Simultaneous Analysis of the NMR and EPR Data on Gd^{3+} and Eu^{2+} Ions in Anhydrous Acetonitrile Solution

III.2.2.1 ^{14}N NMR Spectroscopy

The ^{14}N NMR measurements provide the longitudinal and transverse relaxation rates and angular frequencies of the paramagnetic solutions, $1/T_1$, $1/T_2$ and ω , and of the acetonitrile reference, $1/T_{1A}$, $1/T_{2A}$ and ω_A . This allows the calculation of the reduced relaxation rates and chemical shift, $1/T_{1r}$, $1/T_{2r}$ and $\Delta\omega_r$ (Eq. III-1 to III-3)^[1, 28]

$$\frac{1}{T_{1r}} = \frac{1}{P_m} \left[\frac{1}{T_1} - \frac{1}{T_{1A}} \right] = \frac{1}{T_{1m} + \tau_m} + \frac{1}{T_{1os}} \quad \text{Eq. III-1}$$

$$\frac{1}{T_{2r}} = \frac{1}{P_m} \left[\frac{1}{T_2} - \frac{1}{T_{2A}} \right] = \frac{1}{\tau_m} \frac{T_{2m}^{-2} + \tau_m^{-1} T_{2m}^{-1} + \Delta\omega_m^2}{(\tau_m^{-1} + T_{2m}^{-1})^2 + \Delta\omega_m^2} + \frac{1}{T_{2os}} \quad \text{Eq. III-2}$$

$$\Delta\omega_r = \frac{1}{P_m} (\omega - \omega_A) = \frac{\Delta\omega_m}{(1 + \tau_m T_{2m}^{-1})^2 + \tau_m^2 \Delta\omega_m^2} + \Delta\omega_{os} \quad \text{Eq. III-3}$$

The parameters $1/T_{1m}$ and $1/T_{2m}$ are the longitudinal and transverse relaxation rates of the bound acetonitriles and $\Delta\omega_m$ is the chemical shift difference between bound and bulk acetonitriles in the absence of exchange. The term τ_m is the mean residence time of the bound

acetonitrile molecules (its inverse is the acetonitrile exchange rate k_{ex}) and P_m is the mole fraction of the bound acetonitriles.

It was found that the outer-sphere contributions ($1/T_{1os}$ and $1/T_{2os}$) to the reduced transverse and longitudinal ^{17}O relaxations rates for Gd^{3+} complexes are negligible.^[22] As the outer-sphere contribution depend on the square of the gyromagnetic ratio and as γ^2 for the ^{14}N nucleus is about 3 times smaller than that for ^{17}O nucleus, one can conclude that outer-sphere contributions to the ^{14}N relaxations are also negligible.

The chemical shift of the bound acetonitrile molecules, $\Delta\omega_m$, depends on the hyperfine interaction between the metal ($Ln = Gd^{3+}$, Eu^{2+}) electron spin S and the ^{14}N nuclear spin I . $\Delta\omega_m$ is directly proportional to the scalar coupling constant, A/\hbar , as expressed in Eq. III-4.^[29] The isotropic Landé factor g_L for Gd^{3+} and Eu^{2+} is equal to 2.0, B represents the magnetic field, T the temperature and k_B is the Boltzmann constant.

$$\Delta\omega_m = \frac{g_L \mu_B S(S+1) B}{3k_B T} \frac{A}{\hbar} \quad \text{Eq. III-4}$$

The outer-sphere contribution to the ^{14}N chemical shift is assumed to be linearly related to $\Delta\omega_m$, through an empirical constant C_{os} (Eq. III-5):^[30]

$$\Delta\omega_{os} = C_{os} \Delta\omega_m \quad \text{Eq. III-5}$$

The ^{14}N longitudinal relaxation rates of the bound acetonitriles, $1/T_{1m}$, in Gd^{3+} and Eu^{2+} solutions are the sum of the contributions of the dipole-dipole, $1/T_{1dd}$, and quadrupolar, $1/T_{1q}$, mechanisms as expressed by Eq. III-6 to III-10; where γ_S is the electron and γ_I is the nuclear gyromagnetic ratio ($\gamma_S = 1.76 \times 10^{11} \text{ rad s}^{-1} \text{ T}^{-1}$, $\gamma_I = 1.93 \times 10^7 \text{ rad s}^{-1} \text{ T}^{-1}$ for ^{14}N), ω_S is the Larmor frequency of the electron spin and ω_I is the ^{14}N resonance frequency, r_{LnN} is the effective distance between the electron spins and the ^{14}N nucleus, I is the nuclear spin (1 for ^{14}N), χ is the quadrupolar coupling constant and η is an asymmetry parameter, τ_R is the rotational correlation time for $Ln-N$ ($Ln = Gd^{3+}$, Eu^{2+}) vector:

$$\frac{1}{T_{1m}} = \frac{1}{T_{1dd}} + \frac{1}{T_{1q}} \quad \text{Eq. III-6}$$

where:

$$\frac{1}{T_{1dd}} = \frac{2}{15} \left(\frac{\mu_0}{4\pi} \right)^2 \frac{\hbar^2 \gamma_I^2 \gamma_S^2}{r_{LnN}^6} S(S+1) \left[3J(\omega_I; \tau_{d1}) + 7 \sum_{k=1}^4 I_k J(\omega_S; \tau_{d2k}) \right]; \quad \text{Eq. III-7}$$

$$\text{with: } J(\omega, \tau) = \frac{\tau}{1 + \omega^2 \tau^2}$$

$$\frac{1}{T_{1q}} = \frac{3\pi^2}{10} \frac{2I+3}{I^2(2I-1)} \chi^2 (1 + \eta^2 / 3) \left[0.2J_1(\omega_I; \tau_R) + 0.8J_2(\omega_I; \tau_R) \right]; \quad \text{Eq. III-8}$$

$$\text{with: } J_n(\omega, \tau) = \frac{\tau}{1 + n^2 \omega^2 \tau^2}; \quad n=1, 2$$

$$\frac{1}{\tau_{1d}} = \frac{1}{\tau_m} + \frac{1}{\tau_R} + \frac{1}{T_{1e}} \quad \text{Eq. III-9}$$

$$\frac{1}{\tau_{2dk}} = \frac{1}{\tau_m} + \frac{1}{\tau_R} + \frac{1}{T_{2ek}} \quad \text{Eq. III-10}$$

The longitudinal electron spin relaxation, $1/T_{1e}$, and the four transverse electron spin relaxation rates, $1/T_{2ek}$, as well as the intensities, I_k , are calculated within the Redfield approximation.^[31]

The second order rotational correlation time, τ_R , is assumed to have a simple exponential temperature dependence, with the τ_R^{298} value at 298.15 K and an E_R activation energy, as given in Eq. III-11:

$$\tau_R = \tau_R^{298} \exp \left[\frac{E_R}{R} \left(\frac{1}{T} - \frac{1}{298.15} \right) \right] \quad \text{Eq. III-11}$$

The ^{14}N transverse relaxation rate of bound acetonitrile, $1/T_{2m}$, in the Gd^{3+} and Eu^{2+} solutions are the sum of the contributions of the scalar ($1/T_{2sc}$), dipole-dipole ($1/T_{2dd}$) and quadrupolar ($1/T_{2q}$) relaxation mechanisms described by the Eq. III-12 to III-17, where A/\hbar is the scalar coupling constant.

$$\frac{1}{T_{2m}} = \frac{1}{T_{2sc}} + \frac{1}{T_{2dd}} + \frac{1}{T_{2q}} \quad \text{Eq. III-12}$$

where:

$$\frac{1}{T_{2sc}} = \left(\frac{A}{\hbar} \right)^2 \frac{S(S+1)}{3} \left[\tau_{sl} + \sum_{k=1}^4 I_k \frac{\tau_{2sk}}{1 + \omega^2 \tau_{2sk}} \right] \quad \text{Eq. III-13}$$

$$\frac{1}{T_{2dd}} = \frac{1}{15} \left(\frac{\mu_0}{4\pi} \right)^2 \frac{\hbar^2 \gamma_I^2 \gamma_S^2}{r_{LnN}^6} S(S+1) \left[4J(0; \tau_{d1}) + 3J(\omega_1; \tau_{d1}) + 13 \sum_{k=1}^4 I_k J(\omega_S; \tau_{d2k}) \right]; \text{Eq. III-14}$$

$$\text{with: } J(\omega, \tau) = \frac{\tau}{1 + \omega^2 \tau^2}$$

$$\frac{1}{T_{2q}} = \frac{3\pi^2}{10} \frac{2I+3}{I^2(2I-1)} \chi^2 (1 + \eta^2 / 3) \left[0.3J_1(0; \tau_R) + 0.5J_1(\omega_1; \tau_R) + 0.2J_2(\omega_1; \tau_R) \right]; \text{Eq. III-15}$$

$$\text{with: } J_n(\omega, \tau) = \frac{\tau}{1 + n^2 \omega^2 \tau^2} ; n=1, 2$$

$$\frac{1}{\tau_{1s}} = \frac{1}{\tau_m} + \frac{1}{T_{1e}} \quad \text{Eq. III-16}$$

$$\frac{1}{\tau_{2sk}} = \frac{1}{\tau_m} + \frac{1}{T_{2ek}} \quad \text{Eq. III-17}$$

The temperature dependence of the acetonitrile exchange rate is described by the Eyring^[32] equation given in Eq. III-18, where ΔS^\ddagger and ΔH^\ddagger are the entropy and enthalpy of activation for the acetonitrile exchange process, and k_{ex}^{298} is the acetonitrile exchange at 298.15 K. R is the perfect gas constant, h and k_B are the Planck and Boltzmann constants, respectively.

$$\frac{1}{\tau_m} = k_{ex} = \frac{k_B T}{h} \exp \left\{ \frac{\Delta S^\ddagger}{R} - \frac{\Delta H^\ddagger}{RT} \right\} = \frac{k_{ex}^{298} T}{298.15} \exp \left\{ \frac{\Delta H^\ddagger}{R} \left(\frac{1}{298.15} - \frac{1}{T} \right) \right\} \quad \text{Eq. III-18}$$

III.2.2.2 1H NMRD

The measured longitudinal proton relaxation rate, R_1^{obs} , is the sum of a paramagnetic and a diamagnetic contribution as expressed in Eq. III-19, where r_1 is the proton relaxivity

(normally expressed in $\text{mM}^{-1} \text{s}^{-1}$) and $\text{Ln} = \text{Gd}^{3+}$ and Eu^{2+} . The metal content is expressed in millimolarity (mmol l^{-1}):

$$R_1^{\text{obs}} = R_1^{\text{d}} + R_1^{\text{p}} = R_1^{\text{d}} + r_1 [\text{Ln}]; r_1 = \frac{R_1^{\text{obs}} - R_1^{\text{d}}}{[\text{Ln}]} \quad \text{Eq. III-19}$$

The relaxivity r_1 can be divided into an inner- and an outer-sphere term as follows:

$$r_1 = r_{1\text{is}} + r_{1\text{os}} \quad \text{Eq. III-20}$$

The inner-sphere term is given in Eq. III-21, where q is the number of inner sphere acetonitrile molecules, 19.15 is the molarity of pure acetonitrile (by using 0.786 g cm^{-3} as the acetonitrile density at room temperature) and T_{1m}^H is the relaxation time of the protons from the acetonitriles directly bound to $\text{Ln} = \text{Gd}^{3+}$ and Eu^{2+} :

$$r_{1\text{is}} = \frac{1}{1000} \frac{q}{19.15} \frac{1}{T_{1m}^H + \tau_m} \quad \text{Eq. III-21}$$

In case of water as solvent media $MW = 18 \text{ g mol}^{-1}$ and therefore $1000/MW = 55.56 \text{ mol dm}^{-3}$. For non-aqueous solvents, for example for acetonitrile $MW = 41.052 \text{ g mol}^{-1}$ and therefore $1000/MW = 24.36 \text{ mol kg}^{-1}$ of solvent. The density of CH_3CN (at ambient temperature) is 0.786 kg dm^{-3} and we obtain **$1000/MW = 19.15 \text{ mol dm}^{-3}$** .

The longitudinal relaxation rate of inner-sphere acetonitrile protons, $1/T_{1m}^H$, is governed by dipolar interaction with the electron spin S , where r_{LnH} is the effective distance between the electron spins and the ^1H nucleus, γ_S is the electron and γ_I nuclear gyromagnetic ratio ($\gamma_I = 2.68 \times 10^8 \text{ rad s}^{-1} \text{T}^{-1}$ for protons), ω_I is the proton resonance frequency and ω_S is the Larmor frequency of the electron spin:

$$\frac{1}{T_{1m}^H} = \frac{2}{15} \left(\frac{\mu_0}{4\pi} \right)^2 \frac{\hbar^2 \gamma_I^2 \gamma_S^2}{r_{\text{LnH}}^6} S(S+1) \left[3J(\omega_I; \tau_{d1}) + 7 \sum_{k=1}^4 I_k J(\omega_S; \tau_{d2k}) \right] \quad \text{Eq. III-22}$$

The outer-sphere contribution to proton relaxivity can be described by Freed's model^[33], where N_A is the Avogadro constant, a_{LnH} is the distance of closest approach of a second-sphere acetonitrile proton to the metal center, D_{LnH} is the mutual diffusion of bulk acetonitriles and the complex, τ_{LnH} is the correlation time for translational diffusion such that $\tau_{LnH} = a_{LnH}^2/D_{LnH}$ and J_{os} is its associated spectral density function.

$$r_{1os} = \frac{32N_A\pi}{405} \left(\frac{\mu_0}{4\pi} \right)^2 \frac{\hbar^2 \gamma_S^2 \gamma_I^2}{a_{LnH} D_{LnH}} S(S+1) \left[3J_{os}(\omega_I, T_{1e}) + 7 \sum_{k=1}^4 I_k J_{os}(\omega_S; T_{2ek}) \right] \quad \text{Eq. III-23}$$

$$J_{os}(\omega, T_{je}) = \text{Re} \left[\frac{1 + \frac{1}{4} \left(i\omega\tau_{LnH} + \frac{\tau_{LnH}}{T_{je}} \right)^{1/2}}{1 + \left(i\omega\tau_{LnH} + \frac{\tau_{LnH}}{T_{je}} \right)^{1/2} + \frac{4}{9} \left(i\omega\tau_{LnH} + \frac{\tau_{LnH}}{T_{je}} \right) + \frac{1}{9} \left(i\omega\tau_{LnH} + \frac{\tau_{LnH}}{T_{je}} \right)^{3/2}} \right]; j = 1, 2 \quad \text{Eq. III-24}$$

The diffusion coefficient, D_{LnH} , for the diffusion of an acetonitrile proton relative to a $Ln = Gd^{3+}$, Eu^{2+} complex is assumed to obey an Arrhenius law, with an activation energy E_{LnH} , and D_{LnH}^{298} the diffusion coefficient at 298.15 K.

$$D_{LnH} = D_{LnH}^{298} \exp \left\{ \frac{E_{LnH}}{R} \left(\frac{1}{298.15} - \frac{1}{T} \right) \right\} \quad \text{Eq. III-25}$$

III.2.2.3 EPR Spectroscopy

Gd^{3+} and Eu^{2+} both have $S = 7/2$ electronic spins. The electron spin relaxations (T_{1e} and T_{2e}) for $S = 7/2$ ions are dominated by zero field splitting (ZFS) interactions. The longitudinal electronic relaxation times, T_{1e} , of $S = 7/2$ ions are too short (≤ 10 ns) to be directly measured by the presently available techniques. Nevertheless, the transverse electronic relaxation time, T_{2e} , (determined indirectly from EPR line widths) allows an estimation of T_{1e} within a framework of a given model of the electronic relaxation. The basic theory of the electronic relaxation for paramagnetic ions, such as Gd^{3+} , was developed by Hudson and Lewis.^[34] In absence of hyperfine coupling they predict the general line shape to be the sum of four Lorentzian curves with different widths and intensities. Since the observed apparent line

shape is nearly Lorentzian, McLachlan^[35] and Powell^[36, 37] used the concept of mean relaxation rates.

$$\left\langle \frac{1}{T_{1e}} \right\rangle = \sum_{k=1}^4 \frac{I_k}{T_{1ek}} \quad \text{and} \quad \left\langle \frac{1}{T_{2e}} \right\rangle = \sum_{k=1}^4 \frac{I_k}{T_{2ek}} \quad \text{Eq. III-26}$$

More recently, Rast, Fries and Borel developed a refined theoretical description of electron spin relaxation including static and transient zero field splitting.^[38-40] In this model the static ZFS is described up to 6th order leading to the three parameters a_2 , a_4 , a_6 . The temporal fluctuation of the static ZFS is described by the rotational diffusion of the complex which itself is linked to the rotational correlation time. The transient ZFS is described using only second order terms by the parameter a_{2T} , and its associated correlation time τ_v . It is assumed that the temperature variation of the correlation times is given by an Arrhenius behavior with activation energies E_R and E_v , respectively.

$$\tau = \tau^{298} \exp \left\{ \frac{E}{R} \left(\frac{1}{T} - \frac{1}{298.15} \right) \right\} \quad \text{Eq. III-27}$$

In the simultaneous analysis of the data only the apparent peak-to-peak widths, ΔH_{pp} , extracted from the experimental EPR spectra was used. Theoretical values of ΔH_{pp} have been obtained from spectra calculated using the Rast, Fries and Borel model within the Redfield approximation together with the parameters mentioned above. Because the lines are relatively narrow hyperfine coupling between the electron spin and the nuclear spin could not be neglected and sums of Lorentzian lines were fitted to the calculated spectra to obtain ΔH_{pp} .^[12, 41]

III.3 RESULTS AND DISCUSSIONS

In order to determine the acetonitrile exchange rate, rotational correlation times and electronic relaxation parameters of the Gd^{3+} **3** and Eu^{2+} **2a** complexes, measurements at variable-temperature ^{14}N NMR at two magnetic fields (9.4 and 18.8 T), multiple fields variable-temperature proton relaxation rates as well as variable-temperature EPR at two frequencies

(9.4 and 35 GHz) were undertaken. All experimental ^{14}N NMR, 1H NMRD and EPR data have been analyzed together in a simultaneous fitting procedure by using the electronic spin relaxation model as developed by Rast, Fries and Borel^[38-40] within the Redfield limit (for equations see Section III.2.2). This analysis results in physically meaningful parameters to describe the electron spin relaxation and it allows an improved combined fit of variable-field ^{14}N NMR, 1H NMRD and electronic relaxation rates compared to the Solomon-Bloembergen-Morgan theory.

In the fitting procedures, the diffusion constant D_{MH}^{298} was fixed at $43.7 \times 10^{-10} \text{ m}^2 \text{ s}^{-1}$, the value of the diffusion of pure acetonitrile.^[42] Proton relaxivities only above 6 MHz were included in the fit, within the validity of the Redfield relaxation theory. The experimental data and the fitted curves for both complexes are shown in Figure III-1 (^{14}N NMR and EPR data) and Figure III-2 (1H NMRD data). The parameters obtained in the fitting procedures are presented in Table III-1.

To analyze the ^{14}N NMR and 1H relaxation experimental data it is necessary to know the number of the acetonitrile molecules coordinated in the first coordination sphere to the metal ions (q). In the solid state nine acetonitrile molecules are coordinated to the metal ion in the Gd^{3+} **3** complex. Several attempts to get crystals of the Eu^{2+} **2a** complex failed, therefore only a hypothesis of a coordination number of nine can be made in concordance with the crystal structure of the Eu^{3+} **2** complex (see Chapter II). In solution, conductivity and ^{19}F NMR data strengthened the supposition that there is no anion coordination to the metal center for any of these complexes. UV-Vis spectroscopic results showed the absence of coordination equilibrium in the Eu^{3+} **2** complex. In consequence, it was assumed that the coordination equilibrium for complexes Eu^{2+} **2a** and Gd^{3+} **3** is totally shifted towards the nine-coordinated species. However, since no unambiguous proof was found to confirm which is the coordination number in solution of both complexes, two separate fits were performed with $q = 8$ and 9 (the most common coordination number of lanthanides in water and organic solvents are 8 or 9 ^[5-10, 12, 15, 43]). In Table III-1, in concordance with the X-ray crystal data, the parameters obtained in the simultaneous fit using a coordination number of nine are presented for both complexes. However, it should be mentioned that the variation of the inner-sphere coordination number would have only a slight effect on the parameters listed in Table III-1. By using a coordination number of eight, which can not be totally excluded, the molar fraction of the coordinated acetonitrile molecules, P_m , is changed. Therefore, the acetonitrile

exchange rate, k_{ex} , would increase with 9/8 (which represents about 12 %) as well as the rotational correlation time, τ_{R} , and the hyperfine coupling constant, A/\hbar . The activation entropy would become higher by $0.8 \text{ J mol}^{-1} \text{ K}^{-1}$. The electronic relaxation parameters would change by less than 4 %.

III.3.1 Determination of the Solvent Exchange Rate Constants

The acetonitrile exchange rate $k_{\text{ex}} = 1/\tau_{\text{m}}$ is directly determining the reduced transverse relaxation rates in the slow exchange region, at low temperatures, where $1/T_{2\text{r}}$ increases with temperature (Figure III-1). At high temperatures, an inverse tendency is observed: $1/T_{2\text{r}}$ is decreasing with temperature. In the fast exchange region, $1/T_{2\text{r}}$ is determined by the transverse relaxation rate of bound acetonitrile, which itself is influenced by k_{ex} , the longitudinal electronic relaxation rates, $1/T_{1\text{e}}$, and by the hyperfine or scalar coupling constant, A/\hbar . By comparing the plots of the ^{14}N transverse relaxation rates ($1/T_{2\text{r}}$) as a function of the inverse of the temperature for the Gd^{3+} and Eu^{2+} complexes, one can observe the presence of two distinct areas in the case of Gd^{3+} . At low temperature $1/T_{2\text{r}}$ increases with the temperature until a maximum and then decreases. This maximum of $1/T_{2\text{r}}$ is characteristic of the changeover from the slow to the fast exchange region. The same changeover between these regimes is also manifested in the reduced chemical shifts: the maximum of $1/T_{2\text{r}}$ corresponds to the inflection point in $\Delta\omega_{\text{r}}$. As this changeover can be observed neither for the temperature dependence of the transverse relaxation rate nor for the chemical shifts of the Eu^{2+} complex, it can be concluded that, even without the knowledge of the fitted results, the acetonitrile exchange rate for the Eu^{2+} complex is faster than that for Gd^{3+} . From Table III-1, it can be seen that the mean lifetime of an acetonitrile molecule ($\tau_{\text{m}} = 1/k_{\text{ex}}$) in the first coordination sphere of Gd^{3+} ($1.8 \times 10^{-8} \text{ s}$) is about 2 orders of magnitude longer than that for the Eu^{2+} ($6.5 \times 10^{-10} \text{ s}$). This can be explained by the quite different ionic radii's of Gd^{3+} (1.107 \AA) and Eu^{2+} (1.300 \AA)^[44] and by the lower charge of europium. In consequence, the electronic attraction of the metal for the acetonitrile nitrogen is larger in the Gd^{3+} complex.

The ^{14}N transverse relaxation rates of bound acetonitrile molecules, $1/T_{2\text{m}}$, are dominated by the scalar relaxation mechanism: $\sim 99 \%$ for the Gd^{3+} complex and $\sim 83 \%$ for the Eu^{2+} complex (see Eq. III- 12 and Appendix Table A III-7 and III-8).

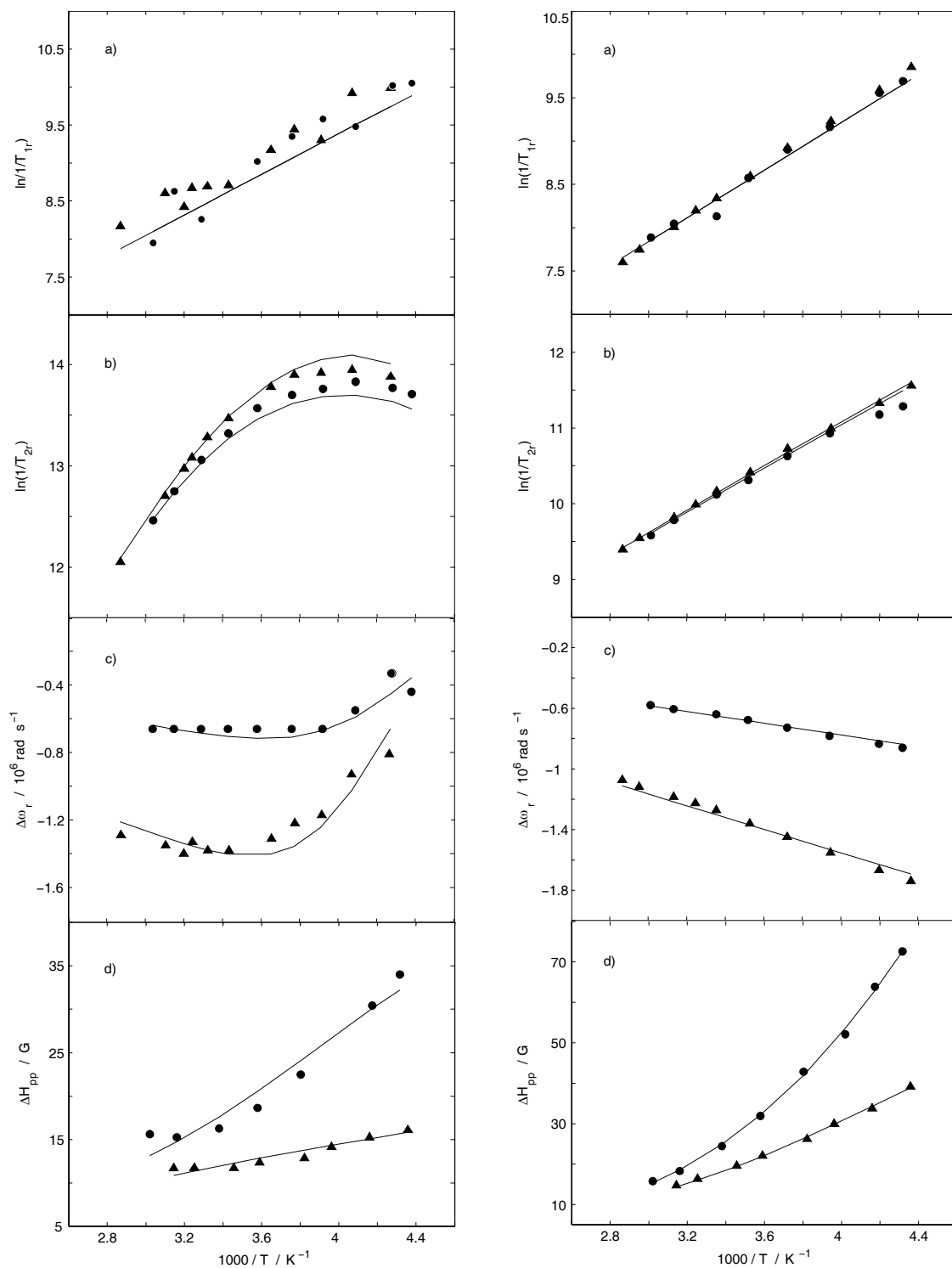


Figure III-1. $[Gd(CH_3CN)_9][Al(OC(CF_3)_3)_4]_3$ (left boxes) and $[Eu(CH_3CN)_9][Al(OC(CF_3)_3)_4]_2$ (right boxes) temperature dependence of the reduced a) longitudinal $1/T_{1r}$ and b) transverse $1/T_{2r}$ ^{14}N relaxation rates; c) ^{14}N chemical shifts $\Delta\omega_r$ at $B = 9.4$ T (●) and 18.8 T (▲); d) EPR peak to peak line widths ΔH_{pp} at X-band (●) and Q-band (▲). The lines through the data points result from the simultaneous least-square fit treatments using Rast-Fries-Borel equations.

The differences between the scalar contributions to the transverse relaxation rates of the bound acetonitrile molecules for the two complexes arise from the differences between the hyperfine coupling constants, A/\hbar . Since in Eq. III-13 A/\hbar is at the second power, small variations of their values ($-2.5 \times 10^6 \text{ rad s}^{-1}$ for Eu^{2+} and $-3.2 \times 10^6 \text{ rad s}^{-1}$ for Gd^{3+}) give the above mentioned influence of the scalar contribution to the transverse relaxation rates of the bound acetonitrile molecules. As A/\hbar is determined by the degree of interaction between the electron spin of the metal and the ^{14}N nucleus it is evident that the hyperfine coupling constant for Eu^{2+} should be lower. The larger, less charged Eu^{2+} ion interacts less strongly with the nitrogen donor atom. This trend has also been observed for $[\text{Eu}(\text{H}_2\text{O})_8]^{2+}$ and $[\text{Gd}(\text{H}_2\text{O})_8]^{3+}$ ions in water.^[11]

The reduced longitudinal relaxation rates, $1/T_{1r}$, in solutions are determined by the rotational correlation time for the Ln-N vector, τ_R , its activation energy, E_R , the quadrupolar coupling constant, $\chi^2(1+\eta^2/3)$, and the Ln-N distance, r_{LnN} (see Eq. III-6 to III-8). For nuclei with spin $I > 1/2$ (for N $I = 1$), the energy of interaction of the nuclear quadrupole moment with the electric field gradient at the nucleus may be quite high. Thus, in the ^{14}N longitudinal relaxation of bound acetonitrile molecules, $1/T_{1m}$, the quadrupolar contribution $\sim 87\%$ becomes the dominant relaxation mechanism for both complexes (Appendix Table A III-7 and A III-8), whilst the dipole-dipole relaxation mechanism has only $\sim 13\%$ contribution. Therefore, the rotational correlation times of the acetonitrile complexes can be determined from ^{14}N NMR longitudinal relaxation rates if the quadrupole coupling constant of the bound acetonitrile ^{14}N nucleus is known (Eq. III-8). In the literature, values like 3.74 MHz (for the solid state)^[45] and 4.22 MHz (for the gas phase)^[46] can be found for the quadrupolar coupling constant of the ^{14}N acetonitrile nucleus. For the Gd^{3+} and Eu^{2+} complexes the quadrupolar coupling constant reached the maximal value of 4.5 MHz in the fitting procedures. Small discrepancies of the quadrupolar coupling constant values from that of the pure solvent have already been presented for gadolinium aqua complexes.^[47] From Table III-1, it can be observed that the relatively smaller Gd^{3+} (1.107 \AA)^[44] complex has a slightly longer rotational correlation time $\tau_R = 14.5 \times 10^{-12} \text{ s}$ than the Eu^{2+} (1.300 \AA) complex $\tau_R = 11.8 \times 10^{-12} \text{ s}$, which is in concordance with the measured $1/T_{1r}$ data. The smaller the rotational correlation time the smaller the reduced longitudinal relaxation rates (if $\chi^2(1+\eta^2/3)$ is the same).

In the fitting procedures, the metal-nitrogen distances r_{LnN} were let to vary between the limit of Ln-N distances found in the X-ray crystal structures for the nine coordinated species (2.40

and 2.60 Å). Finally, r_{LnN} for both complexes, within experimental errors, reached the 2.40 Å value. The r_{LnN} is obtained from the dipole-dipole relaxation (Eq. III-7), which has only a 13 % contribution to $1/T_{1m}$. Due to this low sensitivity of $1/T_{1m}$ to the r_{LnN} values, the metal-nitrogen distances obtained in the fitting procedures may be subject to large errors.

Table III-1. Parameters obtained from the simultaneous fit of ^{14}N NMR, 1H NMRD and EPR data using the Rast-Borel approach to describe electron spin relaxation. Underlined parameters were fixed in the fit.

	$[Gd(CH_3CN)_9]^{3+}$	$[Eu(CH_3CN)_9]^{2+}$
$k_{ex} / 10^6 s^{-1}$	54.9 ± 14.7	1530 ± 202
$\Delta H^\ddagger / kJ mol^{-1}$	25.5 ± 4.5	9.1 ± 1.2
$\Delta S^\ddagger / J mol^{-1} K^{-1}$	-11.1 ± 15.7	-36.2 ± 4.4
$(A/\hbar) / 10^6 rad s^{-1}$	-3.2 ± 0.3	-2.5 ± 0.2
C_{os}	<u>0</u>	<u>0.2</u>
g	1.9927 ± 0.42	1.9933 ± 0.24
$\tau_R^{298} / 10^{-12} s$	14.5 ± 1.8	11.8 ± 1.1
$E_R / kJ mol^{-1}$	10.6 ± 1.4	11.3 ± 0.3
τ_{RH} / τ_R	<u>1</u>	<u>1</u>
$\tau_v^{298} / 10^{-12} s$	0.11 ± 0.1	0.65 ± 0.1
$E_v / kJ mol^{-1}$	0.95 ± 1.8	14.2 ± 0.5
$a_2 / 10^{10} s^{-1}$	0.048 ± 0.027	<u>0</u>
$a_4 / 10^{10} s^{-1}$	<u>0</u>	<u>0</u>
$a_6 / 10^{10} s^{-1}$	0.005 ± 0.0007	0.007 ± 0.0008
$a_{2T} / 10^{10} s^{-1}$	0.65 ± 0.29	0.34 ± 0.02
$D_{LnH}^{298} / 10^{-10} m^2 s^{-1}$	<u>43.7</u>	<u>43.7</u>
$E_{DLnH} / kJ mol^{-1}$	14.4 ± 4.8	13.7 ± 3.4
χ / MHz	<u>4.5</u>	<u>4.5</u>
$r_{LnN} / \text{\AA}$	2.4 ± 0.6	2.4 ± 0.4
$r_{LnH \text{ 1st sphere}} / \text{\AA}$	5.2 ± 1.1	5.3 ± 1.2
$a_{LnH \text{ bulk}} / \text{\AA}$	5.7 ± 5.0	5.4 ± 4.0

Unfortunately, the lack of the high pressure data does not allow for a reliable attribution of the exchange mechanisms. The values of the activation entropies ΔS^\ddagger , $-11.1 J mol^{-1} K^{-1}$ for Gd^{3+} and $-36.2 J mol^{-1} K^{-1}$ for Eu^{2+} , point to an associative activation mode for both complexes.

However, it should be mentioned that since the value of the activation entropy ΔS^\ddagger is obtained by extrapolation to an infinitely high temperature (Eq. III-18), its determination is prone to relatively high uncertainties. Therefore, the sign of the activation entropy can not be used as a precise assessment of the exchange mechanism. Moreover, an associative activation mode implies the formation of a ten-coordinated transition state during the exchange mechanism, coordination number which is quite improbable for lanthanide ions even with the rod-like ligand, CH_3CN .

III.3.2 Rotational Correlation Times by ^1H NMRD

The increase of the longitudinal ^1H relaxation rates for the acetonitrile protons were measured at different temperatures (Figure III-2) and normalized to the millimolar (mmol L^{-1}) concentration of the metal to obtain the proton relaxivities, r_1 , in $\text{mM}^{-1} \text{s}^{-1}$.

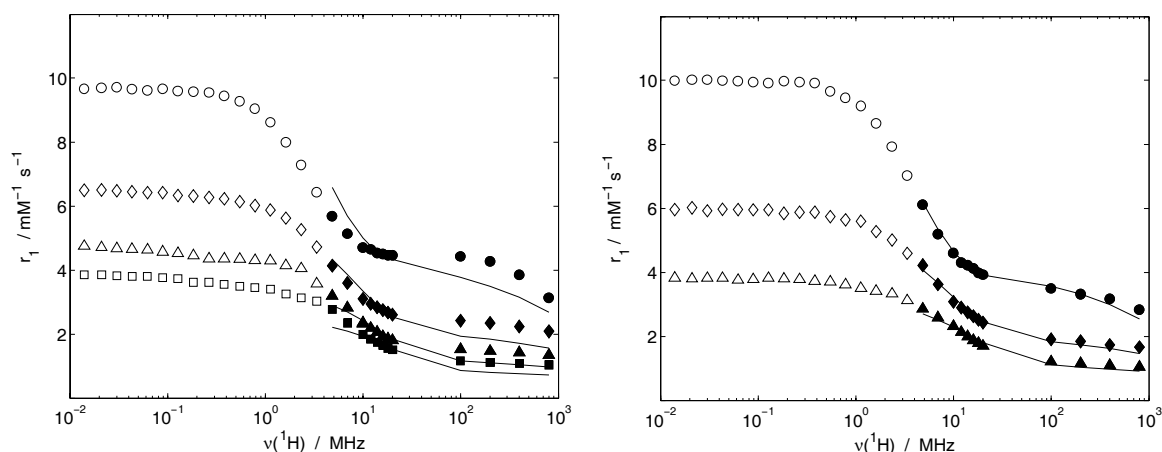


Figure III-2. ^1H NMRD profiles of $[\text{Gd}(\text{CH}_3\text{CN})_9][\text{Al}(\text{OC}(\text{CF}_3)_3)_4]_3$ (left) and $[\text{Eu}(\text{CH}_3\text{CN})_9][\text{Al}(\text{OC}(\text{CF}_3)_3)_4]_2$ (right) at 238 K (\circ), 268.5 K (\diamond), 298 K (\triangle) and 319 K (\square). The lines through the data points result from the least-square fit treatments using Rast-Borel equations. Only high fields (full filled symbols) were considered for the simultaneous fit.

The relaxivity term is widely used in the field of MRI contrast agents, where it is defined as the paramagnetic relaxation rate enhancement of the bulk protons in the presence of 1 mM concentration of the metal.^[48] In the case of MRI contrast agents, the water proton relaxivities are recorded in aqueous media at relatively low metal concentration, when the density is very close to that of the neat water (1 g cm^{-3}). The density of water varies only moderately with

temperature and therefore this variation has been neglected in the calculation of r_1 . Working in non-aqueous solvents, the density variation with temperature could be rather strong. To be compatible with data on aqueous solutions, in this work, the density variation with temperature were not included in the calculation of the r_1 values. However, it should be noted that this variation has influence only on the presentation of the data in the NMRD profiles, but not on the fitted parameters (the variation of the metal concentration, $[Ln]$, in Eq. III-19 and that of the molarity of the pure acetonitrile, 19.15 mol L^{-1} , in Eq. III-21 has the same dependency with the temperature through the density). In this way, the relaxivity values, r_1 , reported in Figure III-2 do not contain corrections due to the density with the temperature.

The 1H NMRD data together with the ^{14}N longitudinal relaxation rates, both hardly influenced by the electronic relaxation, are determining the rotational parameters (see the equations in III.2.2). Due to the lack of an appropriate theory describing the zero-field splitting relaxation mechanism at low fields, the rotational parameters were determined only at high fields (above 10 MHz) since in this region the effect of the electronic relaxation is small. The 1H NMRD profiles have the characteristic line shape of small, rapidly rotating molecules, for which the relaxivity is normally limited by the rotational correlation time, τ_R . By decreasing the temperature, the tumbling slows down, which enhances the relaxivity, as observed in Figure III-2. The rotational correlation time found were: 14.5 and 11.8 ps for the Gd^{3+} and Eu^{2+} complexes, respectively.

Desreux and his coworkers^[49] have determined a rotational correlation time of 51 ps, by using 1H NMRD measured data, for a $Gd(ClO_4)_3$ complex in acetonitrile. They admitted the coordination of one ClO_4^- anion to the Gd^{3+} ion, using therefore a coordination number of eight. It should be mentioned that the presence of an anion in the first coordination sphere of the metal ion can considerably change the acetonitrile exchange rate value. In their data treatments they used a residence time of the acetonitrile in the first coordination sphere of the metal of $\tau_m = 3000 \text{ ps}$ as well as an outer-sphere metal-proton distance of 10.5 \AA which both seems to be overestimated compared to the parameters presented in Table III-1. Hence, it can be concluded that 51 ps is not a relevant value concerning the rotational correlation time for an acetonitrile complex of Gd^{3+} in acetonitrile solution.

According to the observations made by Dunand *et al.*^[50] on the aqua ion the two rotational correlation times for the Ln-N and Ln-H vectors, due to rapid internal rotation of the $-CH_3$

groups, should be different. In the case of acetonitrile, the ratio of the rotational correlation times for Ln-H vector, τ_{RH} , and the overall rotational correlation time, τ_R , is 1, which can be explained by the fact that the Ln-N and Ln-H vectors are nearly collinear.

III.3.3 Electron Spin Relaxation by EPR

The EPR spectra of both complexes were interpreted as superimposed isotropic hyperfine structures of the naturally abundant ^{151}Eu (47.82 %, $I = 5/2$, $\gamma = 6.55 \times 10^7 \text{ T}^{-1} \text{ s}^{-1}$) and ^{153}Eu (52.18 %, $I = 5/2$, $\gamma = 2.94 \times 10^7 \text{ T}^{-1} \text{ s}^{-1}$) isotopes; and ^{155}Gd (14.8 %, $I = 3/2$, $\gamma = -0.83 \times 10^7 \text{ T}^{-1} \text{ s}^{-1}$), ^{157}Gd (15.65 %, $I = 3/2$, $\gamma = -1.08 \times 10^7 \text{ T}^{-1} \text{ s}^{-1}$) isotopes, respectively. For the fitting procedures, the hyperfine coupling constants ($A/g\mu_B$) published by Caravan *et al.*^[12] (37.3 G for ^{151}Eu and 16.4 G for ^{153}Eu) and those published by Borel *et al.*^[41] (4.34 G for ^{155}Gd and 5.67 G for ^{157}Gd) were used. To confirm the validity of the used hyperfine coupling constants for both complexes a test fit were undertaken. The fitting procedures, within experimental errors, gave the hyperfine coupling constants values as published by Caravan *et al.*^[12] and Borel *et al.*^[41] For example at 9.4 GHz and 331 K values like 37.3 ± 0.01 G for ^{151}Eu and 16.6 ± 0.02 G for ^{153}Eu were found; while for Gd values like 4.77 ± 0.11 G for ^{155}Gd and 6.06 ± 0.07 G for ^{157}Gd have been determined (see Appendix Figure A III-1). The splitting due to the hyperfine coupling between the electronic spin and the metal nuclear spin can be seen only in EPR spectra of the Eu^{2+} complex. The splitting becomes more evident at high temperatures. A representative EPR spectrum of the Eu^{2+} complex is shown in Figure III-3.

The electronic relaxation rates, $1/T_{ic}$ ($i = 1, 2$), influence both ^{14}N and ^1H NMR relaxation in both complexes and are generally governed by the static and transient zero-field splitting.^[38, 39] The peak-to-peak widths, ΔH_{pp} , and central fields, B_0 , were extracted by fitting a superposition of Lorentzian's to the experimental spectra with automatic phase and baseline adjustments. The line widths and shifts were analyzed within the framework of the Rast-Borel model,^[38, 39] using only the reduced values for ΔH_{pp} and B_0 instead of the full line shape. This model assumes that the electron spin relaxation is determined by the so-called static or average ZFS, which is rapidly modulated by molecular tumbling, and by the transient ZFS, which is modulated by rapid random distortions of the complex. The least-squares fit procedure yields the following parameters: the static ZFS magnitude parameters a_2 , a_4 , a_6 , and the rotational correlation time τ_R and the activation energy E_R ; the transient ZFS magnitude

a_{2T} , the associated correlation time τ_v and activation energy E_v , plus the natural g -factor (for the fitted values see Table III-1). It has to be mentioned that, the central fields, B_0 , values were excluded from the simultaneous fit for both complexes, due to the fact that a precise determination of B_0 is difficult, and in our case gave unsatisfactory results. Therefore, only the fitted and measured data of ΔH_{pp} are presented in Figure III-1. From Table III-1 can be seen the presence of the second, a_2 , and six order contribution, a_6 , of the static ZFS for the Gd^{3+} complex, while for Eu^{2+} only a small contribution of the six order term of the static ZFS is present. Also, it can be concluded that for both complexes the major contribution to the electron spin relaxation arises from the transient ZFS, a_{2T} . The fact that the static ZFS contributions are very small (even close to zero for Eu) shows that the first coordination sphere around the metal have relatively high symmetry. For the two complexes the line widths (ΔH_{pp}) decreases both with the temperature and the resonance frequency (Figure IV-1). This is consistent with a modulated transient zero field splitting relaxation mechanism.^[51] The Gd^{3+} complex presents sharper lines than the Eu^{2+} complex at both frequencies.

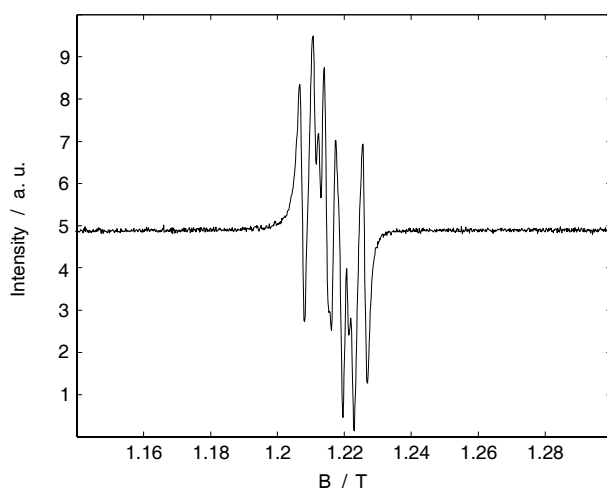


Figure III-3. Representative Q-band EPR spectrum of $[Eu(CH_3CN)_9][Al(OC(CF_3)_3)_4]_2$ in anhydrous acetonitrile at $T = 318$ K.

In 1989 Veselov *et al.*^[52] published the ERP line widths of the $Gd(NO_3)_3$ ion in different solvents. They found that, in acetonitrile the peak-to-peak line widths, ΔH_{pp} , of Gd^{3+} vary from 130 to 300 G. The large line broadening in the work of Veselov compared to those observed in this work (see Figure III-1) can be attributed to the coordination of NO_3^- anion to the metal center, coordination which causes the lowering of the symmetry around the metal center. A similar EPR line broadening due to anion coordination can be seen in the spectra of an acetonitrile solution of $GdCl_3$ as it can be seen in Figure III-4, where the dashed lines

represents the line broadening of Gd^{3+} in the acetonitrile solution of GdCl_3 and the continues one those of the Gd^{3+} in complex **3**. From these examples it is quite evident that the EPR line widths are strongly correlated with the symmetry around the metal center: more the symmetry is high more the line widths are sharp. Consequently, the extremely sharp lines in the EPR spectra of complexes **2a** and **3** bring further proves that the $[\text{Al}(\text{OC}(\text{CF}_3)_3)_4]^-$ anion does not coordinates to the metal center in the acetonitrile solution of Gd^{3+} and Eu^{2+} ions. In this way, one can conclude that the acetonitrile exchange rates measured for these complexes are really the solvent exchange rates of homoleptic acetonitrile lanthanide solvates.

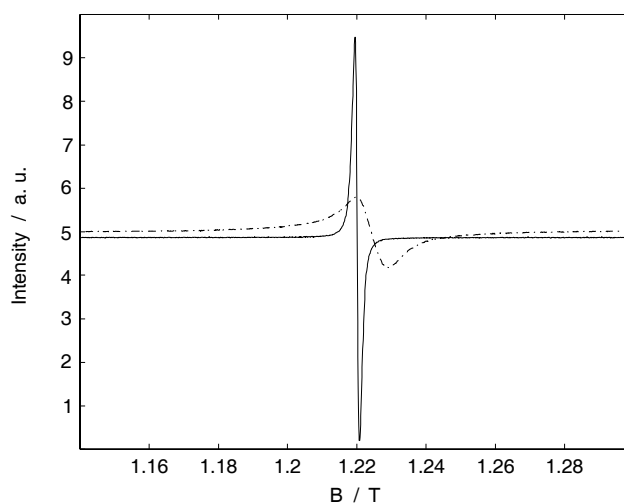


Figure III-4. Comparison between the Q-band EPR spectra of GdCl_3 (---) and $[\text{Gd}(\text{CH}_3\text{CN})_9][\text{Al}(\text{OC}(\text{CF}_3)_3)_4]_3$ (—) in anhydrous acetonitrile at $T = 272 \text{ K}$.

III.4 CONCLUSION

In this chapter it have been described the acetonitrile exchange on the fully solvated Gd^{3+} and Eu^{2+} ions, as a function of temperature, by a combined ^{14}N NMR, ^1H NMRD and EPR study. The approach taken to analyse the experimental data was the same as it was described for the corresponding aqua ions.^[12, 31, 37] The obtained kinetic parameters k_{ex}^{298} (10^6 s^{-1}), ΔH^\ddagger (kJ mol^{-1}) and ΔS^\ddagger ($\text{J mol}^{-1} \text{ K}^{-1}$) for the two complexes were: 55 ± 14.7 , 25.5 ± 4.5 , and -11.1 ± 15.7 for Gd^{3+} , while for Eu^{2+} the corresponding values were 1530 ± 202 , 9.1 ± 1.2 , and -36.2 ± 4.4 . As expected, the larger, less highly charged $[\text{Eu}(\text{CH}_3\text{CN})_9]^{2+}$ ion undergoes acetonitrile exchange faster than $[\text{Gd}(\text{CH}_3\text{CN})_9]^{3+}$. To our best knowledge, this is the first time when a non-aqueous solvent exchange was measured on a divalent lanthanide ion.

III.5 REFERENCES

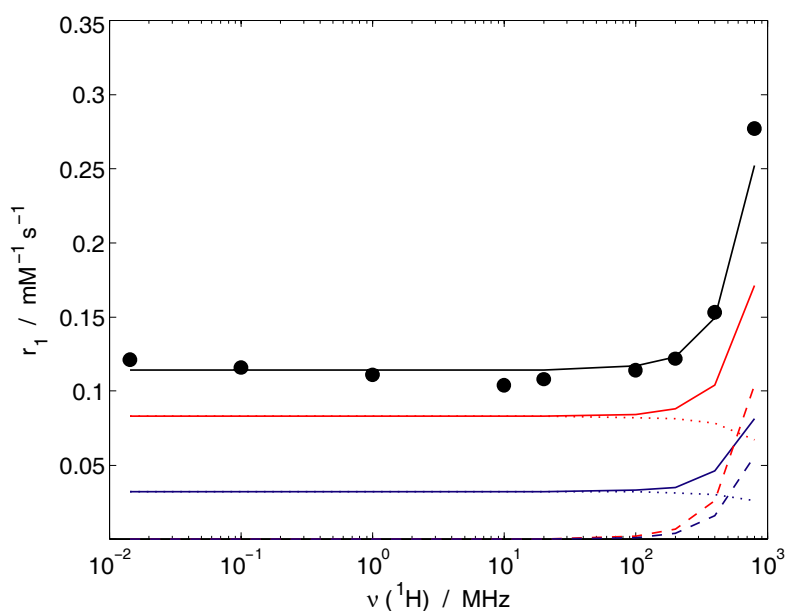
- [1] T. J. Swift, R. E. Connick, *J. Chem. Phys.* **1962**, 37, 307.
- [2] L. Helm, A. E. Merbach, *Chem. Rev.* **2005**, 105, 1923.
- [3] J.-C. G. Bünzli, M. M. Vuckovic, *Inorg. Chim. Acta* **1983**, 73, 53.
- [4] J.-C. G. Bünzli, A. Milicic-Tang, in *Handbook on the Physics and Chemistry of Rare Earth* (Eds.: K. A. Gschneidner, L. a. J. Eyring), Elsevier Science B. V., **1995**, pp. 305.
- [5] G. Moreau, R. Scopelliti, L. Helm, J. Purans, A. E. Merbach, *J. Phys. Chem. A* **2002**, 106, 9612.
- [6] R. Dessapt, L. Helm, A. E. Merbach, *J. Phys. Condens. Matter* **2004**, 14, S1027.
- [7] C. Cossy, L. Helm, A. E. Merbach, *Inorg. Chem.* **1988**, 27, 1973.
- [8] C. Cossy, L. Helm, A. E. Merbach, *Inorg. Chem.* **1989**, 28, 2699.
- [9] K. Micskei, D. H. Powell, L. Helm, E. Brücher, A. E. Merbach, *Magn. Reson. Chem.* **1993**, 31, 1011.
- [10] D. H. Powell, A. E. Merbach, *Magn. Reson. Chem.* **1994**, 32, 739.
- [11] P. Caravan, A. E. Merbach, *Chem. Comm.* **1997**, 2147.
- [12] P. Caravan, É. Tóth, A. Rockenbauer, A. E. Merbach, *J. Am. Chem. Soc.* **1999**, 121, 10403.
- [13] G. Moreau, L. Helm, J. Purans, A. E. Merbach, *J. Phys. Chem. A* **2002**, 106, 3034.
- [14] D. L. Pisaniello, L. Helm, D. Zbinden, A. E. Merbach, *Helv. Chim. Acta* **1983**, 66, 1872.
- [15] D. L. Pisaniello, L. Helm, P. Meier, A. E. Merbach, *J. Am. Chem. Soc.* **1983**, 105, 4528.
- [16] P. Di Bernardo, G. R. Choppin, R. Portanova, P. L. Zanonato, *Inorg. Chim. Acta* **1993**, 207, 85.
- [17] E. Toth, L. Burai, A. E. Merbach, *Coord. Chem. Rev.* **2001**, 216-217, 363.
- [18] J. F. Coetzee, D. K. McGuire, J. L. Hedrick, *J. Phys. Chem.* **1963**, 9, 1814.
- [19] S. D. Clerc, R. A. Jewsbury, M. G. Mortimer, J. Zeng, *Anal. Chim. Acta* **1997**, 339, 225.
- [20] C. Ammann, P. Meier, A. E. Merbach, *J. Magn. Reson.* **1982**, 46, 319.
- [21] A. D. Hugi, L. Helm, A. E. Merbach, *Helv. Chim. Acta* **1985**, 68, 508.
- [22] K. Micskei, L. Helm, E. Brucher, A. E. Merbach, *Inorg. Chem.* **1993**, 32, 3844.
- [23] R. L. Vold, J. S. Waugh, M. P. Klein, D. E. Phelps, *J. Chem. Phys.* **1968**, 48, 3831.

- [24] S. Meiboom, D. Gill, *Rev. Sci. Instrum.* **1958**, 29, 688.
- [25] F. Yerly, *VISUALISEUR 2.3.5* ed., Université de Lausanne: Lausanne, Switzerland, **1999**.
- [26] F. Yerly, *OPTIMISEUR 3.0.0* ed., Université de Lausanne: Lausanne, Switzerland, **1999**.
- [27] L. Helm, A. Borel, F. Yerly, *NMRICMA 3.0.4* ed., EPFL: Lausanne, Switzerland **2004**.
- [28] J. R. Zimmerman, W. E. Brittin, *J. Phys. Chem.* **1957**, 61, 1328.
- [29] H. G. Brittain, J. F. Desreux, *Inorg. Chem.* **1984**, 23, 4459.
- [30] G. Gonzalez, D. H. Powell, V. Tissieres, A. E. Merbach, *J. Phys. Chem.* **1994**, 98, 53.
- [31] A. Borel, F. Yerly, L. Helm, A. E. Merbach, *J. Am. Chem. Soc.* **2002**, 124, 2042.
- [32] H. Eyring, *J. Chem. Phys.* **1935**, 3, 107.
- [33] J. H. Freed, *J. Chem. Phys.* **1978**, 68, 4034.
- [34] A. Hudson, J. W. E. Lewis, *Trans. Faraday Soc.* **1970**, 66, 1297.
- [35] A. D. McLachlan, *Proc. Roy. Soc. (London) Ser. A* **1964**, 280, 271.
- [36] D. H. Powell, A. E. Merbach, G. Gonzalez, E. Brücher, K. Micskei, M. F. Ottaviani, K. Köhler, A. Zelewsky, O. Y. Grinberg, Y. S. Lebedev, *Helv. Chim. Acta* **1993**, 76, 2129.
- [37] D. H. Powell, O. M. Ni Dhubhghaill, D. Pubanz, L. Helm, Y. S. Lebedev, W. Schlaepfer, A. E. Merbach, *J. Am. Chem. Soc.* **1996**, 118, 9333.
- [38] S. Rast, P. H. Fries, *J. Chem. Phys.* **2000**, 113, 8724.
- [39] S. Rast, A. Borel, L. Helm, E. Belorizky, P. H. Fries, A. E. Merbach, *J. Am. Chem. Soc.* **2001**, 123, 2637.
- [40] S. Rast, P. H. Fries, E. Belorizky, A. Borel, L. Helm, A. E. Merbach, *J. Chem. Phys.* **2001**, 115, 7554.
- [41] A. Borel, H. Kang, C. Gateau, M. Mazzanti, R. B. Clarkson, R. L. Belford, *J. Phys. Chem. A* **2006**, 110, 12434.
- [42] M. Holz, H. Weingärtner, *J. Magn. Reson.* **1991**, 92, 115.
- [43] D. L. Pisaniello, A. E. Merbach, *Helv. Chim. Acta* **1982**, 65, 573.
- [44] R. D. Shannon, *Acta Cryst., Sect. A* **1976**, A32, 751.
- [45] P. A. Casabella, P. J. Bray, *J. Chem. Phys.* **1958**, 29, 1105.
- [46] M. K. Kemp, J. M. Pochan, W. H. Flygare, *J. Phys. Chem.* **1967**, 71, 765.
- [47] O. V. Yazyev, L. Helm, *J. Chem. Phys.* **2006**, 125, 054503.

- [48] A. E. Merbach, E. Toth, *The Chemistry of Contrast Agents in Medical Magnetic Resonance Imaging*, Wiley: Chichester ed., **2001**.
- [49] B. Lambert, V. Jacques, A. Shivanyuk, S. E. Matthews, A. Tunayar, M. Baaden, G. Wipff, V. Böhmer, J. F. Desreux, *Inorg. Chem.* **2000**, 39, 2033.
- [50] F. A. Dunand, A. Borel, A. E. Merbach, *J. Am. Chem. Soc.* **2002**, 124, 710.
- [51] L. Banci, I. Bertini, C. Luchinat, *Nuclear and Electron Relaxation*, VCH: New York, **1991**.
- [52] I. A. Veselov, V. G. Shtyrilin, A. V. Zakharov, *Koord. Khim.* **1989**, 15, 567.

Chapter IV

Acetonitrile exchange on
 $[\text{Ln}(\text{CH}_3\text{CN})_n][\text{Al}(\text{OC}(\text{CF}_3)_3)_4]_3$ where
 $n = 9$, $\text{Ln}^{3+} = \text{Nd}$ and Dy ;
 $n = 8$, $\text{Ln}^{3+} = \text{Tm}$



IV.1 INTRODUCTION

Since the pioneering work of Swift and Connick^[1] only a few solvent exchange reactions in non-aqueous solvents have been published with lanthanide ions (for references see Chapter I Section I.5.2). None of these works is dealing with non-aqueous solvent exchange reaction on light lanthanides, mainly due to the fact that for these metals even at relatively high magnetic fields (9.4 and 14.1 T) the kinetic effect ($\Delta\omega_m^2/k_{\text{ex}}$) is too small. Measurements performed at an even higher magnetic field (18.8 T) enabled, for the first time, the determination of a non-aqueous solvent exchange rate on the light lanthanide ion Nd^{3+} . The acetonitrile exchange reaction have been studied for Dy^{3+} and Tm^{3+} ions as well, in order to get an insight into the evolution of the acetonitrile exchange rate over the lanthanide series.

For lanthanide ions (except for the isoelectronic Gd^{3+} and Eu^{2+} with $S = 7/2$), the electronic relaxation times govern the correlation times and therefore, indirectly, the relaxation times. In this way, they play a crucial role in the estimation of the solvent exchange rates. Up to now, the electronic relaxation times of lanthanide ions have been determined only in aqueous solution.^[2] It was found that they are very short, magnetic field independent and substantially temperature independent. The order of magnitude of the electronic relaxation times for lanthanide ions is about 10^{-12} - 10^{-13} s, except for the isoelectronic Gd^{3+} and Eu^{2+} ions^[3] for which they are about 10^{-8} - 10^{-9} s. In view of their importance, and since they have never been studied in non-aqueous solvent, it seems to be worth to determine the electronic relaxation times of lanthanide ions in anhydrous acetonitrile.

In this chapter the study of the acetonitrile exchange reaction on three lanthanide complexes $[\text{Ln}(\text{CH}_3\text{CN})_n][\text{Al}(\text{OC}(\text{CF}_3)_3)_4]_3$ ($n = 9$, $\text{Ln} = \text{Nd}$ **1** and Dy **4**; $n = 8$, $\text{Ln} = \text{Tm}$ **5**), by ^{14}N NMR and ^1H NMRD spectroscopy, will be presented. The variable temperature and magnetic field ^{14}N NMR study yields the kinetic parameters (k_{ex} , ΔH^\ddagger and ΔS^\ddagger) for the exchange of acetonitriles from the first coordination sphere of lanthanides and that of the bulk. The ^1H NMRD data coupled with those of the ^{14}N NMR longitudinal relaxation rates led to the determination of the electronic relaxation times (τ_S) and the rotational correlation times (τ_R) of the Nd^{3+} **1**, Dy^{3+} **4** and Tm^{3+} **5** complexes in anhydrous acetonitrile.

IV.2 ACETONITRILE EXCHANGE ON Nd³⁺, Dy³⁺ AND Tm³⁺ IONS

IV.2.1 Experimental Part

IV.2.1.1 Sample Preparation

Acetonitrile solutions of [Ln(CH₃CN)_n][Al(OC(CF₃)₃)₄]₃ (n = 9, Ln = Nd³⁺ **1**, Dy³⁺ **4**; n = 8, Ln = Tm³⁺ **5**) were prepared by dissolving the solid lanthanide salts in pure, anhydrous acetonitrile. The pure solvent was kept over molecular sieves and the water content - analyzed by Karl Fischer titration - was less than 5 ppm. The metal content in the solutions was determined by the bulk magnetic susceptibility techniques described in Chapter II Section 2.5.2.

IV.2.1.2 ¹⁴N NMR Spectroscopy

Longitudinal and transverse ¹⁴N relaxation rates as well as chemical shift measurements on [Nd(CH₃CN)₉][Al(OC(CF₃)₃)₄]₃ **1** (c_{Nd} = 15.98 mmol kg⁻¹), [Dy(CH₃CN)₉][Al(OC(CF₃)₃)₄]₃ **4** (c_{Dy} = 15.92 mmol kg⁻¹) and [Tm(CH₃CN)₈][Al(OC(CF₃)₃)₄]₃ **5** (c_{Tm} = 70.72 mmol kg⁻¹), were performed at temperatures between 228.15 and 349.15 K on Bruker ARX-400 (9.4 T, 28.9 MHz) and Avance II-800 (18.8 T, 57.8 MHz) spectrometers. Bruker BVT-3000 temperature control units were used to maintain a constant temperature, which was measured by the substitution technique.^[4] The samples were sealed in glass spheres adapted to 10 mm NMR tubes to avoid susceptibility correction to the chemical shifts.^[5, 6] The longitudinal and transverse relaxation times, *T*₁ and *T*₂, were obtained with the inversion-recovery^[7] and the Carr-Purcell-Meiboom-Gill^[8] spin echo techniques, respectively. Pure acetonitrile was used as external reference.

IV.2.1.3 ¹H NMRD

Longitudinal ¹H relaxation rates were measured at 238.15 and 298.15 K on [Nd(CH₃CN)₉][Al(OC(CF₃)₃)₄]₃ **1** (c_{Nd} = 11.92 mM), [Dy(CH₃CN)₉][Al(OC(CF₃)₃)₄]₃ **4** (c_{Dy} = 48.45 mM) and [Tm(CH₃CN)₈][Al(OC(CF₃)₃)₄]₃ **5** (c_{Tm} = 70.44 mM). The measurements

were performed on a Stellar Spinmaster FFC (Fast Field Cycling) relaxometer covering a continuum of magnetic fields from 7×10^{-4} to 0.47 T (corresponding to a proton Larmor frequency range 0.01 – 20 MHz) equipped with a VTC90 temperature control unit. The temperature was regulated by an air or N_2 gas flow. At higher fields, the measurements were performed on different Bruker spectrometers: an Avance 200 (2.3 T, 100 MHz; 4.7 T, 200 MHz), ARX-400 (9.4 T, 400 MHz) and Avance II- 800 (18.8T, 800 MHz). In each case, the temperature was measured by the substitution technique.^[4] The samples were placed in cylindrical sample holders. The diamagnetic correction of the pure acetonitrile to the 1H relaxation rates were 0.104 s^{-1} (238.15 K) and 0.068 s^{-1} (298.15 K).

IV.2.1.4 Data Analysis

The individual least-squares fit of ^{14}N NMR as well as 1H NMRD together with the $1/T_{1r}$ results of ^{14}N NMR data were performed by the Visualiseur/Optimiseur programs,^[9, 10] on a Matlab platform, version 6.5. The errors of the fitted parameters correspond to one standard deviation.

IV.2.2 Equations for the Analysis of ^{14}N NMR and 1H NMRD Data on Nd^{3+} , Dy^{3+} and Tm^{3+} Ions in Acetonitrile Solution

IV.2.2.1 ^{14}N NMR Spectroscopy

The Swift - Connick^[1] and Zimmermann - Brittin^[11] approaches were used to determine the kinetic parameters of the acetonitrile exchange reaction on Nd^{3+} , Dy^{3+} and Tm^{3+} Eq. IV-1 to IV-3:

$$\frac{1}{T_2} - \frac{1}{T_{2A}} = P_m \left[k_{ex} \frac{T_{2m}^{-2} + k_{ex} T_{2m}^{-1} + \Delta\omega_m^2}{(k_{ex} + T_{2m}^{-1})^2 + \Delta\omega_m^2} + \frac{1}{T_{2os}} \right] \quad \text{Eq. IV-1}$$

$$\Delta\omega_r = P_m \left[\frac{\Delta\omega_m}{(1+k_{ex}^{-1}T_{2m}^{-1})^2 + \Delta\omega_m^2 k_{ex}^{-2}} + \Delta\omega_{os} \right] \quad \text{Eq. IV-2}$$

$$\frac{1}{T_1} - \frac{1}{T_{1A}} = P_m \left[\frac{1}{T_{1m} + k_{ex}^{-1}} + \frac{1}{T_{1os}} \right] \quad \text{Eq. IV-3}$$

where $1/T_1$, $1/T_2$ and ω are the longitudinal and transverse relaxation rates, respectively, and the angular frequencies of the paramagnetic solutions; $1/T_{1A}$, $1/T_{2A}$ and ω_A are the longitudinal and transverse relaxation rates and the angular frequencies, respectively, of the pure acetonitrile reference solution. The parameters $1/T_{1m}$ and $1/T_{2m}$ are the longitudinal and transverse relaxation rates of the bound acetonitrile and $\Delta\omega_m$ is the chemical shift difference between bound and bulk acetonitriles in the absence of exchange. P_m is the mole fraction of the bound acetonitriles and k_{ex} is the acetonitrile exchange rate ($k_{ex} = 1/\tau_m$, where τ_m is the mean residence time of an acetonitrile molecule in the first coordination sphere of the metal ions). $1/T_{1os}$, $1/T_{2os}$ and $\Delta\omega_{os}$ are the corresponding outer-sphere contributions to the longitudinal and transverse relaxation rates and the chemical shift of the paramagnetic solutions.

In the case of fast exchange reaction it is justified to use the following hypotheses (see demonstration in Section IV.3.1):

$$k_{ex} \gg \frac{1}{T_{1m}} \quad \text{Eq. IV-4}$$

$$k_{ex} \gg \frac{1}{T_{2m}} \quad \text{Eq. IV-5}$$

$$k_{ex}^2 \gg \Delta\omega_m^2 \quad \text{Eq. IV-6}$$

Therefore, Eq. IV-1 to IV-3 become:

$$\frac{1}{T_2} - \frac{1}{T_{2A}} = P_m \left[\frac{\Delta\omega_m^2}{k_{ex}} + \frac{1}{T_{2m}} + \frac{1}{T_{2os}} \right] \quad \text{Eq. IV-7}$$

$$\Delta\omega_r = P_m [\Delta\omega_m + \Delta\omega_{os}] \quad \text{Eq. IV-8}$$

$$\frac{1}{T_1} - \frac{1}{T_{1A}} = P_m \left[\frac{1}{T_{1m}} + \frac{1}{T_{1os}} \right] \quad \text{Eq. IV-9}$$

As it was first presented by Cossy^[12] for the water exchange on lanthanides, Eq. IV-10 results by subtracting Eq. IV-9 from Eq. IV-7, where the term corresponding to the reference $1/T_{2A}-1/T_{1A}$ disappears, due to the fact that the relaxation of pure acetonitrile is mainly due to the quadrupolar relaxation mechanism. The quadrupolar longitudinal and transverse relaxation rates are equal ($1/T_{1q} = 1/T_{2q}$) in the case of the extreme narrowing conditions:

$$\frac{1}{T_2} - \frac{1}{T_1} = P_m \left[\frac{\Delta\omega_m^2}{k_{ex}} + \frac{1}{T_{2m}} - \frac{1}{T_{1m}} + \frac{1}{T_{2os}} - \frac{1}{T_{1os}} \right] \quad \text{Eq. IV-10}$$

Eq. IV-10 can be further simplified to Eq. IV-13 using the following equations (demonstration in Section IV.3.1):

$$\frac{\Delta\omega_m^2}{k_{ex}} \gg \frac{1}{T_{2m}} - \frac{1}{T_{1m}} \quad \text{Eq. IV-11}$$

$$\frac{\Delta\omega_m^2}{k_{ex}} \gg \frac{1}{T_{2os}} - \frac{1}{T_{1os}} \quad \text{Eq. IV-12}$$

$$\frac{1}{T_2} - \frac{1}{T_1} = P_m \frac{\Delta\omega_m^2}{k_{ex}} \quad \text{Eq. IV-13}$$

Therefore, k_{ex} can be determined from the difference of the transverse and longitudinal relaxation rates if $\Delta\omega_m$ is known.

The temperature dependence of the acetonitrile exchange rate is described by the Eyring^[13] equation given in Eq. IV-14, where ΔS^\ddagger and ΔH^\ddagger are the entropy and enthalpy of activation for the acetonitrile exchange process, and k_{ex}^{298} is the acetonitrile exchange at 298.15 K. R is the perfect gas constant, h and k_B are the Planck and Boltzmann constants, respectively.

$$\frac{1}{\tau_m} = k_{ex} = \frac{k_B T}{h} \exp \left\{ \frac{\Delta S^\ddagger}{R} - \frac{\Delta H^\ddagger}{RT} \right\} = \frac{k_{ex}^{298} T}{298.15} \exp \left\{ \frac{\Delta H^\ddagger}{R} \left(\frac{1}{298.15} - \frac{1}{T} \right) \right\} \quad \text{Eq. IV-14}$$

In Eq. IV-8 $\Delta\omega_m$ is the chemical shift difference of the ^{14}N NMR signals between the bound and bulk acetonitrile molecules in the absence of exchange, P_m is the mole fraction of the

bound acetonitrile and $\Delta\omega_{os}$ is the outer-sphere contribution to the chemical shift, which can, in general, be neglected for ^{14}N NMR:

$$\Delta\omega_r = P_m \Delta\omega_m \quad \text{Eq. IV-15}$$

The temperature dependence of $\Delta\omega_m$ in the case of paramagnetic ions was first discussed by Bloembergen^[14] in terms of the electron-nucleus hyperfine coupling constant. He concluded an inverse proportional relationship of $\Delta\omega_m$ with the temperature. Granot and Fiat^[15] showed that $\Delta\omega_m$ can be described as the sum of a contact, B_1 , and a pseudo-contact contribution, B_2 , as follows:

$$\Delta\omega_m = \omega_0 \left(\frac{B_1}{T} + \frac{B_2}{T^2} \right) \quad \text{Eq. IV-16}$$

where ω_0 is the ^{14}N nucleus resonance frequency (in rad s^{-1}), B_1 and B_2 are constants described by Lewis^[16] and Bleaney,^[17] respectively. In Eq. IV-17 g_J is the Landé g factor, J is the total angular quantum number, μ_B is the Bohr magneton, k_B is the Boltzmann constant, γ_1 is the nuclear gyromagnetic ratio for ^{14}N ($\gamma_1 = 1.93 \times 10^7 \text{ rad s}^{-1} \text{ T}^{-1}$), A/\hbar is the scalar or contact hyperfine coupling constant:

$$B_1 = \frac{g_J (g_J - 1) J (J + 1) \mu_B A}{3k_B \gamma_1 \hbar} \quad \text{Eq. IV-17}$$

For lanthanide complexes having axial symmetry, the constants B_2 describing the pseudo-contact contribution to the chemical shift have been predicted by Bleaney^[17]:

$$B_2 = \frac{g_J^2 \mu_B^2 J (J + 1) (2J - 1) (2J + 3)}{60k_B} \frac{D_z (3 \cos^2 \theta - 1)}{r^3} \quad \text{Eq. IV-18}$$

where D_z is the axial component of the zero field splitting tensor and θ is the angle between the vector of length r joining the nucleus to the metal ion and the principal axis of symmetry. In the case of solvated complexes, the first coordination sphere molecules have different orientations with respect to the principal axis, therefore having different θ values. Since in

solution, due to rapid molecular motion, it is quite impossible to assess each θ no further evaluation of B_2 was possible. Thus, in the treatment of the chemical shifts data B_2 is used as a constant representing the mean of all individual B_2 values:

$$\Delta\omega_r = \omega_0 P_m \left(\frac{g_J (g_J - 1) J (J + 1) \mu_B}{3k_B \gamma_1 T} \frac{A}{\hbar} + \frac{B_2}{T^2} \right) \quad \text{Eq. IV-19}$$

IV.2.2.2 1H NMRD

The measured longitudinal proton relaxation rate, R_1^{obs} , is the sum of a paramagnetic and a diamagnetic contribution as expressed in Eq. IV-20, where r_1 is the proton relaxivity and $[Ln]$ is the milimolar concentration (mmol l^{-1}) of the metal ion:

$$R_1^{\text{obs}} = R_1^d + R_1^p = R_1^d + r_1 [Ln]; \quad r_1 = \frac{R_1^{\text{obs}} - R_1^d}{[Ln]} \quad \text{Eq. IV-20}$$

The relaxivity r_1 can be divided into an inner and an outer sphere term as follows:

$$r_1 = r_{is} + r_{os} \quad \text{Eq. IV-21}$$

The inner-sphere term is given in Eq. IV-22, where q is the number of inner sphere acetonitrile molecules, 19.15 is the molarity of pure acetonitrile (by using 0.786 g cm^{-3} as the acetonitrile density at room temperature) and T_{1m}^H is the relaxation time of the bound acetonitrile protons to $Ln = Nd^{3+}$, Dy^{3+} and Tm^{3+} :

$$r_{is} = \frac{1}{1000} \frac{q}{19.15} \frac{1}{T_{1m}^H + \tau_m} \quad \text{Eq. IV-22}$$

In case of water as solvent media $MW = 18 \text{ g mol}^{-1}$ and therefore $1000/MW = 55.56 \text{ mol dm}^{-3}$. For non-aqueous solvents, for example for acetonitrile $MW = 41.052 \text{ g mol}^{-1}$ and therefore $1000/MW = 24.36 \text{ mol kg}^{-1}$ of solvent. The density of CH_3CN (at ambient temperature) is 0.786 kg dm^{-3} and we obtain **$1000/MW = 19.15 \text{ mol dm}^{-3}$** (see also Chapter III Section 3.2).

The relaxation rate of inner-sphere protons, $1/T_{1m}^H$, is the sum of two contributions: a dipolar one, $1/T_{1dd}^H$, and a Curie one, $1/T_{1Curie}^H$, as expressed by Eq. IV-23. Because the acetonitrile protons have negligible scalar coupling to the electron spins the relaxation due to scalar coupling can be neglected:

$$\frac{1}{T_{1m}^H} = \frac{1}{T_{1dd}^H} + \frac{1}{T_{1Curie}^H} \quad \text{Eq. IV-23}$$

The basic equations describing the paramagnetic relaxation of the inner-sphere acetonitrile protons due to the dipole-dipole interaction between the proton spins and the electrons spins, $1/T_{1dd}^H$, have been first described by Solomon and Bloembergen.^[18, 19] In Eq. IV-24,^[20] the electron spins are described by J (the total angular quantum number) instead of S (the spin quantum number), and r_{LnH} is the effective distance between the electron spins and the ^1H nucleus, γ_I is the nuclear gyromagnetic ratio for protons ($\gamma_I = 2.68 \times 10^8 \text{ rad s}^{-1} \text{ T}^{-1}$), μ_B is the Bohr magneton, ω_I is the proton resonance frequency and ω_S is the Larmor frequency of the electron spin. τ_c is the correlation time which modulates nuclear relaxation described by Eq. IV-25:

$$\frac{1}{T_{1dd}^H} = \frac{2}{15} \left(\frac{\mu_0}{4\pi} \right)^2 \frac{\gamma_I^2 \mu_B^2 g_J^2 J(J+1)}{r_{LnH}^6} \left[\frac{3\tau_c}{1 + \omega_I^2 \tau_c^2} + \frac{7\tau_c}{1 + \omega_S^2 \tau_c^2} \right] \quad \text{Eq. IV-24}$$

$$\frac{1}{\tau_c} = \frac{1}{\tau_R} + \frac{1}{\tau_S} + \frac{1}{\tau_m} \quad \text{Eq. IV-25}$$

$$\mu_{eff} = g_J \sqrt{J(J+1)} \mu_B \quad \text{Eq. IV-26}$$

The contribution of the rotational correlation time, τ_R ($\sim 10^{-11}$ s) and that of the chemical exchange, τ_m ($\sim 10^{-9}$ s) to the overall correlation time, τ_c , can be neglected, since for lanthanides like Nd^{3+} , Dy^{3+} and Tm^{3+} the electronic relaxation time, τ_S , is $\sim 10^{-13}$ s. So, Eq. IV-24 can be written as:

$$\frac{1}{T_{1dd}^H} = \frac{2}{15} \left(\frac{\mu_0}{4\pi} \right)^2 \frac{\gamma_I^2 \mu_{eff}^2}{r_{LnH}^6} \left[\frac{3\tau_S}{1 + \omega_I^2 \tau_S^2} + \frac{7\tau_S}{1 + \omega_S^2 \tau_S^2} \right] \quad \text{Eq. IV-27}$$

The basic equation describing the paramagnetic relaxation of the inner-sphere acetonitrile protons due to the Curie relaxation, $1/T_{1Curie}^H$, is given by Eq. IV-28 and represents the interaction between the proton spins and the small difference in the population of the electron spin levels according to the Boltzmann distribution.^[2, 20] In Eq. III-28 k_B is the Boltzmann constant and T is the temperature.

$$\frac{1}{T_{1Curie}^H} = \frac{2}{5} \left(\frac{\mu_0}{4\pi} \right)^2 \frac{\gamma_I^2 \mu_B^2 g_J^2 \langle S_z \rangle^2}{r_{LnH}^6} \left[\frac{3\tau_R}{1 + \omega_I^2 \tau_R^2} \right] \quad \text{Eq. IV-28}$$

$$\langle S_z \rangle = -J(J+1) \frac{\mu_B g_J B_0}{3k_B T} \quad \text{Eq. IV-29}$$

From Eq. IV-26, IV-28 and IV-29, Eq. IV-30 results as follow:

$$\frac{1}{T_{1Curie}^H} = \frac{2}{5} \left(\frac{\mu_0}{4\pi} \right)^2 \frac{\omega_I^2 \mu_{eff}^4}{(3k_B T)^2 r_{LnH}^6} \left[\frac{3\tau_R}{1 + \omega_I^2 \tau_R^2} \right] \quad \text{Eq. IV-30}$$

The relaxivity of the outer-sphere protons is also given as the sum of dipolar and Curie relaxations:

$$r_{1os} = r_{1os}^{dd} + r_{1os}^{Curie} \quad \text{Eq. IV-31}$$

The dipole-dipole relaxation to r_{1os} is described by the following equations as developed by Freed^[21, 22] and Ayant,^[23] where N_A is the Avogadro constant, a_{LnH} is the distance of closest approach of an outer-sphere acetonitrile proton to the metal center, D_{LnH} is the mutual diffusion of bulk acetonitriles and the complex, τ_{LnH} is the correlation time for translational diffusion and J_{os} is its associated spectral density function. If one sets $T_{1e} = T_{2e} = \tau_s^{[2]} r_{1os}^{dd}$ can be described as:

$$r_{1os}^{dd} = \frac{32N_A \pi}{405} \left(\frac{\mu_0}{4\pi} \right)^2 \frac{\hbar^2 \gamma_S^2 \gamma_I^2}{a_{LnH} D_{LnH}} J(J+1) [3J_{os}(\omega_I; \tau_s) + 7J_{os}(\omega_S; \tau_s)] \quad \text{Eq. IV-32}$$

$$\gamma_S = \frac{g_J \mu_B}{\hbar} \quad \text{Eq. IV-33}$$

$$r_{Ios}^{dd} = \frac{32N_A\pi}{405} \left(\frac{\mu_0}{4\pi} \right)^2 \frac{g_J^2 \mu_B^2 \gamma_I^2}{a_{LnH} D_{LnH}} J(J+1) [3J_{os}(\omega_I; \tau_s) + 7J_{os}(\omega_s; \tau_s)] \quad \text{Eq. IV-34}$$

$$\mu_{eff} = g_J \sqrt{J(J+1)} \mu_B \quad \text{Eq. IV-35}$$

$$r_{Ios}^{dd} = \frac{32N_A\pi}{405} \left(\frac{\mu_0}{4\pi} \right)^2 \frac{\mu_{eff}^2 \gamma_I^2}{a_{LnH} D_{LnH}} [3J_{os}(\omega_I; \tau_s) + 7J_{os}(\omega_s; \tau_s)] \quad \text{Eq. IV-36}$$

$$J_{os}(\omega, \tau_s) = \text{Re} \left[\frac{1 + \frac{1}{4} \left(i\omega\tau_{LnH} + \frac{\tau_{LnH}}{\tau_s} \right)^{1/2}}{1 + \left(i\omega\tau_{LnH} + \frac{\tau_{LnH}}{\tau_s} \right)^{1/2} + \frac{4}{9} \left(i\omega\tau_{LnH} + \frac{\tau_{LnH}}{\tau_s} \right) + \frac{1}{9} \left(i\omega\tau_{LnH} + \frac{\tau_{LnH}}{\tau_s} \right)^{3/2}} \right] \quad \text{Eq. IV-37}$$

$$\tau_{LnH} = \frac{a_{LnH}^2}{D_{LnH}} \quad \text{Eq. IV-38}$$

The Curie relaxation to r_{Ios} has been described by Fries:^[24]

$$r_{Ios}^{Curie} = \frac{96\pi}{405} \left(\frac{\mu_0}{4\pi} \right)^2 \frac{N_A \gamma_I^2 (g_J \mu_B)}{a_{LnH} D_{LnH}} \langle S_z \rangle^2 [3J_{os}^{Curie}(\omega_I, \tau_{LnH})] \quad \text{Eq. IV-39}$$

$$r_{Ios}^{Curie} = \frac{96\pi}{405} \left(\frac{\mu_0}{4\pi} \right)^2 \frac{\gamma_I^2 \mu_{eff}^4}{(3k_B T)^2} \frac{N_A}{a_{LnH} D_{LnH}} [3J_{os}^{Curie}(\omega_I, \tau_{LnH})] \quad \text{Eq. IV-40}$$

$$J_{os}^{Curie}(\omega, \tau_{LnH}) = \text{Re} \left[\frac{1 + \frac{1}{4} (i\omega\tau_{LnH})^{1/2}}{1 + (i\omega\tau_{LnH})^{1/2} + \frac{4}{9} (i\omega\tau_{LnH}) + \frac{1}{9} (i\omega\tau_{LnH})^{3/2}} \right] \quad \text{Eq. IV-41}$$

One has to keep in mind that the outer-sphere spectral density function J_{os}^{Curie} as defined by Eq. IV-41 is $4/27$ that of Fries, \bar{j}_2 .

All correlation times, τ , and the diffusion constant, D_{LnH} , are supposed to obey an Arrhenius law:

$$\tau = \tau^{298} \exp \left\{ \frac{E_a}{R} \left(\frac{1}{T} - \frac{1}{298.15} \right) \right\} \quad \text{Eq. IV-42}$$

$$D_{LnH} = D_{LnH}^{298} \exp \left\{ \frac{E_{LnH}}{R} \left(\frac{1}{298.15} - \frac{1}{T} \right) \right\} \quad \text{Eq. IV-43}$$

IV.3 RESULTS AND DISCUSSIONS

With the objective of determining the acetonitrile exchange rates, the rotational correlation times and the electronic relaxation times of the Nd^{3+} **1**, Dy^{3+} **4** and Tm^{3+} **5** complexes, variable-temperature ^{14}N NMR at two magnetic fields (9.4 T and 18.8 T) and multiple fields variable-temperature acetonitrile proton relaxation studies were completed. The measured ^{14}N NMR data, allowing the determination of the kinetic parameters which describe the acetonitrile exchange reaction, have been analyzed in a nonlinear fitting procedure. The experimental ^{14}N NMR data and their fitted curves for the three complexes are shown in Figure IV-1, while their corresponding kinetic parameters are reported in Table IV-1. The rotational correlation times and the electronic relaxation times were obtained from a simultaneous fitting procedure of the 1H NMRD and $1/T_{1r}$ ^{14}N NMR data. The 1H NMRD profiles and the experimental $1/T_{1r}$ data, with their fitted curves for the three complexes are shown in Figure IV-2. The parameters obtained in the fitting procedures are presented in Table IV-4.

In order to analyze the ^{14}N NMR and 1H NMRD data, first, one has to determine the mole fraction of the bound acetonitrile molecules, P_m ; which implies the necessity of knowledge of the number of acetonitrile molecules coordinated to the metal center. In the solid state of the Nd^{3+} and Dy^{3+} complexes nine acetonitrile molecules coordinate to the metal center, while for Tm^{3+} eight acetonitriles were found to coordinate to the metal center. In their anhydrous acetonitrile solutions, in the following study, the same coordination numbers were assumed for the three lanthanide complexes as it was found in their solid state structures: nine for Nd^{3+} and Dy^{3+} and eight for Tm^{3+} . Thus, all parameters, presented in Table IV-1 and IV-4, were obtained by using the coordination numbers in concordance with the X-ray crystal data (Chapter II).

IV.3.1 Determination of the Solvent Exchange Rate Constants

The acetonitrile exchange reaction on lanthanides can be described by the classical Swift and Coonick equations.^[1] The temperature dependences of the relaxation rate differences and the chemical shifts of the anhydrous acetonitrile solutions of Nd^{3+} , Dy^{3+} and Tm^{3+} ions revealed that the acetonitrile exchange reaction on these ions is very fast. The experimental data,

measured at 9.4 and 18.8 T, as well as the results of the least-square fits of $\ln(1/T_2 - 1/T_1)/P_m$ and $\Delta\omega_r$ versus the reciprocal of the temperature, using Eq. IV-13, Eq. IV-14 and IV-19, are illustrated in Figure IV-1. The adjustable parameters were k_{ex}^{298} , ΔH^\ddagger , ΔS^\ddagger , A/\hbar and B_2 , as presented in Table IV-1.

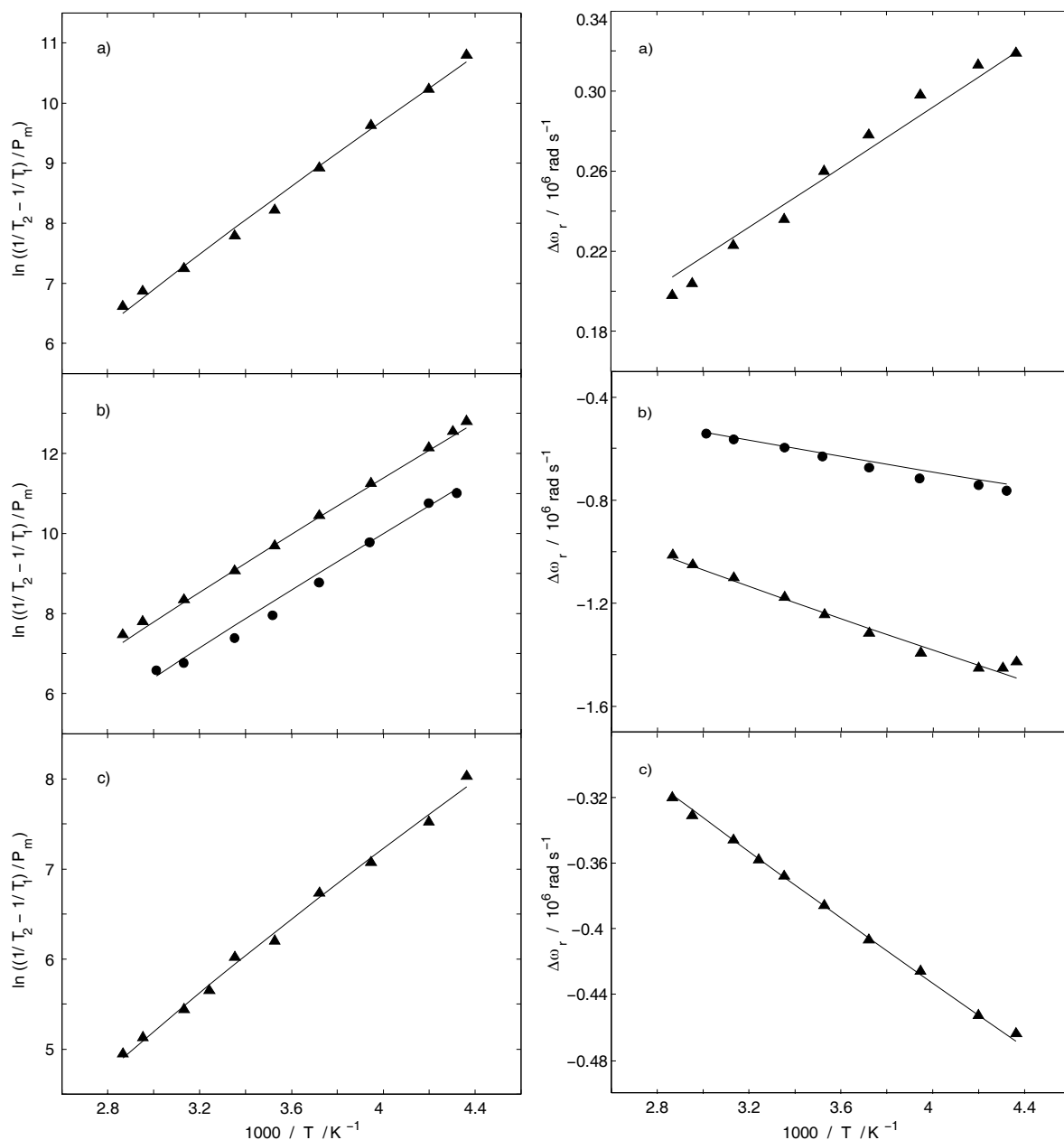


Figure IV-1. Temperature dependence of the ^{14}N reduced relaxation rate differences, $\ln((1/T_2 - 1/T_1)/P_m)$, and chemical shifts, $\Delta\omega_r$, at $B = 9.4$ T (●) and 18.8 T (▲) of: a) $[\text{Nd}(\text{CH}_3\text{CN})_9][\text{Al}(\text{OC}(\text{CF}_3)_3)_4]_3$, b) $[\text{Dy}(\text{CH}_3\text{CN})_9][\text{Al}(\text{OC}(\text{CF}_3)_3)_4]_3$ and c) $[\text{Tm}(\text{CH}_3\text{CN})_8][\text{Al}(\text{OC}(\text{CF}_3)_3)_4]_3$ complexes. The lines through the data points result from the least-square fit treatments of the ^{14}N NMR data using the simplified Swift and Connick equations.

From Figure IV-1 it can be seen that, for the Nd^{3+} and Tm^{3+} ions only data measured at 18.8 T were fitted. This is due to the fact that at lower magnetic field, for these ions, the kinetic effect, $\Delta\omega_m^2/k_{ex}$, is too small with respect to the experimental errors on $1/T_2-1/T_1$. The kinetic effect being proportional to the square of the magnetic field (see Eq. IV-16), it is obvious that, by reducing the magnetic field from 18.8 T, the chemical shift difference between the bound and bulk acetonitrile signals will become smaller. For the acetonitrile solution of these ions, at low magnetic field (9.4 T) the difference between the transverse and longitudinal relaxation rates is very small (less than 10 %) and as a result the uncertainties on $(1/T_2-1/T_1)/P_m$ are large. In conclusion, for the Nd^{3+} and Tm^{3+} ions only the data measured at 18.8 T allowed the determination of the kinetic parameters describing the acetonitrile exchange reaction. In the case of the Dy^{3+} ion, the chemical shift, $\Delta\omega_m$, is larger than for Nd^{3+} and Tm^{3+} , mainly due to the pseudo contact (B_2) contribution^[17] (Table IV-1), therefore, for this ion low field results could be included in the fitting procedures. It is worth to be noted that, this is the first time when a solvent exchange rate could be determined for the Nd^{3+} ion. In 1994 Powell^[25] managed to determine only a lower limit of the water exchange rate on Nd^{3+} and Pr^{3+} ions, by ^{17}O NMR relaxation rate measurements at 14.1 T (the highest magnetic field available at that time).

Table IV-1. Parameters obtained from the least-square fit of the ^{14}N NMR data.

	$[Nd(CH_3CN)_9]^{3+}$	$[Dy(CH_3CN)_9]^{3+}$	$[Tm(CH_3CN)_8]^{3+}$
$k_{ex}^{298} / 10^6 s^{-1}$	21.5 ± 5.7	159 ± 12	357 ± 39
$\Delta H^\ddagger / kJ mol^{-1}$	16.1 ± 3.6	23.3 ± 1.0	10.1 ± 1.6
$\Delta S^\ddagger / J mol^{-1} K^{-1}$	-50.5 ± 13.6	-9.9 ± 3.8	-47.4 ± 5.7
$(A/\hbar) / 10^6 rad s^{-1}$	-3.42 ± 2.9	-3.32 ± 0.6	-3.36 ± 1.1
B_2	1.6 ± 43	31.7 ± 52	6.8 ± 28

The data presented in Table IV-1 show that, the acetonitrile exchange on lanthanides become faster as the lanthanide ionic radii decrease: $Nd^{3+}_{(CN=9)} = 1.16 \text{ \AA}$, $Dy^{3+}_{(CN=9)} = 1.08 \text{ \AA}$ and $Tm^{3+}_{(CN=8)} = 0.99 \text{ \AA}$.^[26] This result is in contradiction with the expected trend due to electrostatic interaction if one take into account the strength of the Ln-N bonds: $r_{Nd-N} = 2.64 \text{ \AA}$, $r_{Dy-N} = 2.52 \text{ \AA}$ and $r_{Tm-N} = 2.41 \text{ \AA}$ (Chapter II Table II-2). Therefore, if the electrostatic effect would be decisive for the lability of the acetonitrile molecules, one should expect that the lability decreases while the ionic radii decrease. The experimental data show the contrary.

Therefore, one can conclude that steric effects play a more important role in the lability of the acetonitrile molecules than does the electrostatic one. In this way, as the ionic radii decrease, the steric constraints produced between the bound acetonitrile molecules in the first coordination sphere of the lanthanide ions will increase, increasing in consequence the exchange rate of the acetonitrile molecules.

The data analyses of the ^{14}N NMR results were undertaken using the fast exchange hypotheses and the simplified Swift and Coonick equations as first presented by Cossy *et al.*^[12] in the case of water exchange on lanthanides (for equations see section IV.2.2.1). In order to confirm the validity of the fast exchange hypotheses for the acetonitrile exchange reaction on lanthanides, using the results of the data fitting (Table IV-1) and the Eq. IV-7, IV-9, IV-14 and IV-19, it was possible to estimate the magnitude of the contribution of $1/T_{1m}+1/T_{1os}$ and $1/T_{2m}+1/T_{2os}$ to the observed longitudinal and transverse relaxation rates, respectively (Table IV-2). Since $\Delta\omega_m^2/k_{ex}$ varies regularly with temperature, by calculating their values for the two extremities of the used temperature range will prove the validity of these hypotheses for the entire temperature range. From the data presented in Table IV-2 it can be seen that $1/T_{1m}+1/T_{1os}$ and $1/T_{2m}+1/T_{2os}$ are always at least 3 orders of magnitude smaller than k_{ex} , implying that also $1/T_{1m}$ and $1/T_{2m}$ are considerably smaller than k_{ex} (justification of Eq. IV-4 and IV-5). Table IV-2 clearly shows that even at the lowest temperature $\Delta\omega_m^2$ is also at least 10 times smaller than k_{ex}^2 (justification of Eq. IV-6).

Table IV-2. Data calculated at 18.8 T and used to demonstrate the fast exchange hypotheses.

Ln^{3+}	T	k_{ex}	k_{ex}^2	$\Delta\omega_m^2$	$1/T_{1m} + 1/T_{1os}$	$1/T_{2m} + 1/T_{2os}$
	/ K	/ s^{-1}	/ s^{-1}	/ $\text{rad}^2 \text{s}^{-2}$	/ s^{-1}	/ s^{-1}
Nd	229	2.34×10^6	5.46×10^{12}	1.02×10^{11}	1.98×10^4	3.00×10^4
	349	6.52×10^7	4.25×10^{15}	4.30×10^{10}	2.46×10^3	2.68×10^3
Dy	229	7.17×10^6	5.15×10^{13}	2.27×10^{12}	2.22×10^4	6.84×10^4
	349	7.31×10^8	5.34×10^{17}	1.08×10^{12}	2.63×10^3	2.92×10^3
Tm	229	8.06×10^7	6.50×10^{15}	2.08×10^{11}	2.72×10^4	2.98×10^4
	349	7.56×10^8	5.72×10^{17}	9.63×10^{10}	2.77×10^3	2.79×10^3

To confirm the validity of the simplification leading to Eq. IV-13, $1/T_{2m} - 1/T_{1m}$ and $1/T_{2os} - 1/T_{1os}$ need to be considerably smaller than $\Delta\omega_m^2/k$. The ^{14}N transverse and longitudinal relaxation rates of the bound acetonitriles, $1/T_{2m}$ and $1/T_{1m}$, in Nd^{3+} , Dy^{3+} and Tm^{3+} solutions

are the sum of the contributions of the scalar, $1/T_{isc}$, dipole-dipole, $1/T_{idd}$, and quadrupolar, $1/T_{iq}$ ($i = 1, 2$), mechanisms as expressed by Eq. IV-44 to IV-50;^[27] where γ_s is the electron and γ_l is the nuclear gyromagnetic ratio ($\gamma_s = 1.76 \times 10^{11} \text{ rad s}^{-1} \text{ T}^{-1}$, $\gamma_l = 1.93 \times 10^7 \text{ rad s}^{-1} \text{ T}^{-1}$ for ^{14}N), ω_s is the angular resonance frequency of the electron spin and ω_l is the ^{14}N angular resonance frequency, r_{LnN} is the effective distance between the electron spins and the ^{14}N nucleus, I is the nuclear spin (1 for ^{14}N), A/\hbar is the scalar coupling constant, χ is the quadrupolar coupling constant, η is an asymmetry parameter, τ_R is the rotational correlation time for Ln-N vector and τ_s is the electron-spin relaxation time:

$$\frac{1}{T_{2m}} - \frac{1}{T_{1m}} = \left(\frac{1}{T_{2sc}} - \frac{1}{T_{1sc}} \right) + \left(\frac{1}{T_{2dd}} - \frac{1}{T_{1dd}} \right) + \left(\frac{1}{T_{2q}} - \frac{1}{T_{1q}} \right) \quad \text{Eq. IV-44}$$

$$\frac{1}{T_{1sc}} = \frac{J(J+1)}{3} \left(\frac{A}{\hbar} \right)^2 \left(\frac{2\tau_s}{1 + \omega_s^2 \tau_s^2} \right) \quad \text{Eq. IV-45}$$

$$\frac{1}{T_{2sc}} = \frac{J(J+1)}{3} \left(\frac{A}{\hbar} \right)^2 \left(\tau_s + \frac{\tau_s}{1 + \omega_s^2 \tau_s^2} \right) \quad \text{Eq. IV-46}$$

$$\frac{1}{T_{1dd}} = \frac{2}{15} \left(\frac{\mu_0}{4\pi} \right)^2 \frac{\hbar^2 \gamma_l^2 \gamma_s^2}{r_{LnN}^6} J(J+1) \left(3\tau_s + \frac{7\tau_s}{1 + \omega_s^2 \tau_s^2} \right) \quad \text{Eq. IV-47}$$

$$\frac{1}{T_{2dd}} = \frac{1}{15} \left(\frac{\mu_0}{4\pi} \right)^2 \frac{\hbar^2 \gamma_l^2 \gamma_s^2}{r_{LnN}^6} J(J+1) \left(7\tau_s + \frac{13\tau_s}{1 + \omega_s^2 \tau_s^2} \right) \quad \text{Eq. IV-48}$$

$$\frac{1}{T_{1q}} = \frac{3\pi^2}{10} \frac{2I+3}{I^2(2I-1)} \chi^2 (1 + \eta^2/3) \left(\frac{0.2\tau_R}{1 + \omega_l^2 \tau_R^2} + \frac{0.8\tau_R}{1 + 4\omega_l^2 \tau_R^2} \right) \quad \text{Eq. IV-49}$$

$$\frac{1}{T_{2q}} = \frac{3\pi^2}{10} \frac{2I+3}{I^2(2I-1)} \chi^2 (1 + \eta^2/3) \left(0.3\tau_R + \frac{0.5\tau_R}{1 + \omega_l^2 \tau_R^2} + \frac{0.2\tau_R}{1 + 4\omega_l^2 \tau_R^2} \right) \quad \text{Eq. IV-50}$$

The relaxation rates, given in Table IV-3, corresponding to the different relaxation mechanisms (see Eq. IV-45 to IV-50), were calculated using the following estimations for the parameters: the values of the scalar coupling constants (A/\hbar) as presented in Table IV-1; the distances between the electron spins and the ^{14}N nucleus (r_{LnN}) as predicted from the X-ray crystal structures (2.64 Å for Nd^{3+} , 2.52 Å for Dy^{3+} and 2.41 Å for Tm^{3+}); 4.5 MHz for the quadrupolar coupling constant ($\chi^2(1+\eta^2/3)$) as used in Chapter III; and the values of the rotational correlation times (τ_R) and the electron-spin relaxation times (τ_s) were calculated for the two extremities of the used temperature range according to the ^1H NMRD data (Section

IV.3.2). In case of the validity of the extreme narrowing conditions, the quadrupolar longitudinal and transverse relaxation rates are equal ($1/T_{1q} = 1/T_{2q}$); in consequence their difference in Eq. IV-44 is equal to zero. Their estimated values for the three complexes at 25°C are: $4.9 \times 10^3 \text{ s}^{-1}$ for Nd^{3+} , $5.3 \times 10^3 \text{ s}^{-1}$ for Dy^{3+} and $5.7 \times 10^3 \text{ s}^{-1}$ for Tm^{3+} . The extreme narrowing condition is fulfilled if $(\omega_I \tau_R)^2 \ll 1$, where τ_R is the molecular reorientation correlation time and ω_I is the ^{14}N angular resonance frequency (which at 18.8 T is $3.63 \times 10^8 \text{ rad s}^{-1}$). From the τ_R values presented in Table IV-3 follow that $(\omega_I \tau_R)^2 < 10^{-5}$, proving the validity of the extreme narrowing condition. The results in Table IV-3 clearly show that $1/T_{2m} - 1/T_{1m}$ is always small compared to $\Delta\omega_m^2/k_{\text{ex}}$ (less than 5 %, except for Tm^{3+} at 349 K), therefore the effect of neglecting this difference in Eq. IV-10 will be comparable with the experimental errors on the kinetic parameters.

Table IV-3. Data used for the discussions employed for the simplifications considered in the relaxation data treatments. The data were calculated at 18.8 T.

Ln^{3+}	T / K	τ_R / 10^{-12} s	τ_S / 10^{-12} s	$1/T_{2sc}$ / s^{-1}	$1/T_{1sc}$ / s^{-1}	$1/T_{2dd}$ / s^{-1}	$1/T_{1dd}$ / s^{-1}	$1/T_{2m} - 1/T_{1m}$ / s^{-1}	$\Delta\omega_m^2/k_{\text{ex}}$ / s^{-1}
Nd	229	67	0.44	56	28	32	30	30	4.36×10^4
	349	8.2	0.17	29	25	18	18	4	6.60×10^2
Dy	229	72	0.45	138	67	109	103	77	3.17×10^5
	349	8.9	0.23	89	69	78	76	22	1.48×10^3
Tm	229	89	0.46	95	45	95	89	56	2.58×10^3
	349	9.1	0.31	74	49	79	76	28	1.27×10^2

The ^{14}N transverse and longitudinal relaxation rates of the outer-sphere acetonitriles, $1/T_{2os}$ and $1/T_{1os}$, are governed by the quadrupolar relaxation mechanisms Eq. IV-49 and IV-50. Since, here the extreme narrowing condition is valid the quadrupolar longitudinal and transverse relaxation rates are equal ($1/T_{1q} = 1/T_{2q}$) as well as the outer-sphere relaxation rates. In consequence, $1/T_{2os} - 1/T_{1os}$ in Eq. IV-10 can be neglected.

Finally, one can conclude that, all hypotheses describing the acetonitrile exchange reaction on lanthanides as a rapid exchange reaction, and the simplifications leading to Eq. IV-13 are justified.

IV.3.2 Rotational Correlation Times and Electron Spin Relaxation by 1H NMRD and $1/T_{1r}$ of ^{14}N NMR

The acetonitrile proton relaxivity values have been recorded at 298 and 238 K from 0.01 to 800 MHz for the fully solvated Nd^{3+} , Dy^{3+} and Tm^{3+} ions in anhydrous acetonitrile (Figure IV-2). The NMRD profiles are relatively different from those observed for the Gd^{3+} and Eu^{2+} ions, presenting a flat profile between 0.01 and 50 MHz which increases continuously with the magnetic field above 100 MHz. The same tendency has already been observed by Bertini *et al.*^[2] in the case of the water proton relaxation study on some lanthanide aqua ions. They have interpreted their profiles as due to inner-sphere proton relaxations arising from proton-electron dipolar coupling and Curie relaxation mechanisms. However, in their data treatments, Bertini *et al.*^[2] neglected the outer-sphere contribution to the observed relaxivity. In this study, it will be shown that the outer-sphere relaxation can not be neglected, since it has a considerable influence on the total proton relaxivity.

Since the 1H NMRD profiles of the Nd^{3+} , Dy^{3+} and Tm^{3+} ions in acetonitrile are quite similar to those observed in the aqueous solution of Pr^{3+} , Sm^{3+} , Dy^{3+} , Ho^{3+} , Er^{3+} and Yb^{3+} ions,^[2] it was assumed that the relaxation is also due to the dipole-dipole and the Curie relaxation mechanisms. In case of aqueous solution with six or more inner-sphere water molecules, the outer-sphere contribution can be neglected in respect to the relaxation enhancement due to the inner-sphere molecules.^[2] In acetonitrile, the protons of inner-sphere solvent molecules are much further away from the paramagnetic center than in water ($r_{LnH} > 5 \text{ \AA}$). Due to the r_{LnH}^{-6} dependence the inner-sphere contribution is therefore smaller than in water and the outer-sphere contribution has to be taken into account. In this work, the acetonitrile proton relaxivities data have been treated as a sum of an inner- and an outer-sphere contribution (r_{1is} , r_{1os}). Both contributions arise from their corresponding dipole-dipole (r_{1is}^{dd} , r_{1os}^{dd}), as presented in Eq. IV-27 and IV-30, and Curie relaxation mechanisms (r_{1is}^{Curie} , r_{1os}^{Curie}), as presented in Eq. IV-36 and IV-40. These equations show that, the correlation time describing the proton-electron dipolar coupling can be attributed to the electron relaxation time, τ_s , while the Curie relaxation to the rotational correlation time of the acetonitrile complexes, τ_R . The Curie nuclear longitudinal relaxation enhancement depends on the square of the external field, therefore its contribution is more pronounced at high magnetic fields. Thus, only data measured at 200, 400 and 800 MHz can have a significant input to the determination of the rotational correlation time of the acetonitrile complexes, τ_R . This scarce number of data can

not give reliable τ_R values. But, as it has been shown in the previous section, the ^{14}N longitudinal relaxation rates are determined by the quadrupolar relaxation mechanisms, $1/T_{1q}$, and from Eq. IV-50 can be seen that $1/T_{1q}$ allow as well an accurate determination of τ_R , if the quadrupolar coupling constant is known.

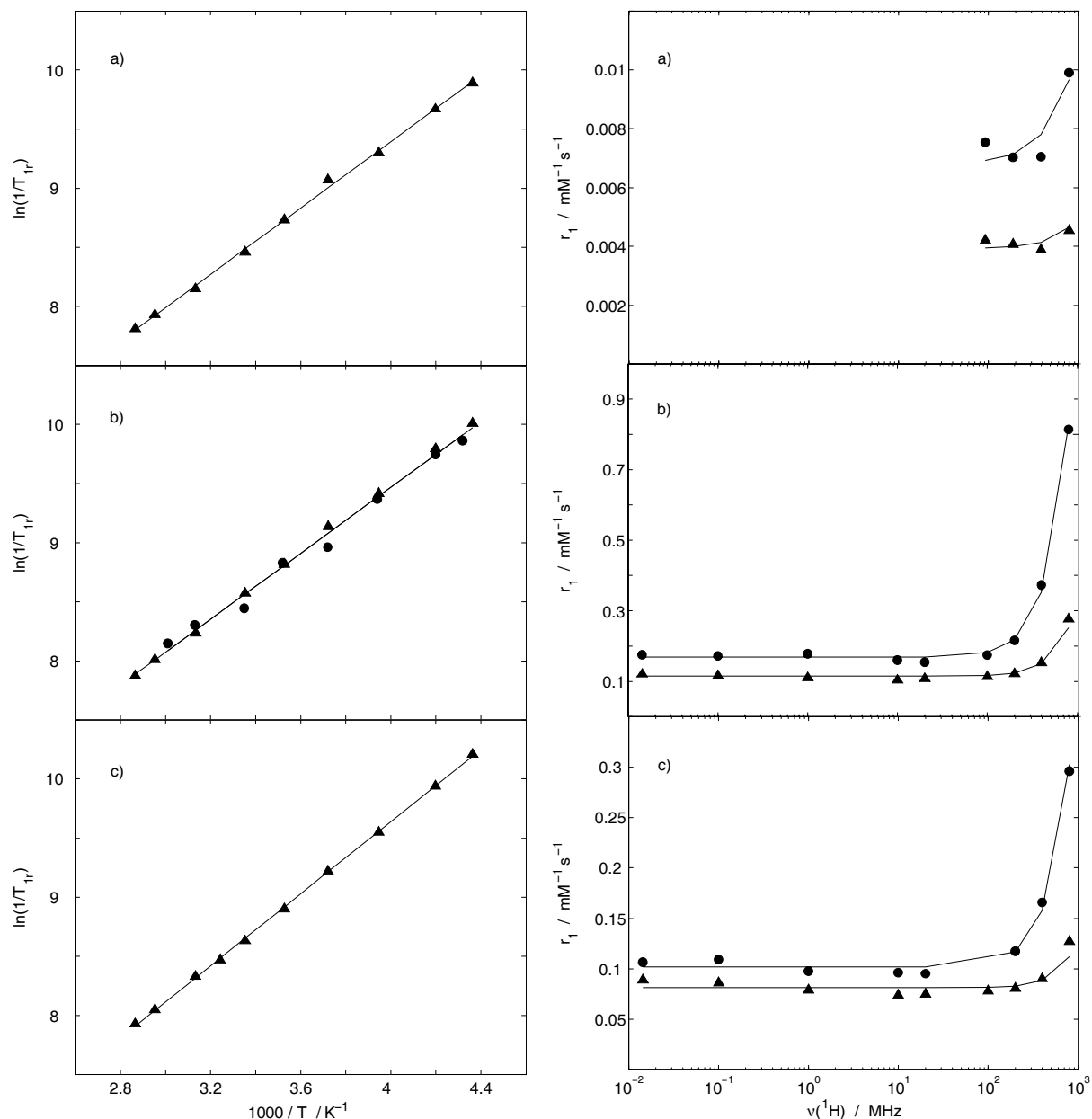


Figure IV-2. Temperature dependence of the ^{14}N reduced longitudinal relaxation rates, $1/T_{1r}$, at $B = 9.4$ T (●) and 18.8 T (▲) and ^1H NMRD profiles at 238 K (●) and 298 K (▲) of: a) $[\text{Nd}(\text{CH}_3\text{CN})_9][\text{Al}(\text{OC}(\text{CF}_3)_3)_4]_3$, b) $[\text{Dy}(\text{CH}_3\text{CN})_9][\text{Al}(\text{OC}(\text{CF}_3)_3)_4]_3$ and c) $[\text{Tm}(\text{CH}_3\text{CN})_8][\text{Al}(\text{OC}(\text{CF}_3)_3)_4]_3$ complexes. The lines through the data points result from the simultaneous least-square fit treatments of the longitudinal ^{14}N NMR and ^1H NMRD data using the contributions of the Curie relaxations to both inner and outer sphere relaxations.

By using a quadrupolar coupling constant of 4.5 MHz and by combining the 1H NMRD data with those of the ^{14}N NMR $1/T_{1r}$ data, simultaneous fitting procedures were undertaken in order to obtain the electronic and rotational correlation times of the Nd^{3+} , Dy^{3+} and Tm^{3+} ions in anhydrous acetonitrile. The simultaneous fits allowed to get more meaningful values for the rotational correlation times, τ_R . In Figure IV-2 the temperature dependence of both, ^{14}N NMR reduced longitudinal relaxation rates and 1H NMRD data together with their fitted curves are shown. The parameters obtained in the simultaneous fitting procedures are presented in Table IV-4.

Since the simultaneously fitted curves match perfectly to the experimental data, the model of dipolar and Curie relaxations for the inner-sphere as well as for the outer-sphere relaxations of 1H nuclear spins is confirmed. Therefore, at relatively low magnetic fields the correlation time for nuclear relaxation is the electronic relaxation time, τ_S , which in this region is magnetic field independent. At high magnetic field a strong magnetic field dependency can be seen, which can be attributed to the Curie relaxation mechanism and indirectly to the rotational correlation time of the acetonitrile complexes, τ_R . The relaxivity increase at high magnetic field is more pronounced for Dy^{3+} than for Nd^{3+} and Tm^{3+} ions which, is in concordance with their magnetic moment values, μ_{eff} , (see Chapter II Table II-10). As a general trend, one can observe that, when the temperature is decreased, the relaxivities at high magnetic fields increase substantially, while at low magnetic fields the increase is much less pronounced. This behavior leads to the conclusion that, the electronic relaxation time has smaller variation with the temperature than the rotational correlation time has.

Table IV-4. Parameters obtained from the simultaneous least-square fit of 1H NMRD and ^{14}N NMR $1/T_{1r}$ data. Underlined parameters were fixed in the fit.

	$[Nd(CH_3CN)_9]^{3+}$	$[Dy(CH_3CN)_9]^{3+}$	$[Tm(CH_3CN)_8]^{3+}$
$\tau_R / 10^{-12} \text{ s}$	16.2 ± 0.1	17.6 ± 0.2	19.1 ± 0.07
$E_R / \text{kJ mol}^{-1}$	11.7 ± 0.1	11.6 ± 0.2	12.7 ± 0.06
$\tau_S / 10^{-12} \text{ s}$	$0.23 \pm 1.6^*$	0.28 ± 0.04	0.35 ± 0.02
$E_S / \text{kJ mol}^{-1}$	$5.3 \pm 37^*$	3.8 ± 1.5	2.1 ± 0.7
$r_{LnH \text{ 1st sphere}} / \text{\AA}$	$7.48 \pm 43^*$	5.0 ± 0.06	4.7 ± 0.04
$a_{LnH \text{ bulk}} / \text{\AA}$	<u>5.7</u>	<u>5.7</u>	<u>5.7</u>

* the significant errors for these parameters arise due to the lack of the relaxivity data at low magnetic fields

In the fitting procedures, the diffusion constant D_{LnH}^{298} was fixed at $43.7 \times 10^{-10} \text{ m}^2 \text{ s}^{-1}$, the value of the diffusion of pure acetonitrile,^[28] whilst E_{DLnH} was fixed at the value of 14.1 kJ mol^{-1} , as obtained in Chapter III from the data treatment of the Gd^{3+} complex. In a first attempt, the data of the Tm^{3+} ion were fitted using the distance between the metal center and the first coordination sphere acetonitrile protons, $r_{\text{LnH 1st sphere}}$, fixed to 5.4 \AA (value estimated from the X-ray crystal structure of the Tm^{3+} complex). The fitted value for the distance of the closest approach between the metal center and bulk acetonitrile protons, $a_{\text{LnH bulk}}$, was $3.55 \pm 0.14 \text{ \AA}$. This value is too short and not reasonable. Therefore, in the fitting procedures of all three Ln^{3+} solutions, the distances between the metal center and the first coordination sphere acetonitrile protons were fitted, by keeping constant the distance between the metal center and bulk protons at the value of 5.7 \AA (value found in the fitting procedure of the Gd^{3+} complex). This choice is sustained also by the fact that, the refinement of the crystal structures of the nine-coordinated complexes does not allow a prediction of the metal-first coordination sphere hydrogen distances.

Since the experimental profiles have been interpreted as the sum of an inner- and outer-sphere contribution (r_{1is} , r_{1os}), the magnitude of their individual contributions to the observed relaxivity has been calculated. This is, to our best knowledge, the first time when the outer-sphere contribution to the relaxivity is quantified for the Dy^{3+} and Tm^{3+} ions. Figure IV-3 gives an insight to the importance of each contribution to the observed relaxivity for the Dy^{3+} ion (for Tm^{3+} the same contributions are presented in the Appendix Figure A IV-1). Both, inner- and outer-sphere contributions arise from the corresponding proton-electron dipolar coupling (r_{1is}^{dd} , r_{1os}^{dd}) and Curie relaxation mechanisms (r_{1is}^{Curie} , r_{1os}^{Curie}) (for equation see Section IV.2.2.2). For both of them at low magnetic fields the dipole-dipole relaxation, at high magnetic fields the Curie relaxation mechanisms dominates. For the Dy^{3+} ion, the total inner-sphere contribution (r_{1is}) to the relaxivity is 68 % at 298 K and 800 MHz, while that of the outer-sphere one (r_{1os}) is 32 %; these values become 70 % and 30 % at 238 K, respectively. A complete temperature and magnetic field dependency of the individual dipole-dipole and Curie relaxation contributions to the inner- (r_{1is}^{dd} , r_{1is}^{Curie}) and outer-sphere (r_{1os}^{dd} , r_{1os}^{Curie}) proton relaxivities, for the two ions, are presented in Appendix Table A IV-7 and A IV-8. One can see that, the outer-sphere contribution is significant mostly at high magnetic field, and it can be attributed mainly to the Curie relaxation (r_{1os}^{Curie}).

As in acetonitrile the outer-sphere relaxivity seems to be quite important, a cross check of the outer-sphere contribution to the observed relaxivity for the Dy^{3+} aqua ion have been done using the measured data of Bertini *et al.*^[2] (see Appendix Table A IV-9 and Figure A IV-2). In the case of water the contribution of the outer-sphere relaxation is smaller than in acetonitrile, being only 18 % which, however, can not be neglected.

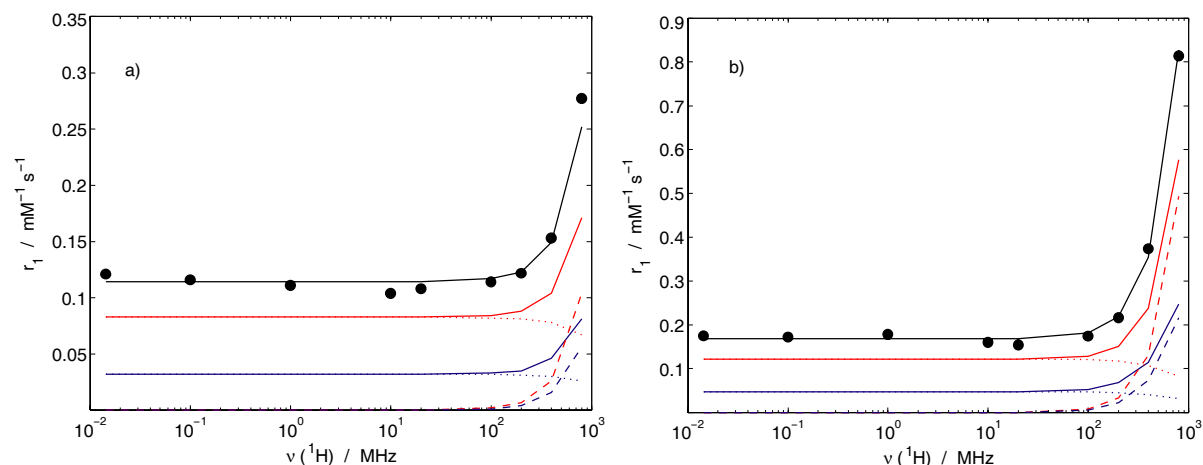


Figure IV-3. 1H NMRD profile of the Dy^{3+} ion in acetonitrile at: a) 298 K and b) 238 K. The measured relaxivity points are represented as filled symbols (●) and the line through the data points (—) result from the simultaneous least-square fit of the 1H NMRD and ^{14}N NMR $1/T_{1r}$ data. The continuous lines (—) and (—) represent the total inner- and outer-sphere contributions (r_{1is} , r_{1os}), respectively, to the relaxivity curve. The dotted lines (· · ·) and (· · ·) represent the dipole-dipole contributions to the inner- and outer-sphere relaxivities (r_{1is}^{dd} , r_{1os}^{dd}) respectively. The dashed lines (---) and (---) represent the Curie contributions to the inner- and outer-sphere relaxivities (r_{1os}^{Curie} , r_{1os}^{Curie}) respectively.

Table IV-5 gives an overview of the dynamic parameters characterizing the lanthanides ions in water^[2] and acetonitrile. It can be seen that, Dy^{3+} is the only lanthanide ion for which a direct comparison is possible.

Table IV-5. Calculated rotational correlation time and electronic relaxation time values at 298 K for Ln^{3+} ions in water and anhydrous acetonitrile :

		Pr	Nd	Sm	Dy	Ho	Er	Tm	Tb
$\tau_S / 10^{-12} s$	$H_2O^{[2]}$	0.082	-	0.079	0.39 / 0.28 ^{a)}	0.27	0.31	-	0.22
	$CH_3CN^{b)}$		(0.23)		0.28			0.35	
$\tau_R / 10^{-12} s$	$H_2O^{[2]}$	63	-	67	63 / 40 ^{a)}	65	61	-	68
	$CH_3CN^{b)}$		16.2		17.6			19.1	

a) obtained by taking into account the outer sphere relaxation

b) this work

If the outer-sphere contribution is taken into account, the rotational correlation time, τ_R , and the electronic relaxation time, τ_S , become significantly smaller than those determined by Bertini *et al.*:^[2] 40×10^{-12} s and 0.28×10^{-12} s, respectively. Thus, it can be seen that, the electronic relaxation time of the Dy^{3+} ion in acetonitrile and water is equal. Accordingly, one can conclude that, for this ion, the electron spin relaxation, represented by τ_S , is independent from the nature of the coordinated solvent molecule. This statement is probably valid for all lanthanide ions except for those having an $S = 7/2$ state (Gd^{3+} and Eu^{2+}). The rotational correlation times τ_R are considerably shorter in acetonitrile than in water. This reflects the about three times lower viscosity of the acetonitrile compared to that of the water.

IV.4 CONCLUSION

In this study the acetonitrile exchange reaction of the fully solvated Nd^{3+} , Dy^{3+} and Tm^{3+} ions has been described. The kinetic parameters have been determined by variable temperature ^{14}N NMR measurements at 9.4 T and 18.8 T in anhydrous acetonitrile. For Nd^{3+} , k_{ex}^{298} (10^6 s^{-1}), ΔH^\ddagger (kJ mol^{-1}) and ΔS^\ddagger ($\text{J mol}^{-1} \text{ K}^{-1}$) are respectively 21.5 ± 5.7 , 16.1 ± 3.6 , and -50.5 ± 13.6 ; for Dy^{3+} , 159 ± 12 , 23.3 ± 1 , and -9.9 ± 3.8 ; while for Tm^{3+} the corresponding values are 357 ± 39 , 10.1 ± 1.6 , and -47.4 ± 5.7 . The systematic increase of the acetonitrile exchange rate as the lanthanide ionic radii decrease have been interpreted as an increase in the steric crowding produced by the coordinated acetonitrile molecules to the metal center.

For the three complexes, ^1H NMRD profiles of acetonitrile protons have been investigated between 0.01 and 800 MHz. The shapes of the NMRD profiles are quite similar to those observed for the lanthanide aqua ions.^[2] In the present case, the experimental profiles have been interpreted as due to inner- and outer-sphere contributions of both proton-electron dipolar coupling and Curie relaxation mechanisms. For the first time, the magnitude of the outer-sphere contribution to the observed relaxivity has been outlined for the Dy^{3+} and Tm^{3+} ions. The correlation time describing the proton-electron dipolar coupling has been attributed to the electron relaxation time (τ_S) whereas for the Curie relaxation, the rotational correlation time of the acetonitrile complexes (τ_R) is important. As it was already observed for the lanthanide ions in aqueous solutions, in acetonitrile as well very fast electron-spin relaxation times were found: 2.3×10^{-13} s for Nd^{3+} , 2.8×10^{-13} s for Dy^{3+} and 3.5×10^{-13} s for Tm^{3+} . The combined analysis of the ^1H NMRD data with the ^{14}N NMR longitudinal relaxation rates

allowed a more accurate determination of the rotational correlation time of the acetonitrile complexes, giving: 1.6×10^{-11} s for Nd^{3+} , 1.8×10^{-11} s for Dy^{3+} and 1.9×10^{-11} s for Tm^{3+} .

IV.5 REFERENCES

- [1] T. J. Swift, R. E. Connick, *J. Chem. Phys.* **1962**, 37, 307.
- [2] I. Bertini, F. Capozzi, C. Luchinat, G. Nicastrò, Z. Xia, *J. Phys. Chem.* **1993**, 97, 6351.
- [3] S. Rast, P. H. Fries, *J. Chem. Phys.* **2000**, 113, 8724.
- [4] C. Ammann, P. Meier, A. E. Merbach, *J. Magn. Reson.* **1982**, 46, 319.
- [5] A. D. Hugi, L. Helm, A. E. Merbach, *Helv. Chim. Acta* **1985**, 68, 508.
- [6] K. Micskei, L. Helm, E. Brucher, A. E. Merbach, *Inorg. Chem.* **1993**, 32, 3844.
- [7] R. L. Vold, J. S. Waugh, M. P. Klein, D. E. Phelps, *J. Chem. Phys.* **1968**, 48, 3831.
- [8] S. Meiboom, D. Gill, *Rev. Sci. Instrum.* **1958**, 29, 688.
- [9] F. Yerly, *VISUALISEUR 2.3.5* ed., Université de Lausanne: Lausanne, Switzerland, **1999**.
- [10] F. Yerly, *OPTIMISEUR 3.0.0* ed., Université de Lausanne: Lausanne, Switzerland, **1999**.
- [11] J. R. Zimmerman, W. E. Brittin, *J. Phys. Chem.* **1957**, 61, 1328.
- [12] C. Cossy, L. Helm, A. E. Merbach, *Inorg. Chem.* **1988**, 27, 1973.
- [13] H. Eyring, *J. Chem. Phys.* **1935**, 3, 107.
- [14] N. Bloembergen, *J. Chem. Phys.* **1957**, 27, 595.
- [15] J. Granot, D. Fiat, *J. Magn. Reson.* **1975**, 19, 372.
- [16] W. B. Lewis, J. A. Jackson, J. F. Lemons, H. Taube, *J. Chem. Phys.* **1962**, 36, 694.
- [17] B. Bleaney, *J. Magn. Reson.* **1972**, 8, 91.
- [18] I. Solomon, *Phys. Rev.* **1955**, 99, 559.
- [19] N. Bloembergen, *J. Chem. Phys.* **1957**, 27, 572.
- [20] I. Bertini, C. Luchinat, G. Parigi, in *Solution NMR of Paramagnetic Molecules*, Vol. 2, Elsevier, Amsterdam, **2001**, p. 100.
- [21] L.-P. Hwang, J. H. Freed, *J. Chem. Phys.* **1975**, 63, 1975.
- [22] J. H. Freed, *J. Chem. Phys.* **1978**, 68, 4034.
- [23] Y. Ayant, E. Belorizky, P. H. Fries, J. Rosset, *J. Phys.* **1977**, 38, 325.
- [24] C. Vigouroux, E. Belorizky, P. H. Fries, *Eur. Phys. J. D* **1999**, 5, 243.
- [25] D. H. Powell, A. E. Merbach, *Magn. Reson. Chem.* **1994**, 32, 739.
- [26] R. D. Shannon, *Acta Cryst., Sect. A* **1976**, A32, 751.
- [27] B. M. Alsaadi, F. J. C. Rossotti, R. J. P. Williams, *J. Chem. Soc. Dalton Trans.* **1980**, 2147.

- [28] M. Holz, H. Weingärtner, *J. Magn. Reson.* **1991**, 92, 115.

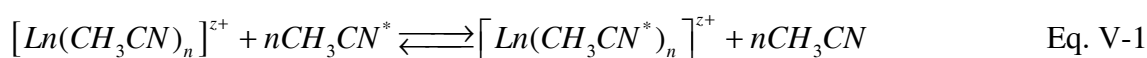
Chapter V

Conclusions

V.1 CONCLUSIONS

In this work extensive studies have been carried out regarding the acetonitrile exchange reaction on some representative lanthanide ions from the Ln(III/II) series: Nd(III), Gd(III), Dy(III), Tm(III) and Eu(II).

The knowledge of the exchange reaction (Eq. V-1) of an acetonitrile molecule between the first coordination sphere of the lanthanide ions and bulk acetonitriles is fundamental to the understanding of the reactivity of these ions in non-aqueous solutions.



The presence of the anion in the first coordination sphere of the metal ion can considerably change the solvent exchange rates; consequently the solvent exchange reaction has to be studied on homoleptic metal complexes. The choice of the counter anion for the synthesis of homoleptic metal complexes is very important. For lanthanides, the generally known “non-coordinating” anions such as $[CF_3SO_3]^-$, $[ClO_4]^-$, $[BF_4]^-$ or $[AlCl_4]^-$ compete with the uncharged CH_3CN ligands for coordination sites to the metal center. Within this work, it has been shown that the extremely robust perfluorinated $[Al(OC(CF_3)_3)_4]^-$ anion has no direct contact to the metal center neither in solid state nor in solution. It represents therefore a new generation of “non-coordinating” anions with respect to lanthanides in non-aqueous solvents. The effect of temperature on the ^{14}N NMR relaxation rates and the chemical shifts, measured at different magnetic fields, allowed the determination of the kinetic parameters describing the acetonitrile exchange reaction on Nd^{3+} , Gd^{3+} , Dy^{3+} , Tm^{3+} and Eu^{2+} ions in their corresponding homoleptic acetonitrile complexes. The obtained kinetic parameters are summarized in Table V-1. The overall labilities of the CH_3CN ligand are the highest ones so far measured on lanthanides in non-aqueous solvents (Table V-2).

Table V-1. Kinetic parameters for CH_3CN exchange on $[Ln(CH_3CN)_n]^{z+}$ in anhydrous acetonitrile with $n = 9$ for $Ln = Nd^{3+}$, Eu^{2+} , Gd^{3+} and Dy^{3+} ; and $n = 8$ for $Ln = Tm^{3+}$.

	Nd^{3+}	Gd^{3+}	Dy^{3+}	Tm^{3+}	Eu^{2+}
$k_{ex}^{298} 10^6 / s^{-1}$	21.5 ± 5.7	55 ± 14.7	159 ± 12	357 ± 39	1530 ± 202
$\Delta H^\ddagger / kJ mol^{-1}$	16.1 ± 3.6	25.5 ± 4.5	23.3 ± 1.0	10.1 ± 1.6	9.1 ± 1.2
$\Delta S^\ddagger / J mol^{-1} K^{-1}$	-50.5 ± 13.6	-11.1 ± 15.7	-9.9 ± 3.8	-47.4 ± 5.7	-36.2 ± 4.4

Table V-2. Rate constants and activation parameters for the non-aqueous solvent exchange reactions on some lanthanide ions.^[1]

Ln^{3+}	$r_{\text{Ln}}^{\text{a)}}$ / pm	k_{ex}^{298} / s ⁻¹	ΔH^\ddagger / kJ mol ⁻¹	ΔS^\ddagger / J K ⁻¹ mol ⁻¹	ΔV^\ddagger / cm ³ mol ⁻¹	Mech.	Ref.
[Ln(TMU)₆]³⁺							
Tb ³⁺	92.3	1380	38.2	-56.7	-	-	[2]
Dy ³⁺	91.2	1290	38.6	-56.0	-	-	[2]
Ho ³⁺	90.1	510	40.9	-55.9	-	-	[2]
Y ³⁺	90.0	253	27.1	-108	-	D	[3]
Er ³⁺	89.0	214	35.5	-81.3	-	D	[2]
Tm ³⁺	88.0	145	29.3	-105	-	D	[4]
Yb ³⁺	86.8	65.5	38.3	-81.8	-	D	[2]
Lu ³⁺	86.1	41.9	41.7	-74	-	D	[5]
Sc ³⁺	74.5	0.90	68.6	-15.7	-	D	[6]
[Ln(DMSO)₈]³⁺							
Gd ³⁺	105.3	6.2×10^6	32.8	-4.7	+8.2	I_d	[7]
[Ln(DMF)₈]³⁺							
Tb ³⁺	104.0	19×10^6	14.1	-58	+5.2	I_d	[8]
Dy ³⁺	102.7	6.3×10^6	13.8	-69	+6.1	I_d	[8]
Ho ³⁺	101.5	3.6×10^6	15.3	-68	+5.2	I_d	[8]
Er ³⁺	100.4	13×10^6	23.6	-30	+5.4	D and I_d	[8]
Tm ³⁺	99.4	31×10^6	33.2	+10	+7.4	D	[8]
Yb ³⁺	98.5	99×10^6	39.3	+40	+11.8	D	[8]
[Ln(CH₃CN)₉]³⁺							
Nd ³⁺	116.3	21.5×10^6	16.1	-50.5	-	d (D or I_d)	this work
Gd ³⁺	110.7	54.9×10^6	25.5	-11.1	-	d (D or I_d)	this work
Dy ³⁺	108.3	159×10^6	23.3	-9.9	-	d (D or I_d)	this work
[Ln(CH₃CN)₈]³⁺							
Tm ³⁺	99.4	357×10^6	10.1	-47.4	-	a (A or I_a)	this work
[Ln(CH₃CN)₉]²⁺							
Eu ²⁺	130	1530×10^6	9.1	-36.2	-	d (D or I_d)	this work

a) six-, eight- and nine-coordinated ionic radii from ref.^[9]

The high coordination numbers and the absence of crystal field stabilisation are responsible for the substantial lability of acetonitrile on these ions. The increasing steric repulsion between the coordinated solvent molecules causes most likely the systematic increase of the acetonitrile exchange rates as the lanthanide ionic radii decrease. As expected, the acetonitrile exchange reaction on the larger, less highly charged Eu^{2+} ion is even much faster. The rotational molecular dynamics of all complexes and the electronic relaxation times of the corresponding lanthanide ions could be determined from the ^1H NMRD profiles, from the ^{14}N longitudinal relaxation and/or the EPR measurements (Table V-3). The electronic relaxation times of lanthanides such as Nd^{3+} , Dy^{3+} and Tm^{3+} in anhydrous acetonitrile are considerably shorter (10^{-12} - 10^{-13} s) than those of Gd^{3+} or Eu^{2+} ions having $S = 7/2$ states (10^{-8} - 10^{-9} s). The same tendency to have very short relaxation times have been observed for these ions in aqueous solution.^[10-12] As the electronic relaxation time of the Dy^{3+} ion in water and anhydrous acetonitrile have the same value, one can conclude that for this ion the electronic relaxation time is independent from the nature of the directly coordinated solvent molecules. This statement is probably true for all lanthanide ions except those having an $S = 7/2$ state.

TableV-3. Rotational correlation times and electronic relaxation times for the $[\text{Ln}(\text{CH}_3\text{CN})_n]^{z+}$ complexes in anhydrous acetonitrile with $n = 9$ for $\text{Ln} = \text{Nd}^{3+}$, Eu^{2+} , Gd^{3+} and Dy^{3+} ; and $n = 8$ for $\text{Ln} = \text{Tm}^{3+}$.

	Nd^{3+}	Gd^{3+}	Dy^{3+}	Tm^{3+}	Eu^{2+}
$\tau_R / 10^{-12} \text{ s}$	16.2 ± 0.1	14.7 ± 2.0	17.6 ± 0.2	19.1 ± 0.07	11.8 ± 1.1
$\tau_S / 10^{-12} \text{ s}$	(0.23 ± 1.6)	4080^{a}	0.28 ± 0.04	0.35 ± 0.02	2700^{a}

^{a)} T_{1e} values calculated at 10 MHz and 298 K using equations from ref.^[13]

To have a deeper view about the reactivity of metal ions in solutions, in addition to the knowledge of the rate constants of the solvent exchange reactions, one needs to know the mechanisms which govern these reactions. There are two frequently used methods for determining the solvent exchange mechanisms on metal ions: establishing the rate laws and measuring the activation volumes.^[1] The former requires the measurement of the solvent exchange rates in an inert diluent. The latter involve high pressure measurements. Determination of the solvent exchange mechanism by the rate law measurements could be performed in the case of the $\text{TMU}^{[4]}$ and $\text{DMF}^{[8]}$ exchange on lanthanides, where first- or second-order rate laws allowed to distinguish between **I_d** or **D** mechanisms. Unfortunately, for acetonitrile, as it is the case of water as well,^[14] an inert diluent does not exist. Therefore, for these solvents, high pressure measurements are needed to determine the reaction mechanisms.

Generally, the sign of the activation volumes (ΔV^\ddagger) is decisive in the interpretation of the reaction mechanisms: negative activation volumes are characteristic for associatively (**a**-) activated reactions and positive activation volumes for the dissociatively (**d**-) activated ones.^[15] For the Gd^{3+} , Dy^{3+} and Eu^{2+} complexes the activation volumes can be determined by high pressure measurements using ^{14}N NMR at 9.4 T, while for Nd^{3+} and Tm^{3+} the use of the higher magnetic field at 18.8 T is mandatory. Unfortunately, the variable frequency high pressure probe-head working at 9.4 T^[16] available in our group is broken, preventing us to perform these measurements. No high pressure probe-head working at 18.8 T is actually available in our laboratory. As a consequence, the high pressure NMR studies could not be carried out and, hence the activation volumes could not be determined. Therefore, in this study, only a hypothesis of the acetonitrile exchange reaction mechanisms on lanthanide ions can be made.

The variation of the enthalpy, ΔH^\ddagger , and entropy, ΔS^\ddagger , of activation obtained from variable temperature NMR experiments can be a guide to a mechanistic change. Thus **d**-activated reactions tend to have greater ΔH^\ddagger values than do **a**-activated reactions, and ΔS^\ddagger tends to be positive for **d**- and negative for **a**-activated reactions.^[1] The negative activation entropies determined for the acetonitrile exchange on the lanthanide complexes seem to support an associatively activated exchange mechanism. However, mechanism attribution basing on entropy values, which are obtained from extrapolation, should be considered with care due to the inherent error of the extrapolation (ΔS^\ddagger is obtained from extrapolation to infinitely high temperature). In this way, negative activation entropies were found for all non-aqueous solvent exchange reactions on lanthanides (Table V-2) and nevertheless, in each case, dissociatively activated mechanisms (**D** or **I_d**) have been attributed. In the case of TMU,^[2] the exchange reaction mechanisms were attributed by determining the reaction rate laws in CD_3CN as inert diluent. The observed first-order rate constants let to the attribution of a dissociative (**D**) mechanism despite the negative activation entropy values. In the case of DMSO^[7] dissociatively activated interchange **I_d** reaction mechanism have been attributed, for the Gd^{3+} ion, by the sign of the volume of activation. In the case of DMF^[8] the exchange reaction mechanisms have been determined by both the activation volumes and rate law constants. The change from second- to first-order exchange rate laws (as determined in nitromethane diluent), the variation of ΔS^\ddagger from negative to positive values and the irregular variation of the DMF exchange rate along the Ln series sustained a mechanistic crossover at Er^{3+} from an **I_d** to a limiting **D** mechanism.^[8] In the case of the CH_3CN , the regular increase

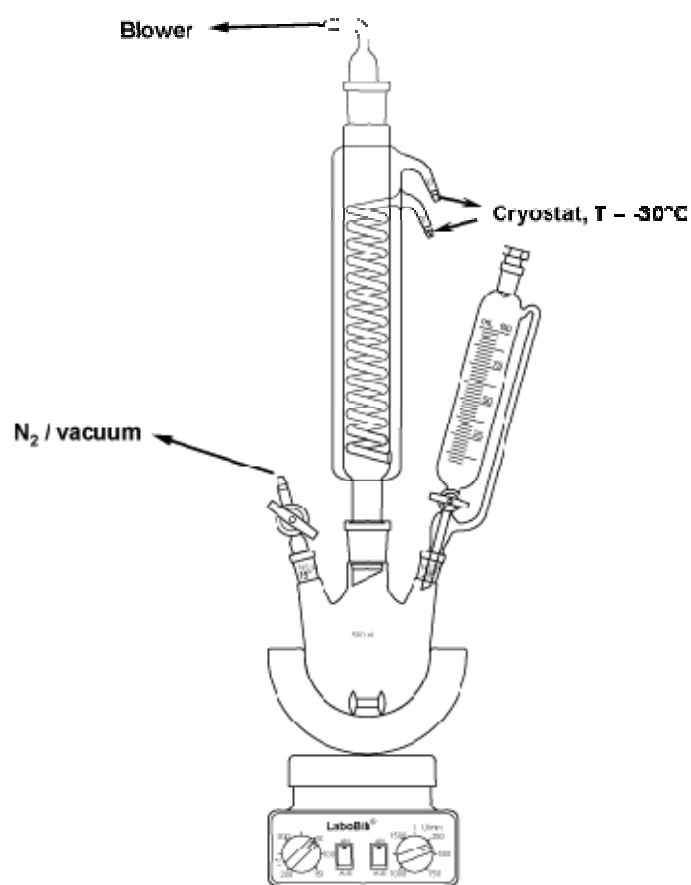
of ΔS^\ddagger from Nd^{3+} to Dy^{3+} (CN = 9) and its drastic decrease while passing to Tm^{3+} (CN = 8) strongly suggest that the mechanism of the exchange reaction varies along the lanthanide series. In this way, for the nine coordinated Nd^{3+} , Gd^{3+} , Dy^{3+} and Eu^{2+} ions the exchange processes most probably take place by a dissociatively activated **d**- (**D** or **I_d**) mechanism. This statement is supported by the fact that generally dissociatively activated mechanisms were observed for all studied non-aqueous solvent exchange reactions on lanthanides and by the fact that a coordination number of ten is not representative for these ions. The steric effects which dominate the lability of the CH_3CN ligands also sustain the hypothesis of a dissociatively activated **d**- (**D** or **I_d**) mechanism. As the ionic radii of lanthanides decrease, the steric repulsion of the coordinated ligands becomes significant. Thus, it become more and more easy to release one ligand to form an eight coordinated intermediate or transition state, which result in acceleration of the exchange processes as it were experimentally observed. In contrast, for the eight coordinated Tm^{3+} ion, the drastic decrease of the activation entropy value clearly points to a mechanistic change. Thus, for this ion most likely an associatively activated **a**- exchange mechanism (**A** or **I_a**) should be attributed. This hypothesis is also in concordance with the observed rapid exchange rate and the stronger bound strengths for the smaller Tm^{3+} ion, as well as with the less pronounced steric repulsion due to only eight coordinated solvent molecules.

V.2 REFERENCES

- [1] L. Helm, A. E. Merbach, *Chem. Rev.* **2005**, *105*, 1923.
- [2] S. F. Lincoln, A. White, *Inorg. Chim. Acta* **1990**, *168*, 265.
- [3] D. L. Pisaniello, S. F. Lincoln, A. F. Williams, A. Jones, *Aust. J. Chem.* **1981**, *34*, 495.
- [4] S. F. Lincoln, A. White, *Polyhedron* **1986**, *5*, 1351.
- [5] S. F. Lincoln, A. M. Hounslow, A. Jones, *Aust. J. Chem.* **1982**, *35*, 2393.
- [6] D. L. Pisaniello, S. F. Lincoln, *J. Chem. Soc., Dalton Trans.* **1980**, 699.
- [7] R. Dessapt, L. Helm, A. E. Merbach, *J. Phys. Condens. Matter* **2004**, *14*, S1027.
- [8] D. L. Pisaniello, L. Helm, P. Meier, A. E. Merbach, *J. Am. Chem. Soc.* **1983**, *105*, 4528.
- [9] R. D. Shannon, *Acta Cryst., Sect. A* **1976**, *A32*, 751.
- [10] J. Reuben, D. Fiat, *J. Chem. Phys.* **1969**, *51*, 4918.
- [11] S. Rast, P. H. Fries, *J. Chem. Phys.* **2000**, *113*, 8724.
- [12] I. Bertini, F. Capozzi, C. Luchinat, G. Nicastro, Z. Xia, *J. Phys. Chem.* **1993**, *97*, 6351.
- [13] E. Belorizky, P. H. Fries, *Phys. Chem. Chem. Phys.* **2004**, *6*, 2341.
- [14] C. Cossy, L. Helm, A. E. Merbach, *Inorg. Chem.* **1988**, *27*, 1973.
- [15] A. E. Merbach, *Pure Appl. Chem.* **1987**, *59*, 161.
- [16] U. Frey, L. Helm, A. E. Merbach, *High Press. Res.* **1990**, *2*, 237.

Chapter VI

Experimental section



This chapter presents the general experimental techniques used in the previously described work, as well as the synthesis of all used compounds and the characterization of those which have never been reported before in the literature. For the compounds which have already been characterized and published, the syntheses with respect to their original publications were slightly modified, and therefore, only their synthesis will be described herein.

VI.1. GENERAL EXPERIMENTAL TECHNIQUES AND MEASUREMENTS

VI.1.1 General Procedures and Starting Materials

Due to air- and moisture sensitivity of most materials all manipulations (if not mentioned otherwise) were undertaken using standard vacuum and Schlenk techniques as well as a glove box with an argon or nitrogen filled atmosphere (H_2O and $\text{O}_2 < 0.1$ ppm). Reagents and solvents were purchased from commercial sources with high quality grade (Table VI-1). Most of them were used without further purification.

Table VI-1. Sources of the starting materials sources and some purification methods.

Starting material	Source	Purity or purification method
LiAlH_4	Aldrich	extraction with Et_2O
$\text{R}^{\text{F}}\text{OH}$	P M Invest, Russia	distillation
AgF	Apollo Scientific, UK	99 %
NdCl_3	Aldrich	Anhydrous, 99.99 %
EuCl_3	Aldrich	Anhydrous, 99.99 %
GdCl_3	Abr	Anhydrous, 99.9 % (REO)
DyCl_3	Aldrich	Anhydrous, 99.99 %
TmCl_3	Aldrich	Anhydrous, 99.99 %
$\text{Bu}_4\text{N CF}_3\text{SO}_3$	Fluka	Puriss, 99.0 %
CH_3CN	Fluka	Puriss, over molecular sieves ($\text{H}_2\text{O} < 0.001$ %)
CH_2Cl_2	Fluka	Puriss, over molecular sieves ($\text{H}_2\text{O} < 0.005$ %)

VI.1.2 Elemental Analysis

Elemental analyses were performed at Solvias AG analytical laboratories (CH-Basel).

VI.1.3 X-Ray Diffraction and Crystal Structure Determination

Data collection for X-ray structure determinations were performed on a OXFORD DIFFRACTION SAPHIRE/KM4 CCD (kappa geometry) and a BRUKER APEX II diffractometer, all using graphite-monochromated Mo-K α (0.71073 Å) radiation. Single crystals were mounted in perfluoroether oil on top of a glass fiber and then brought into the cold stream of a low temperature device so that the oil solidified. All calculations were performed on PC's using the SHELX97 software package. The structures were solved by the Patterson heavy atom method or direct methods and successive interpretation of the difference Fourier maps, followed by least-squares refinement. All non-hydrogen atoms were refined anisotropically. The hydrogen atoms were included in the refinement in calculated positions by a riding model using fixed isotropic parameters.

VI.1.4 Conductivity

Conductivity measurements were carried out in inert atmosphere in argon filled glove box. The measurements were done at 25°C with a Metrohm 712 Conductometer working with a platinum electrode and having a cell constant of 0.814 cm⁻¹.

VI.1.5 IR and Raman Spectroscopy

All samples for IR and Raman measurements were prepared in inert atmosphere. The IR spectra were recorded on a Nicolet Magna 760 spectrometer using a diamond Orbit ATR unit (extended ATR correction with refraction index 1.5 was used). Raman spectra were recorded at room temperature on a Bruker RAM II FT-Raman spectrometer (using a liquid nitrogen cooled, highly sensitive Ge detector) in sealed melting point capillaries. Both IR and Raman

spectra were recorded by Dr. Ines Raabe at the *Universität Freiburg, Institut für Anorganische und Analytische Chemie*.

VI.1.6 UV-Vis Spectroscopy

UV-Vis spectra were recorded on a Perkin-Elmer Lambda 850 double beam spectrometer. Thermostatizable cylindrical cells with 10 cm optical path length were used for the variable temperature study, in order to maximise the observed absorption. The temperature was controlled by circulating ethanol from a thermostat bath. The temperature was measured using a Pt-resistance thermometer.

VI.1.7 NMR Spectroscopy

NMR spectra were recorded on Bruker Avance 200, DRX-400, ARX-400 and Avance II-800 spectrometers. Bruker BVT-3000 temperature control units were used to maintain a constant temperature, which was measured by the substitution technique.^[1] Chemical shifts were referenced against the TMS resonance frequency, using the unified scale recommendation of IUPAC (see below).^[2] The longitudinal and transverse relaxation times, T_1 and T_2 , were obtained with the Inversion-recovery^[3] and the Carr-Purcell-Meiboom-Gill^[4] spin echo techniques, respectively.

In 2001 IUPAC recommended^[2] a unified scale for reporting the NMR chemical shifts of all nuclei relative to the ^1H resonance of tetramethylsilane (TMS). The unified scale is designed to provide a precise ratio, Ξ , of the resonance frequency of a given nuclide to that of the primary reference, the ^1H resonance of TMS in dilute solution (volume fraction, $\phi < 1\%$) in chloroform. Thus, the chemical shifts of the X nuclei can be determined on the unified (TMS-based) scale just by measuring the resonance frequency of the sample and using a predetermined reference frequency for the nuclide in question. Therefore, only one (sample) tube is required and no reference substance needs to be added. The predetermined reference frequency is obtained by measuring the proton resonance of TMS under similar condition to the sample (with the same lock compound) in a single experiment for the spectrometer being

used. Then, the frequency of the usual secondary reference for the nucleus X can be calculated using the predetermined value of TMS, Eq. VI-1:

$$\nu_{X,\text{ref}} = (\nu_{\text{TMS}} \Xi_{\text{ref}}) / 100 \quad \text{Eq. VI-1}$$

where:

$\nu_{X,\text{ref}}$	resonance frequency of a given nuclei (X) whit respect to TMS
ν_{TMS}	proton resonance frequency of TMS
Ξ_{ref}	frequency ratio between the secondary reference frequency and that of the ^1H in TMS ^[2]

Hence, the chemical shift of a given X nuclei in the sample can be easily derived form Eq. VI-2:

$$\delta_{X,\text{sample}} = \frac{\nu_{X,\text{sample}} - \nu_{X,\text{ref}}}{\nu_{X,\text{ref}}} 10^6 \quad \text{Eq. VI-2}$$

where:

$\nu_{X,\text{sample}}$	resonance frequency of a given nuclei (X) in the sample
$\delta_{X,\text{sample}}$	chemical shift of a given nuclei (X) in the sample whit respect to TMS

If the lock substance in the sample solution is not the same as that of the reference solution, a lock correction must be applied, Eq. VI-3:

$$\delta_{\text{true}} = \delta_{\text{measured}} + (\delta_{\text{sample}}^{\text{lock}} - \delta_{\text{reference}}^{\text{lock}}) \quad \text{Eq. VI-3}$$

VI.1.8 ^1H NMRD

Longitudinal ^1H relaxation rate measurements were performed on a Stelar Spinmaster FFC (Fast Field Cycling) relaxometer covering a continuum of magnetic fields from 7×10^{-4} to 0.47 T (corresponding to a proton Larmor frequency range 0.01 – 20 MHz) equipped with VTC90 temperature control unit. The temperature was regulated by an air or N_2 gas flow. At higher fields, the measurements were performed on different Bruker spectrometers: an

Avance 200 (2.3 T, 100 MHz; 4.7 T, 200 MHz), ARX-400 (9.4 T, 400 MHz) and Avance II-800 (18.8T, 800 MHz). In each case, the temperature was measured by the substitution technique.^[1]

VI.1.9 EPR Spectroscopy

Q-(35 GHz) and X-band (9.4 GHz) EPR spectra were recorded on a Bruker ELEXSYS E500 spectrometer at variable temperatures. A controlled nitrogen gas flow was used to maintain a constant temperature, which was measured by a substitution technique. The microwave frequency was measured using a frequency counter embedded in the standard microwave bridge (X-band) or an external Hewlett-Packard 5353B frequency counter (Q-band). Continuous wave EPR was used for all frequencies.

VI.2 SYNTHESIS AND CHARACTERIZATION OF THE COMPOUNDS USED IN THIS WORK

VI.2.1 Synthesis of $\text{Li}[\text{Al}(\text{OC}(\text{CF}_3)_3)_4]$

The synthesis of $\text{Li}[\text{Al}(\text{OC}(\text{CF}_3)_3)_4]$ salt has been performed as previously described.^[5, 6]

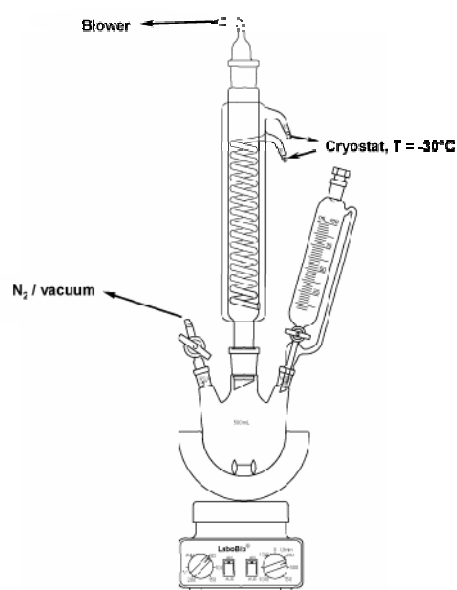


Figure VI-1: Typical installation for the synthesis of Li^+ salt in inert atmosphere

In the glove box, LiAlH_4 (3.28 g, 86.4 mmol; white powder) is weighted in a three neck flask. 350 ml of freshly distilled hexane is used as solvent media. A slight excess (4.1 equivalents) of $\text{HOC}(\text{CF}_3)_3$ (50 ml, $d = 1.693 \text{ g ml}^{-1}$; colorless solution) is added drop wise by rigorous stirring at room temperature (Figure VI-1). When all the alcohol is added the solution mixture is heated to reflux for 3 h. To avoid evaporation of the perfluorinated alcohol due to his low boiling point (b.p. = 45°C), the system is connected to a double reflux condenser which is connected to a cryostat and set to a temperature of -30°C . A bubbler filled with silicon oil is used to allow H_2 evaporation. After the 3 h of reflux, the solution mixture is let to cool down at room temperature, then refrigerated for about 2 h at -25°C . The solvent is decanted and the white solid is dried under vacuum until a constant weight is obtained. If the obtained product has some grayish precipitate (Al^0), purification by extraction with dichloromethane or dichloroethane in an extraction frit is necessary. All manipulations should be done with precautious exclusion of air and water.

Isolated yield: 78.14 g of white solid, 93 %.

VI.2.2 Synthesis of $\text{Ag}[\text{Al}(\text{OC}(\text{CF}_3)_3)_4]$

$\text{Ag}[\text{Al}(\text{OC}(\text{CF}_3)_3)_4]$ was synthesized according to the literature.^[6]

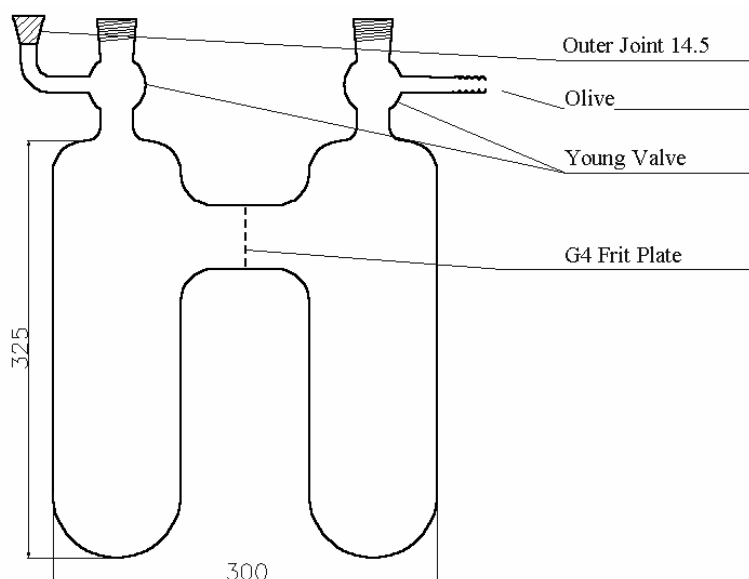


Figure VI-2: Two bulbed Schlenk vessel with Young valves and G4 frit plate. Measures are given in mm.

In the glove box, $\text{Li}[\text{Al}(\text{OC}(\text{CF}_3)_3)_4]$ (28.87 g, 29.64 mmol; white powder) and a slight excess (1.4 equivalents) of AgF (5.28 g, 41.61 mmol; should have light beige color and be stored with exclusion of light) are weighted together into one side of a special two bulbed Schlenk vessel with Young valves and frit plate (Figure VI-2). 150 ml of CH_2Cl_2 is added to the reaction mixture and the vessel is evacuated until the solvent started to boil and left under the vapor pressure of the solvent. The mixture is left in an ultrasonic bath overnight. Prior to filtration the solution should be frozen at -25°C for at least 3 h to check if unreacted $\text{Li}[\text{Al}(\text{OC}(\text{CF}_3)_3)_4]$ is still present (formation of a white microcrystalline precipitate). If not, the reaction is finished and the solution is filtered. Afterwards the resulting solid is dried under vacuum, finely ground in a glove box, placed in a new flask and left directly hooked to a vacuum line (10^{-3} mbar) until a constant weight is achieved. With this procedure one gets rid of the last traces of coordinated solvent and obtains solvent free naked $\text{Ag}[\text{Al}(\text{OC}(\text{CF}_3)_3)_4]$. All manipulations should be done with precautions exclusion of air and water.

Isolated yield: 30.12 g of light beige powder, 95 %.

VI.2.3 Synthesis of $[\text{Bu}_4\text{N}][\text{Al}(\text{OC}(\text{CF}_3)_3)_4]$

$[\text{Bu}_4\text{N}][\text{Al}(\text{OC}(\text{CF}_3)_3)_4]$ was synthesized according to the literature.^[7]

$\text{Li}[\text{Al}(\text{OC}(\text{CF}_3)_3)_4]$ (7.871 g, 8.08 mmol; white solid) dissolved in 800 ml of bi-distilled water is reacted with a slight excess (1.2 equivalents) of Bu_4NCl (2.761 g, 9.93 mmol; white solid) dissolved in 80 ml of bi-distilled water. The reaction mixture is stirred overnight at 50°C . 100 ml of acetone is added before the filtration of the suspension over a Büchner frit. The precipitate is washed with water until no more Cl^- is present. The white, crystalline product is dried overnight at 120°C .

Isolated yield: 8.8 g of white solid, 90 %.

VI.2.4 Synthesis of $[\text{Nd}(\text{CH}_3\text{CN})_9][\text{Al}(\text{OC}(\text{CF}_3)_3)_4]_3$ 1

In the glove box, anhydrous NdCl_3 (0.453 g, 1.81 mmol; pale violet powder) dissolved in 600 ml of anhydrous acetonitrile (the solubility of the anhydrous NdCl_3 is quite low in acetonitrile) is reacted with a slight excess (3.1 equivalents) of $\text{Ag}[\text{Al}(\text{OC}(\text{CF}_3)_3)_4]$ (6.11 g, 5.68 mmol; light beige powder) at room temperature. AgCl is generated instantaneously. After 10 minutes of stirring the solution is let in dark overnight so that all the precipitate is deposited. The suspension is filtered to eliminate AgCl . The solvent is removed under vacuum and the obtained pale pink solid is washed with dichloromethane in order to get rid of the unreacted $\text{Ag}[\text{Al}(\text{OC}(\text{CF}_3)_3)_4]$ (approximately seven times with 20 ml). X-ray diffraction quality crystals are obtained at room temperature, in a few days, by slow diffusion of dichloromethane over the concentrated acetonitrile solution of the neodymium salt.

Isolated yield: 4.2 g of pale pink powder, 67 %.

^1H NMR (400 MHz, CH_3CN / TMS, 25°C): $\delta = 1.96$ (s, CH_3).

^{13}C NMR (101 MHz, CH_3CN / TMS, 25°C): $\delta = 0.78$ (q, $J_{(\text{C,H})} = 136.18$ Hz, CH_3),
117.71 (s, CN), 121.14 (q, $J_{(\text{C,F})} = 292.6$ Hz, CF_3), 78.44 (m, O-C).

^{19}F NMR (376 MHz, CH_3CN / TMS, 25°C): $\delta = -76.01$ (s, $\Delta\nu_{1/2} = 8.33$ Hz, CF_3).

^{27}Al NMR (104 MHz, CH_3CN / TMS, 25°C): $\delta = 34.50$ (s, $\Delta\nu_{1/2} = 4.02$ Hz).

^{14}N NMR (29 MHz, CH_3CN / TMS, 25°C): $\delta = -131.61$ (s, $\Delta\nu_{1/2} = 114.67$ Hz, CN).

Elemental analysis: Found: C 22.72 %, H 1.01 %, N 3.86 %, F 51.00 %, Nd 4.12 %; required for $\text{C}_{66}\text{H}_{27}\text{N}_9\text{O}_{12}\text{F}_{108}\text{Al}_3\text{Nd}$: C 23.21 %, H 0.8 %, N 3.69 %, F 60.08%, Nd 4.22 %.

IR: $\tilde{\nu} = 289$ (w), 315 (m), 327 (w), 355 (vw), 376 (w), 399 (m), 447 (ms), 537 (ms), 561 (ms), 572 (m), 727 (ms), 755 (vw), 832 (mw), 933 (vw), 972 (vs), 1168 (m), 1218 (vs), 1244 (vs), 1275 (s), 1299 (ms), 1353 (m), 2281 (m), 2310 (w), 2955 (vw).

Raman: $\tilde{\nu} = 233$ (w), 288 (w), 323 (w), 368 (w), 408 (w), 538 (w), 562 (w), 572 (sh,w), 746 (ms), 798 (ms), 936 (vw), 978 (w), 1245 (w), 1274 (w), 1377 (m), 2284 (vs), 2312 (ms), 2956 (s), 3022 (mw).

VI.2.5 Synthesis of $[\text{Eu}(\text{CH}_3\text{CN})_9][\text{Al}(\text{OC}(\text{CF}_3)_3)_4]_3$ **2**

In the glove box, anhydrous EuCl_3 (0.463 g, 1.79 mmol; yellow powder) dissolved in 180 ml of anhydrous acetonitrile is reacted with a slight excess (3.1 equivalents) of $\text{Ag}[\text{Al}(\text{OC}(\text{CF}_3)_3)_4]$ (5.97 g, 5.55 mmol; light beige powder) at room temperature. AgCl is generated instantaneously. After 10 minutes of stirring the solution is let in dark overnight so that all the precipitate is deposited. The suspension is filtered to eliminate AgCl . The solvent is removed under vacuum and the obtained white solid is washed with dichloromethane in order to get rid of the unreacted $\text{Ag}[\text{Al}(\text{OC}(\text{CF}_3)_3)_4]$ (approximately seven times with 20 ml). X-ray diffraction quality crystals are obtained at room temperature, in a few days, by slow diffusion of dichloromethane over the concentrated acetonitrile solution of the europium salt.

Isolated yield: 4.23 g of white powder, 69 %.

^1H NMR (400 MHz, CH_3CN / TMS, 25°C): $\delta = 1.98$ (s, CH_3).

^{13}C NMR (101 MHz, CH_3CN / TMS, 25°C): $\delta = 0.70$ (q, $J_{(\text{C},\text{H})} = 136.18$ Hz, CH_3),
116.92 (s, CN), 120.94 (q, $J_{(\text{C},\text{F})} = 292.6$ Hz, CF_3), 78.88 (m, O-C).

^{19}F NMR (376 MHz, CH_3CN / TMS, 25°C): $\delta = -75.99$ (s, $\Delta\nu_{1/2} = 7.6$ Hz, CF_3).

^{27}Al NMR (104 MHz, CH_3CN / TMS, 25°C): $\delta = 34.47$ (s, $\Delta\nu_{1/2} = 3.35$ Hz).

^{14}N NMR (29 MHz, CH_3CN / TMS, 25°C): $\delta = -140.03$ (s, $\Delta\nu_{1/2} = 84.67$ Hz CN).

Elemental analysis: Found: C 22.16 %, H 0.9 %, N 3.93 %, F 56.71 %, Eu 4.56 %; required for $\text{C}_{66}\text{H}_{27}\text{N}_9\text{O}_{12}\text{F}_{108}\text{Al}_3\text{Eu}$: C 23.16 %, H 0.8 %, N 3.68 %, F 59.95 %, Eu 4.44 %.

IR: $\tilde{\nu} = 283$ (w), 315 (w), 376 (w), 447 (m), 537 (mw), 561 (w), 572 (vw, sh), 727 (s), 756 (vw), 832 (w), 935 (w), 972 (vs), 1170 (ms), 1216 (vs), 1244 (vs), 1275 (s), 1299 (ms), 1353 (m), 1377 (vw), 2283 (m), 2311 (w), 2956 (vw).

Raman: $\tilde{\nu} = 234$ (w), 288 (w), 322 (m), 368 (w), 409 (mw), 538 (m), 561 (mw), 572 (sh, w), 746 (s), 797 (s), 938 (w), 973 (vw), 1135 (vw), 1218 (vw), 1244 (vs), 1273 (w), 1307 (w), 1377 (m), 1416 (vw), 2285 (vs), 2313 (s), 2956 (vs), 3021 (w).

Reduction of $[\text{Eu}(\text{CH}_3\text{CN})_9][\text{Al}(\text{OC}(\text{CF}_3)_3)_4]_3$ to $[\text{Eu}(\text{CH}_3\text{CN})_9][\text{Al}(\text{OC}(\text{CF}_3)_3)_4]_2$ 2a

An acetonitrile solution of $[\text{Eu}(\text{CH}_3\text{CN})_9][\text{Al}(\text{OC}(\text{CF}_3)_3)_4]_3$ is passed over a glass column filled with Zn/Hg amalgam at least 7 times. The more the initial solution is concentrated in Eu^{3+} , the more the reduced solution will be yellow (due to Eu^{2+}).

Preparation of Zn/Hg amalgam:^[8]

Zn (76 g, 1.16 mol, 20 mesh) is stirred manually with a plastic spatula in 50 ml of HCl (1 M) for 5 min. The activated zinc is washed with distilled water, then is manually stirred in 50 ml of HgCl_2 (0.125 M in HCl 0.1 M) for 15 min. The amalgam formation is instantaneous. The Zn/Hg amalgam is washed several times with distilled water, until no more Cl^- is present. Prior to use the Zn/Hg is dried under nitrogen flux for at least 3 – 4 days.

VI.2.6 Synthesis of $[\text{Gd}(\text{CH}_3\text{CN})_9][\text{Al}(\text{OC}(\text{CF}_3)_3)_4]_3$ 3

In the glove box, anhydrous GdCl_3 (0.490 g, 1.86 mmol; white powder) dissolved in 120 ml of anhydrous acetonitrile is reacted with a slight excess (3.1 equivalents) of $\text{Ag}[\text{Al}(\text{OC}(\text{CF}_3)_3)_4]$ (6.19 g, 5.76 mmol; light beige powder) at room temperature. AgCl is generated instantaneously. After 10 minutes of stirring the solution is let in dark overnight so that all the precipitate is deposited. The suspension is filtered to eliminate AgCl . The solvent is removed under vacuum and the obtained white solid is washed with dichloromethane in order to get rid of the unreacted $\text{Ag}[\text{Al}(\text{OC}(\text{CF}_3)_3)_4]$ (approximately seven times with 20 ml). X-ray diffraction quality crystals are obtained at room temperature, in a few days, by slow diffusion of dichloromethane over the concentrated acetonitrile solution of the gadolinium salt.

Isolated yield: 4.46 g of white powder, 70 %.

^1H NMR (400 MHz, CH_3CN / TMS, 25°C): δ = 2.04 (s, CH_3).

^{13}C NMR (101 MHz, CH_3CN / TMS, 25°C): δ = 0.30 (q, $J_{(\text{C},\text{H})}$ = 136.18 Hz, CH_3),

114.72 (s, CN), 120.95 (q, $J_{(\text{C},\text{F})}$ = 292.6 Hz, CF_3), 78.69 (m, O-C).

^{19}F NMR (376 MHz, CH_3CN / TMS, 25°C): $\delta = -76.21$ (s, $\Delta\nu_{1/2} = 4.02$ Hz, CF_3).

^{27}Al NMR (104 MHz, CH_3CN / TMS, 25°C): $\delta = 34.47$ (s, $\Delta\nu_{1/2} = 4.02$ Hz).

^{14}N NMR (29 MHz, CH_3CN / TMS, 25°C): $\delta = -139.05$ (s, $\Delta\nu_{1/2} = 94.78$ Hz, CN).

Elemental analysis: Found: C 22.90 %, H 0.78 %, N 4.13 %, F 59.48 %, Gd 4.6 %; required for $\text{C}_{66}\text{H}_{27}\text{N}_9\text{O}_{12}\text{F}_{108}\text{Al}_3\text{Gd}$: C 23.12 %, H 0.79 %, N 3.68 %, F 59.86 %, Gd 4.59 %.

IR: $\tilde{\nu} = 283$ (w), 315 (w), 376 (w), 404 (w), 447 (mw), 537 (w), 561 (vw), 572 (vw, sh), 727 (ms), 756 (vw), 833 (w), 934 (vw), 972 (vs), 1171 (m), 1218 (vs), 1245 (vs), 1275 (s), 1299 (ms), 1353 (m), 2283 (mw), 2312 (vw), 2955 (vw).

Raman: $\tilde{\nu} = 236$ (w), 291 (w), 324 (ms), 370 (w), 417 (m), 540 (w), 563 (w), 571 (sh, w), 748 (s), 799 (s), 942 (w), 977 (vw), 1276 (w), 1308 (w), 1379 (m), 1420 (vw), 2290 (vs), 2318 (s), 2957 (vs), 3023 (mw).

VI.2.7 Synthesis of $[\text{Dy}(\text{CH}_3\text{CN})_9][\text{Al}(\text{OC}(\text{CF}_3)_3)_4]_3$ **4**

In the glove, box anhydrous DyCl_3 (0.488 g, 1.82 mmol; white powder) dissolved in 90 ml of anhydrous acetonitrile is reacted with a slight excess (3.1 equivalents) of $\text{Ag}[\text{Al}(\text{OC}(\text{CF}_3)_3)_4]$ (6.05 g, 5.63 mmol; light beige powder) at room temperature. AgCl is generated instantaneously. After 10 minutes of stirring the solution is let in dark overnight so that all the precipitate is deposited. The suspension is filtered to eliminate AgCl . The solvent is removed under vacuum and the obtained white solid is washed with dichloromethane in order to get rid of the unreacted $\text{Ag}[\text{Al}(\text{OC}(\text{CF}_3)_3)_4]$ (approximately seven times with 20 ml). X-ray diffraction quality crystals are obtained at room temperature, in a few days, by slow diffusion of dichloromethane over the concentrated acetonitrile solution of the dysprosium salt.

Isolated yield: 4.5 g of white powder, 72 %.

^1H NMR (400 MHz, CH_3CN / TMS, 25°C): $\delta = 1.81$ (s, CH_3)

^{13}C NMR (101 MHz, CH_3CN / TMS, 25°C): $\delta = 0.28$ (q, $J_{(\text{C},\text{H})} = 136.18$ Hz, CH_3), 113.51 (s, CN), 121.34 (q, $J_{(\text{C},\text{F})} = 292.6$ Hz, CF_3), 78.90 (m, O-C).

^{19}F NMR (376 MHz, CH_3CN / TMS, 25°C): $\delta = -76.19$ (s, $\Delta\nu_{1/2} = 5.67$ Hz, CF_3).

^{27}Al NMR (104 MHz, CH_3CN / TMS, 25°C): $\delta = 34.28$ (s, $\Delta\nu_{1/2} = 3.68$ Hz).

^{14}N NMR (29 MHz, CH_3CN / TMS, 25°C): $\delta = -136.25$ (s, $\Delta\nu_{1/2} = 109.02$ Hz, CN).

Elemental analysis: Found: C 22.10 %, H 0.86 %, N 3.66 %, F 51.55 %, Dy 4.71 %; required for $\text{C}_{66}\text{H}_{27}\text{N}_9\text{O}_{12}\text{F}_{108}\text{Al}_3\text{Dy}$: C 23.09 %, H 0.79 %, N 3.67 %, F 59.76 %, Dy 4.73 %.

IR: $\tilde{\nu} = 287$ (w), 315 (m), 331 (vw), 368 (w), 380 (w), 417 (vw), 449 (ms), 537 (ms), 561 (ms), 572 (mw), 727 (ms), 756 (vw), 832 (w), 937 (vw), 972 (vs), 1171 (m), 1217 (vs), 1245 (vs), 1275 (vs), 1299 (s), 1353 (8m), 1376 (vw), 2284 (m), 2313 (w), 2955 (vw).

Raman: $\tilde{\nu} = 233$ (w), 287 (w), 323 (w), 368 (w), 414 (w), 539 (w), 562 (w), 572 (sh, w), 746 (ms), 798 (ms), 938 (vw), 1271 (mw), 1308 (w), 1377 (m), 2286 (vs), 2314 (ms), 2955 (w), 3024 (vs).

VI.2.8 Synthesis of $[\text{Tm}(\text{CH}_3\text{CN})_8][\text{Al}(\text{OC}(\text{CF}_3)_3)_4]_3$ **5**

In the glove box, anhydrous TmCl_3 (0.493 g, 1.80 mmol; white powder) dissolved in 25 ml of anhydrous acetonitrile is reacted with a slight excess (3.1 equivalents) of $\text{Ag}[\text{Al}(\text{OC}(\text{CF}_3)_3)_4]$ (6.00 g, 5.58 mmol; light beige powder) at room temperature. AgCl is generated instantaneously. After 10 minutes of stirring the solution is let in dark overnight so that all the precipitate is deposited. The suspension is filtered to eliminate AgCl . The solvent is removed under vacuum and the obtained white solid is washed with dichloromethane in order to get rid of the unreacted $\text{Ag}[\text{Al}(\text{OC}(\text{CF}_3)_3)_4]$ (approximately seven times with 20 ml). X-ray diffraction quality crystals are obtained at room temperature, in a few days, by slow diffusion of dichloromethane over the concentrated acetonitrile solution of the thulium salt.

Isolated yield: 4.75 g of white powder, 77 %.

^1H NMR (400 MHz, CH_3CN / TMS, 25°C): $\delta = 1.97$ (s, CH_3).

^{13}C NMR (101 MHz, CH_3CN / TMS, 25°C): $\delta = 0.70$ (q, $J_{(\text{C},\text{H})} = 136.18$ Hz, CH_3), 116.93 (s, CN), 121.34 (q, $J_{(\text{C},\text{F})} = 292.6$ Hz, CF_3), 79.12 (m, O-C).

^{19}F NMR (376 MHz, CH_3CN / TMS, 25°C): $\delta = -75.83$ (s, $\Delta\nu_{1/2} = 4.81$ Hz, CF_3).

^{27}Al NMR (104 MHz, CH_3CN / TMS, 25°C): $\delta = 34.60$ (s, $\Delta\nu_{1/2} = 3.35$ Hz).

^{14}N NMR (29 MHz, CH_3CN / TMS, 25°C): $\delta = -140.24$ (s, $\Delta\nu_{1/2} = 103.16$ Hz, CN).

Elemental analysis: Found: C 22.08 %, H 0.86 %, N 3.62 %, F 51.78 %, Tm 4.91 %; required for $\text{C}_{64}\text{H}_{24}\text{N}_8\text{O}_{12}\text{F}_{108}\text{Al}_3\text{Tm}$: C 22.62 %, H 0.71 %, N 3.3 %, F 60.37 %, Tm 4.97 %.

IR: $\tilde{\nu} = 289$ (w), 315 (m), 328 (w), 355 (vw), 370 (w), 375 (w), 407 (w), 448 (ms), 537 (ms), 561 (ms), 572 (m), 727 (ms), 756 (vw), 832 (mw), 972 (vs), 1217 (vs), 1245 (s), 1275 (s), 1299 (ms), 1353 (m), 2286 (m), 2314 (w), 2955 (vw).

Raman: $\tilde{\nu} = 235$ (w), 291 (w), 324 (m), 370 (w), 418 (m), 549 (w), 563 (w), 572 (sh, w), 748 (ms), 799 (ms), 942 (w), 977 (w), 1276 (w), 1308 (w), 1379 (m), 1420 (vw), 2290 (vs), 2318 (ms), 3023 (vs).

VI.2.9 Synthesis of $\text{Ln}(\text{CH}_3\text{CN})_3(\text{CF}_3\text{SO}_3)_3$, Ln = Eu, Gd

In a glove box, $\text{Ln}(\text{H}_2\text{O})_9(\text{CF}_3\text{SO}_3)_3$ (1 g, 1.30 mmol; white powder) is dissolved under rigorous stirring in TEOF (4 g, 27.03 mmol; colorless solution $d = 1.69 \text{ g ml}^{-1}$) (if necessary, some drops of ethanol can be added to complete the dissolution). The mixture solution is heated to 50°C for 1h, then CH_3CN (1.5 g, 36.58 mmol) is added. After 15 min of stirring, the filtrated solution is let to crystallize at room temperature. Crystals are formed within 2-3 days. The highly hygroscopic crystals are dried under vacuum.

Isolated yield of $\text{Ln}(\text{CH}_3\text{CN})_3(\text{CF}_3\text{SO}_3)_3$: 0.76 g of white powder, 80 %.

VI.3 REFERENCES

- [1] C. Ammann, P. Meier, A. E. Merbach, *J. Magn. Reson.* **1982**, 46, 319.
- [2] R. K. Harris, E. D. Becker, S. M. Cabral de Menezes, R. Goodfellow, P. Grangere, *Pure Appl. Chem.* **2001**, 73, 1795.
- [3] R. L. Vold, J. S. Waugh, M. P. Klein, D. E. Phelps, *J. Chem. Phys.* **1968**, 48, 3831.
- [4] S. Meiboom, D. Gill, *Rev. Sci. Instrum.* **1958**, 29, 688.
- [5] I. Krossing, *Chem. Eur. J.* **2001**, 7, 490.
- [6] I. Krossing, A. Reisinger, *Coord. Chem. Rev.* **2006**, 250, 2721.
- [7] I. Raabe, I. Krossing, K. Wagner, K. Guttsche, *in preparation*.
- [8] S. D. Clerc, R. A. Jewsbury, M. G. Mortimer, J. Zeng, *Anal. Chim. Acta* **1997**, 339, 225.

Chapter VII

Appendix

VII.1 GENERALITIES

Table A-1. Spectroscopic properties of selected nuclides.

Nucleus	Spin, I	Natural abundance (%)	Measured NMR freq. (rel. ^1H ref.) (MHz)	Gyromagnetic ratio, γ ($10^7 \text{ rad s}^{-1} \text{ T}^{-1}$)
^1H	1/2	99.989	100.0000	26.75
^{13}C	1/2	1.07	25.145	6.73
^{14}N	1	99.63	7.226	1.93
^{17}O	5/2	0.038	13.557	-3.63
^{19}F	1/2	100	94.094	25.16
^{27}Al	5/2	100	26.057	6.98
^{151}Eu	5/2	47.81	-	6.65
^{153}Eu	5/2	52.19	-	2.94
^{155}Gd	3/2	14.80	-	-0.82
^{157}Gd	3/2	15.65	-	-1.08

Table A-2. Lanthanide ions electronic properties.

ION	$^{2S+1}L_J$	S	L	J	g_J (calc)	μ_{eff} (in μ_B)
Ce^{3+}	$^2F_{5/2}$	1/2	3	5/2	6/7	2.535
Pr^{3+}	3H_4	1	5	4	4/5	3.578
Nd^{3+}	$^4I_{9/2}$	3/2	6	9/2	8/11	3.618
Pm^{3+}	5I_4	2	6	4	3/5	2.683
Sm^{3+}	$^6H_{5/2}$	5/2	5	5/2	2/7	0.845
Eu^{3+}	7F_0	3	3	0	-	0.000
Gd^{3+}	$^8S_{7/2}$	7/2	0	7/2	2	7.937
Tb^{3+}	7F_6	3	3	6	3/2	9.721
Dy^{3+}	$^6H_{15/2}$	5/2	5	15/2	4/3	10.646
Ho^{3+}	5I_8	2	6	8	5/4	10.607
Er^{3+}	$^4I_{15/2}$	3/2	6	15/2	6/5	9.581
Tm^{3+}	3H_6	1	5	6	7/6	7.561
Yb^{3+}	$^2F_{7/2}$	1/2	3	7/2	8/7	4.536

Lanthanides:
$$g_J = 1 + \frac{J(J+1) - L(L+1) + S(S+1)}{2J(J+1)}$$

VII.2 EXPERIMENTAL DATA FOR CHAPTER II

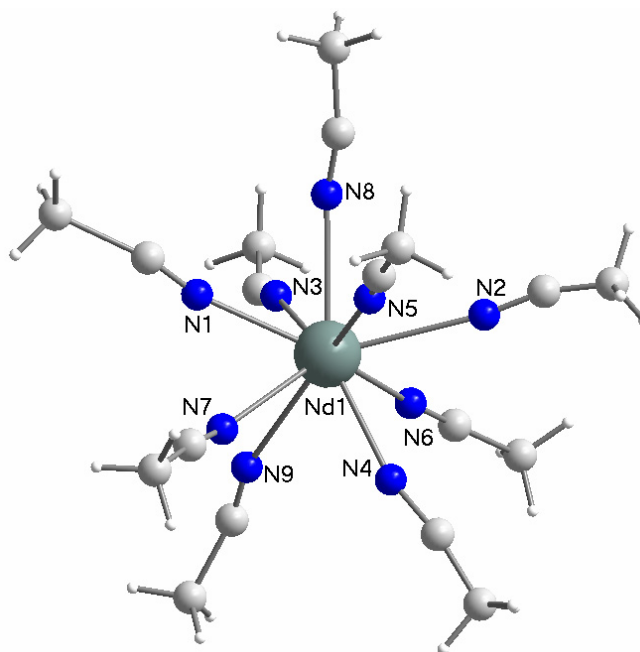


Figure A II-1. Ball and stick representation of the solid-state structure of the $[\text{Nd}(\text{CH}_3\text{CN})_9]^{3+}$ cation in compound **1**. The $[\text{Al}(\text{OC}(\text{CF}_3)_3)_4]^-$ anions as well as the embedded solvent molecules ($4\text{CH}_2\text{Cl}_2$) have been omitted for clarity.

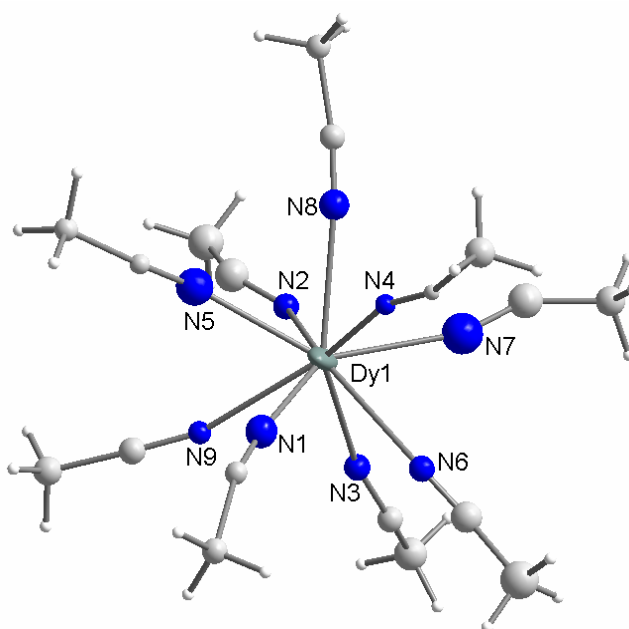


Figure A II-2. Solid-state structure of the $[\text{Dy}(\text{CH}_3\text{CN})_9]^{3+}$ cation in compound **4**. The ellipsoids are drawn at the 25% probability level. The $[\text{Al}(\text{OC}(\text{CF}_3)_3)_4]^-$ anions as well as the embedded solvent molecules ($3\text{CH}_2\text{Cl}_2$ and CH_3CN) have been omitted for clarity.

Table A II-1. Crystal data and structure refinement for [Tm(CH₃CN)₈][Al(OC(CF₃)₃)₄]₃·2CH₂Cl₂·2CH₃CN (**5**·2CH₂Cl₂·2CH₃CN).

Identification code	gb15	
Empirical formula	C70 H34 Al3 Cl4 F108 N10 O12 Tm	
Formula weight	3650.74	
Temperature	140(2) K	
Wavelength	0.71073 Å	
Crystal system	Monoclinic	
Space group	P2(1)/n	
Unit cell dimensions	a = 14.2601(3) Å	α = 90°.
	b = 32.5092(6) Å	β = 95.8031(18)°.
	c = 26.3378(5) Å	γ = 90°.
Volume	12147.2(4) Å ³	
Z	4	
Density (calculated)	1.996 Mg/m ³	
Absorption coefficient	1.063 mm ⁻¹	
F(000)	7072	
Crystal size	0.33 x 0.26 x 0.14 mm ³	
Theta range for data collection	2.62 to 26.37°.	
Index ranges	-17 ≤ h ≤ 17, -40 ≤ k ≤ 40, -32 ≤ l ≤ 32	
Reflections collected	105298	
Independent reflections	24607 [R(int) = 0.0509]	
Completeness to theta = 26.37°	99.1 %	
Absorption correction	Semi-empirical from equivalents	
Max. and min. transmission	1.00000 and 0.63891	
Refinement method	Full-matrix least-squares on F ²	
Data / restraints / parameters	24607 / 54 / 1875	
Goodness-of-fit on F ²	1.052	
Final R indices [I > 2σ(I)]	R1 = 0.0813, wR2 = 0.1894	
R indices (all data)	R1 = 0.1101, wR2 = 0.2096	
Largest diff. peak and hole	1.773 and -1.744 e.Å ⁻³	

Table A II-2. Atomic coordinates ($\times 10^4$) and equivalent isotropic displacement parameters ($\text{\AA}^2 \times 10^3$) for $[\text{Tm}(\text{CH}_3\text{CN})_8][\text{Al}(\text{OC}(\text{CF}_3)_3)_4]_3 \cdot 2\text{CH}_2\text{Cl}_2 \cdot 2\text{CH}_3\text{CN}$ (**5** $2\text{CH}_2\text{Cl}_2 \cdot 2\text{CH}_3\text{CN}$). $U(\text{eq})$ is defined as one third of the trace of the orthogonalized U^{ij} tensor.

	x	y	z	U(eq)
Tm(1)	7636(1)	4006(1)	7139(1)	26(1)
N(1)	8834(4)	3512(2)	6988(2)	34(1)
N(2)	6750(4)	3378(2)	7022(2)	34(1)
N(3)	8013(4)	3641(2)	7925(2)	37(2)
N(4)	6281(4)	4071(2)	7604(2)	32(1)
N(5)	8131(4)	4512(2)	7773(2)	38(2)
N(6)	6784(4)	4613(2)	6820(2)	32(1)
N(7)	8893(4)	4402(2)	6814(2)	35(1)
N(8)	7324(4)	3916(2)	6226(2)	27(1)
C(1)	9369(5)	3259(2)	6969(3)	34(2)
C(2)	10067(6)	2930(3)	6964(3)	46(2)
C(3)	6312(6)	3087(2)	7038(3)	39(2)
C(4)	5734(8)	2724(3)	7058(4)	60(3)
C(5)	8044(5)	3454(2)	8294(3)	34(2)
C(6)	8058(7)	3218(3)	8758(3)	54(2)
C(7)	5691(5)	4066(2)	7858(3)	31(2)
C(8)	4935(6)	4055(3)	8186(3)	47(2)
C(9)	8323(6)	4744(3)	8089(3)	39(2)
C(10)	8574(7)	5036(3)	8491(3)	56(2)
C(11)	6229(6)	4852(2)	6708(3)	36(2)
C(12)	5479(7)	5153(3)	6563(5)	64(3)
C(13)	9485(5)	4593(2)	6687(3)	34(2)
C(14)	10239(6)	4844(3)	6516(4)	59(3)
C(15)	7147(5)	3870(2)	5801(3)	28(1)
C(16)	6919(6)	3809(2)	5254(3)	39(2)
Al(1)	7981(1)	6522(1)	10257(1)	23(1)
F(1)	8137(5)	7763(2)	10165(3)	81(2)
F(2)	6863(6)	7404(2)	10140(3)	110(3)
F(3)	7041(5)	7856(2)	9562(3)	90(2)
F(4)	6375(6)	7059(3)	9231(4)	139(4)
F(5)	7484(8)	6744(2)	8913(3)	131(4)
F(6)	7212(7)	7375(3)	8711(3)	126(4)
F(7)	8687(5)	7793(2)	9165(3)	83(2)
F(8)	9094(7)	7183(2)	8977(3)	122(3)
F(9)	9521(5)	7418(2)	9708(4)	99(3)
F(10)	8602(4)	5413(2)	9766(3)	86(2)
F(11)	8431(4)	5961(2)	9318(2)	72(2)
F(12)	9665(5)	5589(2)	9287(3)	96(3)
F(13)	9913(4)	6457(2)	9402(2)	68(2)
F(14)	11070(4)	6085(2)	9739(3)	68(2)
F(15)	10518(4)	6575(2)	10159(2)	60(1)
F(16)	10574(5)	5397(2)	10202(3)	94(3)
F(17)	10715(4)	5894(2)	10752(3)	75(2)

F(18)	9514(5)	5496(2)	10708(3)	90(2)
F(19)	8597(6)	7500(2)	11207(3)	93(2)
F(20)	9550(4)	7087(2)	10912(2)	74(2)
F(21)	9635(5)	7189(2)	11716(2)	84(2)
F(22)	9719(5)	6372(2)	11393(3)	85(2)
F(23)	9047(6)	6450(3)	12085(3)	100(3)
F(24)	8428(6)	6070(2)	11478(3)	98(2)
F(25)	7935(5)	7101(3)	12103(3)	105(3)
F(26)	7094(6)	6586(3)	11803(3)	117(3)
F(27)	6971(5)	7177(3)	11427(3)	101(3)
F(28)	7093(5)	5537(2)	10436(3)	94(2)
F(29)	6462(5)	5899(2)	10961(2)	72(2)
F(30)	5617(5)	5486(2)	10503(3)	90(2)
F(31)	5736(5)	6613(2)	10631(3)	93(2)
F(32)	4641(4)	6200(2)	10372(4)	111(3)
F(33)	5107(6)	6635(2)	9875(3)	99(2)
F(34)	4954(4)	5725(2)	9555(2)	88(2)
F(35)	5799(5)	6145(2)	9196(2)	84(2)
F(36)	6374(5)	5573(2)	9465(3)	83(2)
O(1)	8202(4)	6914(2)	9847(2)	46(1)
O(2)	8926(4)	6191(2)	10288(2)	42(1)
O(3)	7900(4)	6683(2)	10876(2)	43(1)
O(4)	6951(4)	6291(2)	10029(2)	43(1)
C(17)	7907(6)	7234(2)	9548(3)	37(2)
C(18)	7476(8)	7572(3)	9856(4)	62(3)
C(19)	7249(12)	7100(4)	9093(5)	92(5)
C(20)	8824(9)	7416(3)	9347(5)	66(3)
C(21)	9559(5)	5983(2)	10045(3)	35(2)
C(22)	9067(7)	5732(3)	9594(4)	60(3)
C(23)	10274(6)	6275(3)	9837(4)	47(2)
C(24)	10099(8)	5692(3)	10439(5)	66(3)
C(25)	8331(6)	6784(3)	11335(3)	39(2)
C(26)	9036(7)	7142(3)	11292(4)	57(2)
C(27)	8873(8)	6417(3)	11578(4)	65(3)
C(28)	7556(8)	6923(5)	11674(4)	76(4)
C(29)	6152(5)	6080(2)	10090(3)	35(2)
C(30)	6326(6)	5743(3)	10496(3)	46(2)
C(31)	5390(6)	6377(3)	10245(4)	50(2)
C(32)	5812(7)	5882(3)	9569(3)	52(2)
Al(2)	2509(1)	3827(1)	5236(1)	23(1)
F(37)	-385(4)	3988(2)	4745(2)	74(2)
F(38)	164(5)	3463(2)	4424(2)	78(2)
F(39)	-960(5)	3393(3)	4880(3)	122(4)
F(40)	598(9)	2850(2)	5089(3)	136(4)
F(41)	-113(5)	2991(2)	5733(2)	99(3)
F(42)	1377(5)	3037(2)	5799(2)	75(2)
F(43)	-666(6)	3797(4)	5779(3)	147(5)
F(44)	675(5)	3709(2)	6190(2)	74(2)
F(45)	464(9)	4209(2)	5658(3)	140(4)
F(46)	3467(5)	3123(2)	6477(2)	80(2)

F(47)	2617(5)	3532(3)	6860(3)	106(3)
F(48)	4117(4)	3514(2)	7063(2)	67(2)
F(49)	2349(5)	4296(3)	6451(4)	113(3)
F(50)	3594(5)	4562(2)	6200(3)	72(2)
F(51)	3622(6)	4312(2)	6960(2)	96(2)
F(52)	4929(4)	3474(2)	6106(2)	71(2)
F(53)	5137(3)	4033(2)	6523(2)	63(2)
F(54)	4664(4)	4051(2)	5726(2)	70(2)
F(55)	4168(4)	4664(2)	4843(2)	64(2)
F(56)	3564(4)	5121(2)	5292(2)	61(1)
F(57)	3474(4)	5187(2)	4476(2)	62(2)
F(58)	1748(5)	4985(2)	5478(3)	84(2)
F(59)	1739(5)	5329(2)	4784(3)	89(2)
F(60)	860(5)	4798(3)	4815(3)	95(2)
F(61)	1895(5)	4840(2)	3952(2)	76(2)
F(62)	2999(5)	4391(2)	4053(2)	65(2)
F(63)	1624(5)	4231(2)	4222(2)	74(2)
F(64)	4927(6)	3243(2)	4975(5)	152(5)
F(65)	4624(6)	3724(2)	4423(5)	150(5)
F(66)	4790(7)	3101(3)	4172(5)	153(5)
F(67)	3216(9)	3557(3)	3731(3)	132(4)
F(68)	2976(11)	2908(3)	3786(3)	183(6)
F(69)	1977(8)	3340(4)	4040(4)	164(5)
F(70)	3811(5)	2551(2)	4651(3)	84(2)
F(71)	2380(6)	2737(4)	4733(5)	170(5)
F(72)	3474(7)	2875(3)	5304(3)	109(3)
O(5)	1381(4)	3673(2)	5177(2)	65(2)
O(6)	2980(5)	3733(2)	5851(2)	57(2)
O(7)	2594(5)	4349(2)	5137(2)	56(2)
O(8)	3089(6)	3584(3)	4803(2)	88(3)
C(33)	551(5)	3550(2)	5306(3)	32(2)
C(34)	-157(6)	3590(3)	4827(3)	50(2)
C(35)	617(8)	3100(3)	5485(4)	59(3)
C(36)	214(10)	3814(4)	5741(4)	75(3)
C(37)	3544(5)	3834(2)	6264(3)	35(2)
C(38)	3433(7)	3497(3)	6675(4)	58(3)
C(39)	3271(7)	4254(3)	6477(4)	59(3)
C(40)	4577(6)	3852(3)	6156(3)	44(2)
C(41)	2494(6)	4671(3)	4815(3)	47(2)
C(42)	3431(7)	4912(3)	4856(4)	51(2)
C(43)	1713(8)	4951(3)	4978(5)	67(3)
C(44)	2247(7)	4531(3)	4253(4)	56(2)
C(45)	3409(6)	3259(3)	4555(3)	44(2)
C(46)	4443(9)	3334(4)	4512(7)	92(5)
C(47)	2906(12)	3242(5)	4026(5)	97(5)
C(48)	3280(8)	2852(4)	4827(5)	77(3)
Al(3)	1943(2)	6139(1)	7665(1)	26(1)
F(73)	2397(8)	6863(3)	6600(5)	147(4)
F(74)	1493(9)	6410(6)	6241(5)	223(8)
F(75)	2931(8)	6551(3)	5944(3)	142(4)

F(76)	1807(7)	5610(3)	6583(3)	142(4)
F(77)	2584(10)	5757(3)	5960(3)	189(7)
F(78)	3306(9)	5496(3)	6704(7)	308(14)
F(79)	4298(7)	6079(3)	6394(7)	250(11)
F(80)	4246(9)	6086(5)	7205(7)	273(12)
F(81)	4041(11)	6670(3)	6763(5)	200(8)
F(82)	2106(7)	4900(2)	7407(4)	124(3)
F(83)	3575(6)	5087(4)	7720(5)	160(5)
F(84)	2675(12)	4621(3)	8112(5)	231(8)
F(85)	3797(5)	5647(2)	8334(4)	108(3)
F(86)	3596(7)	5099(3)	8735(5)	178(6)
F(87)	2702(11)	5675(3)	8901(3)	198(7)
F(88)	1841(7)	4959(4)	8829(5)	225(8)
F(89)	1037(8)	5478(5)	8586(4)	211(8)
F(90)	898(6)	4970(4)	8031(6)	211(8)
F(91)	4200(8)	6459(3)	8306(5)	180(6)
F(92)	3582(7)	6471(3)	9069(3)	150(4)
F(93)	4252(8)	7033(3)	8704(5)	196(7)
F(94)	1832(8)	6624(3)	9025(3)	140(4)
F(95)	2658(11)	7171(3)	9119(3)	228(9)
F(96)	1413(9)	7159(4)	8493(6)	179(6)
F(97)	2928(4)	7509(2)	8215(3)	74(2)
F(98)	2090(5)	7157(2)	7646(3)	103(3)
F(99)	3618(7)	7066(3)	7718(3)	134(4)
F(100)	-106(15)	6108(3)	8310(3)	223(9)
F(101)	-229(8)	6735(2)	8150(3)	126(4)
F(102)	-1388(11)	6329(4)	7956(6)	195(7)
F(103)	230(5)	6991(2)	7266(3)	85(2)
F(104)	-1173(5)	6812(2)	7131(3)	102(3)
F(105)	-247(8)	6587(3)	6641(2)	124(3)
F(106)	-1474(7)	5992(3)	7025(4)	125(3)
F(107)	-135(9)	5798(3)	6814(4)	149(4)
F(108)	-556(7)	5600(2)	7517(3)	115(3)
O(9)	2512(8)	6213(2)	7143(3)	104(4)
O(10)	2076(5)	5639(2)	7837(2)	54(2)
O(11)	2422(6)	6446(2)	8144(2)	71(2)
O(12)	810(6)	6239(3)	7509(5)	126(4)
C(49)	2840(6)	6168(2)	6698(3)	36(2)
C(50)	2454(13)	6544(5)	6356(5)	98(5)
C(51)	2576(10)	5750(4)	6450(4)	112(6)
C(52)	3932(11)	6252(6)	6771(6)	198(14)
C(53)	2305(6)	5323(2)	8144(3)	44(2)
C(54)	2689(14)	4969(4)	7824(6)	210(16)
C(55)	3169(12)	5436(4)	8561(6)	131(7)
C(56)	1528(12)	5170(5)	8393(6)	360(40)
C(57)	2762(6)	6792(2)	8364(3)	45(2)
C(58)	3701(11)	6704(4)	8620(6)	260(20)
C(59)	2103(11)	6940(4)	8772(6)	185(13)
C(60)	2792(8)	7144(3)	7988(5)	104(6)
C(61)	-117(6)	6292(3)	7460(3)	41(2)

C(62)	-539(15)	6361(4)	7974(4)	99(6)
C(63)	-324(7)	6675(3)	7120(3)	56(2)
C(64)	-566(10)	5918(4)	7196(5)	73(3)
N(9)	3011(7)	5733(4)	11050(4)	97(4)
C(65)	2989(7)	5472(4)	10128(4)	65(3)
C(66)	3004(6)	5613(3)	10650(4)	57(2)
N(10)	4332(7)	6962(3)	11696(4)	76(3)
C(67)	4832(11)	7478(4)	11036(5)	89(4)
C(68)	4566(8)	7190(3)	11406(4)	60(3)
Cl(1)	-4018(3)	5139(1)	8220(2)	119(1)
Cl(2)	-3300(3)	5756(2)	7602(3)	144(2)
C(69)	-4083(12)	5649(5)	8030(6)	120(6)
Cl(3)	3129(4)	2497(2)	2629(2)	126(2)
Cl(4)	4138(7)	3152(2)	2217(5)	248(4)
C(70)	3451(16)	3036(9)	2595(9)	207(14)

Table A II-3. Bond lengths [Å] and angles [°] for [Tm(CH₃CN)₈][Al(OC(CF₃)₃)₄]₃·2CH₂Cl₂·2CH₃CN (**5**·2CH₂Cl₂·2CH₃CN).

Tm(1)-N(5)	2.400(6)
Tm(1)-N(4)	2.400(6)
Tm(1)-N(3)	2.400(6)
Tm(1)-N(2)	2.405(6)
Tm(1)-N(1)	2.407(6)
Tm(1)-N(8)	2.418(6)
Tm(1)-N(6)	2.421(6)
Tm(1)-N(7)	2.430(7)
N(1)-C(1)	1.127(9)
N(2)-C(3)	1.136(10)
N(3)-C(5)	1.144(10)
N(4)-C(7)	1.126(9)
N(5)-C(9)	1.136(10)
N(6)-C(11)	1.127(9)
N(7)-C(13)	1.128(9)
N(8)-C(15)	1.132(9)
C(1)-C(2)	1.463(10)
C(2)-H(2A)	0.9800
C(2)-H(2B)	0.9800
C(2)-H(2C)	0.9800
C(3)-C(4)	1.444(12)
C(4)-H(4A)	0.9800
C(4)-H(4B)	0.9800
C(4)-H(4C)	0.9800
C(5)-C(6)	1.443(11)
C(6)-H(6A)	0.9800
C(6)-H(6B)	0.9800
C(6)-H(6C)	0.9800
C(7)-C(8)	1.449(10)
C(8)-H(8A)	0.9800
C(8)-H(8B)	0.9800
C(8)-H(8C)	0.9800
C(9)-C(10)	1.440(11)
C(10)-H(10A)	0.9800
C(10)-H(10B)	0.9800
C(10)-H(10C)	0.9800
C(11)-C(12)	1.471(11)
C(12)-H(12A)	0.9800
C(12)-H(12B)	0.9800
C(12)-H(12C)	0.9800
C(13)-C(14)	1.455(11)
C(14)-H(14A)	0.9800
C(14)-H(14B)	0.9800
C(14)-H(14C)	0.9800
C(15)-C(16)	1.457(10)
C(16)-H(16A)	0.9800
C(16)-H(16B)	0.9800

C(16)-H(16C)	0.9800
Al(1)-O(4)	1.705(5)
Al(1)-O(1)	1.720(6)
Al(1)-O(2)	1.721(6)
Al(1)-O(3)	1.725(5)
F(1)-C(18)	1.334(13)
F(2)-C(18)	1.326(11)
F(3)-C(18)	1.317(12)
F(4)-C(19)	1.340(19)
F(5)-C(19)	1.306(16)
F(6)-C(19)	1.345(13)
F(7)-C(20)	1.324(11)
F(8)-C(20)	1.323(13)
F(9)-C(20)	1.303(14)
F(10)-C(22)	1.335(12)
F(11)-C(22)	1.330(13)
F(12)-C(22)	1.319(10)
F(13)-C(23)	1.344(11)
F(14)-C(23)	1.339(10)
F(15)-C(23)	1.316(10)
F(16)-C(24)	1.360(13)
F(17)-C(24)	1.318(13)
F(18)-C(24)	1.313(12)
F(19)-C(26)	1.329(12)
F(20)-C(26)	1.313(11)
F(21)-C(26)	1.343(11)
F(22)-C(27)	1.354(14)
F(23)-C(27)	1.337(12)
F(24)-C(27)	1.307(12)
F(25)-C(28)	1.335(11)
F(26)-C(28)	1.340(15)
F(27)-C(28)	1.299(16)
F(28)-C(30)	1.306(11)
F(29)-C(30)	1.323(10)
F(30)-C(30)	1.314(10)
F(31)-C(31)	1.328(11)
F(32)-C(31)	1.287(11)
F(33)-C(31)	1.318(11)
F(34)-C(32)	1.322(11)
F(35)-C(32)	1.302(11)
F(36)-C(32)	1.329(12)
O(1)-C(17)	1.346(9)
O(2)-C(21)	1.340(9)
O(3)-C(25)	1.342(9)
O(4)-C(29)	1.353(9)
C(17)-C(19)	1.509(14)
C(17)-C(18)	1.532(13)
C(17)-C(20)	1.575(14)
C(21)-C(23)	1.533(11)
C(21)-C(22)	1.548(12)

C(21)-C(24)	1.552(13)
C(25)-C(27)	1.529(14)
C(25)-C(26)	1.549(13)
C(25)-C(28)	1.556(13)
C(29)-C(30)	1.533(11)
C(29)-C(31)	1.540(12)
C(29)-C(32)	1.550(11)
Al(2)-O(8)	1.673(6)
Al(2)-O(5)	1.676(6)
Al(2)-O(6)	1.716(6)
Al(2)-O(7)	1.724(6)
F(37)-C(34)	1.344(11)
F(38)-C(34)	1.267(11)
F(39)-C(34)	1.331(10)
F(40)-C(35)	1.320(11)
F(41)-C(35)	1.332(13)
F(42)-C(35)	1.310(11)
F(43)-C(36)	1.270(15)
F(44)-C(36)	1.338(13)
F(45)-C(36)	1.357(15)
F(46)-C(38)	1.326(13)
F(47)-C(38)	1.310(12)
F(48)-C(38)	1.341(10)
F(49)-C(39)	1.317(11)
F(50)-C(39)	1.345(13)
F(51)-C(39)	1.333(11)
F(52)-C(40)	1.339(10)
F(53)-C(40)	1.327(10)
F(54)-C(40)	1.321(10)
F(55)-C(42)	1.328(11)
F(56)-C(42)	1.329(11)
F(57)-C(42)	1.348(10)
F(58)-C(43)	1.317(13)
F(59)-C(43)	1.332(12)
F(60)-C(43)	1.345(13)
F(61)-C(44)	1.344(10)
F(62)-C(44)	1.322(12)
F(63)-C(44)	1.316(10)
F(64)-C(46)	1.372(19)
F(65)-C(46)	1.321(14)
F(66)-C(46)	1.306(16)
F(67)-C(47)	1.386(18)
F(68)-C(47)	1.267(16)
F(69)-C(47)	1.367(19)
F(70)-C(48)	1.346(14)
F(71)-C(48)	1.335(13)
F(72)-C(48)	1.259(14)
O(5)-C(33)	1.326(9)
O(6)-C(37)	1.328(9)
O(7)-C(41)	1.346(9)

O(8)-C(45)	1.348(10)
C(33)-C(35)	1.539(12)
C(33)-C(34)	1.539(10)
C(33)-C(36)	1.546(12)
C(37)-C(40)	1.529(12)
C(37)-C(39)	1.542(13)
C(37)-C(38)	1.559(12)
C(41)-C(43)	1.535(15)
C(41)-C(42)	1.544(12)
C(41)-C(44)	1.554(13)
C(45)-C(47)	1.503(14)
C(45)-C(46)	1.510(14)
C(45)-C(48)	1.526(16)
Al(3)-O(12)	1.658(7)
Al(3)-O(9)	1.683(7)
Al(3)-O(10)	1.693(5)
Al(3)-O(11)	1.698(6)
F(73)-C(50)	1.227(15)
F(74)-C(50)	1.44(2)
F(75)-C(50)	1.338(16)
F(76)-C(51)	1.267(12)
F(77)-C(51)	1.292(12)
F(78)-C(51)	1.440(15)
F(79)-C(52)	1.296(15)
F(80)-C(52)	1.303(15)
F(81)-C(52)	1.368(17)
F(82)-C(54)	1.328(15)
F(83)-C(54)	1.374(18)
F(84)-C(54)	1.362(14)
F(85)-C(55)	1.318(14)
F(86)-C(55)	1.314(12)
F(87)-C(55)	1.404(15)
F(88)-C(56)	1.374(14)
F(89)-C(56)	1.349(16)
F(90)-C(56)	1.402(18)
F(91)-C(58)	1.396(15)
F(92)-C(58)	1.429(15)
F(93)-C(58)	1.331(14)
F(94)-C(59)	1.307(13)
F(95)-C(59)	1.372(14)
F(96)-C(59)	1.366(15)
F(97)-C(60)	1.335(10)
F(98)-C(60)	1.278(10)
F(99)-C(60)	1.458(13)
F(100)-C(62)	1.313(16)
F(101)-C(62)	1.361(17)
F(102)-C(62)	1.21(2)
F(103)-C(63)	1.329(12)
F(104)-C(63)	1.292(12)
F(105)-C(63)	1.307(11)

F(106)-C(64)	1.349(15)
F(107)-C(64)	1.292(14)
F(108)-C(64)	1.333(14)
O(9)-C(49)	1.311(10)
O(10)-C(53)	1.328(9)
O(11)-C(57)	1.334(9)
O(12)-C(61)	1.327(11)
C(49)-C(51)	1.539(14)
C(49)-C(52)	1.573(19)
C(49)-C(50)	1.583(18)
C(53)-C(56)	1.432(18)
C(53)-C(54)	1.56(2)
C(53)-C(55)	1.61(2)
C(57)-C(58)	1.464(15)
C(57)-C(60)	1.516(12)
C(57)-C(59)	1.573(16)
C(61)-C(64)	1.511(14)
C(61)-C(63)	1.543(13)
C(61)-C(62)	1.554(15)
N(9)-C(66)	1.123(13)
C(65)-C(66)	1.447(14)
C(65)-H(65A)	0.9800
C(65)-H(65B)	0.9800
C(65)-H(65C)	0.9800
N(10)-C(68)	1.138(13)
C(67)-C(68)	1.430(16)
C(67)-H(67A)	0.9800
C(67)-H(67B)	0.9800
C(67)-H(67C)	0.9800
Cl(1)-C(69)	1.733(18)
Cl(2)-C(69)	1.699(18)
C(69)-H(69A)	0.9900
C(69)-H(69B)	0.9900
Cl(3)-C(70)	1.82(3)
Cl(4)-C(70)	1.513(18)
C(70)-H(70A)	0.9900
C(70)-H(70B)	0.9900
N(5)-Tm(1)-N(4)	77.3(2)
N(5)-Tm(1)-N(3)	73.4(2)
N(4)-Tm(1)-N(3)	74.1(2)
N(5)-Tm(1)-N(2)	141.7(2)
N(4)-Tm(1)-N(2)	72.6(2)
N(3)-Tm(1)-N(2)	76.0(2)
N(5)-Tm(1)-N(1)	114.1(2)
N(4)-Tm(1)-N(1)	139.9(2)
N(3)-Tm(1)-N(1)	73.2(2)
N(2)-Tm(1)-N(1)	77.5(2)
N(5)-Tm(1)-N(8)	141.9(2)
N(4)-Tm(1)-N(8)	116.2(2)

N(3)-Tm(1)-N(8)	143.1(2)
N(2)-Tm(1)-N(8)	74.28(19)
N(1)-Tm(1)-N(8)	79.4(2)
N(5)-Tm(1)-N(6)	77.6(2)
N(4)-Tm(1)-N(6)	72.8(2)
N(3)-Tm(1)-N(6)	139.8(2)
N(2)-Tm(1)-N(6)	114.2(2)
N(1)-Tm(1)-N(6)	145.6(2)
N(8)-Tm(1)-N(6)	73.64(19)
N(5)-Tm(1)-N(7)	72.9(2)
N(4)-Tm(1)-N(7)	142.5(2)
N(3)-Tm(1)-N(7)	117.2(2)
N(2)-Tm(1)-N(7)	143.2(2)
N(1)-Tm(1)-N(7)	74.5(2)
N(8)-Tm(1)-N(7)	77.4(2)
N(6)-Tm(1)-N(7)	79.0(2)
C(1)-N(1)-Tm(1)	171.8(6)
C(3)-N(2)-Tm(1)	170.3(6)
C(5)-N(3)-Tm(1)	169.2(6)
C(7)-N(4)-Tm(1)	171.8(6)
C(9)-N(5)-Tm(1)	175.8(6)
C(11)-N(6)-Tm(1)	165.2(6)
C(13)-N(7)-Tm(1)	176.6(6)
C(15)-N(8)-Tm(1)	177.6(6)
N(1)-C(1)-C(2)	178.0(8)
C(1)-C(2)-H(2A)	109.5
C(1)-C(2)-H(2B)	109.5
H(2A)-C(2)-H(2B)	109.5
C(1)-C(2)-H(2C)	109.5
H(2A)-C(2)-H(2C)	109.5
H(2B)-C(2)-H(2C)	109.5
N(2)-C(3)-C(4)	178.7(9)
C(3)-C(4)-H(4A)	109.5
C(3)-C(4)-H(4B)	109.5
H(4A)-C(4)-H(4B)	109.5
C(3)-C(4)-H(4C)	109.5
H(4A)-C(4)-H(4C)	109.5
H(4B)-C(4)-H(4C)	109.5
N(3)-C(5)-C(6)	178.6(9)
C(5)-C(6)-H(6A)	109.5
C(5)-C(6)-H(6B)	109.5
H(6A)-C(6)-H(6B)	109.5
C(5)-C(6)-H(6C)	109.5
H(6A)-C(6)-H(6C)	109.5
H(6B)-C(6)-H(6C)	109.5
N(4)-C(7)-C(8)	179.5(9)
C(7)-C(8)-H(8A)	109.5
C(7)-C(8)-H(8B)	109.5
H(8A)-C(8)-H(8B)	109.5
C(7)-C(8)-H(8C)	109.5

H(8A)-C(8)-H(8C)	109.5
H(8B)-C(8)-H(8C)	109.5
N(5)-C(9)-C(10)	179.5(10)
C(9)-C(10)-H(10A)	109.5
C(9)-C(10)-H(10B)	109.5
H(10A)-C(10)-H(10B)	109.5
C(9)-C(10)-H(10C)	109.5
H(10A)-C(10)-H(10C)	109.5
H(10B)-C(10)-H(10C)	109.5
N(6)-C(11)-C(12)	178.0(9)
C(11)-C(12)-H(12A)	109.5
C(11)-C(12)-H(12B)	109.5
H(12A)-C(12)-H(12B)	109.5
C(11)-C(12)-H(12C)	109.5
H(12A)-C(12)-H(12C)	109.5
H(12B)-C(12)-H(12C)	109.5
N(7)-C(13)-C(14)	179.1(10)
C(13)-C(14)-H(14A)	109.5
C(13)-C(14)-H(14B)	109.5
H(14A)-C(14)-H(14B)	109.5
C(13)-C(14)-H(14C)	109.5
H(14A)-C(14)-H(14C)	109.5
H(14B)-C(14)-H(14C)	109.5
N(8)-C(15)-C(16)	179.8(9)
C(15)-C(16)-H(16A)	109.5
C(15)-C(16)-H(16B)	109.5
H(16A)-C(16)-H(16B)	109.5
C(15)-C(16)-H(16C)	109.5
H(16A)-C(16)-H(16C)	109.5
H(16B)-C(16)-H(16C)	109.5
O(4)-Al(1)-O(1)	108.1(3)
O(4)-Al(1)-O(2)	112.5(3)
O(1)-Al(1)-O(2)	107.5(3)
O(4)-Al(1)-O(3)	109.2(3)
O(1)-Al(1)-O(3)	113.8(3)
O(2)-Al(1)-O(3)	105.8(3)
C(17)-O(1)-Al(1)	150.9(6)
C(21)-O(2)-Al(1)	148.7(6)
C(25)-O(3)-Al(1)	149.1(5)
C(29)-O(4)-Al(1)	152.5(5)
O(1)-C(17)-C(19)	111.9(7)
O(1)-C(17)-C(18)	111.4(7)
C(19)-C(17)-C(18)	112.2(10)
O(1)-C(17)-C(20)	105.4(7)
C(19)-C(17)-C(20)	108.3(9)
C(18)-C(17)-C(20)	107.4(7)
F(3)-C(18)-F(2)	108.9(9)
F(3)-C(18)-F(1)	107.2(9)
F(2)-C(18)-F(1)	108.3(10)
F(3)-C(18)-C(17)	112.5(9)

F(2)-C(18)-C(17)	108.9(8)
F(1)-C(18)-C(17)	111.0(8)
F(5)-C(19)-F(4)	106.9(11)
F(5)-C(19)-F(6)	108.0(12)
F(4)-C(19)-F(6)	107.5(12)
F(5)-C(19)-C(17)	112.5(11)
F(4)-C(19)-C(17)	109.5(12)
F(6)-C(19)-C(17)	112.1(9)
F(9)-C(20)-F(8)	106.5(10)
F(9)-C(20)-F(7)	109.5(10)
F(8)-C(20)-F(7)	107.8(9)
F(9)-C(20)-C(17)	110.8(9)
F(8)-C(20)-C(17)	110.2(9)
F(7)-C(20)-C(17)	111.9(9)
O(2)-C(21)-C(23)	111.4(6)
O(2)-C(21)-C(22)	110.9(6)
C(23)-C(21)-C(22)	108.6(7)
O(2)-C(21)-C(24)	107.5(7)
C(23)-C(21)-C(24)	108.2(7)
C(22)-C(21)-C(24)	110.2(8)
F(12)-C(22)-F(11)	108.0(10)
F(12)-C(22)-F(10)	107.9(8)
F(11)-C(22)-F(10)	106.6(8)
F(12)-C(22)-C(21)	112.7(8)
F(11)-C(22)-C(21)	110.8(7)
F(10)-C(22)-C(21)	110.6(9)
F(15)-C(23)-F(14)	107.0(7)
F(15)-C(23)-F(13)	106.0(7)
F(14)-C(23)-F(13)	107.3(7)
F(15)-C(23)-C(21)	111.8(7)
F(14)-C(23)-C(21)	113.0(7)
F(13)-C(23)-C(21)	111.4(7)
F(18)-C(24)-F(17)	108.8(10)
F(18)-C(24)-F(16)	106.2(9)
F(17)-C(24)-F(16)	107.9(9)
F(18)-C(24)-C(21)	111.0(8)
F(17)-C(24)-C(21)	111.6(8)
F(16)-C(24)-C(21)	111.1(9)
O(3)-C(25)-C(27)	110.6(7)
O(3)-C(25)-C(26)	111.1(7)
C(27)-C(25)-C(26)	108.2(8)
O(3)-C(25)-C(28)	107.6(7)
C(27)-C(25)-C(28)	110.2(9)
C(26)-C(25)-C(28)	109.0(8)
F(20)-C(26)-F(19)	106.2(9)
F(20)-C(26)-F(21)	106.9(8)
F(19)-C(26)-F(21)	106.8(8)
F(20)-C(26)-C(25)	111.7(7)
F(19)-C(26)-C(25)	111.8(8)
F(21)-C(26)-C(25)	112.9(8)

F(24)-C(27)-F(23)	107.9(9)
F(24)-C(27)-F(22)	105.5(10)
F(23)-C(27)-F(22)	106.7(9)
F(24)-C(27)-C(25)	112.0(9)
F(23)-C(27)-C(25)	113.0(9)
F(22)-C(27)-C(25)	111.3(9)
F(27)-C(28)-F(25)	109.5(11)
F(27)-C(28)-F(26)	109.7(10)
F(25)-C(28)-F(26)	107.9(10)
F(27)-C(28)-C(25)	110.8(10)
F(25)-C(28)-C(25)	111.2(9)
F(26)-C(28)-C(25)	107.7(10)
O(4)-C(29)-C(30)	111.4(6)
O(4)-C(29)-C(31)	109.8(7)
C(30)-C(29)-C(31)	109.5(7)
O(4)-C(29)-C(32)	107.2(6)
C(30)-C(29)-C(32)	109.6(7)
C(31)-C(29)-C(32)	109.3(7)
F(28)-C(30)-F(30)	109.3(9)
F(28)-C(30)-F(29)	105.3(8)
F(30)-C(30)-F(29)	105.8(7)
F(28)-C(30)-C(29)	111.2(7)
F(30)-C(30)-C(29)	113.2(7)
F(29)-C(30)-C(29)	111.7(7)
F(32)-C(31)-F(33)	106.1(8)
F(32)-C(31)-F(31)	108.3(9)
F(33)-C(31)-F(31)	105.2(9)
F(32)-C(31)-C(29)	114.4(8)
F(33)-C(31)-C(29)	112.0(8)
F(31)-C(31)-C(29)	110.3(7)
F(35)-C(32)-F(34)	106.9(8)
F(35)-C(32)-F(36)	107.8(9)
F(34)-C(32)-F(36)	106.2(8)
F(35)-C(32)-C(29)	111.9(7)
F(34)-C(32)-C(29)	112.9(8)
F(36)-C(32)-C(29)	110.8(7)
O(8)-Al(2)-O(5)	109.4(5)
O(8)-Al(2)-O(6)	112.7(4)
O(5)-Al(2)-O(6)	108.4(3)
O(8)-Al(2)-O(7)	108.2(4)
O(5)-Al(2)-O(7)	111.1(4)
O(6)-Al(2)-O(7)	107.0(3)
C(33)-O(5)-Al(2)	159.9(6)
C(37)-O(6)-Al(2)	151.2(5)
C(41)-O(7)-Al(2)	149.0(6)
C(45)-O(8)-Al(2)	156.4(8)
O(5)-C(33)-C(35)	109.6(7)
O(5)-C(33)-C(34)	107.1(6)
C(35)-C(33)-C(34)	110.3(7)
O(5)-C(33)-C(36)	112.0(8)

C(35)-C(33)-C(36)	108.4(7)
C(34)-C(33)-C(36)	109.5(8)
F(38)-C(34)-F(39)	108.5(9)
F(38)-C(34)-F(37)	106.4(7)
F(39)-C(34)-F(37)	106.4(9)
F(38)-C(34)-C(33)	113.3(8)
F(39)-C(34)-C(33)	111.9(7)
F(37)-C(34)-C(33)	109.9(7)
F(42)-C(35)-F(40)	110.6(10)
F(42)-C(35)-F(41)	106.6(8)
F(40)-C(35)-F(41)	105.6(10)
F(42)-C(35)-C(33)	111.3(8)
F(40)-C(35)-C(33)	110.4(8)
F(41)-C(35)-C(33)	112.1(9)
F(43)-C(36)-F(44)	108.6(9)
F(43)-C(36)-F(45)	109.4(12)
F(44)-C(36)-F(45)	105.7(11)
F(43)-C(36)-C(33)	114.6(11)
F(44)-C(36)-C(33)	110.6(9)
F(45)-C(36)-C(33)	107.4(8)
O(6)-C(37)-C(40)	111.8(7)
O(6)-C(37)-C(39)	111.3(7)
C(40)-C(37)-C(39)	108.5(7)
O(6)-C(37)-C(38)	107.4(7)
C(40)-C(37)-C(38)	108.9(7)
C(39)-C(37)-C(38)	108.9(8)
F(47)-C(38)-F(46)	107.2(9)
F(47)-C(38)-F(48)	108.6(8)
F(46)-C(38)-F(48)	106.5(9)
F(47)-C(38)-C(37)	110.6(8)
F(46)-C(38)-C(37)	111.2(8)
F(48)-C(38)-C(37)	112.5(8)
F(49)-C(39)-F(51)	108.1(9)
F(49)-C(39)-F(50)	106.8(9)
F(51)-C(39)-F(50)	107.3(9)
F(49)-C(39)-C(37)	111.1(9)
F(51)-C(39)-C(37)	112.8(8)
F(50)-C(39)-C(37)	110.4(8)
F(54)-C(40)-F(53)	107.7(7)
F(54)-C(40)-F(52)	107.1(7)
F(53)-C(40)-F(52)	106.0(7)
F(54)-C(40)-C(37)	110.8(7)
F(53)-C(40)-C(37)	113.7(7)
F(52)-C(40)-C(37)	111.2(7)
O(7)-C(41)-C(43)	108.5(8)
O(7)-C(41)-C(42)	108.4(7)
C(43)-C(41)-C(42)	109.0(8)
O(7)-C(41)-C(44)	111.9(7)
C(43)-C(41)-C(44)	109.8(8)
C(42)-C(41)-C(44)	109.2(8)

F(55)-C(42)-F(56)	106.8(8)
F(55)-C(42)-F(57)	106.6(8)
F(56)-C(42)-F(57)	107.0(7)
F(55)-C(42)-C(41)	111.7(7)
F(56)-C(42)-C(41)	111.5(8)
F(57)-C(42)-C(41)	112.8(8)
F(58)-C(43)-F(59)	107.9(10)
F(58)-C(43)-F(60)	106.9(9)
F(59)-C(43)-F(60)	106.3(9)
F(58)-C(43)-C(41)	112.0(9)
F(59)-C(43)-C(41)	113.0(9)
F(60)-C(43)-C(41)	110.4(10)
F(63)-C(44)-F(62)	106.9(9)
F(63)-C(44)-F(61)	108.0(8)
F(62)-C(44)-F(61)	106.9(8)
F(63)-C(44)-C(41)	111.2(8)
F(62)-C(44)-C(41)	111.3(8)
F(61)-C(44)-C(41)	112.3(8)
O(8)-C(45)-C(47)	108.9(9)
O(8)-C(45)-C(46)	107.0(9)
C(47)-C(45)-C(46)	108.3(11)
O(8)-C(45)-C(48)	113.0(8)
C(47)-C(45)-C(48)	109.6(10)
C(46)-C(45)-C(48)	109.9(9)
F(66)-C(46)-F(65)	109.8(14)
F(66)-C(46)-F(64)	107.1(11)
F(65)-C(46)-F(64)	106.0(12)
F(66)-C(46)-C(45)	113.5(11)
F(65)-C(46)-C(45)	112.2(10)
F(64)-C(46)-C(45)	107.8(12)
F(68)-C(47)-F(69)	109.9(14)
F(68)-C(47)-F(67)	107.9(13)
F(69)-C(47)-F(67)	101.9(12)
F(68)-C(47)-C(45)	116.1(12)
F(69)-C(47)-C(45)	109.9(12)
F(67)-C(47)-C(45)	110.1(12)
F(72)-C(48)-F(71)	108.2(12)
F(72)-C(48)-F(70)	108.2(10)
F(71)-C(48)-F(70)	107.2(12)
F(72)-C(48)-C(45)	113.0(11)
F(71)-C(48)-C(45)	108.4(10)
F(70)-C(48)-C(45)	111.6(10)
O(12)-Al(3)-O(9)	108.0(6)
O(12)-Al(3)-O(10)	109.6(5)
O(9)-Al(3)-O(10)	107.8(4)
O(12)-Al(3)-O(11)	112.1(5)
O(9)-Al(3)-O(11)	109.4(4)
O(10)-Al(3)-O(11)	109.8(3)
C(49)-O(9)-Al(3)	163.4(7)
C(53)-O(10)-Al(3)	156.9(6)

C(57)-O(11)-Al(3)	156.9(6)
C(61)-O(12)-Al(3)	170.5(11)
O(9)-C(49)-C(51)	112.5(8)
O(9)-C(49)-C(52)	108.1(9)
C(51)-C(49)-C(52)	113.7(10)
O(9)-C(49)-C(50)	106.8(9)
C(51)-C(49)-C(50)	112.5(9)
C(52)-C(49)-C(50)	102.6(10)
F(73)-C(50)-F(75)	118.4(13)
F(73)-C(50)-F(74)	104.6(17)
F(75)-C(50)-F(74)	112.7(12)
F(73)-C(50)-C(49)	113.0(11)
F(75)-C(50)-C(49)	107.4(13)
F(74)-C(50)-C(49)	99.0(11)
F(76)-C(51)-F(77)	112.1(11)
F(76)-C(51)-F(78)	105.8(11)
F(77)-C(51)-F(78)	113.2(12)
F(76)-C(51)-C(49)	112.5(10)
F(77)-C(51)-C(49)	112.5(10)
F(78)-C(51)-C(49)	100.1(10)
F(79)-C(52)-F(80)	111.3(14)
F(79)-C(52)-F(81)	111.3(15)
F(80)-C(52)-F(81)	113.4(15)
F(79)-C(52)-C(49)	107.6(13)
F(80)-C(52)-C(49)	106.4(14)
F(81)-C(52)-C(49)	106.4(11)
O(10)-C(53)-C(56)	113.2(9)
O(10)-C(53)-C(54)	108.7(8)
C(56)-C(53)-C(54)	108.8(11)
O(10)-C(53)-C(55)	111.3(8)
C(56)-C(53)-C(55)	109.9(10)
C(54)-C(53)-C(55)	104.5(10)
F(82)-C(54)-F(84)	106.2(12)
F(82)-C(54)-F(83)	113.2(15)
F(84)-C(54)-F(83)	114.1(15)
F(82)-C(54)-C(53)	110.1(13)
F(84)-C(54)-C(53)	106.6(13)
F(83)-C(54)-C(53)	106.4(11)
F(86)-C(55)-F(85)	106.2(12)
F(86)-C(55)-F(87)	118.2(13)
F(85)-C(55)-F(87)	112.9(13)
F(86)-C(55)-C(53)	110.1(12)
F(85)-C(55)-C(53)	108.6(11)
F(87)-C(55)-C(53)	100.5(11)
F(89)-C(56)-F(88)	101.0(13)
F(89)-C(56)-F(90)	106.2(13)
F(88)-C(56)-F(90)	117.9(15)
F(89)-C(56)-C(53)	111.8(13)
F(88)-C(56)-C(53)	110.8(13)
F(90)-C(56)-C(53)	108.8(12)

O(11)-C(57)-C(58)	108.1(9)
O(11)-C(57)-C(60)	112.7(7)
C(58)-C(57)-C(60)	111.3(8)
O(11)-C(57)-C(59)	109.8(8)
C(58)-C(57)-C(59)	109.1(9)
C(60)-C(57)-C(59)	105.8(8)
F(93)-C(58)-F(91)	103.3(13)
F(93)-C(58)-F(92)	113.9(13)
F(91)-C(58)-F(92)	107.2(11)
F(93)-C(58)-C(57)	114.7(11)
F(91)-C(58)-C(57)	109.7(12)
F(92)-C(58)-C(57)	107.8(11)
F(94)-C(59)-F(96)	116.8(13)
F(94)-C(59)-F(95)	105.6(11)
F(96)-C(59)-F(95)	114.1(14)
F(94)-C(59)-C(57)	109.7(12)
F(96)-C(59)-C(57)	103.9(11)
F(95)-C(59)-C(57)	106.2(11)
F(98)-C(60)-F(97)	110.7(9)
F(98)-C(60)-F(99)	106.0(10)
F(97)-C(60)-F(99)	106.6(8)
F(98)-C(60)-C(57)	114.4(8)
F(97)-C(60)-C(57)	113.0(9)
F(99)-C(60)-C(57)	105.4(8)
O(12)-C(61)-C(64)	108.2(9)
O(12)-C(61)-C(63)	106.9(9)
C(64)-C(61)-C(63)	109.6(8)
O(12)-C(61)-C(62)	113.7(11)
C(64)-C(61)-C(62)	109.5(10)
C(63)-C(61)-C(62)	108.8(7)
F(102)-C(62)-F(100)	112.0(18)
F(102)-C(62)-F(101)	112.2(13)
F(100)-C(62)-F(101)	102.4(13)
F(102)-C(62)-C(61)	115.2(13)
F(100)-C(62)-C(61)	107.5(12)
F(101)-C(62)-C(61)	106.5(13)
F(104)-C(63)-F(105)	105.5(9)
F(104)-C(63)-F(103)	104.9(9)
F(105)-C(63)-F(103)	110.0(9)
F(104)-C(63)-C(61)	112.9(9)
F(105)-C(63)-C(61)	110.8(9)
F(103)-C(63)-C(61)	112.5(7)
F(107)-C(64)-F(108)	106.6(11)
F(107)-C(64)-F(106)	108.1(12)
F(108)-C(64)-F(106)	107.3(11)
F(107)-C(64)-C(61)	112.9(11)
F(108)-C(64)-C(61)	110.8(10)
F(106)-C(64)-C(61)	110.9(9)
C(66)-C(65)-H(65A)	109.5
C(66)-C(65)-H(65B)	109.5

H(65A)-C(65)-H(65B)	109.5
C(66)-C(65)-H(65C)	109.5
H(65A)-C(65)-H(65C)	109.5
H(65B)-C(65)-H(65C)	109.5
N(9)-C(66)-C(65)	178.3(14)
C(68)-C(67)-H(67A)	109.5
C(68)-C(67)-H(67B)	109.5
H(67A)-C(67)-H(67B)	109.5
C(68)-C(67)-H(67C)	109.5
H(67A)-C(67)-H(67C)	109.5
H(67B)-C(67)-H(67C)	109.5
N(10)-C(68)-C(67)	178.3(13)
Cl(2)-C(69)-Cl(1)	111.6(8)
Cl(2)-C(69)-H(69A)	109.3
Cl(1)-C(69)-H(69A)	109.3
Cl(2)-C(69)-H(69B)	109.3
Cl(1)-C(69)-H(69B)	109.3
H(69A)-C(69)-H(69B)	108.0
Cl(4)-C(70)-Cl(3)	117.2(15)
Cl(4)-C(70)-H(70A)	108.0
Cl(3)-C(70)-H(70A)	108.0
Cl(4)-C(70)-H(70B)	108.0
Cl(3)-C(70)-H(70B)	108.0
H(70A)-C(70)-H(70B)	107.2

Symmetry transformations used to generate equivalent atoms:

Table A II-4. Anisotropic displacement parameters ($\text{\AA}^2 \times 10^3$) for $[\text{Tm}(\text{CH}_3\text{CN})_8][\text{Al}(\text{OC}(\text{CF}_3)_3)_3 \cdot 2\text{CH}_2\text{Cl}_2 \cdot 2\text{CH}_3\text{CN}]$ (**5** $2\text{CH}_2\text{Cl}_2 \cdot 2\text{CH}_3\text{CN}$). The anisotropic displacement factor exponent takes the form: $-2\pi^2 [h^2 a^{*2} U^{11} + \dots + 2 h k a^* b^* U^{12}]$

	U ¹¹	U ²²	U ³³	U ²³	U ¹³	U ¹²
Tm(1)	26(1)	30(1)	22(1)	0(1)	5(1)	1(1)
N(1)	33(3)	40(4)	31(3)	2(3)	8(3)	6(3)
N(2)	39(3)	33(3)	29(3)	4(3)	5(3)	1(3)
N(3)	33(3)	51(4)	28(3)	1(3)	3(3)	6(3)
N(4)	30(3)	36(3)	32(3)	-2(3)	6(3)	1(3)
N(5)	36(3)	45(4)	33(3)	-5(3)	5(3)	-4(3)
N(6)	39(3)	28(3)	31(3)	-3(2)	7(3)	-1(3)
N(7)	31(3)	37(3)	38(3)	-4(3)	8(3)	4(3)
N(8)	30(3)	24(3)	30(3)	1(2)	8(2)	2(2)
C(1)	36(4)	41(4)	27(4)	5(3)	7(3)	5(3)
C(2)	53(5)	51(5)	35(4)	8(4)	9(4)	26(4)
C(3)	51(5)	31(4)	36(4)	7(3)	12(4)	2(4)
C(4)	82(7)	39(5)	61(6)	0(4)	19(5)	-17(5)
C(5)	35(4)	35(4)	32(4)	-1(3)	-3(3)	9(3)
C(6)	61(6)	57(6)	41(5)	24(4)	-6(4)	-9(4)
C(7)	30(4)	35(4)	29(4)	0(3)	7(3)	4(3)
C(8)	39(4)	68(6)	38(4)	4(4)	19(4)	5(4)
C(9)	38(4)	45(5)	34(4)	-3(4)	0(3)	-12(3)
C(10)	67(6)	56(6)	42(5)	-11(4)	0(4)	-20(5)
C(11)	38(4)	26(4)	45(4)	2(3)	8(3)	3(3)
C(12)	48(5)	48(6)	96(8)	11(5)	9(5)	23(4)
C(13)	35(4)	31(4)	38(4)	-8(3)	8(3)	0(3)
C(14)	45(5)	56(6)	79(7)	-23(5)	25(5)	-20(4)
C(15)	31(4)	24(3)	29(4)	3(3)	6(3)	0(3)
C(16)	49(5)	39(4)	28(4)	-2(3)	-5(3)	-1(4)
Al(1)	24(1)	22(1)	23(1)	-3(1)	3(1)	-1(1)
F(1)	120(6)	49(3)	73(4)	-17(3)	6(4)	6(4)
F(2)	111(6)	82(5)	154(7)	30(5)	99(6)	29(4)
F(3)	76(4)	58(4)	136(6)	24(4)	13(4)	33(3)
F(4)	87(6)	108(7)	202(10)	61(7)	-80(6)	-47(5)
F(5)	244(12)	60(5)	79(5)	-14(4)	-32(6)	-26(6)
F(6)	198(9)	96(6)	71(5)	35(4)	-57(5)	-40(6)
F(7)	106(5)	47(3)	105(5)	22(3)	51(4)	-9(3)
F(8)	186(9)	75(5)	123(7)	16(5)	110(7)	32(5)
F(9)	53(4)	76(5)	169(8)	21(5)	9(5)	-8(3)
F(10)	65(4)	49(3)	149(7)	-42(4)	36(4)	-23(3)
F(11)	65(4)	95(5)	54(3)	-31(3)	-3(3)	-10(3)
F(12)	71(4)	106(5)	118(6)	-80(5)	46(4)	-19(4)
F(13)	80(4)	76(4)	49(3)	9(3)	15(3)	-4(3)
F(14)	46(3)	56(3)	106(5)	1(3)	35(3)	-2(2)
F(15)	70(4)	44(3)	65(3)	-2(2)	0(3)	-23(3)
F(16)	71(4)	38(3)	180(8)	17(4)	43(5)	23(3)
F(17)	54(3)	89(5)	78(4)	23(3)	-9(3)	13(3)

F(18)	73(4)	78(4)	126(6)	55(4)	36(4)	5(3)
F(19)	116(6)	57(4)	105(6)	-8(4)	2(5)	-14(4)
F(20)	66(4)	100(5)	59(4)	-7(3)	17(3)	-31(3)
F(21)	86(4)	108(5)	54(4)	-19(3)	-11(3)	-45(4)
F(22)	61(4)	107(5)	82(5)	-8(4)	-15(3)	23(4)
F(23)	125(6)	114(6)	54(4)	22(4)	-28(4)	-10(5)
F(24)	124(6)	67(4)	97(5)	19(4)	-23(5)	-24(4)
F(25)	86(5)	169(8)	63(4)	-71(5)	21(4)	-17(5)
F(26)	99(6)	185(9)	76(5)	-49(5)	53(4)	-74(6)
F(27)	69(4)	141(7)	92(5)	-45(5)	5(4)	35(5)
F(28)	107(5)	99(5)	82(5)	36(4)	33(4)	63(4)
F(29)	88(4)	90(4)	37(3)	10(3)	3(3)	-13(3)
F(30)	96(5)	75(4)	95(5)	45(4)	-6(4)	-42(4)
F(31)	68(4)	107(5)	100(5)	-54(4)	-4(4)	28(4)
F(32)	48(4)	88(5)	204(9)	-21(6)	55(5)	-8(3)
F(33)	99(5)	87(5)	109(6)	35(4)	4(4)	38(4)
F(34)	67(4)	121(6)	72(4)	-7(4)	-17(3)	-52(4)
F(35)	125(6)	85(4)	36(3)	11(3)	-20(3)	-34(4)
F(36)	87(5)	88(5)	71(4)	-39(4)	-4(3)	3(4)
O(1)	60(4)	30(3)	47(3)	9(2)	8(3)	0(3)
O(2)	39(3)	40(3)	49(3)	-8(3)	9(3)	10(2)
O(3)	38(3)	62(4)	30(3)	-19(3)	3(2)	-5(3)
O(4)	35(3)	61(4)	32(3)	-4(3)	5(2)	-20(3)
C(17)	49(5)	23(4)	40(4)	7(3)	5(4)	1(3)
C(18)	64(6)	48(6)	77(7)	15(5)	25(6)	6(5)
C(19)	133(13)	58(7)	73(8)	14(6)	-50(8)	-24(8)
C(20)	77(8)	45(6)	78(7)	11(5)	21(6)	3(5)
C(21)	29(4)	28(4)	48(4)	-7(3)	11(3)	3(3)
C(22)	51(6)	58(6)	72(7)	-30(5)	17(5)	-2(5)
C(23)	46(5)	44(5)	54(5)	-2(4)	14(4)	-9(4)
C(24)	56(6)	61(6)	84(8)	22(6)	18(6)	7(5)
C(25)	43(4)	48(5)	27(4)	-9(3)	6(3)	-5(4)
C(26)	58(6)	66(7)	47(5)	-19(5)	2(5)	-12(5)
C(27)	75(7)	67(7)	50(6)	-1(5)	-14(5)	-11(6)
C(28)	63(7)	115(10)	53(6)	-43(7)	19(5)	-24(7)
C(29)	26(4)	45(5)	34(4)	1(3)	0(3)	-9(3)
C(30)	50(5)	55(5)	32(4)	8(4)	5(4)	-5(4)
C(31)	36(5)	57(6)	57(6)	-4(4)	0(4)	1(4)
C(32)	59(6)	57(6)	38(5)	-4(4)	-3(4)	-15(5)
Al(2)	22(1)	25(1)	22(1)	1(1)	1(1)	-2(1)
F(37)	51(3)	101(5)	69(4)	26(4)	-3(3)	22(3)
F(38)	119(5)	89(5)	23(3)	-4(3)	-5(3)	16(4)
F(39)	72(4)	188(9)	93(5)	65(5)	-50(4)	-79(5)
F(40)	293(13)	52(4)	59(4)	-8(3)	-4(6)	20(6)
F(41)	104(5)	122(6)	67(4)	45(4)	-19(4)	-78(5)
F(42)	81(4)	83(4)	58(4)	28(3)	-6(3)	17(3)
F(43)	87(5)	284(13)	78(5)	24(7)	54(5)	89(7)
F(44)	107(5)	90(4)	26(3)	-12(3)	9(3)	-11(4)
F(45)	299(14)	61(5)	64(5)	-22(4)	33(6)	36(6)
F(46)	114(5)	55(4)	63(4)	25(3)	-29(4)	-32(3)

F(47)	64(4)	172(8)	87(5)	53(5)	24(4)	-14(5)
F(48)	74(4)	87(4)	34(3)	15(3)	-20(3)	-8(3)
F(49)	53(4)	138(7)	150(8)	-4(6)	17(4)	40(4)
F(50)	86(4)	42(3)	82(4)	-15(3)	-23(3)	10(3)
F(51)	131(6)	105(5)	50(4)	-38(4)	-3(4)	41(5)
F(52)	75(4)	57(3)	81(4)	-7(3)	13(3)	25(3)
F(53)	36(3)	67(4)	82(4)	-1(3)	-16(3)	-10(2)
F(54)	67(4)	83(4)	67(4)	25(3)	31(3)	8(3)
F(55)	54(3)	45(3)	90(4)	-5(3)	-4(3)	0(3)
F(56)	71(4)	45(3)	68(4)	-7(3)	5(3)	-24(3)
F(57)	77(4)	34(3)	76(4)	11(2)	16(3)	-11(2)
F(58)	80(4)	90(5)	85(5)	-9(4)	25(4)	-7(4)
F(59)	83(5)	59(4)	127(6)	24(4)	25(4)	24(3)
F(60)	54(4)	120(6)	111(6)	26(5)	9(4)	-9(4)
F(61)	87(4)	69(4)	66(4)	39(3)	-13(3)	-2(3)
F(62)	91(4)	50(3)	53(3)	3(3)	4(3)	-9(3)
F(63)	93(4)	66(4)	57(3)	22(3)	-25(3)	-41(3)
F(64)	74(5)	72(5)	288(14)	-33(7)	-93(7)	10(4)
F(65)	79(5)	64(5)	303(15)	21(7)	-3(7)	-3(4)
F(66)	121(7)	109(7)	254(13)	19(7)	137(8)	48(6)
F(67)	267(13)	90(6)	47(4)	-3(4)	51(6)	43(7)
F(68)	388(19)	91(6)	55(5)	-31(4)	-60(8)	-31(9)
F(69)	120(8)	190(11)	160(10)	15(8)	-95(7)	-9(8)
F(70)	114(6)	50(4)	84(5)	-19(3)	-2(4)	-4(4)
F(71)	58(5)	191(10)	253(13)	99(10)	-24(6)	-58(6)
F(72)	145(7)	125(7)	59(4)	22(4)	16(5)	59(6)
O(5)	19(3)	115(6)	58(4)	45(4)	-7(3)	-15(3)
O(6)	79(4)	43(3)	41(3)	11(3)	-32(3)	-25(3)
O(7)	87(5)	30(3)	45(3)	17(3)	-24(3)	-25(3)
O(8)	117(6)	114(6)	37(4)	15(4)	32(4)	90(6)
C(33)	25(3)	45(4)	26(3)	-1(3)	2(3)	-9(3)
C(34)	40(5)	69(6)	39(5)	8(4)	-11(4)	-16(4)
C(35)	88(8)	50(5)	38(5)	0(4)	-5(5)	-3(5)
C(36)	111(10)	80(8)	38(6)	-1(5)	27(6)	17(7)
C(37)	34(4)	41(4)	29(4)	2(3)	-8(3)	-6(3)
C(38)	57(6)	75(7)	42(5)	16(5)	-2(4)	-14(5)
C(39)	46(5)	68(7)	60(6)	-14(5)	-5(5)	17(5)
C(40)	46(5)	39(4)	46(5)	-1(4)	-1(4)	4(4)
C(41)	52(5)	37(4)	49(5)	15(4)	-10(4)	-12(4)
C(42)	61(6)	29(4)	62(6)	9(4)	4(5)	-8(4)
C(43)	61(7)	62(7)	77(8)	17(6)	8(6)	-2(5)
C(44)	62(6)	46(5)	57(6)	19(4)	-10(5)	-13(5)
C(45)	35(4)	59(5)	37(4)	-11(4)	4(3)	11(4)
C(46)	53(7)	54(7)	172(15)	-26(8)	23(8)	3(5)
C(47)	126(13)	96(10)	62(8)	-14(7)	-30(8)	3(9)
C(48)	52(6)	91(9)	87(9)	-3(7)	-2(6)	2(6)
Al(3)	35(1)	19(1)	22(1)	1(1)	1(1)	1(1)
F(73)	149(9)	59(5)	241(13)	43(7)	53(9)	26(5)
F(74)	117(9)	400(20)	134(10)	75(12)	-63(7)	41(12)
F(75)	238(11)	147(8)	38(4)	40(4)	1(5)	-92(8)

F(76)	184(9)	154(8)	94(6)	-46(5)	43(6)	-136(8)
F(77)	386(19)	117(7)	79(6)	-63(5)	92(8)	-139(10)
F(78)	272(17)	94(8)	610(40)	155(14)	310(20)	118(10)
F(79)	94(7)	91(7)	590(30)	-39(12)	174(14)	7(5)
F(80)	142(11)	284(18)	360(20)	206(18)	-158(14)	-90(11)
F(81)	293(17)	157(10)	159(10)	-38(8)	63(11)	-168(12)
F(82)	159(8)	72(5)	132(7)	-48(5)	-32(6)	4(5)
F(83)	72(6)	215(13)	202(12)	-54(10)	53(7)	8(7)
F(84)	380(20)	52(5)	258(16)	41(8)	0(15)	58(9)
F(85)	87(5)	86(5)	148(8)	18(5)	-11(5)	-14(4)
F(86)	113(7)	157(9)	249(13)	142(10)	-49(8)	-11(6)
F(87)	430(20)	124(8)	44(5)	-4(5)	37(8)	7(11)
F(88)	125(8)	329(18)	230(13)	237(14)	65(8)	29(10)
F(89)	156(10)	380(20)	117(8)	54(10)	94(8)	146(13)
F(90)	51(5)	218(14)	360(20)	32(14)	13(9)	-49(7)
F(91)	127(9)	127(9)	292(17)	86(10)	59(10)	57(7)
F(92)	169(9)	152(9)	112(7)	74(7)	-63(7)	-7(7)
F(93)	153(9)	161(10)	241(14)	64(9)	-148(10)	-63(8)
F(94)	227(11)	102(6)	107(7)	-1(5)	103(7)	-38(7)
F(95)	480(20)	137(9)	90(7)	-75(6)	129(11)	-162(12)
F(96)	158(11)	125(9)	261(17)	11(10)	51(11)	68(8)
F(97)	88(4)	33(3)	104(5)	-13(3)	25(4)	-17(3)
F(98)	98(5)	89(5)	111(6)	52(4)	-44(5)	-34(4)
F(99)	191(10)	133(8)	92(6)	-20(5)	84(6)	-78(7)
F(100)	520(30)	106(7)	39(4)	20(4)	6(8)	81(11)
F(101)	243(11)	80(5)	57(4)	-28(4)	30(5)	29(6)
F(102)	205(13)	202(13)	208(14)	-36(10)	176(12)	-32(11)
F(103)	87(5)	74(4)	90(5)	7(4)	-7(4)	-20(4)
F(104)	71(4)	87(5)	138(7)	23(5)	-35(4)	33(4)
F(105)	221(10)	117(6)	36(3)	4(4)	29(5)	-18(7)
F(106)	120(7)	130(7)	114(7)	8(5)	-43(6)	-69(6)
F(107)	268(13)	83(6)	109(7)	-60(5)	80(8)	-9(7)
F(108)	178(9)	50(4)	115(6)	3(4)	8(6)	-10(5)
O(9)	208(11)	62(5)	53(4)	-7(4)	74(6)	-41(6)
O(10)	91(5)	23(3)	47(3)	9(2)	5(3)	13(3)
O(11)	136(7)	38(3)	36(3)	-8(3)	-5(4)	-37(4)
O(12)	48(5)	125(8)	194(12)	-28(8)	-37(6)	55(5)
C(49)	43(4)	41(4)	24(4)	5(3)	8(3)	6(3)
C(50)	166(16)	76(9)	52(7)	-13(6)	17(8)	-34(10)
C(51)	166(16)	104(11)	78(9)	-50(8)	65(10)	-74(11)
C(52)	83(12)	380(40)	125(17)	-50(20)	-25(11)	120(20)
C(53)	60(5)	28(4)	44(5)	18(3)	11(4)	5(4)
C(54)	440(50)	42(8)	130(17)	1(10)	-60(30)	45(17)
C(55)	182(19)	87(11)	117(14)	66(11)	-17(13)	-10(12)
C(56)	170(30)	430(50)	520(60)	430(50)	240(40)	200(30)
C(57)	71(6)	36(4)	27(4)	-5(3)	4(4)	-16(4)
C(58)	220(30)	62(11)	450(50)	-30(20)	-230(30)	24(14)
C(59)	280(30)	147(19)	150(19)	-56(16)	120(20)	-150(20)
C(60)	132(12)	37(6)	123(12)	15(6)	-82(10)	-30(7)
C(61)	44(5)	41(4)	37(4)	-8(3)	-5(3)	19(4)

C(62)	203(18)	59(7)	37(6)	-7(5)	18(8)	43(9)
C(63)	57(6)	74(7)	34(5)	0(4)	-6(4)	6(5)
C(64)	90(9)	61(7)	68(7)	-13(6)	8(6)	-5(6)
N(9)	62(6)	177(12)	52(6)	-11(7)	10(5)	-25(7)
C(65)	50(6)	87(8)	61(6)	-24(6)	13(5)	-15(5)
C(66)	41(5)	79(7)	52(6)	-1(5)	9(4)	-9(5)
N(10)	89(7)	68(6)	72(6)	3(5)	12(5)	-4(5)
C(67)	135(12)	57(7)	76(8)	17(6)	24(8)	34(7)
C(68)	73(7)	51(6)	54(6)	-3(5)	6(5)	21(5)
Cl(1)	84(2)	102(3)	171(4)	-17(3)	13(3)	17(2)
Cl(2)	95(3)	126(4)	219(6)	-22(4)	50(3)	-9(3)
C(69)	126(13)	146(15)	86(10)	-31(10)	0(9)	77(11)
Cl(3)	129(4)	145(4)	106(3)	-18(3)	15(3)	1(3)
Cl(4)	226(9)	137(6)	385(14)	-35(7)	47(9)	-46(6)
C(70)	140(18)	330(40)	180(20)	-60(20)	122(17)	-60(20)

Table A II-5. Hydrogen coordinates ($\times 10^4$) and isotropic displacement parameters ($\text{\AA}^2 \times 10^{-3}$) for $[\text{Tm}(\text{CH}_3\text{CN})_8][\text{Al}(\text{OC}(\text{CF}_3)_3)_4]_3 \cdot 2\text{CH}_2\text{Cl}_2 \cdot 2\text{CH}_3\text{CN}$ (**5** $2\text{CH}_2\text{Cl}_2 \cdot 2\text{CH}_3\text{CN}$).

	x	y	z	U(eq)
H(2A)	10665	3044	6876	69
H(2B)	9842	2722	6710	69
H(2C)	10161	2802	7302	69
H(4A)	5466	2714	7386	90
H(4B)	6121	2479	7022	90
H(4C)	5223	2732	6780	90
H(6A)	7991	2925	8675	80
H(6B)	7535	3305	8948	80
H(6C)	8656	3263	8968	80
H(8A)	4793	3769	8266	71
H(8B)	4371	4185	8010	71
H(8C)	5127	4205	8502	71
H(10A)	8172	4995	8767	83
H(10B)	8486	5316	8356	83
H(10C)	9235	4996	8623	83
H(12A)	5235	5110	6206	96
H(12B)	5736	5432	6606	96
H(12C)	4968	5117	6782	96
H(14A)	10067	4931	6163	88
H(14B)	10821	4682	6536	88
H(14C)	10335	5087	6735	88
H(16A)	6349	3965	5138	58
H(16B)	6811	3516	5184	58
H(16C)	7444	3906	5073	58
H(65A)	2963	5709	9898	98
H(65B)	2434	5298	10044	98
H(65C)	3561	5312	10090	98
H(67A)	5389	7631	11178	133
H(67B)	4311	7670	10947	133
H(67C)	4977	7330	10729	133
H(69A)	-4729	5710	7874	144
H(69B)	-3952	5829	8332	144
H(70A)	2867	3197	2511	249
H(70B)	3725	3123	2938	249

Table A II-6. Torsion angles [°] for [Tm(CH₃CN)₈][Al(OC(CF₃)₃)₄]₃·2CH₂Cl₂·2CH₃CN (**5** 2CH₂Cl₂·2CH₃CN).

N(5)-Tm(1)-N(1)-C(1)	78(5)
N(4)-Tm(1)-N(1)-C(1)	-21(5)
N(3)-Tm(1)-N(1)-C(1)	16(4)
N(2)-Tm(1)-N(1)-C(1)	-63(4)
N(8)-Tm(1)-N(1)-C(1)	-139(5)
N(6)-Tm(1)-N(1)-C(1)	-178(100)
N(7)-Tm(1)-N(1)-C(1)	141(5)
N(5)-Tm(1)-N(2)-C(3)	1(4)
N(4)-Tm(1)-N(2)-C(3)	-39(4)
N(3)-Tm(1)-N(2)-C(3)	38(4)
N(1)-Tm(1)-N(2)-C(3)	114(4)
N(8)-Tm(1)-N(2)-C(3)	-164(4)
N(6)-Tm(1)-N(2)-C(3)	-100(4)
N(7)-Tm(1)-N(2)-C(3)	155(4)
N(5)-Tm(1)-N(3)-C(5)	113(3)
N(4)-Tm(1)-N(3)-C(5)	32(3)
N(2)-Tm(1)-N(3)-C(5)	-44(3)
N(1)-Tm(1)-N(3)-C(5)	-125(3)
N(8)-Tm(1)-N(3)-C(5)	-81(3)
N(6)-Tm(1)-N(3)-C(5)	67(3)
N(7)-Tm(1)-N(3)-C(5)	173(3)
N(5)-Tm(1)-N(4)-C(7)	-90(4)
N(3)-Tm(1)-N(4)-C(7)	-14(4)
N(2)-Tm(1)-N(4)-C(7)	66(4)
N(1)-Tm(1)-N(4)-C(7)	23(4)
N(8)-Tm(1)-N(4)-C(7)	128(4)
N(6)-Tm(1)-N(4)-C(7)	-171(4)
N(7)-Tm(1)-N(4)-C(7)	-128(4)
N(4)-Tm(1)-N(5)-C(9)	19(9)
N(3)-Tm(1)-N(5)-C(9)	-58(10)
N(2)-Tm(1)-N(5)-C(9)	-20(10)
N(1)-Tm(1)-N(5)-C(9)	-121(9)
N(8)-Tm(1)-N(5)-C(9)	135(9)
N(6)-Tm(1)-N(5)-C(9)	94(10)
N(7)-Tm(1)-N(5)-C(9)	176(100)
N(5)-Tm(1)-N(6)-C(11)	-106(2)
N(4)-Tm(1)-N(6)-C(11)	-25(2)
N(3)-Tm(1)-N(6)-C(11)	-61(2)
N(2)-Tm(1)-N(6)-C(11)	36(2)
N(1)-Tm(1)-N(6)-C(11)	140(2)
N(8)-Tm(1)-N(6)-C(11)	100(2)
N(7)-Tm(1)-N(6)-C(11)	180(100)
N(5)-Tm(1)-N(7)-C(13)	11(11)
N(4)-Tm(1)-N(7)-C(13)	50(11)
N(3)-Tm(1)-N(7)-C(13)	-49(11)
N(2)-Tm(1)-N(7)-C(13)	-153(10)
N(1)-Tm(1)-N(7)-C(13)	-111(11)
N(8)-Tm(1)-N(7)-C(13)	167(11)

N(6)-Tm(1)-N(7)-C(13)	91(11)
N(5)-Tm(1)-N(8)-C(15)	-122(13)
N(4)-Tm(1)-N(8)-C(15)	-18(13)
N(3)-Tm(1)-N(8)-C(15)	80(13)
N(2)-Tm(1)-N(8)-C(15)	43(13)
N(1)-Tm(1)-N(8)-C(15)	123(13)
N(6)-Tm(1)-N(8)-C(15)	-79(13)
N(7)-Tm(1)-N(8)-C(15)	-161(13)
Tm(1)-N(1)-C(1)-C(2)	-29(28)
Tm(1)-N(2)-C(3)-C(4)	71(39)
Tm(1)-N(3)-C(5)-C(6)	-7(36)
Tm(1)-N(4)-C(7)-C(8)	-33(100)
Tm(1)-N(5)-C(9)-C(10)	129(100)
Tm(1)-N(6)-C(11)-C(12)	-16(30)
Tm(1)-N(7)-C(13)-C(14)	-123(65)
Tm(1)-N(8)-C(15)-C(16)	-87(100)
O(4)-Al(1)-O(1)-C(17)	42.1(12)
O(2)-Al(1)-O(1)-C(17)	163.8(11)
O(3)-Al(1)-O(1)-C(17)	-79.4(12)
O(4)-Al(1)-O(2)-C(21)	75.5(11)
O(1)-Al(1)-O(2)-C(21)	-43.4(11)
O(3)-Al(1)-O(2)-C(21)	-165.4(10)
O(4)-Al(1)-O(3)-C(25)	156.1(11)
O(1)-Al(1)-O(3)-C(25)	-83.0(12)
O(2)-Al(1)-O(3)-C(25)	34.8(12)
O(1)-Al(1)-O(4)-C(29)	-151.1(12)
O(2)-Al(1)-O(4)-C(29)	90.4(13)
O(3)-Al(1)-O(4)-C(29)	-26.7(13)
Al(1)-O(1)-C(17)-C(19)	-66.7(15)
Al(1)-O(1)-C(17)-C(18)	59.7(14)
Al(1)-O(1)-C(17)-C(20)	175.9(9)
O(1)-C(17)-C(18)-F(3)	-169.3(8)
C(19)-C(17)-C(18)-F(3)	-43.1(12)
C(20)-C(17)-C(18)-F(3)	75.8(11)
O(1)-C(17)-C(18)-F(2)	-48.5(12)
C(19)-C(17)-C(18)-F(2)	77.7(11)
C(20)-C(17)-C(18)-F(2)	-163.5(9)
O(1)-C(17)-C(18)-F(1)	70.6(9)
C(19)-C(17)-C(18)-F(1)	-163.1(9)
C(20)-C(17)-C(18)-F(1)	-44.3(10)
O(1)-C(17)-C(19)-F(5)	-36.3(16)
C(18)-C(17)-C(19)-F(5)	-162.3(11)
C(20)-C(17)-C(19)-F(5)	79.4(13)
O(1)-C(17)-C(19)-F(4)	82.5(11)
C(18)-C(17)-C(19)-F(4)	-43.5(11)
C(20)-C(17)-C(19)-F(4)	-161.8(9)
O(1)-C(17)-C(19)-F(6)	-158.3(11)
C(18)-C(17)-C(19)-F(6)	75.7(15)
C(20)-C(17)-C(19)-F(6)	-42.5(15)
O(1)-C(17)-C(20)-F(9)	-40.4(10)

C(19)-C(17)-C(20)-F(9)	-160.2(9)
C(18)-C(17)-C(20)-F(9)	78.5(10)
O(1)-C(17)-C(20)-F(8)	77.2(10)
C(19)-C(17)-C(20)-F(8)	-42.7(12)
C(18)-C(17)-C(20)-F(8)	-164.0(9)
O(1)-C(17)-C(20)-F(7)	-162.9(9)
C(19)-C(17)-C(20)-F(7)	77.2(11)
C(18)-C(17)-C(20)-F(7)	-44.0(12)
Al(1)-O(2)-C(21)-C(23)	69.6(12)
Al(1)-O(2)-C(21)-C(22)	-51.4(13)
Al(1)-O(2)-C(21)-C(24)	-172.0(9)
O(2)-C(21)-C(22)-F(12)	167.7(9)
C(23)-C(21)-C(22)-F(12)	45.0(11)
C(24)-C(21)-C(22)-F(12)	-73.4(11)
O(2)-C(21)-C(22)-F(11)	46.5(10)
C(23)-C(21)-C(22)-F(11)	-76.1(9)
C(24)-C(21)-C(22)-F(11)	165.5(8)
O(2)-C(21)-C(22)-F(10)	-71.4(10)
C(23)-C(21)-C(22)-F(10)	165.9(7)
C(24)-C(21)-C(22)-F(10)	47.5(10)
O(2)-C(21)-C(23)-F(15)	39.4(10)
C(22)-C(21)-C(23)-F(15)	161.7(7)
C(24)-C(21)-C(23)-F(15)	-78.6(9)
O(2)-C(21)-C(23)-F(14)	160.1(7)
C(22)-C(21)-C(23)-F(14)	-77.5(9)
C(24)-C(21)-C(23)-F(14)	42.2(10)
O(2)-C(21)-C(23)-F(13)	-79.0(9)
C(22)-C(21)-C(23)-F(13)	43.4(9)
C(24)-C(21)-C(23)-F(13)	163.0(8)
O(2)-C(21)-C(24)-F(18)	46.1(11)
C(23)-C(21)-C(24)-F(18)	166.5(9)
C(22)-C(21)-C(24)-F(18)	-74.9(11)
O(2)-C(21)-C(24)-F(17)	-75.5(9)
C(23)-C(21)-C(24)-F(17)	44.9(10)
C(22)-C(21)-C(24)-F(17)	163.6(8)
O(2)-C(21)-C(24)-F(16)	164.0(7)
C(23)-C(21)-C(24)-F(16)	-75.6(10)
C(22)-C(21)-C(24)-F(16)	43.1(10)
Al(1)-O(3)-C(25)-C(27)	-62.5(14)
Al(1)-O(3)-C(25)-C(26)	57.7(14)
Al(1)-O(3)-C(25)-C(28)	177.0(10)
O(3)-C(25)-C(26)-F(20)	-44.8(11)
C(27)-C(25)-C(26)-F(20)	76.8(10)
C(28)-C(25)-C(26)-F(20)	-163.2(9)
O(3)-C(25)-C(26)-F(19)	74.2(10)
C(27)-C(25)-C(26)-F(19)	-164.2(8)
C(28)-C(25)-C(26)-F(19)	-44.3(11)
O(3)-C(25)-C(26)-F(21)	-165.3(8)
C(27)-C(25)-C(26)-F(21)	-43.7(11)
C(28)-C(25)-C(26)-F(21)	76.2(11)

O(3)-C(25)-C(27)-F(24)	-36.9(12)
C(26)-C(25)-C(27)-F(24)	-158.9(9)
C(28)-C(25)-C(27)-F(24)	81.9(11)
O(3)-C(25)-C(27)-F(23)	-159.0(8)
C(26)-C(25)-C(27)-F(23)	79.1(11)
C(28)-C(25)-C(27)-F(23)	-40.1(12)
O(3)-C(25)-C(27)-F(22)	80.9(9)
C(26)-C(25)-C(27)-F(22)	-41.0(10)
C(28)-C(25)-C(27)-F(22)	-160.2(8)
O(3)-C(25)-C(28)-F(27)	-46.4(12)
C(27)-C(25)-C(28)-F(27)	-167.0(9)
C(26)-C(25)-C(28)-F(27)	74.3(10)
O(3)-C(25)-C(28)-F(25)	-168.4(10)
C(27)-C(25)-C(28)-F(25)	70.9(13)
C(26)-C(25)-C(28)-F(25)	-47.7(14)
O(3)-C(25)-C(28)-F(26)	73.6(11)
C(27)-C(25)-C(28)-F(26)	-47.1(11)
C(26)-C(25)-C(28)-F(26)	-165.7(9)
Al(1)-O(4)-C(29)-C(30)	-40.2(15)
Al(1)-O(4)-C(29)-C(31)	81.3(14)
Al(1)-O(4)-C(29)-C(32)	-160.1(10)
O(4)-C(29)-C(30)-F(28)	-45.1(10)
C(31)-C(29)-C(30)-F(28)	-166.8(8)
C(32)-C(29)-C(30)-F(28)	73.4(9)
O(4)-C(29)-C(30)-F(30)	-168.6(8)
C(31)-C(29)-C(30)-F(30)	69.7(10)
C(32)-C(29)-C(30)-F(30)	-50.1(10)
O(4)-C(29)-C(30)-F(29)	72.1(9)
C(31)-C(29)-C(30)-F(29)	-49.5(9)
C(32)-C(29)-C(30)-F(29)	-169.4(7)
O(4)-C(29)-C(31)-F(32)	-172.1(8)
C(30)-C(29)-C(31)-F(32)	-49.4(11)
C(32)-C(29)-C(31)-F(32)	70.6(10)
O(4)-C(29)-C(31)-F(33)	67.1(9)
C(30)-C(29)-C(31)-F(33)	-170.2(8)
C(32)-C(29)-C(31)-F(33)	-50.2(10)
O(4)-C(29)-C(31)-F(31)	-49.7(10)
C(30)-C(29)-C(31)-F(31)	73.0(10)
C(32)-C(29)-C(31)-F(31)	-167.0(8)
O(4)-C(29)-C(32)-F(35)	-48.6(10)
C(30)-C(29)-C(32)-F(35)	-169.7(8)
C(31)-C(29)-C(32)-F(35)	70.4(10)
O(4)-C(29)-C(32)-F(34)	-169.3(8)
C(30)-C(29)-C(32)-F(34)	69.6(10)
C(31)-C(29)-C(32)-F(34)	-50.3(10)
O(4)-C(29)-C(32)-F(36)	71.8(9)
C(30)-C(29)-C(32)-F(36)	-49.3(10)
C(31)-C(29)-C(32)-F(36)	-169.3(8)
O(8)-Al(2)-O(5)-C(33)	137(2)
O(6)-Al(2)-O(5)-C(33)	14(2)

O(7)-Al(2)-O(5)-C(33)	-104(2)
O(8)-Al(2)-O(6)-C(37)	94.7(14)
O(5)-Al(2)-O(6)-C(37)	-144.0(14)
O(7)-Al(2)-O(6)-C(37)	-24.1(15)
O(8)-Al(2)-O(7)-C(41)	51.6(14)
O(5)-Al(2)-O(7)-C(41)	-68.5(14)
O(6)-Al(2)-O(7)-C(41)	173.3(13)
O(5)-Al(2)-O(8)-C(45)	-55.6(18)
O(6)-Al(2)-O(8)-C(45)	65.1(19)
O(7)-Al(2)-O(8)-C(45)	-176.8(17)
Al(2)-O(5)-C(33)-C(35)	-74(2)
Al(2)-O(5)-C(33)-C(34)	166.5(18)
Al(2)-O(5)-C(33)-C(36)	47(2)
O(5)-C(33)-C(34)-F(38)	43.2(10)
C(35)-C(33)-C(34)-F(38)	-76.0(10)
C(36)-C(33)-C(34)-F(38)	164.8(9)
O(5)-C(33)-C(34)-F(39)	166.4(9)
C(35)-C(33)-C(34)-F(39)	47.2(11)
C(36)-C(33)-C(34)-F(39)	-72.0(11)
O(5)-C(33)-C(34)-F(37)	-75.7(9)
C(35)-C(33)-C(34)-F(37)	165.1(8)
C(36)-C(33)-C(34)-F(37)	45.9(10)
O(5)-C(33)-C(35)-F(42)	45.4(10)
C(34)-C(33)-C(35)-F(42)	163.1(8)
C(36)-C(33)-C(35)-F(42)	-77.1(11)
O(5)-C(33)-C(35)-F(40)	-77.8(11)
C(34)-C(33)-C(35)-F(40)	39.8(12)
C(36)-C(33)-C(35)-F(40)	159.6(10)
O(5)-C(33)-C(35)-F(41)	164.8(7)
C(34)-C(33)-C(35)-F(41)	-77.6(9)
C(36)-C(33)-C(35)-F(41)	42.2(10)
O(5)-C(33)-C(36)-F(43)	160.1(9)
C(35)-C(33)-C(36)-F(43)	-78.8(12)
C(34)-C(33)-C(36)-F(43)	41.5(12)
O(5)-C(33)-C(36)-F(44)	-76.7(11)
C(35)-C(33)-C(36)-F(44)	44.4(12)
C(34)-C(33)-C(36)-F(44)	164.7(9)
O(5)-C(33)-C(36)-F(45)	38.3(12)
C(35)-C(33)-C(36)-F(45)	159.4(10)
C(34)-C(33)-C(36)-F(45)	-80.3(11)
Al(2)-O(6)-C(37)-C(40)	-61.1(16)
Al(2)-O(6)-C(37)-C(39)	60.4(16)
Al(2)-O(6)-C(37)-C(38)	179.5(12)
O(6)-C(37)-C(38)-F(47)	-72.6(10)
C(40)-C(37)-C(38)-F(47)	166.1(8)
C(39)-C(37)-C(38)-F(47)	48.0(10)
O(6)-C(37)-C(38)-F(46)	46.3(10)
C(40)-C(37)-C(38)-F(46)	-74.9(9)
C(39)-C(37)-C(38)-F(46)	166.9(8)
O(6)-C(37)-C(38)-F(48)	165.7(8)

C(40)-C(37)-C(38)-F(48)	44.4(11)
C(39)-C(37)-C(38)-F(48)	-73.7(10)
O(6)-C(37)-C(39)-F(49)	39.9(12)
C(40)-C(37)-C(39)-F(49)	163.4(8)
C(38)-C(37)-C(39)-F(49)	-78.3(10)
O(6)-C(37)-C(39)-F(51)	161.5(8)
C(40)-C(37)-C(39)-F(51)	-75.0(11)
C(38)-C(37)-C(39)-F(51)	43.4(11)
O(6)-C(37)-C(39)-F(50)	-78.4(9)
C(40)-C(37)-C(39)-F(50)	45.1(9)
C(38)-C(37)-C(39)-F(50)	163.4(7)
O(6)-C(37)-C(40)-F(54)	45.1(9)
C(39)-C(37)-C(40)-F(54)	-78.0(9)
C(38)-C(37)-C(40)-F(54)	163.6(7)
O(6)-C(37)-C(40)-F(53)	166.6(7)
C(39)-C(37)-C(40)-F(53)	43.5(9)
C(38)-C(37)-C(40)-F(53)	-74.9(9)
O(6)-C(37)-C(40)-F(52)	-73.9(9)
C(39)-C(37)-C(40)-F(52)	163.0(7)
C(38)-C(37)-C(40)-F(52)	44.6(9)
Al(2)-O(7)-C(41)-C(43)	114.8(13)
Al(2)-O(7)-C(41)-C(42)	-126.9(11)
Al(2)-O(7)-C(41)-C(44)	-6.5(18)
O(7)-C(41)-C(42)-F(55)	46.6(11)
C(43)-C(41)-C(42)-F(55)	164.6(8)
C(44)-C(41)-C(42)-F(55)	-75.5(9)
O(7)-C(41)-C(42)-F(56)	-72.9(10)
C(43)-C(41)-C(42)-F(56)	45.1(10)
C(44)-C(41)-C(42)-F(56)	165.1(7)
O(7)-C(41)-C(42)-F(57)	166.7(8)
C(43)-C(41)-C(42)-F(57)	-75.3(10)
C(44)-C(41)-C(42)-F(57)	44.7(10)
O(7)-C(41)-C(43)-F(58)	39.7(11)
C(42)-C(41)-C(43)-F(58)	-78.1(10)
C(44)-C(41)-C(43)-F(58)	162.3(8)
O(7)-C(41)-C(43)-F(59)	161.8(9)
C(42)-C(41)-C(43)-F(59)	44.0(12)
C(44)-C(41)-C(43)-F(59)	-75.6(11)
O(7)-C(41)-C(43)-F(60)	-79.3(10)
C(42)-C(41)-C(43)-F(60)	162.8(8)
C(44)-C(41)-C(43)-F(60)	43.3(11)
O(7)-C(41)-C(44)-F(63)	41.8(12)
C(43)-C(41)-C(44)-F(63)	-78.8(10)
C(42)-C(41)-C(44)-F(63)	161.7(8)
O(7)-C(41)-C(44)-F(62)	-77.3(9)
C(43)-C(41)-C(44)-F(62)	162.1(7)
C(42)-C(41)-C(44)-F(62)	42.6(9)
O(7)-C(41)-C(44)-F(61)	162.9(8)
C(43)-C(41)-C(44)-F(61)	42.3(11)
C(42)-C(41)-C(44)-F(61)	-77.2(10)

Al(2)-O(8)-C(45)-C(47)	110.0(18)
Al(2)-O(8)-C(45)-C(46)	-133.1(18)
Al(2)-O(8)-C(45)-C(48)	-12(2)
O(8)-C(45)-C(46)-F(66)	-163.4(11)
C(47)-C(45)-C(46)-F(66)	-46.1(16)
C(48)-C(45)-C(46)-F(66)	73.6(16)
O(8)-C(45)-C(46)-F(65)	-38.1(16)
C(47)-C(45)-C(46)-F(65)	79.1(15)
C(48)-C(45)-C(46)-F(65)	-161.1(13)
O(8)-C(45)-C(46)-F(64)	78.2(10)
C(47)-C(45)-C(46)-F(64)	-164.5(10)
C(48)-C(45)-C(46)-F(64)	-44.8(12)
O(8)-C(45)-C(47)-F(68)	-165.2(15)
C(46)-C(45)-C(47)-F(68)	78.8(17)
C(48)-C(45)-C(47)-F(68)	-41.1(19)
O(8)-C(45)-C(47)-F(69)	-39.7(15)
C(46)-C(45)-C(47)-F(69)	-155.7(11)
C(48)-C(45)-C(47)-F(69)	84.3(13)
O(8)-C(45)-C(47)-F(67)	71.8(14)
C(46)-C(45)-C(47)-F(67)	-44.2(14)
C(48)-C(45)-C(47)-F(67)	-164.1(10)
O(8)-C(45)-C(48)-F(72)	-41.8(13)
C(47)-C(45)-C(48)-F(72)	-163.4(11)
C(46)-C(45)-C(48)-F(72)	77.6(13)
O(8)-C(45)-C(48)-F(71)	78.1(13)
C(47)-C(45)-C(48)-F(71)	-43.5(15)
C(46)-C(45)-C(48)-F(71)	-162.5(12)
O(8)-C(45)-C(48)-F(70)	-164.0(9)
C(47)-C(45)-C(48)-F(70)	74.3(12)
C(46)-C(45)-C(48)-F(70)	-44.7(13)
O(12)-Al(3)-O(9)-C(49)	-76(3)
O(10)-Al(3)-O(9)-C(49)	43(4)
O(11)-Al(3)-O(9)-C(49)	162(3)
O(12)-Al(3)-O(10)-C(53)	-116.9(17)
O(9)-Al(3)-O(10)-C(53)	125.8(17)
O(11)-Al(3)-O(10)-C(53)	6.6(18)
O(12)-Al(3)-O(11)-C(57)	-74(2)
O(9)-Al(3)-O(11)-C(57)	46(2)
O(10)-Al(3)-O(11)-C(57)	164.3(19)
O(9)-Al(3)-O(12)-C(61)	169(5)
O(10)-Al(3)-O(12)-C(61)	52(6)
O(11)-Al(3)-O(12)-C(61)	-70(6)
Al(3)-O(9)-C(49)-C(51)	-5(4)
Al(3)-O(9)-C(49)-C(52)	-132(3)
Al(3)-O(9)-C(49)-C(50)	118(3)
O(9)-C(49)-C(50)-F(73)	35.0(16)
C(51)-C(49)-C(50)-F(73)	158.9(12)
C(52)-C(49)-C(50)-F(73)	-78.5(15)
O(9)-C(49)-C(50)-F(75)	167.5(10)
C(51)-C(49)-C(50)-F(75)	-68.6(13)

C(52)-C(49)-C(50)-F(75)	54.0(12)
O(9)-C(49)-C(50)-F(74)	-75.1(12)
C(51)-C(49)-C(50)-F(74)	48.7(13)
C(52)-C(49)-C(50)-F(74)	171.3(11)
O(9)-C(49)-C(51)-F(76)	28.8(15)
C(52)-C(49)-C(51)-F(76)	152.1(12)
C(50)-C(49)-C(51)-F(76)	-91.8(13)
O(9)-C(49)-C(51)-F(77)	156.5(12)
C(52)-C(49)-C(51)-F(77)	-80.2(15)
C(50)-C(49)-C(51)-F(77)	35.9(16)
O(9)-C(49)-C(51)-F(78)	-83.0(11)
C(52)-C(49)-C(51)-F(78)	40.3(12)
C(50)-C(49)-C(51)-F(78)	156.4(10)
O(9)-C(49)-C(52)-F(79)	159.0(11)
C(51)-C(49)-C(52)-F(79)	33.3(15)
C(50)-C(49)-C(52)-F(79)	-88.5(14)
O(9)-C(49)-C(52)-F(80)	39.5(16)
C(51)-C(49)-C(52)-F(80)	-86.1(14)
C(50)-C(49)-C(52)-F(80)	152.1(13)
O(9)-C(49)-C(52)-F(81)	-81.7(13)
C(51)-C(49)-C(52)-F(81)	152.7(11)
C(50)-C(49)-C(52)-F(81)	30.9(13)
Al(3)-O(10)-C(53)-C(56)	93(2)
Al(3)-O(10)-C(53)-C(54)	-145.5(16)
Al(3)-O(10)-C(53)-C(55)	-31(2)
O(10)-C(53)-C(54)-F(82)	-49.3(14)
C(56)-C(53)-C(54)-F(82)	74.4(14)
C(55)-C(53)-C(54)-F(82)	-168.2(11)
O(10)-C(53)-C(54)-F(84)	-164.1(11)
C(56)-C(53)-C(54)-F(84)	-40.4(16)
C(55)-C(53)-C(54)-F(84)	77.0(14)
O(10)-C(53)-C(54)-F(83)	73.7(13)
C(56)-C(53)-C(54)-F(83)	-162.6(12)
C(55)-C(53)-C(54)-F(83)	-45.2(13)
O(10)-C(53)-C(55)-F(86)	-157.8(10)
C(56)-C(53)-C(55)-F(86)	76.0(14)
C(54)-C(53)-C(55)-F(86)	-40.6(14)
O(10)-C(53)-C(55)-F(85)	-41.9(13)
C(56)-C(53)-C(55)-F(85)	-168.1(11)
C(54)-C(53)-C(55)-F(85)	75.3(12)
O(10)-C(53)-C(55)-F(87)	76.8(10)
C(56)-C(53)-C(55)-F(87)	-49.4(12)
C(54)-C(53)-C(55)-F(87)	-166.0(9)
O(10)-C(53)-C(56)-F(89)	-45.8(16)
C(54)-C(53)-C(56)-F(89)	-166.8(12)
C(55)-C(53)-C(56)-F(89)	79.3(13)
O(10)-C(53)-C(56)-F(88)	-157.7(12)
C(54)-C(53)-C(56)-F(88)	81.3(16)
C(55)-C(53)-C(56)-F(88)	-32.7(17)
O(10)-C(53)-C(56)-F(90)	71.1(14)

C(54)-C(53)-C(56)-F(90)	-49.9(14)
C(55)-C(53)-C(56)-F(90)	-163.8(11)
Al(3)-O(11)-C(57)-C(58)	-127(2)
Al(3)-O(11)-C(57)-C(60)	-3(2)
Al(3)-O(11)-C(57)-C(59)	115(2)
O(11)-C(57)-C(58)-F(93)	158.2(12)
C(60)-C(57)-C(58)-F(93)	33.9(16)
C(59)-C(57)-C(58)-F(93)	-82.5(14)
O(11)-C(57)-C(58)-F(91)	42.6(12)
C(60)-C(57)-C(58)-F(91)	-81.7(12)
C(59)-C(57)-C(58)-F(91)	161.9(10)
O(11)-C(57)-C(58)-F(92)	-73.9(12)
C(60)-C(57)-C(58)-F(92)	161.9(10)
C(59)-C(57)-C(58)-F(92)	45.5(13)
O(11)-C(57)-C(59)-F(94)	40.9(14)
C(58)-C(57)-C(59)-F(94)	-77.4(13)
C(60)-C(57)-C(59)-F(94)	162.8(10)
O(11)-C(57)-C(59)-F(96)	-84.7(11)
C(58)-C(57)-C(59)-F(96)	157.1(11)
C(60)-C(57)-C(59)-F(96)	37.2(12)
O(11)-C(57)-C(59)-F(95)	154.6(10)
C(58)-C(57)-C(59)-F(95)	36.4(13)
C(60)-C(57)-C(59)-F(95)	-83.5(11)
O(11)-C(57)-C(60)-F(98)	38.0(14)
C(58)-C(57)-C(60)-F(98)	159.7(11)
C(59)-C(57)-C(60)-F(98)	-81.9(12)
O(11)-C(57)-C(60)-F(97)	166.0(9)
C(58)-C(57)-C(60)-F(97)	-72.4(13)
C(59)-C(57)-C(60)-F(97)	46.0(11)
O(11)-C(57)-C(60)-F(99)	-78.1(10)
C(58)-C(57)-C(60)-F(99)	43.6(11)
C(59)-C(57)-C(60)-F(99)	162.0(8)
Al(3)-O(12)-C(61)-C(64)	-91(6)
Al(3)-O(12)-C(61)-C(63)	151(5)
Al(3)-O(12)-C(61)-C(62)	31(6)
O(12)-C(61)-C(62)-F(102)	-166.2(13)
C(64)-C(61)-C(62)-F(102)	-45.0(15)
C(63)-C(61)-C(62)-F(102)	74.7(15)
O(12)-C(61)-C(62)-F(100)	-40.5(18)
C(64)-C(61)-C(62)-F(100)	80.7(17)
C(63)-C(61)-C(62)-F(100)	-159.6(13)
O(12)-C(61)-C(62)-F(101)	68.7(13)
C(64)-C(61)-C(62)-F(101)	-170.1(11)
C(63)-C(61)-C(62)-F(101)	-50.4(14)
O(12)-C(61)-C(63)-F(104)	-166.0(9)
C(64)-C(61)-C(63)-F(104)	76.9(11)
C(62)-C(61)-C(63)-F(104)	-42.7(13)
O(12)-C(61)-C(63)-F(105)	76.0(11)
C(64)-C(61)-C(63)-F(105)	-41.1(12)
C(62)-C(61)-C(63)-F(105)	-160.8(11)

O(12)-C(61)-C(63)-F(103)	-47.5(11)
C(64)-C(61)-C(63)-F(103)	-164.6(9)
C(62)-C(61)-C(63)-F(103)	75.8(12)
O(12)-C(61)-C(64)-F(107)	-43.8(14)
C(63)-C(61)-C(64)-F(107)	72.5(13)
C(62)-C(61)-C(64)-F(107)	-168.3(11)
O(12)-C(61)-C(64)-F(108)	75.7(13)
C(63)-C(61)-C(64)-F(108)	-168.1(10)
C(62)-C(61)-C(64)-F(108)	-48.8(13)
O(12)-C(61)-C(64)-F(106)	-165.3(11)
C(63)-C(61)-C(64)-F(106)	-49.0(12)
C(62)-C(61)-C(64)-F(106)	70.3(12)

Symmetry transformations used to generate equivalent atoms:

Table A II-7. ^{19}F -NMR data measured on $[\text{Nd}(\text{CH}_3\text{CN})_9][\text{Al}(\text{OC}(\text{CF}_3)_3)_4]_3$ **1** at 376 MHz, 25°C in CH_3CN (5 mm NMR tubes).

Sample	[Ln] (mmol kg ⁻¹)	[anion]/[Ln]	$\Delta\nu_{1/2}$ (Hz)	$1/T_{2\text{obs}}$ (s ⁻¹)
$[\text{Nd}(\text{CH}_3\text{CN})_9][\text{Al}(\text{OC}(\text{CF}_3)_3)_4]_3$ 1	16.00	3	6.3	20
		6	8.0	25
		9	6.3	20

Table A II-8. ^{19}F -NMR data measured on $\text{Eu}(\text{CH}_3\text{CN})_3(\text{CF}_3\text{SO}_3)_2$ and $[\text{Eu}(\text{CH}_3\text{CN})_9][\text{Al}(\text{OC}(\text{CF}_3)_3)_4]_2$ **2a** at 376 MHz, 25°C in CH_3CN (5 mm NMR tubes).

Sample	[Ln] (mmol kg ⁻¹)	[anion]/[Ln]	$\Delta\nu_{1/2}$ (Hz)	$1/T_{2\text{obs}}$ (s ⁻¹)
$\text{Eu}(\text{CH}_3\text{CN})_3(\text{CF}_3\text{SO}_3)_2$	9.43	3	316	991
		6	282	887
		9	253	795
$[\text{Eu}(\text{CH}_3\text{CN})_9][\text{Al}(\text{OC}(\text{CF}_3)_3)_4]_2$ 2a	10.08	3	11.4	36
		6	11.3	36
		9	10.4	33

Table A II-9. ^{19}F -NMR data measured on $\text{Gd}(\text{CH}_3\text{CN})_3(\text{CF}_3\text{SO}_3)_3$ and $[\text{Gd}(\text{CH}_3\text{CN})_9][\text{Al}(\text{OC}(\text{CF}_3)_3)_4]_3$ **3** at 376 MHz, 25°C in CH_3CN (5 mm NMR tubes).

Sample	[Ln] (mmol kg ⁻¹)	[anion]/[Ln]	$\Delta\nu_{1/2}$ (Hz)	$1/T_{2\text{obs}}$ (s ⁻¹)
$\text{Gd}(\text{CH}_3\text{CN})_3(\text{CF}_3\text{SO}_3)_3$	12.51	3	817	2568
		6	497	1561
		9	385	1210
$[\text{Gd}(\text{CH}_3\text{CN})_9][\text{Al}(\text{OC}(\text{CF}_3)_3)_4]_3$ 3	13.37	3	46	143
		6	51	159
		9	53	167
	8.56	3	45	140
		6	50	158
		9	45	142
	1.35	3	26	82

Table A II-10. ^{19}F -NMR data measured on $[\text{Dy}(\text{CH}_3\text{CN})_9][\text{Al}(\text{OC}(\text{CF}_3)_3)_4]_3$ **4** at 376 MHz, 25°C in CH_3CN (5 mm NMR tubes).

Sample	[Ln] (mmol kg ⁻¹)	[anion]/[Ln]	$\Delta\nu_{1/2}$ (Hz)	$1/T_{2\text{obs}}$ (s ⁻¹)
$[\text{Dy}(\text{CH}_3\text{CN})_9][\text{Al}(\text{OC}(\text{CF}_3)_3)_4]_3$ 4	78.20	3	6.9	22
		3	6.9	22
	44.67	6	6.5	20
		9	8.5	27
	27.87	3	5.7	18

Table A II-11. ^{19}F -NMR data measured on $[\text{Tm}(\text{CH}_3\text{CN})_8][\text{Al}(\text{OC}(\text{CF}_3)_3)_4]_3$ **5** at 376 MHz, 25°C in CH_3CN (5 mm NMR tubes).

Sample	[Ln] (mmol kg ⁻¹)	[anion]/[Ln]	$\Delta\nu_{1/2}$ (Hz)	$1/T_{2\text{obs}}$ (s ⁻¹)
$[\text{Tm}(\text{CH}_3\text{CN})_8][\text{Al}(\text{OC}(\text{CF}_3)_3)_4]_3$ 5	130	3	6.8	21
		3	5.9	18
	70.72	6	8.0	25
		9	8.2	26
	18.11	3	4.8	15

VII.3 EXPERIMENTAL DATA FOR CHAPTER III

Table A III-1. ^{14}N longitudinal ($1/T_1$) and transverse ($1/T_2$) relaxation rates and chemical shifts (ν) as a function of temperature, at 9.4 T and 18.8 T for $[\text{Gd}(\text{CH}_3\text{CN})_9][\text{Al}(\text{OC}(\text{CF}_3)_3)_4]_3$ **3** ($c_{\text{Gd}} = 1.34 \text{ mmol kg}^{-1}$, $P_{\text{m}} = 4.94 \times 10^{-4}$), for the reference (pure acetonitrile) $1/T_{1\text{A}}$, $1/T_{2\text{A}}$, ν_{A} , and the reduced values, $1/T_{1\text{r}}$, $1/T_{2\text{r}}$, $\Delta\omega_{\text{r}}$.

B = 9.4 T

T (K)	$1/T_1$ (s^{-1})	$1/T_{1\text{A}}$ (s^{-1})	$\ln(1/T_{1\text{r}})$
228.45	694.93	683.53	10.05
233.45	628.73	617.67	10.02
244.25	521.92	515.46	9.48
255.25	436.49	429.37	9.58
266.25	374.39	368.73	9.35
279.45	314.47	310.37	9.02
291.55	272.85	271.30	8.05
304.05	241.66	239.75	8.26
317.35	212.81	210.04	8.63
328.45	192.34	190.95	7.95

B = 9.4 T

T (K)	$1/T_2$ (s^{-1})	$1/T_{2\text{A}}$ (s^{-1})	$\ln(1/T_{2\text{r}})$
228.45	1117.57	673.17	13.71
233.45	1078.63	604.56	13.77
244.25	992.06	492.51	13.83
255.25	895.18	428.60	13.76
266.25	808.15	368.66	13.70
279.45	699.30	311.20	13.57
291.55	573.75	273.07	13.32
304.05	471.39	239.23	13.06
317.35	382.07	211.69	12.75
328.45	319.44	191.42	12.46

B = 9.4 T

T (K)	ν (Hz)	ν_{A} (Hz)	$\Delta\omega_{\text{r}}$ (10^6 rad s^{-1})
228.45	4395.5	4430.4	-0.443
233.45	4404.2	4429.9	-0.327
244.25	4395.5	4439.1	-0.554
255.25	4395.5	4447.8	-0.665
266.25	4395.5	4447.8	-0.665

279.45	4404.2	4456.5	-0.665
291.55	4404.2	4456.5	-0.665
304.05	4412.9	4465.2	-0.665
317.35	4421.6	4474.0	-0.665
328.45	4421.6	4474.0	-0.665

B = 18.8 T

T (K)	$1/T_1$ (s ⁻¹)	$1/T_{1A}$ (s ⁻¹)	$\ln(1/T_{1r})$
234.25	630.72	619.96	9.99
245.45	518.40	508.39	9.92
255.85	432.15	426.73	9.30
265.25	382.56	376.36	9.44
273.85	340.25	335.51	9.17
291.65	274.73	271.74	8.71
300.95	253.81	250.88	8.69
308.35	232.02	229.15	8.67
312.25	224.06	221.83	8.42
322.45	204.58	201.90	8.60
348.95	163.57	161.83	8.17

B = 18.8 T

T (K)	$1/T_2$ (s ⁻¹)	$1/T_{2A}$ (s ⁻¹)	$\ln(1/T_{2r})$
234.25	1139.99	614.40	13.88
245.45	1064.96	501.71	13.95
255.85	973.14	425.10	13.92
265.25	915.25	374.50	13.90
273.85	813.27	334.67	13.78
291.65	623.05	271.92	13.47
300.95	541.71	251.31	13.28
308.35	465.98	229.46	13.08
312.25	435.12	222.32	12.97
322.45	365.26	202.68	12.70
348.95	246.06	161.60	12.05

B = 18.8 T

T (K)	ν (Hz)	ν_A (Hz)	$\Delta\omega_t$ (10 ⁶ rad s ⁻¹)
291.65	11669.7	11778.5	-1.38
273.85	11646.9	11750.1	-1.31

255.85	11637.1	11729.0	-1.17
234.25	11635.7	11699.3	-0.81
245.45	11641.4	11714.8	-0.93
265.25	11645.6	11741.7	-1.22
300.95	11678.1	11786.9	-1.38
322.45	11704.9	11810.9	-1.35
312.25	11690.8	11801.0	-1.40
308.35	11646.9	11751.5	-1.33
348.95	11695.0	11796.7	-1.29

Table A III-2. ^{14}N longitudinal ($1/T_1$) and transverse ($1/T_2$) relaxation rates and chemical shifts (ν) as a function of temperature, at 9.4 T and 18.8 T for $[\text{Eu}(\text{CH}_3\text{CN})_9][\text{Al}(\text{OC}(\text{CF}_3)_3)_4]_2$ **2a** ($c_{\text{Eu}} = 17.43 \text{ mmol kg}^{-1}$, $P_{\text{m}} = 6.43 \times 10^{-3}$), for the reference (pure acetonitrile) $1/T_{1\text{A}}$, $1/T_{2\text{A}}$, ν_{A} , and the reduced values, $1/T_{1\text{r}}$, $1/T_{2\text{r}}$, $\Delta\omega_{\text{r}}$.

B = 9.4 T

T (K)	$1/T_1$ (s^{-1})	$1/T_{1\text{A}}$ (s^{-1})	$\ln(1/T_{1\text{r}})$
231.45	746.83	642.67	9.69
238.15	654.88	564.02	9.56
253.65	502.77	441.31	9.16
268.65	401.28	353.98	8.90
284.15	327.12	293.00	8.58
298.15	274.65	252.78	8.13
319.15	226.35	206.27	8.05
331.95	201.78	184.67	7.89

B = 9.4 T

T (K)	$1/T_2$ (s^{-1})	$1/T_{2\text{A}}$ (s^{-1})	$\ln(1/T_{2\text{r}})$
231.45	1130.97	619.20	11.28
238.15	1020.62	562.15	11.17
253.65	798.47	439.60	10.93
268.65	616.98	351.28	10.63
284.15	483.54	290.12	10.31
298.15	409.65	250.06	10.12
319.15	319.98	205.76	9.78
331.95	277.80	184.64	9.58

B = 9.4 T

T (K)	ν (Hz)	ν_{A} (Hz)	$\Delta\omega_{\text{r}}$ (10^6 rad s^{-1})
231.45	3518.9	4399.6	-0.86
238.15	3545.7	4399.3	-0.83

253.65	3596.8	4397.4	-0.78
268.65	3659.3	4403.1	-0.73
284.15	3716.1	4408.8	-0.68
298.15	3763.1	4417.0	-0.64
319.15	3807.0	4425.9	-0.60
331.95	3841.3	4434.2	-0.58

B = 18.8 T

T (K)	$1/T_1$ (s ⁻¹)	$1/T_{1A}$ (s ⁻¹)	$\ln(1/T_{1r})$
229.15	809.78	687.76	9.85
238.15	666.67	572.74	9.59
253.35	512.69	447.13	9.23
268.65	408.75	360.62	8.92
283.55	333.11	298.42	8.59
298.15	280.82	253.94	8.34
308.15	252.46	229.15	8.20
319.15	226.19	206.91	8.01
338.65	190.91	175.98	7.75
348.95	174.67	161.83	7.60

B = 18.8 T

T (K)	$1/T_2$ (s ⁻¹)	$1/T_{2A}$ (s ⁻¹)	$\ln(1/T_{2r})$
229.15	1346.62	677.05	11.55
238.15	1105.95	573.23	11.32
253.35	825.63	444.60	10.99
268.65	651.64	359.51	10.72
283.55	513.29	298.94	10.41
298.15	421.30	254.47	10.16
308.15	369.69	229.46	9.99
319.15	325.31	207.30	9.82
338.65	266.43	176.18	9.55
348.95	239.01	161.60	9.40

B = 18.8 T

T (K)	ν (Hz)	ν_A (Hz)	$\Delta\omega_t$ (10 ⁶ rad s ⁻¹)
229.15	9879.6	11661.2	-1.74
238.15	9943.0	11649.8	-1.67
253.35	10101.4	11688.0	-1.55
268.65	10228.5	11710.6	-1.45
283.55	10330.2	11721.9	-1.36

298.15	10440.4	11743.1	-1.27
308.15	10496.9	11751.5	-1.23
319.15	10547.8	11760.0	-1.18
338.65	10632.5	11776.9	-1.12
348.95	10697.5	11796.7	-1.07

Table A III-3. Proton relaxivities, r_1 ($\text{mM}^{-1} \text{s}^{-1}$) of $[\text{Gd}(\text{CH}_3\text{CN})_9][\text{Al}(\text{OC}(\text{CF}_3)_3)_4]_3$ **3** ($c_{\text{Gd}} = 8.58 \text{ mmol l}^{-1}$) as a function of temperature and magnetic field.

$\nu(^1\text{H})$ (MHz)	-35°C	-4.5°C	25°C	46°C
0.010	9.72	6.51	4.77	3.84
0.014	9.68	6.50	4.76	3.86
0.021	9.70	6.51	4.72	3.86
0.030	9.72	6.48	4.68	3.83
0.043	9.66	6.45	4.67	3.80
0.062	9.63	6.43	4.64	3.80
0.089	9.68	6.43	4.58	3.77
0.127	9.61	6.34	4.53	3.75
0.183	9.60	6.32	4.46	3.63
0.264	9.57	6.27	4.36	3.63
0.379	9.46	6.23	4.36	3.55
0.546	9.28	6.14	4.35	3.50
0.784	9.05	6.02	4.32	3.46
1.13	8.64	5.88	4.31	3.41
1.62	8.01	5.64	4.15	3.26
2.34	7.30	5.27	4.06	3.14
3.36	6.44	4.73	3.59	3.03
4.83	5.70	4.14	3.20	2.78
6.95	5.15	3.60	2.83	2.35
10	4.72	3.11	2.36	2.00
10	4.72	3.11	2.33	2.00
12	4.66	2.95	2.19	1.85
14	4.54	2.85	2.07	1.75
16	4.51	2.75	1.93	1.66
18	4.48	2.68	1.86	1.56
20	4.48	2.61	1.81	1.51
100	4.44	2.43	1.53	1.17
200	4.28	2.35	1.48	1.12
400	3.86	2.24	1.43	1.09
800	3.15	2.09	1.36	1.04

Table A III-4. Proton relaxivities, r_1 ($\text{mM}^{-1} \text{s}^{-1}$) of $[\text{Eu}(\text{CH}_3\text{CN})_9][\text{Al}(\text{OC}(\text{CF}_3)_3)_4]_2$ **2a** ($c_{\text{Eu}} = 12.93 \text{ mmol l}^{-1}$) as a function of temperature and magnetic field.

$\nu(^1\text{H})$ (MHz)	-35°C	-4.5°C	25°C
0.010	10.00	5.89	3.82
0.014	10.00	5.97	3.83
0.021	10.03	6.02	3.81
0.030	10.03	5.93	3.82
0.043	10.00	5.98	3.83
0.062	9.98	5.97	3.77
0.089	9.95	5.96	3.79
0.127	9.93	5.96	3.82
0.183	9.98	5.84	3.81
0.264	9.95	5.88	3.78
0.379	9.93	5.89	3.73
0.546	9.67	5.74	3.71
0.784	9.46	5.65	3.63
1.13	9.21	5.61	3.51
1.62	8.67	5.28	3.42
2.34	7.95	5.02	3.34
3.36	7.04	4.60	3.13
4.83	6.13	4.22	2.86
6.95	5.20	3.63	2.58
10	4.60	3.09	2.33
12	4.32	2.91	2.14
14	4.24	2.75	2.01
16	4.13	2.63	1.88
18	3.99	2.52	1.79
20	3.94	2.44	1.71
100	3.50	1.92	1.22
200	3.33	1.85	1.16
400	3.19	1.74	1.10
800	2.85	1.67	1.06

Table A III-5. EPR peak-to-peak widths (ΔH_{pp}) and central fields (B_0) of $[\text{Gd}(\text{CH}_3\text{CN})_9][\text{Al}(\text{OC}(\text{CF}_3)_3)_4]_3$ **3** ($c_{\text{Gd}} = 19.23 \text{ mmol Kg}^{-1}$) at X-band (9.4 GHz) and Q-band (35 GHz) as a function of temperature and spectrometer frequency.

X-Band

T (K)	ν (Hz)	ΔH_{pp} (G)	B_0 (G)
231.65	9.446E+09	34.02	3380.1
239.55	9.437E+09	30.42	3377.5
243.65	9.442E+09	29.45	3380.2
248.75	9.388E+09	26.85	3364.5
262.95	9.437E+09	22.48	3378.9
274.25	9.440E+09	19.32	3381.2
279.35	9.443E+09	18.66	3381.5
293.75	9.438E+09	16.28	3381.6
295.85	9.441E+09	16.28	3381.5
315.35	9.439E+09	15.08	3382.1
316.35	9.442E+09	15.26	3382.0
331.05	9.437E+09	15.62	3380.3

Q-Band

T (K)	ν (Hz)	ΔH_{pp} (G)	B_0 (G)
229.45	3.406E+10	16.07	12214
231.85	3.400E+10	15.74	12193
239.05	3.401E+10	14.97	12192
240.45	3.403E+10	15.24	12201
244.35	3.404E+10	14.72	12206
249.95	3.400E+10	14.20	12189
252.35	3.396E+10	14.14	12187
261.65	3.398E+10	12.85	12181
265.75	3.400E+10	12.81	12191
272.25	3.404E+10	12.24	12204
277.55	3.400E+10	12.36	12187
278.55	3.396E+10	12.34	12173
284.35	3.399E+10	11.86	12188
289.35	3.396E+10	11.73	12175
293.15	3.400E+10	11.43	12186
293.75	3.404E+10	11.35	12204
304.75	3.399E+10	11.43	12187
307.55	3.395E+10	11.73	12171
311.55	3.404E+10	11.34	12206
315.55	3.400E+10	11.56	12188
318.05	3.396E+10	11.71	12175

Table A III-6. EPR peak-to-peak widths (ΔH_{pp}) and central fields (B_0) of $[\text{Eu}(\text{CH}_3\text{CN})_9][\text{Al}(\text{OC}(\text{CF}_3)_3)_4]_2$ **2a** ($c_{\text{Eu}} = 17.43 \text{ mmol Kg}^{-1}$) at X-band (9.4 GHz) and Q-band (35 GHz) as a function of temperature and spectrometer frequency.

X-Band			
T (K)	ν (Hz)	ΔH_{pp} (G)	B_0 (G)
231.65	9.443E+09	72.65	3374.1
239.55	9.439E+09	63.88	3373.9
248.75	9.407E+09	52.13	3364.7
262.95	9.438E+09	42.89	3376.7
279.35	9.438E+09	31.92	3377.9
295.85	9.441E+09	24.49	3379.5
316.35	9.439E+09	18.33	3379.4
331.05	9.440E+09	15.81	3380.1

Q-Band			
T (K)	ν (Hz)	ΔH_{pp} (G)	B_0 (G)
229.45	3.407E+10	39.15	12212
240.45	3.403E+10	33.78	12198
252.35	3.396E+10	29.91	12171
261.65	3.398E+10	26.23	12177
278.55	3.395E+10	22.08	12170
289.35	3.396E+10	19.61	12171
307.55	3.395E+10	16.37	12170
318.05	3.396E+10	14.76	12172

Table A III-7. Quadrupolar ($1/T_{1q}$) and dipolar ($1/T_{1dd}$) contribution percentage to the longitudinal bound ^{14}N acetonitrile relaxation rates ($1/T_{1m}$); and quadrupolar ($1/T_{2q}$), dipolar ($1/T_{2dd}$) and scalar ($1/T_{2sc}$) contribution percentage to the transverse bound ^{14}N acetonitrile relaxation rates ($1/T_{2m}$) in function of temperature and magnetic field for $[\text{Gd}(\text{CH}_3\text{CN})_9][\text{Al}(\text{OC}(\text{CF}_3)_3)_4]_3$ **3**.

T (K)	B (T)	$1/T_{1m}$ (s^{-1})	$1/T_{1q}$ %	$1/T_{1dd}$ %	$1/T_{2m}$ (s^{-1})	$1/T_{2q}$ %	$1/T_{2dd}$ %	$1/T_{2sc}$ %
291.5	18.8	5.55E+03	87.65	12.35	6.83E+05	0.71	0.12	99.17
274.0	18.8	7.45E+03	87.66	12.34	9.44E+05	0.69	0.11	99.19
255.8	18.8	1.06E+04	87.66	12.34	1.19E+06	0.78	0.13	99.09
234.2	18.8	1.71E+04	87.66	12.34	1.37E+06	1.10	0.18	98.72
245.7	18.8	1.31E+04	87.66	12.34	1.29E+06	0.89	0.15	98.96
265.3	18.8	8.75E+03	87.66	12.34	1.07E+06	0.72	0.12	99.16
301.2	18.8	4.79E+03	87.65	12.35	5.53E+05	0.76	0.12	99.12

322.6	18.8	3.57E+03	87.65	12.35	3.30E+05	0.95	0.16	98.90
312.5	18.8	4.08E+03	87.65	12.35	4.23E+05	0.84	0.14	99.02
308.6	18.8	4.30E+03	87.65	12.35	4.64E+05	0.81	0.13	99.05
348.4	18.8	2.62E+03	87.64	12.36	1.73E+05	1.33	0.22	98.45
233.6	9.4	1.73E+04	87.67	12.33	9.76E+05	1.56	0.26	98.19
228.3	9.4	1.98E+04	87.68	12.32	9.88E+05	1.76	0.29	97.95
255.1	9.4	1.07E+04	87.66	12.34	8.86E+05	1.06	0.17	98.77
244.5	9.4	1.34E+04	87.67	12.33	9.40E+05	1.25	0.21	98.54
266.0	9.4	8.64E+03	87.65	12.35	8.11E+05	0.93	0.15	98.91
304.0	9.4	4.60E+03	87.61	12.39	4.52E+05	0.89	0.15	98.96
328.9	9.4	3.29E+03	87.57	12.43	2.60E+05	1.11	0.18	98.71
317.5	9.4	3.82E+03	87.59	12.41	3.39E+05	0.99	0.16	98.85
291.5	9.4	5.55E+03	87.63	12.37	5.72E+05	0.85	0.14	99.01
279.3	9.4	6.79E+03	87.64	12.36	6.93E+05	0.86	0.14	99.00

Table A III-8. Quadrupolar ($1/T_{1q}$) and dipolar ($1/T_{1dd}$) contribution percentage to the longitudinal bound ^{14}N acetonitrile relaxation rates ($1/T_{1m}$); and quadrupolar ($1/T_{2q}$), dipolar ($1/T_{2dd}$) and scalar ($1/T_{2sc}$) contribution percentage to the transverse bound ^{14}N acetonitrile relaxation rates ($1/T_{2m}$) in function of temperature and magnetic field for $[\text{Eu}(\text{CH}_3\text{CN})_9][\text{Al}(\text{OC}(\text{CF}_3)_3)_4]_2$ **2a**.

$T(\text{K})$	$B(\text{T})$	$1/T_{1m}(\text{s}^{-1})$	$1/T_{1q} \%$	$1/T_{1dd} \%$	$1/T_{2m}(\text{s}^{-1})$	$1/T_{2q} \%$	$1/T_{2dd} \%$	$1/T_{2sc} \%$
231.4	9.4	1.56E+04	87.83	12.17	9.64E+04	14.18	2.29	83.53
298.2	9.4	4.12E+03	87.78	12.22	2.44E+04	14.82	2.40	82.78
331.9	9.4	2.58E+03	87.69	12.31	1.49E+04	15.23	2.49	82.29
319.2	9.4	3.04E+03	87.73	12.27	1.77E+04	15.07	2.45	82.48
284.2	9.4	5.17E+03	87.80	12.20	3.10E+04	14.66	2.37	82.97
268.7	9.4	6.83E+03	87.82	12.18	4.14E+04	14.49	2.34	83.16
253.7	9.4	9.24E+03	87.83	12.17	5.66E+04	14.35	2.32	83.33
238.2	9.4	1.32E+04	87.83	12.17	8.12E+04	14.22	2.30	83.48
298.2	18.8	4.12E+03	87.83	12.17	2.46E+04	14.70	2.38	82.93
268.7	18.8	6.83E+03	87.83	12.17	4.18E+04	14.36	2.32	83.32
229.1	18.8	1.65E+04	87.82	12.18	1.03E+05	14.03	2.27	83.70
253.4	18.8	9.30E+03	87.83	12.17	5.75E+04	14.21	2.30	83.50
283.5	18.8	5.22E+03	87.83	12.17	3.16E+04	14.52	2.35	83.13
319.2	18.8	3.04E+03	87.82	12.18	1.78E+04	14.97	2.42	82.61
338.6	18.8	2.37E+03	87.81	12.19	1.37E+04	15.24	2.47	82.29
238.2	18.8	1.31E+04	87.83	12.17	8.20E+04	14.09	2.28	83.63
308.2	18.8	3.55E+03	87.83	12.17	2.10E+04	14.83	2.40	82.78
348.9	18.8	2.11E+03	87.80	12.20	1.20E+04	15.39	2.49	82.12

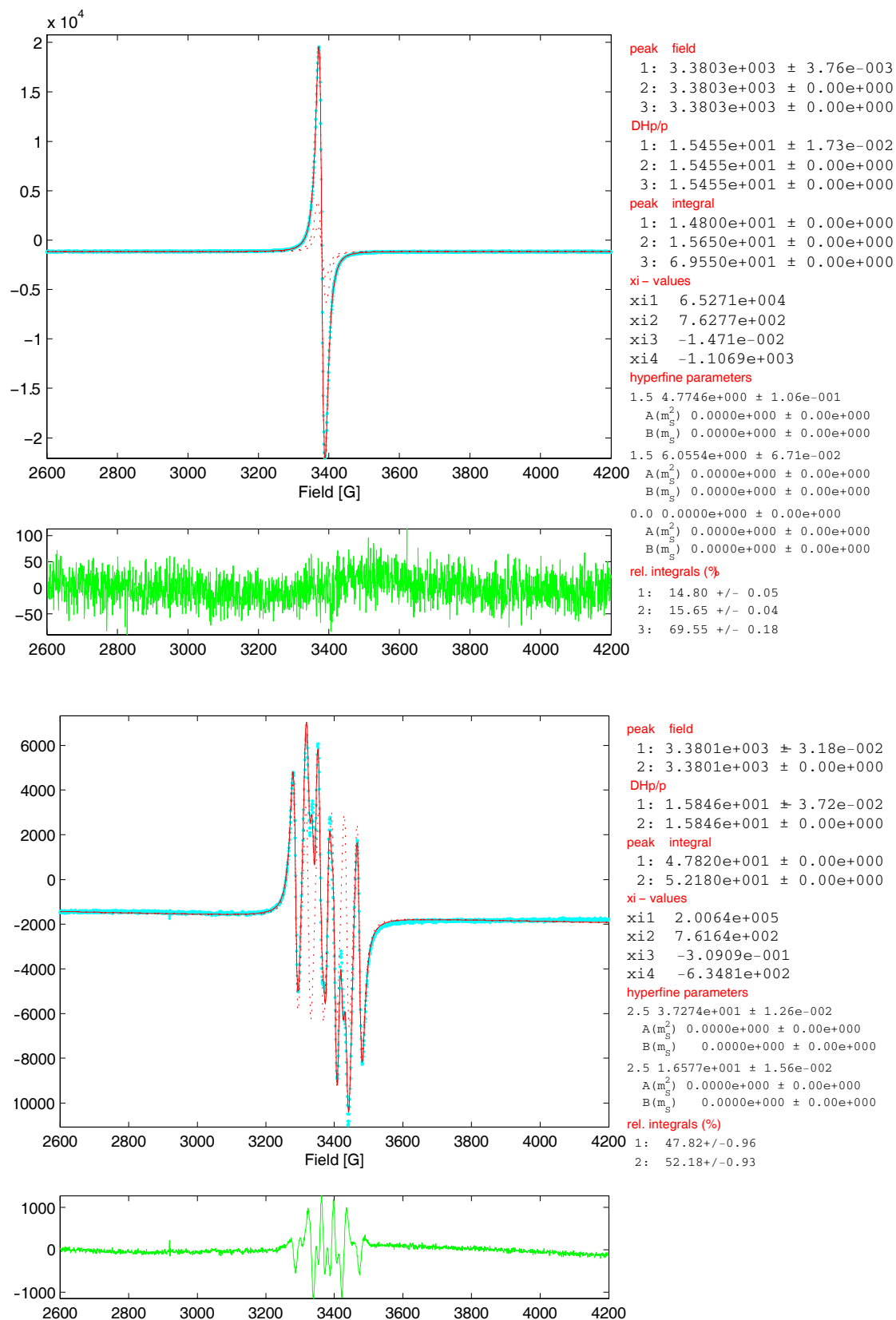


Figure A III-1. EPR spectra of Gd³⁺ (top) and Eu²⁺ (bottom) at 9.4 GHz and 331 K showing their fitted curves and hyperfine coupling constants.

VII.4 EXPERIMENTAL DATA FOR CHAPTER IV

Table A IV-1. ^{14}N longitudinal ($1/T_1$) and transverse ($1/T_2$) relaxation rates and chemical shifts (ν) as a function of temperature, at 18.8 T for $[\text{Nd}(\text{CH}_3\text{CN})_9][\text{Al}(\text{OC}(\text{CF}_3)_3)_4]_3$ **1** ($c_{\text{Nd}} = 15.98 \text{ mmol kg}^{-1}$, $P_{\text{m}} = 5.89 \times 10^{-3}$), $\ln((1/T_2 - 1/T_1)/P_{\text{m}})$ and the reduced values, $\Delta\omega_{\text{r}}$.

B = 18.8 T			
T (K)	$1/T_2$ (s^{-1})	$1/T_1$ (s^{-1})	$\ln((1/T_2 - 1/T_1)/P_{\text{m}})$
229.15	1096.25	806.45	10.80
238.15	831.39	668.00	10.23
253.35	602.77	513.22	9.63
268.65	456.20	412.20	8.92
283.55	356.96	334.95	8.22
298.15	296.47	282.21	7.79
319.15	235.85	227.56	7.25
338.65	198.41	192.75	6.87
348.95	181.29	176.35	6.73

B = 18.8 T			
T (K)	ν (Hz)	ν_{A} (Hz)	$\Delta\omega_{\text{r}}$ (10^6 rad s^{-1})
229.15	11961	11661	0.319
238.15	11944	11650	0.313
253.35	11968	11688	0.298
268.65	11972	11711	0.278
283.55	11966	11722	0.260
298.15	11965	11743	0.236
319.15	11969	11760	0.223
338.65	11969	11777	0.204
348.95	11983	11797	0.198

Table A IV-2. ^{14}N longitudinal ($1/T_1$) and transverse ($1/T_2$) relaxation rates and chemical shifts (ν) as a function of temperature, at 9.4 T and 18.8 T for $[\text{Dy}(\text{CH}_3\text{CN})_9][\text{Al}(\text{OC}(\text{CF}_3)_3)_4]_3$ **4** ($c_{\text{Dy}} = 15.92 \text{ mmol kg}^{-1}$, $P_{\text{m}} = 5.88 \times 10^{-3}$), $\ln((1/T_2 - 1/T_1)/P_{\text{m}})$ and the reduced values, $\Delta\omega_{\text{r}}$.

B = 9.4 T			
T (K)	$1/T_2$ (s^{-1})	$1/T_1$ (s^{-1})	$\ln((1/T_2 - 1/T_1)/P_{\text{m}})$
231.45	1109.9	755.86	11.01
238.15	943.04	664.89	10.76

253.65	614.14	510.20	9.78
268.65	438.10	400.00	8.78
284.15	350.14	333.22	7.96
298.15	289.69	280.19	7.39
319.15	235.18	230.04	6.77
331.95	209.38	205.09	6.59

B = 9.4 T

T (K)	ν (Hz)	ν_A (Hz)	$\Delta\omega$ (10^6 rad s^{-1})
231.45	3684.6	4399.6	-0.764
238.15	3704.7	4399.3	-0.742
253.65	3727.4	4397.4	-0.716
268.65	3772.9	4403.1	-0.673
284.15	3818.3	4408.8	-0.631
298.15	3858.8	4417.0	-0.596
319.15	3897.8	4425.9	-0.564
331.95	3926.4	4434.2	-0.542

B = 18.8 T

T (K)	$1/T_2$ (s^{-1})	$1/T_1$ (s^{-1})	$\ln((1/T_2 - 1/T_1)/P_m)$
229.15	2940.31	820.34	12.80
232.35	2429.54	763.36	12.55
238.15	1776.83	680.27	12.14
253.35	972.57	520.70	11.25
268.65	619.50	415.63	10.45
283.55	433.13	338.29	9.69
298.15	336.47	285.55	9.07
319.15	254.16	229.28	8.35
338.65	208.16	193.84	7.80
348.95	187.69	177.26	7.48

B = 18.8 T

T (K)	ν (Hz)	ν_A (Hz)	$\Delta\omega$ (10^6 rad s^{-1})
229.15	10325	11661	-1.428
232.35	10312	11671	-1.452
238.15	10291	11650	-1.452
253.35	10384	11688	-1.393
268.65	10479	11711	-1.316

283.55	10556	11722	-1.245
298.15	10641	11743	-1.177
319.15	10729	11760	-1.102
338.65	10794	11777	-1.050
348.95	10847	11797	-1.014

Table A IV-3. ^{14}N longitudinal ($1/T_1$) and transverse ($1/T_2$) relaxation rates and chemical shifts (ν) as a function of temperature, at 18.8 T for $[\text{Tm}(\text{CH}_3\text{CN})_8][\text{Al}(\text{OC}(\text{CF}_3)_3)_4]_3$ **5** ($c_{\text{Tm}} = 70.72 \text{ mmol kg}^{-1}$, $P_m = 2.32 \times 10^{-2}$), $\ln((1/T_2 - 1/T_1)/P_m)$ and the reduced values, $\Delta\omega_r$.

B = 18.8 T

$T \text{ (K)}$	$1/T_2 \text{ (s}^{-1}\text{)}$	$1/T_1 \text{ (s}^{-1}\text{)}$	$\ln((1/T_2 - 1/T_1)/P_m)$
229.15	1393.15	1322.14	8.03
238.15	1097.45	1054.63	7.52
253.35	800.64	773.40	7.07
268.65	615.84	596.32	6.73
283.55	479.57	468.16	6.20
298.15	393.48	383.95	6.02
308.35	347.22	340.60	5.65
319.15	308.36	303.03	5.44
338.65	253.14	249.22	5.13
348.95	229.36	226.07	4.95

B = 18.8 T

$T \text{ (K)}$	$\nu \text{ (Hz)}$	$\nu_A \text{ (Hz)}$	$\Delta\omega_r \text{ (10}^6 \text{ rad s}^{-1}\text{)}$
229.15	9946	11661	-0.464
238.15	9977	11650	-0.453
253.35	10114	11688	-0.426
268.65	10207	11711	-0.407
283.55	10293	11722	-0.386
298.15	10381	11743	-0.368
308.35	10429	11751	-0.358
319.15	10480	11760	-0.346
338.65	10553	11777	-0.331
348.95	10613	11797	-0.3203

Table A IV-4. Proton relaxivities, r_1 ($\text{mM}^{-1} \text{s}^{-1}$) of $[\text{Nd}(\text{CH}_3\text{CN})_9][\text{Al}(\text{OC}(\text{CF}_3)_3)_4]_3$ **1** ($c_{\text{Nd}} = 11.92 \text{ mmol l}^{-1}$) as a function of temperature and magnetic field.

$\nu(^1\text{H})$ (MHz)	-35°C	25°C
100	0.0075	0.0042
200	0.0070	0.0041
400	0.0070	0.0039
800	0.0099	0.0045

Table A IV-5. Proton relaxivities, r_1 ($\text{mM}^{-1} \text{s}^{-1}$) of $[\text{Dy}(\text{CH}_3\text{CN})_9][\text{Al}(\text{OC}(\text{CF}_3)_3)_4]_3$ **4** ($c_{\text{Dy}} = 48.45 \text{ mmol l}^{-1}$) as a function of temperature and magnetic field.

$\nu(^1\text{H})$ (MHz)	-35°C	25°C
0.014	0.176	0.121
0.100	0.173	0.116
1.00	0.179	0.111
10	0.161	0.104
20	0.155	0.108
100	0.175	0.114
200	0.217	0.122
400	0.374	0.153
800	0.814	0.277

Table A IV-6. Proton relaxivities, r_1 ($\text{mM}^{-1} \text{s}^{-1}$) of $[\text{Tm}(\text{CH}_3\text{CN})_8][\text{Al}(\text{OC}(\text{CF}_3)_3)_4]_3$ **5** ($c_{\text{Tm}} = 70.44 \text{ mmol l}^{-1}$) as a function of temperature and magnetic field.

$\nu(^1\text{H})$ (MHz)	-35°C	25°C
0.014	0.107	0.089
0.100	0.109	0.086
1.00	0.098	0.079
10	0.096	0.074
20	0.095	0.075
100	-	0.078
200	0.118	0.081
400	0.166	0.090
800	0.296	0.127

Table A IV-7. Dipole-dipole and Curie relaxation contributions to the inner ($r_{1\text{isdd}}$, $r_{1\text{iscu}}$) and outer ($r_{1\text{osdd}}$, $r_{1\text{oscu}}$) sphere proton relaxivities, r_1 ($\text{mM}^{-1} \text{s}^{-1}$), in function of temperature and magnetic field for $[\text{Dy}(\text{CH}_3\text{CN})_9][\text{Al}(\text{OC}(\text{CF}_3)_3)_4]_3$ **4**.

T (K)	$\nu(^1\text{H})$ (MHz)	r_1 ($\text{mM}^{-1}\text{s}^{-1}$)	$r_{1\text{isdd}}$	$r_{1\text{iscu}}$	$r_{1\text{osdd}}$	$r_{1\text{oscu}}$
298.15	0.014	0.114	0.083	0.000	0.032	0.000
298.15	0.1	0.114	0.083	0.000	0.032	0.000
298.15	1	0.114	0.083	0.000	0.032	0.000
298.15	10	0.114	0.083	0.000	0.032	0.000
298.15	20	0.114	0.083	0.000	0.032	0.000
298.15	100	0.117	0.082	0.002	0.032	0.001
298.15	200	0.123	0.081	0.007	0.031	0.004
298.15	400	0.149	0.078	0.026	0.030	0.016
298.15	800	0.252	0.067	0.104	0.026	0.056
238.15	0.014	0.169	0.122	0.000	0.047	0.000
238.15	0.1	0.169	0.122	0.000	0.047	0.000
238.15	1	0.169	0.122	0.000	0.047	0.000
238.15	10	0.169	0.122	0.000	0.047	0.000
238.15	20	0.169	0.122	0.000	0.047	0.000
238.15	100	0.182	0.121	0.008	0.047	0.006
238.15	200	0.219	0.118	0.033	0.045	0.023
238.15	400	0.354	0.107	0.131	0.041	0.074
238.15	800	0.826	0.083	0.494	0.032	0.216

Table A IV-8. Dipole-dipole and Curie relaxation contributions to the inner ($r_{1\text{isdd}}$, $r_{1\text{iscu}}$) and outer ($r_{1\text{osdd}}$, $r_{1\text{oscu}}$) sphere proton relaxivities, r_1 ($\text{mM}^{-1} \text{s}^{-1}$), in function of temperature and magnetic field for $[\text{Tm}(\text{CH}_3\text{CN})_8][\text{Al}(\text{OC}(\text{CF}_3)_3)_4]_3$ **5**.

T (K)	$\nu(^1\text{H})$ (MHz)	r_1 ($\text{mM}^{-1}\text{s}^{-1}$)	$r_{1\text{isdd}}$	$r_{1\text{iscu}}$	$r_{1\text{osdd}}$	$r_{1\text{oscu}}$
298.15	0.014	0.081	0.061	0.000	0.020	0.000
298.15	0.1	0.081	0.061	0.000	0.020	0.000
298.15	1	0.081	0.061	0.000	0.020	0.000
298.15	10	0.081	0.061	0.000	0.020	0.000
298.15	20	0.081	0.061	0.000	0.020	0.000
298.15	100	0.082	0.061	0.001	0.020	0.000
298.15	200	0.083	0.060	0.002	0.019	0.001
298.15	400	0.088	0.057	0.009	0.018	0.004
298.15	800	0.112	0.048	0.034	0.016	0.014

238.15	0.014	0.102	0.077	0.000	0.025	0.000
238.15	0.1	0.102	0.077	0.000	0.025	0.000
238.15	1	0.102	0.077	0.000	0.025	0.000
238.15	10	0.102	0.077	0.000	0.025	0.000
238.15	20	0.102	0.077	0.000	0.025	0.000
238.15	200	0.117	0.075	0.012	0.024	0.006
238.15	400	0.158	0.069	0.048	0.022	0.019
238.15	800	0.303	0.055	0.175	0.018	0.055

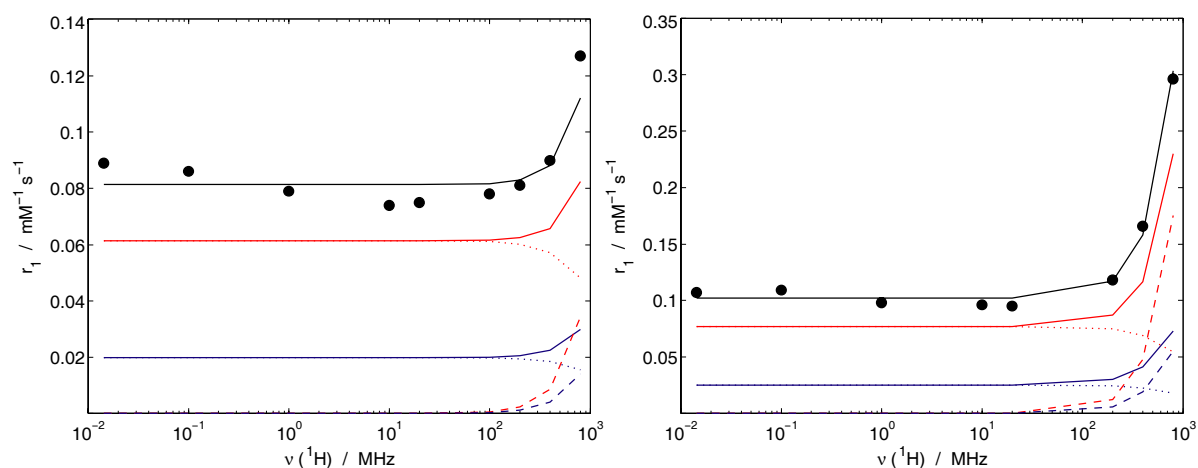


Figure A IV-1. ^1H NMRD profile of the Tm^{3+} ion in acetonitrile at 298 K (left box) and 238 K (right box). The measured relaxivity points are represented as filled symbols (\bullet) and the line through the data points (—) result from the least-square fit treatment of the ^1H NMRD and ^{14}N NMR $1/T_{1r}$ data. The continuous lines (—) and (—) represent the total inner- and outer-sphere contributions, (r_{1is} , r_{1os}), respectively, to the relaxivity curve. The dotted lines (\cdots) and (\cdots) represent the dipole-dipole contributions to the inner- and outer-sphere relaxivities, (r_{1is}^{dd} , r_{1os}^{dd}) respectively. The dashed lines ($---$) and ($---$) represent the Curie contributions to the inner- and outer-sphere relaxivities, (r_{1os}^{Curie} , r_{1os}^{Curie}) respectively.

Table A IV-9. Parameters obtained from the least-square fit of ^1H NMRD data, as measured by Bertini *et al.*,^[1] for the Dy^{3+} aqua ion, using the contribution of the outer-sphere relaxations. In the fitting procedure, D_{LnH}^{298} and E_{DLnH} were used as published by Powell,^[2] while the coordination number and the Ln-H distances were used as published by Cossy.^[3] Underlined parameters were fixed in the fit.

$[\text{Dy}(\text{H}_2\text{O})_8]^{3+}$	
$\tau_R / 10^{-12} \text{ s}$	40.4 ± 3
$E_R / \text{kJ mol}^{-1}$	21.5 ± 9
$\tau_S / 10^{-12} \text{ s}$	0.28 ± 0.04
$E_S / \text{kJ mol}^{-1}$	2.66 ± 1.6
$r_{\text{LnH 1st sphere}} / \text{\AA}$	<u>3.03</u>
$a_{\text{LnH bulk}} / \text{\AA}$	<u>4</u>

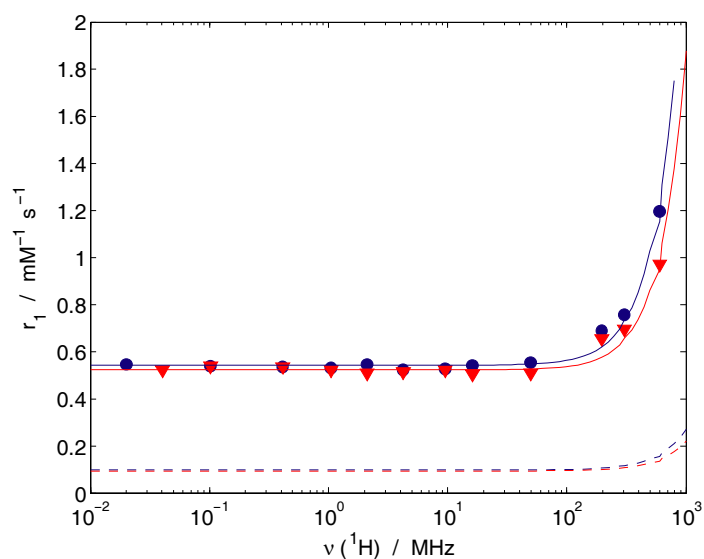


Figure A IV-2. ^1H NMRD profile of the Dy^{3+} aqua ion. The relaxivity points, as measured by Bertini *et al.*,^[1] are represented as filled symbols: (●) for 298 K and (▼) 308 K. The continuous lines through the data points result from the least-square fit treatment of the ^1H NMRD data using the contributions of the outer-sphere relaxations. The dashed lines (---) and (- - -) represent the outer-sphere contributions ($\sim 18\%$) to the relaxivity curves for the corresponding temperatures.

VII.5 REFERENCES

- [1] I. Bertini, F. Capozzi, C. Luchinat, G. Nicastro, Z. Xia, *J. Phys. Chem.* **1993**, *97*, 6351.
- [2] D. H. Powell, O. M. Ni Dhubhghaill, D. Pubanz, L. Helm, Y. S. Lebedev, W. Schlaepfer, A. E. Merbach, *J. Am. Chem. Soc.* **1996**, *118*, 9333.
- [3] C. Cossy, A. C. Barnes, J. E. Enderby, A. E. Merbach, *J. Chem. Phys.* **1989**, *90*, 3254.

CURRICULUM VITAE

Gabriella Éva BÓDIZS

Born 8th of December 1977

Romanian

Married (born GÁBOR)

Education and Diplomas

- 2004 - 2008 **PhD thesis in chemistry**, Ecole Polytechnique Fédérale de Lausanne (EPFL), Switzerland, supervisor Prof. Lothar Helm
- 2001 - 2002 **Master of Science in Advanced Organic Chemistry**, Babeş-Bolyai University (UBB), Faculty of Chemistry and Chemical Engineering, Cluj Napoca, Romania
- 1997 - 2001 **Bachelor of Science in Chemistry**, UBB, Cluj Napoca, Romania
- 1992 - 1996 **Baccalaureate**, Liceul Teoretic “Ion Slavici”, Satu Mare, Romania
Major: chemistry and biology

Work Experiences

- 2004 - 2008 **Research work in coordination chemistry**, Groupe de Chimie Inorganique et Bioinorganique (GCIB), group of Prof. Lothar Helm, EPFL, Switzerland
Study of the solvent exchange reaction mechanisms on lanthanide complexes using multinuclear and high pressure NMR.
Teaching assistant to 1st, 2nd and 3rd year chemistry and pharmacy students (analytical chemistry: UV-Vis spectroscopy; advanced inorganic chemistry: NMR techniques)
- 2003 - 2004 **Scientific collaborator** (1 year), Laboratoire de Chimie Inorganique et Bioinorganique (LCIB), group of Prof. André E. Merbach, EPFL, Switzerland,
Research work related to the coordination chemistry of lanthanides.
- 2003 **Scientific collaborator** (3 months), Laboratoire de Chimie Organometallique et Médicinale (LCOM), group of Prof. Paul J. Dyson, EPFL, Switzerland
Research work related to the formation of heteronuclear ruthenium clusters.
- 1996 - 1997 **Primary school teacher**, Ț coala Generala “Lucian Blaga”, Satu Mare, Romania

Languages

Hungarian/Romanian: bilingual

French: fluent

English: fluent

PUBLICATIONS

- [1] D. M. Chisholm, J. S. McIndoe, G. Bodizs, W. H. Ang, R. Scopelliti, P. J. Dyson, “Investigation into the formation of heteronuclear clusters of formula $[Ru_6C(CO)_{16}Ag_2X]_2^{2-}$ ($X = Cl, Br, \text{ or } I$)”, *J. Cluster Sci.*, **2007**, 18, 303-318
- [2] G. Bodizs, I. Raabe, R. Scopelliti, I. Krossing, L. Helm, “Synthesis, Structure and Characterization of some homoleptic lanthanide complexes: $[Ln(CH_3CN)_n][Al(OC(CF_3)_3)_4]_3$, with $n = 9$, $Ln = Nd, Eu, Gd, Dy$ and $n = 8$, $Ln = Tm$ ”, to be submitted
- [3] G. Bodizs, A. Borel, L. Helm, “Acetonitrile exchange on $[Gd(CH_3CN)_9]^{3+}$ and $[Eu(CH_3CN)_9]^{2+}$: a variable temperature and magnetic field ^{14}N NMR studies”, to be submitted
- [4] G. Bodizs, L. Helm, “ ^{14}N NMR and 1H NMRD variable temperature and magnetic field studies on the exchange of acetonitrile solvent on $[Nd(CH_3CN)_9]^{3+}$, $[Dy(CH_3CN)_9]^{3+}$ and $[Tm(CH_3CN)_8]^{3+}$ complexes”, in preparation
- [5] G. Bodizs, L. Helm, “First variable temperature ^{17}O NMR study at 18.8 T magnetic field for elucidate water exchange kinetics on $[Pr(H_2O)_9]^{3+}$ and $[Nd(H_2O)_9]^{3+}$ ”, in preparation

POSTER PRESENTATION

- [1] Fall meeting of the Swiss Chemical Society, September 13, **2007**, Lausanne, **Switzerland**
Gabriella Bodizs, Lothar Helm, “ ^{14}N NMR studies related to the solvent exchange reaction on $[\text{Ln}(\text{CH}_3\text{CN})_9][\text{Al}(\text{OC}(\text{CF}_3)_3)_4]_3$ ”, in CHIMIA **2007**, 61, No. 7/8
- [2] 5th Conference on Field Cycling NMR Relaxometry, May 31 – June 2, **2007**, Turin, **Italy**
Gabriella Bodizs, Lothar Helm, “NMRD profiles of a homoleptic Gd^{3+} acetonitrile complex with $[\text{Al}(\text{OC}(\text{CF}_3)_3)_4]^-$ as a non-coordinating anion”,
- [3] Fall meeting of the Swiss Chemical Society, October 13, **2006**, Zurich, **Switzerland**
Gabriella Bodizs, Ines Raabe, Ingo Krossing, Lothar Helm, “Straightforward synthesis and characterization of $\text{Gd}(\text{III})$ and $\text{Eu}(\text{III})$ acetonitrile complexes without counter ion in the first coordination sphere of the metal”, in CHIMIA **2006**, 60, No. 7/8
- [4] ICEF6, 6th International Conference on f-Elements, September 4 - 9, **2006**, Wroclaw, **Poland**
Gabriella Bodizs, Ines Raabe, Ingo Krossing, Lothar Helm, “Homoleptic lanthanide complexes in anhydrous acetonitrile using $[\text{Al}(\text{OC}(\text{CF}_3)_3)_4]^-$ as counter ion”
- [5] GDCh-JCF Frühjahrssymposium, 8th young scientists' conference on chemistry, March 16 - 18, **2006**, Konstanz, **Germany**
Gabriella Bodizs, Ines Raabe, Ingo Krossing, Lothar Helm, “Synthesis, Structure and Characterization of $[\text{Ln}(\text{CH}_3\text{CN})_9][\text{Al}(\text{OC}(\text{CF}_3)_3)_4]_3$, with $\text{Ln} = \text{Gd}, \text{Eu}$ ”
- [6] Fall meeting of the Swiss Chemical Society, October 7, **2004**, Zurich, **Switzerland**
Gabriella Bodizs, Lothar Helm, André E. Merbach, “Exchange of acetonitrile on a divalent lanthanide: a variable temperature and pressure ^{14}N NMR study”, in CHIMIA **2004**, 58, No. 7/8
- [7] EHPRG'42, Meeting on Advanced High Pressure Research, September 1 - 4, **2004**, Lausanne, **Switzerland**
Gabriella Bodizs, Lothar Helm, André E. Merbach, “Mechanism of acetonitrile exchange on $\text{Eu}(\text{II})$: A high pressure ^{14}N NMR study”